MATERIAL LAWS OF FRP STRENGTHENED REINFORCED CONCRETE UNDER UNIAXIAL TENSION AND BIAXIAL TENSION-COMPRESSION STRESS FIELDS

A Dissertation

Presented to

the Faculty of the Department of Civil and Environmental Engineering
University of Houston

In Partial Fulfillment
of the Requirements for the Degree
Doctor of Philosophy
in Civil Engineering

by
Guang Yang

August 2015

MATERIAL LAWS OF FRP STRENGTHENED REINFORCED CONCRETE UNDER UNIAXIAL TENSION AND BIAXIAL TENSION-COMPRESSION STRESS FIELDS

Guang Yang

Approved:

Chair of the Committee
Dr. Abdeldjelil Belarbi, Hugh Roy and Lillie Cranz Cullen Distinguished Professor,
Civil and Environmental Engineering

Committee Members:

Dr. Ashraf Ayoub, Professor and Royal Academy of Eng. Pell Frischmann Chair,
Civil Engineering,
City University London

Dr. Yi-Lung Mo, Professor,
Civil and Environmental Engineering

Dr. Bora Gencturk, Assistant Professor,
Civil and Environmental Engineering

Dr. Lu Gao, Assistant Professor,
Construction Management

Dr. Suresh K. Khator, Associate Dean,
Cullen College of Engineering

Dr. Roberto Ballarini
Thomas and Laura Hsu Professor and Chair,
Civil and Environmental Engineering

ACKNOWLEDGMENTS

I would like to express great gratitude and respect to my advisor, Prof. Abdeldjelil Belarbi, for his patience, support and advice throughout this research study. Special thanks are given to other committee members Prof. Ashraf Ayoub, Prof. Yi-Lung Mo, Prof. Bora Gencturk, and Prof. Lu Gao for their criticism and advices.

The experiments in this dissertation were funded by the National Science Foundation Grant No. 1100930. Steel reinforcements and FRP materials were donated by Gerdau Ameristeel Co. and Fyfe Co., respectively. Their support is greatly acknowledged.

I would like to acknowledge my colleague Mehdi Zomorodian for his help during the experimental tests. Special thanks are given to the lab technicians Gerald McTigret and Jeffrey Miller for their support and guidance on lab work. Also, I would like to thank my colleagues Moheb Labib, and Yashar Moslehy for their advice and guidance on the Panel Tester operation. Special thanks are also given to my undergraduate helpers: Ridwan Ajala, Mohammad Amini, Diego Salinas, Andres Villarreal, Damilola Sanni, Jaime Haro, and Ayatullah Muhammad for their help.

Finally, I would like to sincerely thank my wife, Shuang Zhou, my mom, and my friends for their love and support during my study, without which this dissertation would not have been possible.

MATERIAL LAWS OF FRP STRENGTHENED REINFORCED CONCRETE UNDER UNIAXIAL TENSION AND BIAXIAL TENSION-COMPRESSION STRESS FIELDS

An Abstract
of a
Dissertation
Presented to

the Faculty of the Department of Civil and Environmental Engineering
University of Houston

In Partial Fulfillment
of the Requirements for the Degree
Doctor of Philosophy
in Civil Engineering

by
Guang Yang

August 2015

ABSTRACT

Well established analytical models and design guidelines are already available for analyzing and designing FRP strengthened structures under flexural and axial-confinement actions. However, the understanding of the behavior of such members under in-plane stress field remains a subject of on-going discussion among several researchers and practitioners. Several analytical models have been proposed to predict the gain and upgrade of shear capacity due to FRP strengthening, among which, most models resulted in large discrepancies and produced large scatter when compared to experimental database. This is due to the lack of accurate constitutive models for strengthened reinforced concrete (RC) with FRP (FRP-RC) members. An efficient method to study the overall response of an RC member is to identify the characteristic behavior and the contribution of each material constituting the structure, the behavior of that specific element can be predicted by taking into account the inherent characteristics and material laws of the constituents that leads to understanding the global shear response of the structure.

As a first step of developing a shear model of FRP-RC elements, constitutive laws of each material component, namely concrete, steel reinforcement, and FRP sheets were studied in this research project through experimental and analytical investigations. Thirteen full-scale prismatic specimens and six full-scale panels were tested using the Universal Panel Tester (UPT) to study the stress-strain relationships of concrete, steel and FRP in tension as well as concrete in compression and the Poisson effect resulting from the biaxial loading. The results indicate that compared to the un-strengthened RC element, the presence of the externally bonded FRP material typically alters the main characteristics of

the stress-strain relationships for each components in FRP-RC element. These newly developed material laws will be used to further develop a model to predict the behavior of FRP strengthened RC elements subjected to shear and torsion. The results from both experimental and analytical study in this research project will provide a promising contribution to the prediction of the behavior of FRP-RC members under shear that will ultimately improve the accuracy of the available design guidelines.

TABLE OF CONTENTS

LIST OF FIGURES

LIST OF TABLES

NOTATIONS

1	direction of applied principal tensile stress
2	direction of applied principal compressive stress
A_c	area of concrete
A_f	area of FRP sheet
A_s	area of steel bars
B	factor for calculating apparent yielding stress
c	coefficient for tension stiffening
$c_{\exp}$	coefficient for tension stiffening from regression of test data
d	effective depth of beam
d_b	diameter of rebar
d_f	effective depth of FRP
D_{frp}	stress distribution factor
E_c	elastic modulus of concrete
E_f	elastic modulus of FRP sheet
E_s	elastic modulus of bare steel bars
f_c'	cylinder compressive strength of concrete
f_{cK}	specified characteristic cylinder compressive strength
f_{cm}	mean cylinder compressive strength of concrete
f_{cr}	cracking tensile strength of concrete
f_{ctm}	mean tensile strength of concrete

f_{fe}	effective stress of FRP
$f_{pull-off}$	pull-off strength for concrete-FRP interface
f_s	smeared (average) stress in embedded mild steel bars
f_u	tensile strength of steel rebar
$f_{u,FRP}$	tensile strength of FRP sheet
f_y	yield stress of bare steel bars
f_y'	apparent yield stress of steel bars
f_y'	depth of beam
G_f	facture energy
h	effective depth
k	factor calculating Hsu/Zhu ratio
$K_{f/s}$	factor for FRP/steel stiffness ratio
K_w	factor for wrapping scheme
l	direction of longitudinal steel bars
L	effective length of FRP
l_e	effective length of FRP
M	bond parameter
$n_{f/s}$	ratio of Young's Modulus between FRP and steel
P	applied tensile load
P_{cr}	cracking load
R	reduction factor
s_f	spacing of FRP strip

$s(x)$	slip at a distance x from the loaded end
t	direction of transverse steel bars
t_s	direction of transverse steel bars
t_f	width of FRP sheet
T_v	shear contribution of the transverse steel reinforcement
V_c	concrete contribution to the shear capacity
V_f	FRP contribution to the shear capacity
$V_{frp,d}$	FRP contribution to the shear capacity
V_n	nominal shear strength
V_p	shear force provided by the FRP reinforcement
V_s	steel contribution to the shear capacity
α	angle of transverse reinforcement relative to the longitudinal axis
β	deviation angle
$\Delta\varepsilon_1$	change of strain in principal 1-direction
$\Delta\varepsilon_2$	change of strain in principal 2-direction
ε_1	smeared (average) tensile strain in principal 1-direction
ε_{ca}	autogenously shrinkage strain
ε_{cd}	drying shrinkage strain
ε_{cr}	cracking tensile strain of concrete
$\varepsilon_{c,sh}$	strain in concrete due to shrinkage
ε_f	strain in FRP
ε_{fe}	effective strain in FRP

ε_{fu}	ultimate strain in FRP
$\varepsilon_f(x)$	strain in the FRP sheet at a distance x from the crack
$\varepsilon\nu_{cu}$	effective strain in FRP
ε_s	smeared (average) strain of steel bars
ε_{sf}	smeared (average) strain of steel bars that yield first
$\varepsilon_s(x)$	strain in the steel bars at a distance x from the crack
ε_y	yielding strain in bare steel bars
$\varepsilon_y^{'}$	yielding strain in steel bars in smeared model
$\varepsilon_{s,sh}$	strain in steel bars due to shrinkage of concrete
ε_{sh}	shrinkage strain of plain concrete
ϕ_F	resistance factor of FRP
$\gamma_{f,d}$	safety factor for strength of FRP
ν_{12}	Hsu/Zhu ratio (ratio of resulting tensile strain to source compressive strain)
ν_{21}	Hsu/Zhu ratio (ratio of resulting compressive strain to source tensile strain)
θ	angle of diagonal compression
ρ_e	equivalent reinforcement ratio
ρ_f	FRP reinforcement ratio
ρ_s	steel reinforcement ratio
σ_1	smeared (average) tensile stress in principal 1-direction
σ_c	smeared (average) tensile stress in concrete
$\sigma_{c,sh}$	stress in concrete due to shrinkage
σ_f	smeared (average) tensile stress in FRP sheet

$\sigma_f(x)$	stress in the FRP sheet at a distance x from the crack
σ_p	peel-off stress of the FRP sheets
σ_s	smeared (average) tensile stress in steel bars
$\sigma_{s,sh}$	stress in steel rebar due to shrinkage
$\sigma_s(x)$	stress in the steel bars at a distance x from the crack
$\tau(x)$	shear stress at a distance x from the loaded end
τ_{ave}	average shear stress along FRP
ζ	softening coefficient
ζ_f	softening coefficient considering FRP sheet

CHAPTER 1 INTRODUCTION

1.1 GENERAL

Deterioration of civil infrastructures has become an increasingly serious problem for the society. According to 2013 American Society of Civil Engineer (ASCE) Report Card for America's Infrastructures, America's cumulative GPA for infrastructure is only a D+ using a simple A to F grade report card format. Since 1998, this grades have been averaging only Ds (poor condition) due to delayed maintenance and underinvestment across most categories. The potential cost of repair and retrofitting these infrastructures can become a drag on the economy. The main causes of deterioration include environmental corrosion, overloading due to change of use or change of loading condition, and intentional (unintentional) damage by public user, see Fig. 1.1a)–c), respectively. The deterioration causes a reduction of the capacity and serviceability that leads to durability loss or even structure failure.

a) Environmental Corrosion b) Overloading c) Unintentional Damage

Fig. 1.1 Examples of Deterioration of the Civil Infrastructures

Depending on the loads and condition, civil engineers have developed many techniques for strengthening the infrastructure such as cement grout, section enlargement, external plate bonding and external post-tensioning. Besides that, composite materials such as Fiber Reinforced Polymer (FRP) with a combination of high strength, high stiffness,

light weight, and corrosion resistance properties, became very attractive since early 1960s. In 1970s, lower-cost of fabrication methods appeared due to the high market demand (Bakis et al., 2002). By the late 1980s, FRP started being used in civil engineering applications. To date, FRP has been widely used practically in strengthening or building the civil engineering structures under flexural, axial load and shear, see Fig. 1.2.

a) Flexural Strengthening b) Confinement c) Shear Strengthening

Fig. 1.2 Examples of Strengthening of Structure Members Using FRPs

Extensive experimental and analytical investigations have been conducted to study the complex behavior of FRP strengthened structures. In the current literature, well established analytical models are already available for analyzing and designing strengthened beams and columns under flexural and axial-confinement actions. However, the behavior of such members under in-plane shear stress field remains a subject of on-going discussion among several researchers and practitioners due to the high complexity of the mechanism and the failure modes associated with the behavior (Lee and Kim, 2008). Several analytical models were proposed to predict the gain in shear capacity due to the use of FRP for strengthening. However, most models resulted in large discrepancies and produced large scatter when compared to experimental results, and the analytical models for estimating the shear capacity of FRP strengthened Reinforced Concrete (RC) members were mostly developed based on results of simply supported beam tests (Belarbi et al., 2011). Such tests cannot give a full understanding of shear behavior due to the presence of

flexural effects. As a case study in NCHRP report 678 (Belarbi et al., 2011), the FRP contribution to the shear capacity of a rectangular RC beam with U-wrap method (cross section shown in Fig. 1.3) was predicted using 11 models and four code provisions. The vertical axis shows the shear stress contribution due to FRPs, horizontal axis gives the axial rigidity of FRP. The comparison shown in Fig. 1.3 illustrates that there are quite significant differences in the predictions.

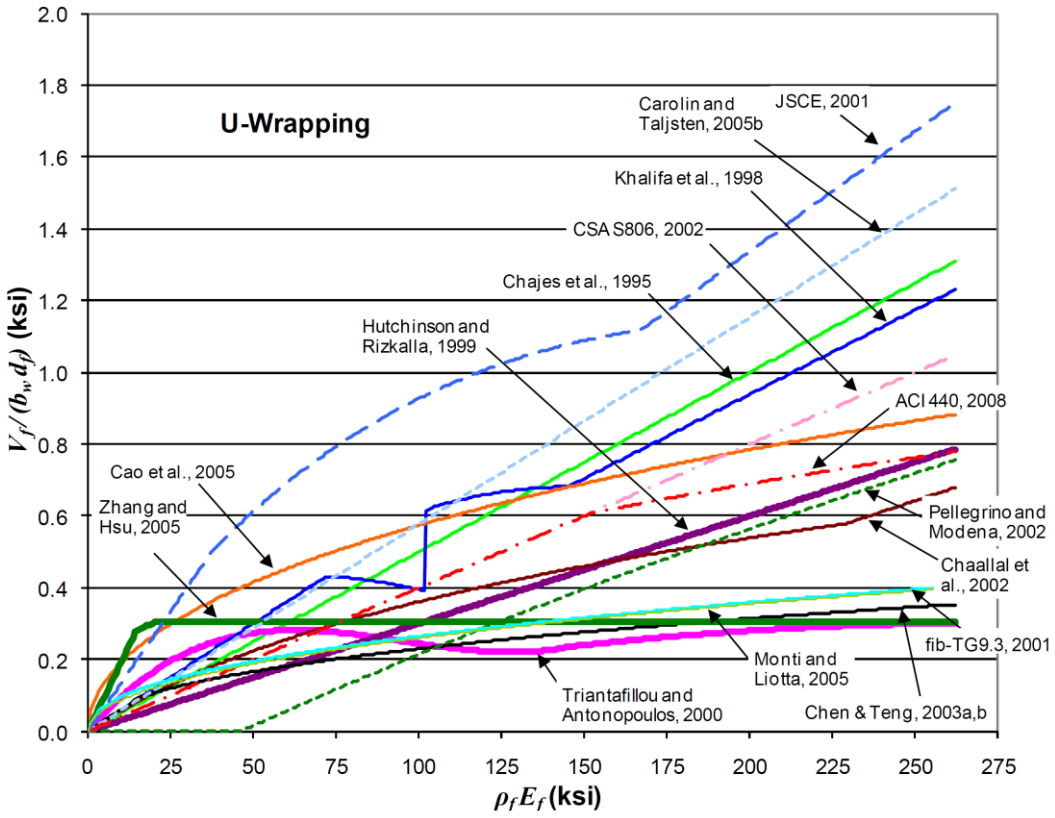

Fig. 1.3 Comparison of FRP Contribution to Shear Capacity Using Different Models and Codes (Adopted from NCHRP Report 678)

1.2 PROBLEM DEFINITION AND RESEARCH APPROACH

The difference of predictions from various models as shown in Fig. 1.3 is partly due to the high level of complexity associated with the shear behavior, but more importantly to the lack of accurate constitutive models for FRP strengthened reinforced

concrete (FRP RC) elements. In the previous proposed models, the stress strain relationships of concrete, steel and FRP were derived independently. For the currently used code and design guidelines, the shear capacity of the FRP RC members are calculated as a superposition of the shear contribution of concrete (V_c), steel (V_s), and FRP (V_f). However, a high level of interaction between these components exists and different parameters that might influence this interaction need to be taken into account (Bousselham and Chaallal, 2008; Chen et al., 2010). To rationally describe the behavior and predict the capacity of FRP RC element in shear, constitutive models of each component and the interactions among them have to be carefully investigated, see Fig. 1.4.

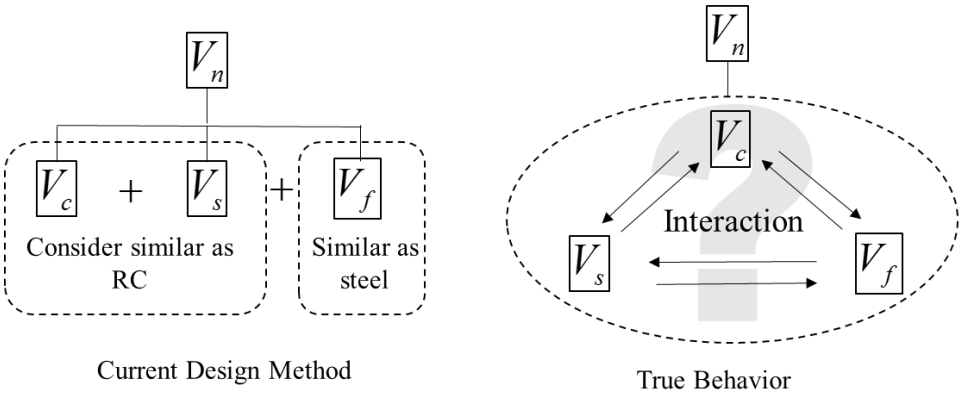

Fig. 1.4 Shear Contribution and Interaction of the Components in FRP RC Members

An efficient method to assess the overall response of an RC member is to identify the characteristic behavior and the contribution of each material constituting the structure. As shown in Fig. 1.5, reinforced concrete members can be considered as an assemblage of elements. If the behavior of such element can be well understood, the behavior of the whole member, even the whole structure can be obtained through finite element method.

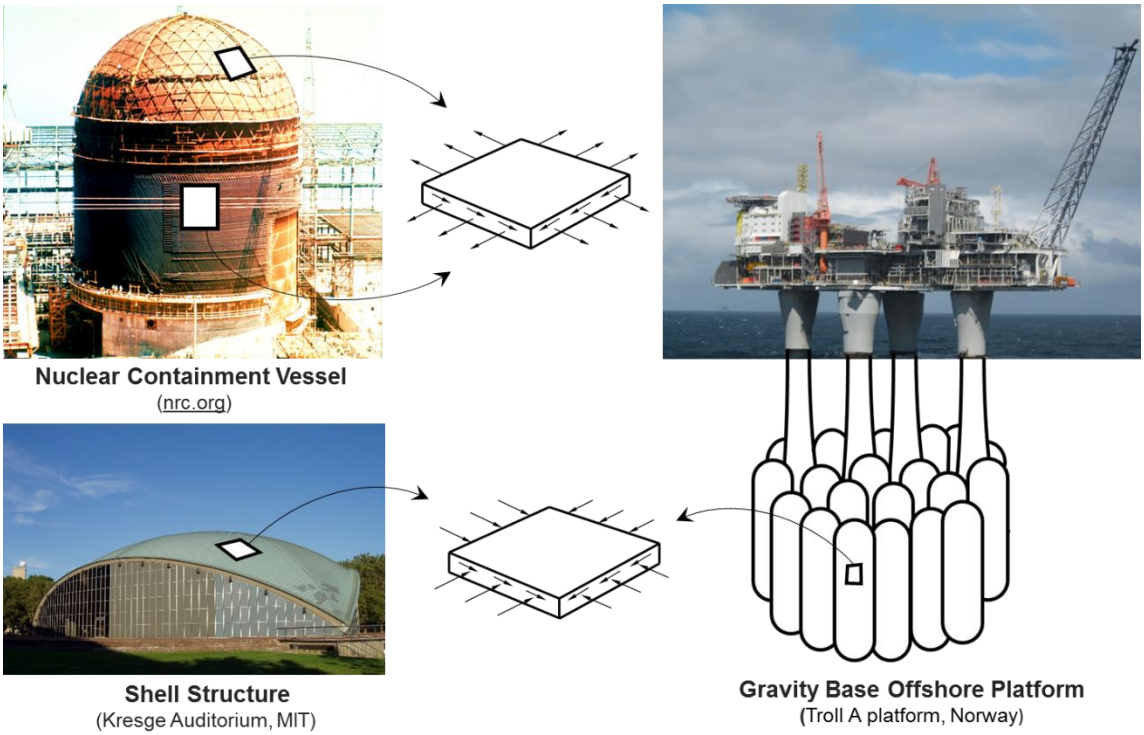

Fig. 1.5 An Efficient Method to Study the Behavior of the Structures Using Elements

This method could be applied to investigate the shear behavior of the FRP RC under shear stress field. As an example, an element from a girder strengthened by FRP sheets that is subjected to shear force can be isolated and the behavior of that specific element can be predicted by taking into account the inherent characteristics and material laws of the constituents that leads to understanding the global shear response of the girder (Fig. 1.6). To investigate the behavior of this shear element, a set of equilibrium equations, compatibility conditions, and materials laws are required for steel and FRP reinforcements in the longitudinal (l) and transverse (t) directions as well as the concrete in tension and compression in the principal directions 1 and 2, respectively.

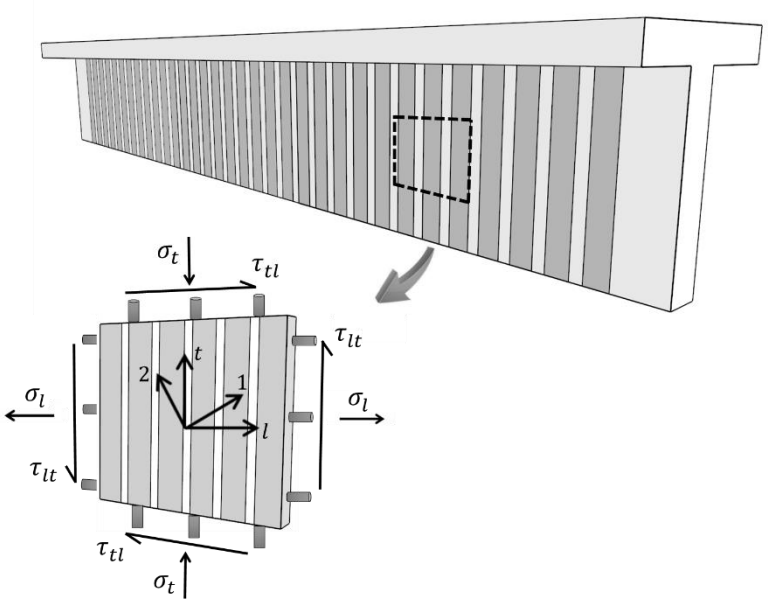

Fig. 1.6 Beam Shear Element with In-plane Stresses

The study of shear behavior of structure element can be conducted by testing full-scale panel elements using the unique Universal Panel Tester (UPT) at the University of Houston (UH). The UPT can apply various combination of in-plane and out-of-plane stresses to the element (Hsu et al., 1995).

The research work conducted by the author is part of an on-going NSF project with the aim of developing the analytical models for FRP strengthened RC elements under shear stress field including membrane stresses. Fig. 1.7 shows the work plan of the project and the contribution of the author. As the first step of developing a shear model of FRP RC elements, constitutive laws of each material component were studied in this research project through experimental and analytical investigations.

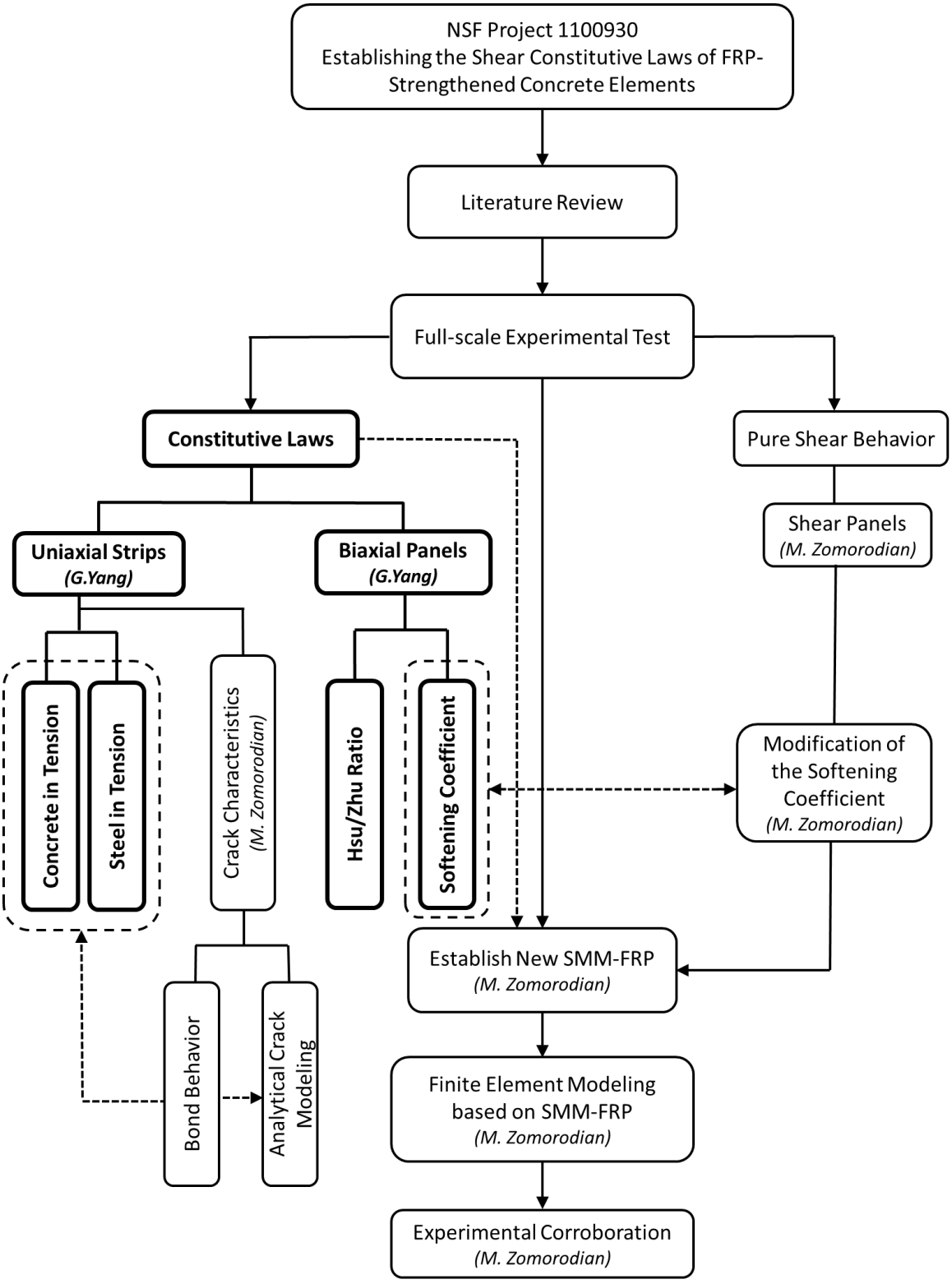

Fig. 1.7 Work Plan of the Project and Contribution of the Author

1.3 RESEARCH OBJECTIVES

To rationally describe the behavior of FRP RC element in shear, the stress strain relationships of each component and the interactions among them have to be carefully investigated. The main objective of this investigation is to derive the uniaxial and biaxial material laws of concrete, steel and FRP required in the truss model theory to predict the behavior of the FRP RC element under in plane shear stress field.

The proposed work in this research includes the following specific objectives:

a) to investigate the parameters affecting the material laws of concrete, steel in uniaxial tension and biaxial tension-compression.
b) to recommend the mathematical expressions for material laws of concrete, steel and FRP in tension, the softening coefficient, and the modified Hsu/Zhu ratio needed for rational prediction of the truss model theory.

The accuracy of the shear model highly depends on the constitutive laws. By carefully investigating these constitutive laws, the research in this study is expected to enhance the understanding of this complex phenomenon that will ultimately improve the accuracy of the available design guidelines.

1.4 OUTLINE OF DISSERTATION

This dissertation is organized in six chapters as

Chapter 1: Presents the statement of problems and the objective of the research.

Chapter 2: Presents the literature review of: a) researches on shear strengthening using externally bonded FRP sheets; b) development of the truss model theories; c) development of the constitutive modeling for RC elements with and without

FRP sheets under uniaxial and biaxial loading. The research gap is also presented in this chapter.

Chapter 3: Presents a brief introduction on the Universal Panel Tester and the detail information of the servo-control system in this particular test program.

Chapter 4: Presents the details of experimental program, including the fabrication of the specimen, test setup, instrumentation method and the loading procedure for the three types of tests in this study.

Chapter 5: Presents the test results and analytical studies of the constitutive modeling. The analysis involves the study on different variables affecting the constitutive laws of the components in FRP RC elements, and development of the mathematical expressions for constitutive laws of concrete, steel in tension, as well as the softened coefficient for concrete and the modified Hsu/Zhu ratio for the FRP RC element.

Chapter 6: Presents conclusions, limitations and recommendations for future research.

CHAPTER 2 LITERATURE REVIEW

2.1 INTRODUCTION

In this chapter, a comprehensive review on the existing knowledge of shear strengthening of RC members using FRP is presented. The flowchart in Fig. 2.1 shows the outline of the presentation in this chapter. It can be seen that the review includes three main parts: review of the experimental and analytical investigations on shear strengthening of RC using FRPs, review of development of the truss model approaches, and review of the constitutive laws of each components in FRP RC members. As the main research topic in this study, the constitutive laws is reviewed in detail in this chapter, including concrete in tension (tension stiffening), steel in tension, FRP in tension; concrete in compression (softening coefficient); and Poisson effect (Hsu/Zhu ratio). Finally, the research gaps related to shear strengthening of RC members using FRP is addressed.

2.2 STUDIES ON SHEAR STRENGTHENING USING FRP

2.2.1 General

The FRPs have been proven as an effective material that considerably increases the strength as well as ductility of the member without significantly affecting the stiffness of the structure (Bakis et al., 2002). Externally bonded FRP materials is one of the effective ways to strengthen the members in shear. The most common wrapping methods include fully (complete) wrapping, U-wrap, and side bonding as shown in Fig. 2.2a)–c), respectively.

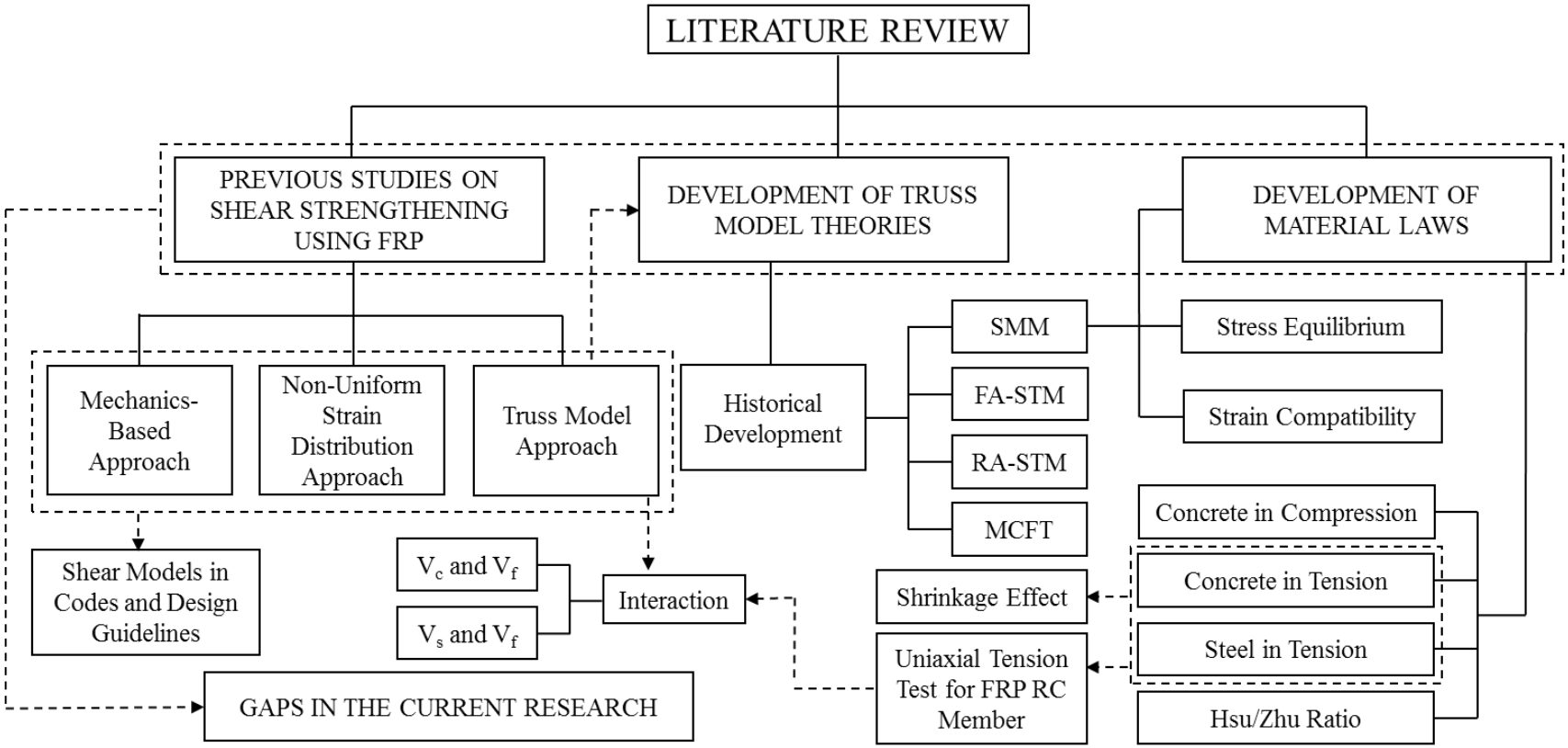

Fig. 2.1 Outline of Literature Review

The FRP sheets can be applied as continuous sheets along the span or as discrete strips. The fibers in the FRP sheets can also be oriented at various angles to meet a range of strengthening requirements, see Fig. 2.3a)-c).

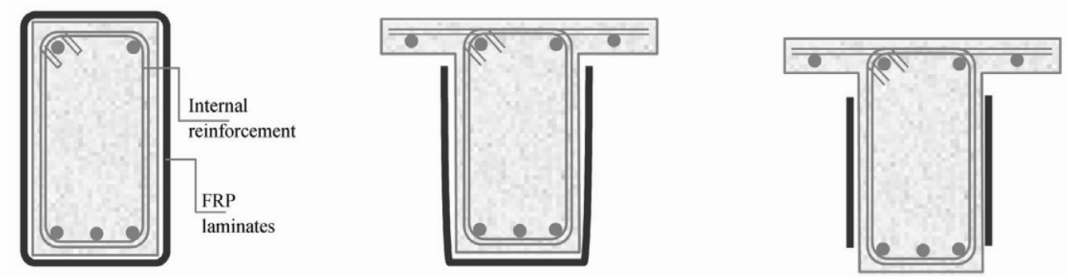

a) Fully Wrap b) U-Wrap c) Side Bonding

Fig. 2.2 Different Wrapping Schemes for Shear Strengthening Using FRP Sheets (Adopted from Belarbi and Bora, 2013)

a) Strips (β=90) b) Strips (β<90) c) Continuous Sheet

Fig. 2.3 Different Configurations for Shear Strengthening Using FRP Sheets

2.2.2 Shear Models for FRP RC Members

The most commonly used analytical approaches to calculate the shear contribution of FRP include truss model approach (Triantafillou, 1998; Khalifa et al., 1998 and 1999; Triantafillou et al., 2000; Chaallal et al., 2002; Pellegrino et al., 2002; Hsu et al., 2003; Chen et al., 2013), mechanics-based model (Malek and Saadatmanesh, 1998; Deniaud and Cheng, 2001, 2004; Monti and Liotta, 2005; Sim et al., 2005) and non-uniform strain distribution approach (Caroline and Taljsten, 2005b; Chen and Teng, 2003a and 2003b; Cao et al., 2005).

Bousselham and Chaallal (2004) reviewed 250 specimens of the shear tests with FRP to study the effect of different parameters. The reported failure modes includes: (a) debonding failure due to delamination, adhesive failure, or concrete substrate failure (e.g.

Deniaud and Cheng, 2001; Kalifa and Nanni, 2002; Triantafillou, 1998); and (b) FRP rupture (e.g. Berset, 1992; Chajes et al., 1995; Funakawa et al., 1997, Challal et al., 2002, Mitsui et al., 1998, and Umezu et al., 1997). The failure modes are affected mainly by: shear span-to-depth ratio, beam depth, internal and externally shear reinforcement ratio, concrete strength, and material properties of FRP (Teng et al., 2004; Bousselham and Chaallal, 2004).

Most of the analytical models have the following format in calculating the shear capacity of the FRP RC members, which defines the nominal shear capacity (V_n) as the summation of three components: concrete (V_c), steel shear reinforcement (V_s), and external FRP shear reinforcement (V_f), as shown in Eqn. (2-1):

$$V_n = V_c + V_s + V_f . \tag{2-1}$$

In the equation, V_c attributes to the shear force in the compression zone, the aggregate interlock and friction along the cracks, and the dowel action of the steel flexural reinforcements, while V_s and V_f attribute to the force in stirrups and FRP reinforcements, respectively. Basically, the shear resistances for concrete and steel shear reinforcement in FRP RC members are assumed to be the same as the un-strengthened RC structures. The FRP sheets are often assumed to work analogously as the stirrups. The FRP sheets are considered as ties to resist the tensile stresses between the concrete struts. However, the effectiveness of the FRP in resisting these tensile stresses is much more complex than stirrups due to: (1) the bond behavior in the concrete-FRP interface, (2) the material properties of the FRP laminates, (3) FRP sheets geometry, (4) shear failure modes, and (5) anchorage system provided.

Most analytical models express the contribution of FRP in terms of the effective strain in FRP, ε_{fe}, which is expressed as a fraction of the ultimate tensile strain and is significantly affected by the failure mode. For the case of rupture of FRP, the effective strain is close but smaller than the ultimate tensile strain of FRP due to a concentration of strains in the FRP; for the case of FRP debonding, the effective strain in the FRP tends to be much lower than the ultimate tensile strain of FRP. The equations used to calculate the effective strain in FRP ε_{fe} have been developed and improved by many researchers with more updated experimental data (Belarbi et al., 2011). The factors determining the effective strain are mainly the stiffness of FRP, the strength of the concrete, the FRP strengthening scheme, and failure modes.

As a summary, Table 2.1 lists the general information of all up-to-date experimental results. Table 2.1 is based on NCHRP 678 and updated with the recent tests between 2011 and 2014. In the following section, several most important analytical models are reviewed in detail categorized by different approaches. The tests related to these analytical models are also presented respectively.

2.2.2.1 Models Based on the Truss Model Approaches

Al-Sulaimani et al. (1994) was the first group of researchers that came up with a set of equations for shear contribution of FRP. They tested sixteen RC beams ($5.9 \times 5.9 \times 49$ in) strengthened with FRP using different bonding schemes including shear strips (side-bonded discrete FRP strips), shear wings (side-bonded continuous FRP sheets), and U-jackets (U-wrapped continuous FRP sheets), with 0.12 in thick fiberglass plates. All beams

Table 2.1 Summary of Experimental Tests (Updated Based on NCHRP Report 678)

Author	Year	Number of Tests	Properties and Parameters																					
			Geometry					Type of Beam				Concrete and Steel			Type of FRP			Strengthening Scheme						
			Rectangular Section	T-Section	Beam Spanning L< 7 ft	Beam Spanning 7 ft <L<13 ft	Beam Spanning L>13 ft	Regular Beams (a/d>2.5)	Deep Beams	Scale Effect	Precracking	Concrete Strength	Longitudinal Reinforcement	Transverse Reinforcement	Carbon	Aramid	Glass	Two-Side Bonding	U-Wrap	Complete Wrap	Continuous	Strips	Angle to Long. Axis=90 °	Angle to Long. Axis ≠90°
Berset	1992	2	■		■			■									■	■			■			■
Uji	1992	4	■		■			■							■			■		■	■		■	■
Al-Sulaimani et al.	1994	4	■		■			■			■						■	■			■	■	■	
Ohuchi et al.	1994	13	■		■				■					■	■					■			■	
Chajes et al.	1995	5		■	■			■							■	■	■		■		■		■	■
Sato et al.	1996	3	■			■		■							■			■	■		■	■	■	
Araki et al.	1997	8	■		■				■						■	■				■	■	■	■	
Funakawa et al.	1997	3	■				■	■							■					■	■		■	
Kamiharako et al.	1997	1	■			■		■	■							■				■			■	
Miyauchi et al.	1997	4	■		■			■	■						■					■		■	■	
Sato et al.	1997	2		■	■			■							■				■		■		■	
Taerwe et al.	1997	3	■				■	■							■				■	■		■	■	
Taljsten	1997	3	■				■	■			■				■			■			■	■		■
Umezu et al.	1997	15	■			■		■					■	■	■	■				■	■	■	■	
Chaallal et al.	1998	2	■		■			■							■			■				■	■	■
Mitsui et al.	1998	6	■			■			■		■				■					■	■		■	
Triantafillou	1998	9	■		■			■							■			■				■	■	■
Khalifa et al.	1999	6	■			■		■							■						■	■	■	
Kachlakev and Barnes	1999	3	■				■	■									■	■			■		■	
Khalifa et al.	2000	4		■		■		■							■				■		■	■	■	
Deniaud and Cheng	2001	5		■		■		■		■		■		■	■		■	■			■	■	■	■
Li et al.	2001a	5	■		■				■						■				■		■		■	
Li et al.	2001b	9	■			■		■					■		■				■			■		■
Park et al.	2001	2	■	■	■			■							■			■			■		■	
Chaallal et al.	2002	10		■			■		■					■	■			■			■		■	
Khalifa and Nanni	2002	4	■			■		■							■			■	■		■		■	
Li et al.	2002	9	■			■		■					■		■				■			■		■
Micelli et al.	2002	10		■		■			■						■	■			■				■	
Pellegrino and Modena	2002	9	■			■		■						■	■			■			■		■	
Beber	2003	28	■			■		■							■			■	■	■		■	■	■
Diagana et al.	2003	8	■			■			■						■				■	■		■	■	■
Hsu et al.	2003	3	■		■			■							■		■	■			■	■	■	■

Table 2.1 (Continued)

Author	Year	Number of Tests	Properties and Parameters																						
			Geometry					Type of Beam				Concrete and Steel			Type of FRP			Strengthening Scheme							
			Rectangular Section	T-Section	Beam Spanning L< 7 ft	Beam Spanning 7 ft <L<13	Beam Spanning L>13 ft	Regular Beams (a/d>2.5)	Deep Beams	Scale Effect	Precracking	Concrete Strength	Longitudinal Reinforcement	Transverse Reinforcement	Carbon	Aramid	Glass	Two-Side Bonding	U-Wrap	Complete Wrap	Continuous	Strips	Angle to Long. Axis=90 °	Angle to Long. Axis ≠90°
Taljsten	2003	6	■				■	■							■				■		■		■	■
Adhikary et al.	2004	8	■			■		■							■	■			■	■	■	■	■		
Xue Song et al.	2004	12	■		■				■						■				■			■	■		
Cao et al.	2005	10	■		■			■	■					■	■		■			■		■	■		
Carolin and Taljsten	2005a	18	■					■				■			■				■	■			■	■	■
Miyajima	2005	4	■			■		■							■					■		■	■		
Monti and Liotta	2005	16	■			■		■							■			■	■	■	■	■	■	■	■
Sim et al.	2005	9	■		■				■						■			■	■	■	■	■	■	■	■
Zhang and Hsu	2005	10		■			■	■						■	■				■					■	■
Barros and Dias	2006	5		■	■				■						■				■			■	■		
Bousselham and Chaallal	2006a	20		■			■	■	■					■	■				■		■		■		
Pellegrino and Modena	2006	8	■			■		■						■	■				■		■		■		
Lees and Kesse	2007	8	■		■			■							■				■				■		
Leung et al.	2007	12	■		■	■		■					■	■	■				■	■	■	■	■	■	
Alrousan et al.	2009	4	■				■	■	■						■				■	■	■	■	■	■	
Arteaga et al.	2009	15	■				■	■		■					■				■	■		■	■	■	■
Gamino et al.	2009	7		■	■			■							■								■		
Rizzo and De Lorenzis	2009	1	■		■			■							■				■		■		■		
Bukhari et al.	2010	7	■			■		■							■			■		■	■	■	■	■	■
El-Ghandour	2011	7	■			■		■					■		■				■			■	■		
Mefidi et al.	2011	14		■		■									■				■		■	■	■		
Belarbi et al.	2012	15		■			■	■			■			■	■				■			■	■	■	■
Murphy et al.	2012	16					■	■			■			■	■				■			■	■	■	■
Dong et al.	2013	14	■		■			■			■		■		■		■		■		■	■	■	■	■
Mostofinejad et al.	2013	32	■		■			■					■	■	■			■				■	■		
Panigrahi et al.	2014	12		■	■			■									■	■	■		■	■	■	■	■
Baggio et al.	2014	9	■			■		■							■		■		■			■	■		
Colalillo and Sheikh	2014	15	■			■		■						■	■				■	■	■	■	■		

were tested as simply supported beams with a span of 47 in and a shear span of 15.7 in. The proposed model is based on an assumed shear crack angle of 45°. Based on the test results, three equations for different strengthening schemes were proposed:

$$V_p = \frac{2F_p d}{S_p} = \frac{2\left[\tau_{ave}\frac{t_s h_s}{2}\right]d}{S_p} \quad \text{(for shear strips)}$$
$$V_p = 2F_p = 2\left[\tau_{ave}\frac{dh_w}{2}\right] \quad \text{(for shear wings)} \qquad (2\text{-}2)$$
$$V_p = 2F_p = 2\left[\tau_{ult}\frac{dh_j}{2}\right] \quad \text{(for U-jackets)},$$

where V_p is the shear force provided by the FRP reinforcement; t_s is the width of the strip; h_s, h_w and h_j are the effective depths of the FRP sheets; d is the effective depth of the beam, τ_{ave} is the average shear stress and S_p is the spacing of the FRP strips. The shear contribution of FRP highly depends on the value of τ_{ave}, but in the model, enough explanation wasn't given on how to decide this value. Also, in the equation, the FRP material properties were not chosen as studied parameter since there is only one type of fiber glass was tested.

Chajes et al. (1995) tested 16 specimens without transverse steel reinforcements under four-point bending. U-wrap was used as the wrapping scheme with two different angle of fiber direction of 45°and 90°with respected to the longitudinal axis. By assuming a perfect bond (i.e. failure happens in the concrete), two equations were proposed as

$$V_f = A_f E_f \varepsilon v_{cu} d \quad \text{for FRP oriented at 0/90 degrees}$$
$$V_f = A_f E_f \varepsilon v_{cu} d\sqrt{2} \quad \text{for FRP oriented at 45/135 degrees}, \qquad (2\text{-}3)$$

where εv_{cu} is the effective strain of the FRP sheets; A_f is the area of the FRP sheets; E_f is the modulus of elasticity of the FRP sheets.

In the equation, the ultimate vertical tensile strain of FRP was taken as 0.005, which cannot account for the differences in ultimate strain resulting from using different FRP and different orientations of wrapping. Also, in this model, the non-uniformity of the strain along the FRP was not taken into account. Last but not least, the assumption of perfect bond is questionable due to different failure modes occurred in practical cases.

Triantafillou (1998a) was one of the first researchers that proposed the shear contribution of FRP in terms of effective FRP strain ($\varepsilon_{frp,e}$). Triantafillou (1998a) tested 9 rectangular RC beams strengthened with side bonded FRP sheets at 90 °. Based on the test results and a database of 33 other tests (Berset, 1992; Uji, 1992; Dolan et al., 1992; Al-Sulaimani et al., 1994; Ohuchi et al., 1994; Chajes et al., 1995; Malvar, 1995; Sato et al., 1996; and Triantafillou, 1997), the equations were proposed in a *Eurocode* format as

$$V_{frp,d} = \frac{0.9}{\gamma_{frp}} \rho_{frp} E_{frp} \varepsilon_{frp,e} b_w d (1+\cot\beta)\sin\beta$$
$$\varepsilon_{frp,e} = 0.0119 - 0.0205(\rho_{frp} E_{frp}) + 0.0104(\rho_{frp} E_{frp})^2 \quad \text{when } 0 \le \rho_{frp} E_{frp} \le 1\text{GPa} \qquad (2\text{-}4)$$
$$\varepsilon_{frp,e} = -0.00065(\rho_{frp} E_{frp}) + 0.00245 \quad \text{when } \rho_{frp} E_{frp} > 1\text{GPa},$$

where $V_{frp,d}$ is the shear capacity provide by FRP sheets; ρ_{frp} and E_{frp} are the reinforcement ratio and the modulus of elasticity of the FRP sheets, respectively; β is the angle of applied FRP sheets in respect of longitudinal axis; ε_{frp} is the proposed effective strain of the FRP sheets.

The model presented two equations to calculate the effective strain of FRP, and it is the first time that FRP rigidity was involved into the equation for calculating effective

strain. By regression, it was found that the effective strain decreases with the increase of FRP rigidity.

Based on Triantafillou's original model (Triantafillou, 1998b), Khalifa et al. (1998) considered further the effect of shear crack opening and loss of aggregate interlock as well as the FRP types into the equations. Additional experimental data were updated to the database for regression (Araki et al., 1997; Chajes et al., 1995; Funakawa et al., 1997; Ohuchi et al., 1994; Sato et al., 1996; Triantafillou, 1997; Umezu et al., 1997; and Uji, 1992). A modified effective strain was proposed based on both fiber rupture and debonding failure by introducing a reduction factor R:

$$R = 0.5622(\rho_f E_f)^2 - 1.2188(\rho_f E_f) + 0.778 \le 0.50 \quad \text{(FRP rupture)}$$
$$R = \frac{0.0042\left(f_c^{'}\right)^{2/3} w_{fe}}{\left(E_f t_f\right)^{0.58} \varepsilon_{fu} d_f} \quad \text{(debonding failure)}, \tag{2-5}$$

where t_f is the thickness of FRP; w_{fe} is the width of FRP; and d_f is the effective depth of the FRP reinforcement.

For calculating the capacity in the case of debonding failure, a concept of effective bond length (L_e) has been adopted by Maeda et al. (1997). The model suggests to use only the portion of FRP extending past the crack by the effective bond length L_e to calculate the shear strength. The effective width was calculated based on 45 °truss model.

$$w_{fe} = d_f - L_e \quad \text{(U-jacket configuration) and}$$
$$w_{fe} = d_f - 2L_e \quad \text{(sheet bonded only on two faces).} \tag{2-6}$$

This equation in ACI format is

$$V_f = \frac{A_f f_{fe}(\sin\beta + \cos\beta) d_f}{s_f}, \quad \text{where: } f_{fe} = R f_{fu}. \tag{2-7}$$

An upper limitation of spacing $s_{f,max}$ of FRP strips was proposed by the author so that all the shear crack will intercept at least one FRP strip:

$$s_{f,\max} = w_f + \frac{d}{4}. \tag{2-8}$$

Later in 2000, Khalifa and Nanni modified the reduction factor as the least of

$$R = 0.5622(\rho_f E_f)^2 - 1.2188(\rho_f E_f) + 0.778 \le 0.50$$
$$R = \frac{\left(f_c'\right)^{2/3} w_{fe}}{\varepsilon_{fu} d_f} \left[738.93 - 4.06(t_f E_{frp})\right] \times 10^{-6} \tag{2-9}$$
$$R = \frac{0.006}{\varepsilon_{fu}}.$$

In 2000, Triantafillou and Antonopoulos proposed an updated model in which the effective strain was calibrated based on the results of more than 75 tests (Berset, 1992; Uji, 1992; Al-Sulaimani et al., 1994; Ohuchi et al., 1994; Chajes et al., 1995; Sato et al., 1996; Antonopoulos, 1996; Miyauchi et al., 1997; Taerwe et al., 1997; Funakawa et al., 1997; Umezu et al., 1997; Araki et al., 1997; Sato et al., 1997a; Ono et al., 1997; and Taljsten, 1997). The $\left(f_c'\right)^{2/3}$ was involved as a parameter to consider the effect of concrete strengthened in tension. Regression was conducted to determine different values of effective strains for different failure modes and different FRP types:

Debonding failure mode:

$$\varepsilon_{f,e} = 0.65\left(\frac{f_c^{2/3}}{E_f \rho_f}\right)\times 10^{-3}.$$

Shear-tension failure combined with or followed by CFRP fracture:

$$\varepsilon_{f,e} = 0.17\left(\frac{f_c^{2/3}}{E_f \rho_f}\right)^{0.30} \varepsilon_{f,u}. \quad (2\text{-}10)$$

Shear-tension failure combined with or followed by AFRP fracture:

$$\varepsilon_{f,e} = 0.048\left(\frac{f_c^{2/3}}{E_f \rho_f}\right)^{0.47} \varepsilon_{f,u}.$$

Based on Khalifa et al. (1998), several researchers have proposed different equations for calculating the reduction factor R. Hsu et al. (2003) tested 15 beams in a three-point bending. Hsu et al. (Hsu et al., 2003 and Zhang and Hsu, 2005) proposed an R factor considering the effect of the concrete compressive strength. Also, in this model the regression was based on $\rho_f E_f / f_c^{'}$ instead of the axial rigidity $\rho_f E_f$:

$$R = 1.8589\left(\rho_f E_f / f_c^{'}\right)^{-0.7488}. \quad (2\text{-}11)$$

Pellegrino and Modena (2002) tested 11 rectangular RC beams with and without the internal steel reinforcement ratio. The FRP wrapping method is side bond only. Based on the results, new R factors were proposed based on the bond mechanism modified by Miller (1999). An additional reduction factor R^* was introduced to account the effect of the transverse steel reinforcement ratio:

$$R = 0.5622(\rho_f E_f)^2 - 1.2188(\rho_f E_f) + 0.778 \le 0.50 \text{ or}$$
$$R = R^* \left\{0.0042(f_{cm})^{2/3} w_{fe} / \left[\left(E_f t_f\right)^{0.58} \varepsilon_{fu} d\right]\right\}$$
$$0 \le R^* = -0.53 \ln \rho_{s,f} + 0.29 \le 1 \text{ or} \quad (2\text{-}12)$$
$$R = \frac{0.006}{\varepsilon_{fu}},$$

where fcm is the mean concrete cylinder compressive strength; $\rho_{s,f}$ is the ratio between the axial rigidities of the transverse steel and FRP sheets.

Chaallal et al. (2002) investigated the effect of transverse steel reinforcement on the FRP effectiveness by testing 12 RC beams that were half-scale T girders. The FRP were multi-layer and fully wrapped in an angle of 90°. A new term called total shear reinforcement ratio was introduced. Also, the author compared the test results with Triantifillou (1998a)'s equations, but the results showed large scatter. The author pointed out that the main reason is due to the factor that Triantifillou (1998a)'s equations are based on the results of small-scale shallow beam. To account for the effect of deep beam, the following equations were recommended:

$$V_f = f\left(\frac{a}{d}, \rho_{tot}\right)\left(\frac{A_f}{s_f}\right) E_f \varepsilon_{eff} d_f$$
$$\varepsilon_{eff} = 3 \times 10^{-5} \times \rho_{tot}^{-0.6522}, \quad \rho_{tot} = n\rho_f + \rho_s \quad (2\text{-}13)$$
New deep beam coefficient:
$$f\left(\frac{a}{d}, \rho_{tot}\right) = \max\left[\frac{1 + 2a/d}{12} + (1000\rho_{tot} - 0.6) \le 1, \frac{1 + 2a/d}{12}\right],$$

where ρ_{tot} is the total shear reinforcement ratio; n is the ratio between the modulus of elasticity of the transverse steel and FRP sheets.

Colotti and Swamy (2011) proposed a model to predict the ultimate load capacity of RC beams strengthened by externally bonded FRP plates/sheets. The approach is based on truss model approach as well as the theory of plasticity and is refined to consider: variable angle crack, non-uniform stress distribution on FRP over the crack, and shear span/depth ratio. The model varies for different failure modes. It is worth mentioning that in the model, mechanics-based approach was also applied when calculate the bond strength (Dai et al., 2006). The prediction of the proposed model was compared with 73 RC beam test in literature and have a well agreement with a mean experimental/theoretical failure load ratio of 1.05.

Chen et al. (2013) proposed a new shear strength model considering the shear interaction among concrete, steel and FRP reinforcements. The main interaction effect that was considered caused an overestimate of the V_s term in the design equations. Since debonding usually happens at a relatively small shear crack width, the internal steel reinforcement may not reach the yielding strain and consequently, the strength of the internal steel reinforcement may not be fully utilized. The shear resistance can be expressed as

$$V_u = V_c + K_s f_y A_{sv} + K_f f_{f,e} A_{frp} . \quad (2\text{-}14)$$

K_s and K_f are called mobilization factors and defined as

$$K_s = \sigma_{s,e} / f_y \text{ and} \quad (2\text{-}15)$$

$$K_f = \sigma_{f,e} / f_{y,e} . \quad (2\text{-}16)$$

$\sigma_{s,e}$ and $\sigma_{f,e}$ are the average stresses in the steel stirrups and FRP strips intersected by the critical shear crack, respectively. The general expression of V_f is shown as

$$V_f = 2 f_{f,e} t_f w_f \frac{h_{f,e}(\sin\theta + \cos\theta)\sin\beta}{s_f}$$

$$f_{f,e} = \sigma_{f,\max} D_{frp}$$

$$\sigma_{f,\max} = \min\begin{cases} f_f \\ \sigma_{db,\max} \end{cases}$$

$$\sigma_{db,\max} = \begin{cases} \sqrt{\dfrac{2E_f G_f}{t_f}} & L_{max} \geq L_e \\ \sin\left(\dfrac{\pi}{2}\cdot\dfrac{L}{L_e}\right)\sqrt{\dfrac{2E_f G_f}{t_f}} & L_{max} < L_e \end{cases}$$

$$L_{\max} = \begin{cases} \dfrac{h_{f,e} + h_t + h_b}{2\sin\beta} & \text{for side strips} \\ \dfrac{h_{f,e} + h_t + h_b}{\sin\beta} & \text{for U strips}, \end{cases} \qquad (2\text{-}17)$$

where D is the stress distribution factor; Gf is the facture energy; L_{max} is the maximum bonding length of FRP.

The new model showed a good performance in prediction the shear contribution of FRP by comparing with the tests results in a large databases. However, the proposed equation, as mentioned by Chen et al. (2012), should be modified in a simpler format for practical applications.

Nehdi and Nikopour (2010) proposed a new model for predicting the shear contribution of FRP using the so-called Genetic Algorithm (GA) method. The GA method is used in computing both exact and approximate solution. This method was applied to 212 RC beams strengthened with externally bonded FRP sheets in the literature. The factors in

the equation were derived by GA method from the test data in literature. The general format of the proposed design equations was proposed as

$$
\begin{aligned}
V_n &= \left(C_1 \sqrt{f_c^{'}} + C_2 \frac{\rho_1}{a/d} \right) b_w d + \frac{A_v f_{steel} d}{s} + \frac{A_f E_f \varepsilon_{fe} d_f}{s_f} (\sin\alpha + \cos\alpha) \\
\varepsilon_{fe} &= C_3 \Gamma_f^{C_4} \varepsilon_{fu} \\
\Gamma_f &= \frac{E_f \rho_f}{f_c^{2/3} (a/d)} \\
\rho_f &= \frac{A_f}{b s_f}.
\end{aligned}
\tag{2-18}
$$

Belarbi et al. (2012) tested 15 full-scale RC T-beam strengthened with externally bonded FRP sheets. The parameters studied includes transverse steel reinforcement and mechanical anchorage system. The test results showed that the FRP strengthened beams with mechanical anchorages exhibited an increase in shear capacity about 23%-26% when compared to the control beam without anchorages. Also, the FRP shear strengthening was more efficient for the tested beams with a greater stirrup spacing (12 in) than for those with smaller spacing (8 in), which indicates that there is an interaction between the internal steel reinforcement and the externally bonded FRP sheets.

Murphy et al. (2012) tested 16 full-scale AASHTO type prestressed I-girders to investigate the parameters of size of the girder, transverse reinforcement, FRP orientation, anchorage systems and the pre-cracking. One of the important conclusion drawn from the test results is that the failure modes of the tested beam highly depends on the cross-sectional shape and shear reinforcement schemes. It was found that debonding of the FRP sheets reduced the web thickness which lead to web crushing failure. Also, the mechanical anchorage was found to postpone the debonding and provided additional capacity

compared to the beams without anchorages. The shear gain of the test specimen were also compared with the predictions from 17 analytical models and none of the model can accurately predict the FRP contribution or the total shear resistance of the tested beams in the study due to the complexity of the shear behavior and the different failure modes.

Mofidi and Chaallal (2014) proposed a model to calculate the contribution of FRP to the shear resistance of RC beams strengthened in shear with externally bonded FRPs. The diminishing effect of the stirrups and the distributed pattern of the shear cracks are quantified. The effective strain was given as

$$\varepsilon_{fe} = \frac{k_c k_L k_w \tau_{eff} L_e}{t_f E_f} = 0.31 k_c k_L k_w \sqrt{\frac{\sqrt{f_c'}}{t_f E_f}} \leq 0.005. \quad (2\text{-}19)$$

The coefficient k_L and k_w were given separately for side bond and U-jack. The total contribution of FRP was given in the format of truss model theory and the maximum effective strain in the FRP is limited to 0.005.

2.2.2.2 Models Based on the Non-uniform Strain Distribution in FRP

Extensive experimental work was conducted by Chen and Teng (2003a and 2003b) by investigating effective stress distribution along FRPs. Assumption was made that the stress distribution in the FRP along the shear crack is non-uniform, and it is affected by: (a) the variation in shear crack width along its length; (b) material properties of FRP; and (c) the bond behavior in the FRP-concrete interface. The contribution of FRP to the shear capacity was calculated by

$$V_f = 2 f_{frp,e} t_{frp} w_{frp} \frac{h_{frp,e}(\sin\beta + \cos\beta) d_f}{s_{frp}}. \quad (2\text{-}20)$$

For the debonding limit state, the non-uniform stress distribution in the FRP is taken into account by introducing a stress distribution factor (D_{frp}) as

$$f_{frp,e} = D_{frp}\sigma_{frp,\max},$$
$$\text{where:} D_{frp} = \frac{\int_{zt}^{zb} \sigma_{frp,z} dz}{h_{frp,e}\sigma_{frp,\max}}. \quad (2\text{-}21)$$

The proposed model was compared with the 46 experimental tests failed by debonding and 58 experimental tests failed by FRP rupture (Uji, 1992: Al-Sulaimani et al, 1994; Chajes et al., 1995;, Kage et al., 1997; Sato et al., 1997a; Taerwe et al., 1997; Araki et al., 1997; Funakawa et al.; 1997; Kamiharako et al., 1997; Ono et al., 1997; Umezu et al., 1997; Triantafillou, 1998a; Khalifa et al., 1998; Chaallal et al., 1998b; Mitsui et al., 1998; Kachlakev and Barnes, 1999b;Hutchinson and Rizkalla, 1999; Mutsuyoshi et al., 1999; and Khalifa and Nanni, 2000). The model shows a good agreement with the test results.

Carolin and Taljsten (2005) derived a model based on a database of 23 rectangular RC beam. The database includes tests with and without internal steel reinforcement and with full wrapping, side bonding FRP in an angel of 45 and 90 degrees. The model is shown as

$$V_f = \eta\varepsilon_{cr}E_f t_f r_f z\frac{\cos\theta}{\sin\theta}$$
$$\varepsilon_{cr} = \min\begin{cases} \varepsilon_{fu} \\ \varepsilon_{bond}\cos^2\theta \\ \varepsilon_{c\max}\cos^2\theta. \end{cases} \quad (2\text{-}22)$$

Cao et al. (2005) tested 12 pre-cracked rectangular RC beams with complete wrap, CFRP/GFRP at an angle of 90-degree. They proposed the first model that considers the effects of pre-cracking. A new expression of the distribution factor $D_{f\theta}$ is given as

$$D_{f\theta} = \left(1 - \frac{\pi - 2}{\lambda_{frp}\pi}\right) \times \begin{cases} 1 & \text{for } \lambda \le 1.4 \\ \dfrac{1}{1 - 0.2(\lambda - 1.4)^2} & \text{for } 1.4 < \lambda < 3 \\ 2.05 & \text{for } \lambda \ge 3, \end{cases} \tag{2-23}$$

where λ_{frp} is the normalized FRP bond length

2.2.2.3 Models Based on the Mechanics-based Approaches

Using a data base of 35 test results, Deniaud and Cheng (2001b) developed a model based on a strip method and shear friction approach. In this model, the interaction between concrete, steel and FRP was addressed. The equation is shown as

$$\begin{aligned} V_r &= 0.25k^2 f_c^{'} b_w h \frac{d_s}{ns} + T_v(n-1) + nT_{FRP} \\ T_{FRP} &= d_f t_f E_f \varepsilon_{\max} R_L \left(\frac{w_{FRP}}{S_{FRP}}\right)\left(\frac{s}{d_s}\sin\alpha + \cos\alpha\right)\sin\alpha, \end{aligned} \tag{2-24}$$

where T_v is the shear contribution of the transverse steel reinforcement.

Monti and Liotta (2005 and 2007) tested 24 FRP strengthened RC beams with different wrapping schemes (U-wrap, side bond and fully wrap), and proposed an equation with closed-form based on mechanics. In this model, V_f is a function of the strengthening schemes and some parameters related to geometry and mechanics. This model was based on the assumptions: (a) the cracks are uniformly distributed along the beam axis, with an angle (θ), (b) crack depth equals the internal lever arm (0.9d) at the ultimate limit state, and (c) the shear mechanism is based on the Mörsch's truss model for U-wrap and fully wrap

schemes and on crack-bridging for side bonding. Two failure criterions are considered in the development of the model. The effective bond length (l_e) and debonding strength (f_{fdd}) can be determined as

$$l_e = \sqrt{\frac{E_f t_f}{2 f_{ctm}}}$$

where: $f_{ctm} = 0.27 R_{ck}^{2/3}$

$$f_{fdd} = \frac{0.80}{\gamma_{f,d}} \sqrt{\frac{2 E_f \Gamma_{Fk}}{t_f}} \tag{2-25}$$

where: $\Gamma_{Fk} = 0.03 k_b \sqrt{f_{ck} f_{ctm}}$

$$k_b = \sqrt{\frac{2 - w_f / \rho_f}{1 + w_f / 400}} \geq 1$$

$$w_f \leq \min(0.9d, hw) \sin(\theta + \beta) / \sin\theta,$$

where fck is the specified characteristic cylinder compressive strength; fctm is the mean axial tensile strength; and $\gamma_{f,d}$ is the safety factor for strength of FRP.

Colalillo and Sheikh (2014) proposed a new analytical method to predict the load-deformation response of FRP strengthened beams and also presented a revision of the FRP strain limits for the design codes when debonding is the failure mode. The bond behavior was model by Yu et al. (2004) and Mohamad Ali et al. (2005). The proposed strain limit can be calculated as

$$\varepsilon_{fe} = D_f \varepsilon_{f\max}. \tag{2-26}$$

And in accordance with Cao et al. (2005), the distribution factor was given as

$$D_f = \frac{\sum_{i=0}^{n} \varepsilon_{f,i}}{n \varepsilon_{f\max}} \cong \frac{\int_0^l \varepsilon_f(x) dx}{l \varepsilon_{f\max}}. \tag{2-27}$$

The distribution factors were give for side-bond, U-wrap and closed wrap strengthening systems. Also the effective debonding strain and effective rupture strain were also given. A total of 119 experimental tests were analyzed and compared with the results of proposed model, ACI 440 2R-08 and CAN/CSA S6-06. It was found that the predictions of the rupture failure for fully wrap are most accurate by the proposed model and the use of the design strain limit 0.004 is overly conservative predictions for the specimens in the database.

2.2.3 Shear Models in Codes and Design Guidelines

Several codes and design provisions have addressed the design method for evaluating the shear contribution of the FRP to the shear capacity of the RC members. Compared with the results from individual researchers, the results in the design codes contains a larger database and provides a wider range of application (Belarbi et al., 2011). In the following section, review is conducted on several widely used design codes that has specifications regarding the shear design of the FRP RC member.

2.2.3.1 ACI 440.2R-08 (2008)

ACI 440.2R-08 proposes the shear model based on 45 degree truss model. This code is to date the most comprehensive. ACI 440.2R-08 calculates the shear contribution of FRP reinforcement by the failure modes. The effective strain of FRP is calculated based on different wrapping schemes and is limited to 0.4%. Also, limits for total reinforcement including FRP and steel stirrups is given. The shear capacity of the FRP is

$$V_f = \frac{A_{fv} f_{fe} (\sin\alpha + \cos\alpha) d_f}{s_f}. \tag{2-28}$$

The effective stress depends on the effective strain:

$$f_{fe} = E_f \varepsilon_{fe}. \tag{2-29}$$

The effective strain is determined by different FRP configurations:

$$\varepsilon_{fe} = 0.004 \le 0.75\varepsilon_{fu} \quad \text{for fully wrap}. \tag{2-30}$$

For the U-wrap and side bond, effective bond length is introduced to consider the reduction of the bond. The effective strain is calculated by

$$\begin{aligned}
&\varepsilon_{fe} = k_v \varepsilon_{fu} \le 0.004 \\
&k_v = \frac{k_1 k_2 L_e}{11{,}900\varepsilon_{fu}} \le 0.75 \quad \text{(SI)} \\
&L_e = \frac{23{,}300}{(nt_f E_f)^{0.58}} \quad \text{(SI)} \\
&k_1 = \begin{cases} \dfrac{d_f - L_e}{d_f} & \text{for U-wrap} \\ \dfrac{d_f - 2L_e}{d_f} & \text{for side bonded.} \end{cases}
\end{aligned} \tag{2-31}$$

In ACI, mechanical anchorages can be used to develop larger tensile forces (Khalifa et al., 1999). The effectiveness of the anchorage has to be verified by physical testing and the effective strain should be, in no cases, exceed 0.004. ACI 440 2R also has a reinforcement limits for the total shear strength provided by both FRP and steel shear reinforcements. The sum of shear strengthen should be limited by

$$V_f + V_s \le 8\sqrt{f_c'} b_w d \quad \text{in in-lb units and} \tag{2-32}$$

$$V_f + V_s \le 0.66\sqrt{f_c'} b_w d \quad \text{in SI units.} \tag{2-33}$$

2.2.3.2 AASHTO FRPS-1 (2012)

Based tests results of RC T-beams and AASHTO type PC I-girders in NCHRP Project 12-75, relevant changes have been suggested to AASHTO LRFD Bridge Design Specifications. The effective FRP strain was expressed by two separate design expression based on different predominant failure modes, namely FRP rupture (complete wrap or U-wrap with anchors) and FRP rupture (side bonding or U-wrap).

The shear contribution follows the

$$V_f = \frac{A_f f_{fe} d_f (\cot\theta + \cot\alpha)\sin\alpha}{s_f} \qquad (2\text{-}34)$$
$$f_{fe} = \varepsilon_{fe} E_f,$$

where θ is the angle of diagonal compression and α is the angle of transverse reinforcement relative to the longitudinal axis of the member.

For the cases with complete wrap or U-wrap with anchors:

$$\varepsilon_{fe} = R\varepsilon_{fu}$$
$$\varepsilon_{fu} = \varepsilon_{fu} / E_f \qquad (2\text{-}35)$$
$$R = 4\left(\rho_f E_f\right)^{-0.67} \le 1.0,$$

where $\rho_f E_f$ is in ksi units and limited to 300 ksi.

For the cases with side bonding or U-wrap without anchors or the "full-anchorage" is not provided:

$$\varepsilon_{fe} = R\varepsilon_{fu} \le 0.012$$
$$\varepsilon_{fu} = \varepsilon_{fu} / E_f \qquad (2\text{-}36)$$
$$R = 3\left(\rho_f E_f\right)^{-0.67} \le 1.0.$$

Since the effective strain ε_{fe} is highly dependent on failure modes. Therefore, the experimental databased contained in NCHRP Report 678 was grouped by the failure modes of the experimental tests. The expressions of *R* in Eqn. (2-35) and (2-36) are then obtained by regression of test data in each group.

2.2.3.3 *fib*-TG 9.3 Bulletin 14 (2001)

fib-TG 9.3 Bulletin 14 calculates the shear contribution of FRP based on Triantafillou and Antonopulos's model (2000). The code provides different safety factors to account for the difference for preformed FRP and wet lay-up FRP system. Debonding is considered using a simplified bilinear bond model. The shear contribution of FRP was proposed as

$$V_{fd} = 0.9\varepsilon_{fd,e} E_{fu} \rho_f b_w d(\cot\theta + \cot\alpha)\sin\alpha . \tag{2-37}$$

The design value for effective strain is calculated by multiplying effective strain by a reduction factor k as

$$\varepsilon_{fd,e} = k\varepsilon_{f,e}, \quad \text{where } k = 0.8. \tag{2-38}$$

The effective strain is given for different FRP types and configurations of FRP:

$$\varepsilon_{f,e} = \begin{cases} 0.17\left(\dfrac{f_{cm}^{2/3}}{E_{fu}\rho_f}\right)^{0.30} \varepsilon_{fu} \text{ for fully wrap (or properly anchored) CFRP} \\ \min\left[0.65\left(\dfrac{f_{cm}^{2/3}}{E_{fu}\rho_f}\right)^{0.56} \times 10^{-3}, 0.17\left(\dfrac{f_{cm}^{2/3}}{E_{fu}\rho_f}\right)^{0.30} \varepsilon_{fu}\right] \text{ for U-wrap and side bonded CFRP} \\ 0.048\left(\dfrac{f_{cm}^{2/3}}{E_{fu}\rho_f}\right)^{0.47} \varepsilon_{fu} \text{ for fully wrap AFRP.} \end{cases} \quad (2\text{-}39)$$

2.2.3.4 Canadian Code

Canadian Codes for Building (CAN/CSA S806, 2002) and Bridges (CAN/CSA S6-06, 2006) used a similar equations as ACI 440.2R-08. The shear contribution of FRP is calculated for different failure modes. The maximum strain of FRP is also limited to 0.4%. The shear capacity from FRP is calculated as

$$V_f = \frac{\phi_F A_F E_F \varepsilon_F d_f}{s_F}, \quad (2\text{-}40)$$

where ϕ_F is the resistance factor of FRP. The code also proposed assumed values for ε_F if there is no precise information: 1) for U-shaped wrapping, ε_F is assumed to be 4000 με; 2) for side bonding, ε_F is assumed to be 2000 με.

The new version of Canadian Codes for Building (CAN/CSA S806, 2012) calculate the contribution of FRP using:

$$V_f = \frac{\phi_F A_F E_F \varepsilon_F d_v (\cot\theta + \cot\alpha_F)\sin\alpha_F}{s_F}, \quad (2\text{-}41)$$

where α_F is the orientation angle of the fibers with respect to the longitudinal axis of the member. The values of ε_F is calculated as follows:

$$\begin{aligned}
&\varepsilon_F = 0.006 < 0.75\varepsilon_{Fu} \text{ (for fully wrap)} \\
&\varepsilon_F = 0.005 < 0.75\varepsilon_{Fu} \text{ (for U-wrap with proven anchoring system)} \\
&\varepsilon_F = k_v\varepsilon_{Fu} < 0.75\varepsilon_{Fu} \text{ (for U-wrap without anchoring or side-bond),}
\end{aligned} \tag{2-42}$$

where k_v is calculated as

$$k_v = \frac{k_1 k_2 L_e}{11900\varepsilon_{Fu}} \le 0.75, \tag{2-43}$$

where the factor k_1 is related to concrete strength:

$$k_1 = \left(\frac{f_c'}{27}\right)^{2/3}, \tag{2-44}$$

the factor k_2 is related to effective bond length:

$$k_2 = \left(\frac{d_F - L_e}{d_F}\right) \text{ and} \tag{2-45}$$

$$L_e = \frac{23300}{(n_F t_F E_F)^{0.58}}. \tag{2-46}$$

2.2.3.5 ISIS Design Manual No. 4 (2001)

The design provisions in the document "Strengthening Reinforced Concrete Structures with Externally-Bonded FRP" (ISIS, 2001) is based on the aforementioned

CAN/CSA S6-06 and CAN/CAS S806-02. Design examples and guidance are given in this report.

2.2.3.6 JSCE Recommendations (2001)

JSCE Recommendations used a performance-based approach to design the RC structures strengthened by externally bonded FRP sheets. The V_f is calculated as

$$V_{fd} = K \frac{A_f f_{fud} \, z(\sin\alpha_f + \cos\alpha_f)}{s_f}, \tag{2-47}$$

where z is the lever arm length set to d/1.15, and K is the shear reinforcing efficiency, which is a function of elastic modulus and the FRP reinforcement ratio:

$$K = 1.68 - 0.67R \quad \text{however, } 0.4 \le K \le 0.8$$
$$R = \left(\rho_f E_f\right)^{1/4} \left(\frac{f_{fud}}{E_f}\right)^{2/3} \left(\frac{1}{f'_{cd}}\right)^{1/3} \quad \text{however, } 0.5 \le R \le 2.0. \tag{2-48}$$

2.2.3.7 Great Britain Technical Report 55 (2004)

This reports gives the same design suggestion as *fib*-TG 9.3 Bulletin 14, and also addressed many issues related to practice in application of FRP materials. The suggested equations are based on truss model approach, and 45-degree was assumes as the crack incline angle. Maximum design value for effective strain is limited to half of the ultimate strain of the material and in no cases exceeds 0.004.

2.2.4 Shear Interaction in the FRP RC Members

In this section, a review of the study related to shear interaction between different components in FRP RC members are presented. For un-strengthened RC members under shear, interaction have been found between V_c and V_s (Bower and Viest, 1960; Bazant and

Kazemi, 1991; Pang and Hsu, 1996; Yoon et al., 1996; Frosch, 1999; Angelakos et al., 2001; Tompos et al., 2002). With the existence of FRP sheets, additional interactions have been observed between V_c and V_f and beween V_s and V_f.

2.2.4.1 Shear Interaction between V_c and V_f

The shear contribution of concrete mainly comes from three parts: the interlock and friction along the cracks; the shear force in the un-cracked compression section; and the dowel action. In order to understand the shear interaction between V_c and V_f, the effect of FRP sheets on the mechanism of V_c has to be carefully studied.

It has been widely accepted that the shear contribution of concrete (V_c) trends to decrease for the cases with fully wrap FRP sheets (Trantalillou and Antonopoulos, 2000). The failure mode for the members with fully wrap FRP sheets is mainly FRP rupture, which results in a larger effective strain developed in the FRP material. And it is reasonably assumed that the shear crack width is proportional to the effective strain. Thus, a larger crack width was developed in this failure state, which compromised the shear resistance mechanism in concrete, which is mainly the friction and aggregate interlock along the cracks.

Since the magnitude of strain along the FRP affects the shear resistance of V_c, the beam size is another factor that affects V_c. A beam with a larger size normally means a longer FRP strip length for deformation in the case of FRP wraps, resulting in a smaller FRP strain for a given crack width. The current code normally recommends a strain limit of about 0.004-0.006 to prevent a significant degradation of the concrete shear resistance mechanism (Khalifa et al., 1998), but does not necessarily prevent the wide cracks.

Another aspect to consider the interaction between V_c and V_f is by the concrete strength. Concrete strength has an influence on the performance of shear strengthening with FRP from both the local and the global points of view. From the local point of view, this influence impacts the bonding performance at the FRP-concrete interface. A higher concrete strength will delay the failure by debonding. From the global point of view, this influence is linked to the failure scenarios proposed, that can differ depending on the concrete strength. A low concrete strength will have early crushing of concrete in the compression zone or in the diagonal struts (Bousselham and Chaallal, 2006a) while it will decrease bond strength at the FRP-concrete interface. However, despite its importance with regards to the performance of shear strengthening with FRP, the effect of concrete strength has not been carefully studied. It should be noted that the guidelines for the design of RC structures strengthened with externally bonded FRPs consider the concrete strength while calculating the FRP contribution to shear resistance (ACI 440.2R-08, 2008; and *fib*-TG 9.3, 2001). Therefore, it may be useful to document this influence analytically and experimentally.

2.2.4.2 Shear Interaction between V_s and V_f

Although the majority of the existing research (Chajes et al, 1995; Khalifa et al, 1998; Triantafillou, 1998; Triantafillou and Antonopoulos, 2000; Taljsten, 2003; Chen and Teng, 2003a, 2003b; Monti and Liotta, 2007) and the main design guidelines (ACI 440-2R-08, CNR-DT 200/2004; ISIS, 2001; *fib*-TG 9.3, 2001; JSCE, 2001) have adopted the assumption that the total shear resistance V_n is a summation of V_c, V_s and V_f. But the validity of this assumption has been questioned by many researchers (Park et al., 2001;

Khalifa and Nanni, 2000, 2002; Teng et al., 2004; Pellegrino and Modena, 2002; Denton et al., 2004; Oehlers et al., 2005; Bousselham and Chaallal, 2004, 2006, 2008).

RC beams with side bonding or U-wraps commonly fail due to the debonding of the FRP sheets from the side of the beam (Chen and Teng, 2003a, 2003b). In this case, the crack width of critical shear crack may not be fully developed. Thus, the shear contribution of concrete V_c normally won't be affected when debonding failure happens. However, since the crack width of the critical shear crack is not large when the debonding failure occurs, the strain in the stirrups that intersects with the shear crack may not reach the yielding strain, which means the stirrups will contribute less than what is predicted using the existing shear design models.

Moreover, the amount of the stirrups was also found to have a significant effect on the shear contribution of FRP sheets, especially for FRP U-wrap (Khalifa and Nanni, 2002; Bousselham and Chaallal, 2004, 2006; Caroline and Taljsten, 2005a; Pellegrino and Modena, 2006) The V_f was found to decrease with the increase of the axial rigidity ratio between the internal steel shear reinforcement and externally bonded FRP sheets (Bousselham and Chaallal, 2004; Pellegrino and Modena, 2006). Since accurately measurement of V_s and V_f in the experimental tests is difficult, the mechanism of shear interaction is not yet well understood (Bousselham and Chaallal, 2004, 2008). In the NCHRP Report 678, available data (include more than 500 tests carried out worldwide) has been summarized to study this interaction. In this study, the updated test results (141 tests) up to 2014 were added, the additional tests were listed in Table 2.1 at the beginning of the chapter. Fig. 2.4 shows the effective strain in FRP for different steel reinforcement ratio. It can be clearly observed that the shear gain increases with the decrease of the

transverse steel reinforcement. The data points were also grouped by the failure mode of the tests. As shown in Fig. 2.5 and 2.6, the aforementioned trend is more significant in the specimens failed by FRP debonding when compared to specimens failed by FRP rupture. Although the influence of the transverse steel reinforcement on the shear contribution of FRP is shown by experimental evidence, the mechanisms that can explain the physical inside of this phenomenon steel remains to be discovered. All figures from Fig. 2.4-2.6 follow E_f in ksi and $f_c^{'}$ in psi.

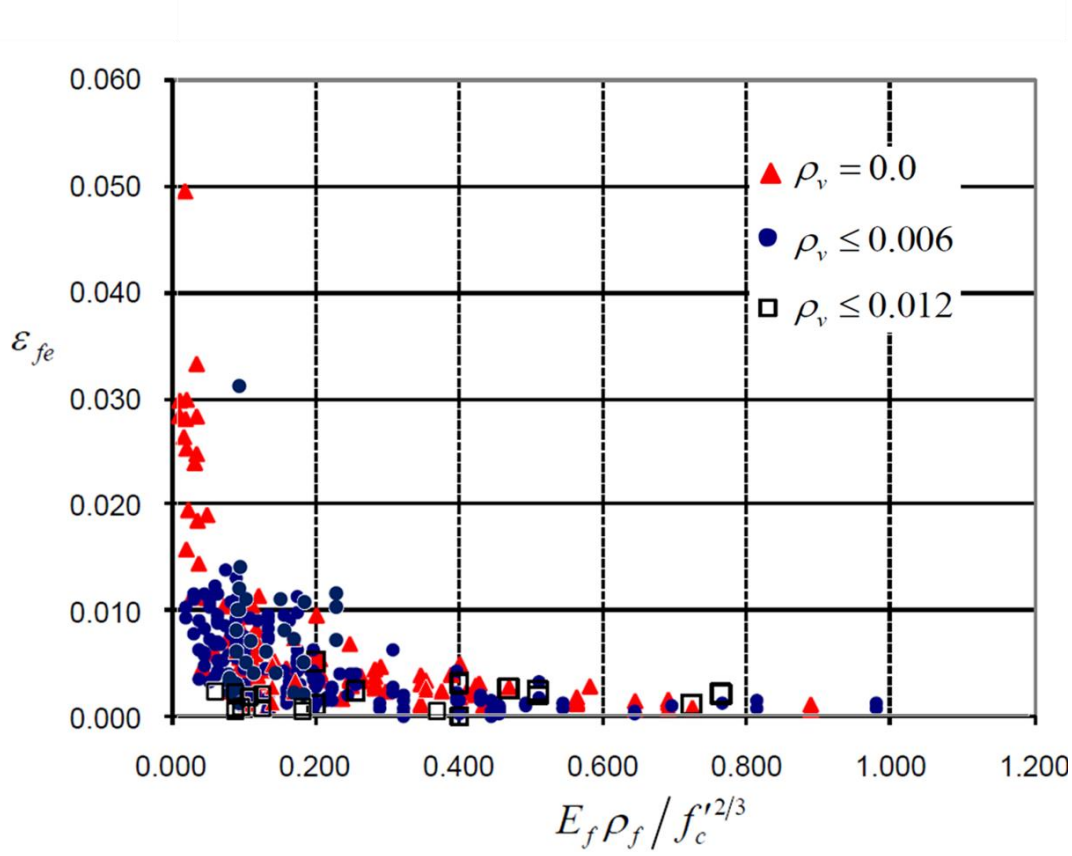

Fig. 2.4 Effective Strain of FRP, ε_{fe} in Terms in Terms of $E_f \rho_f / \left(f_c^{'} \right)^{2/3}$ (Adopted from NCHRP Report 678)

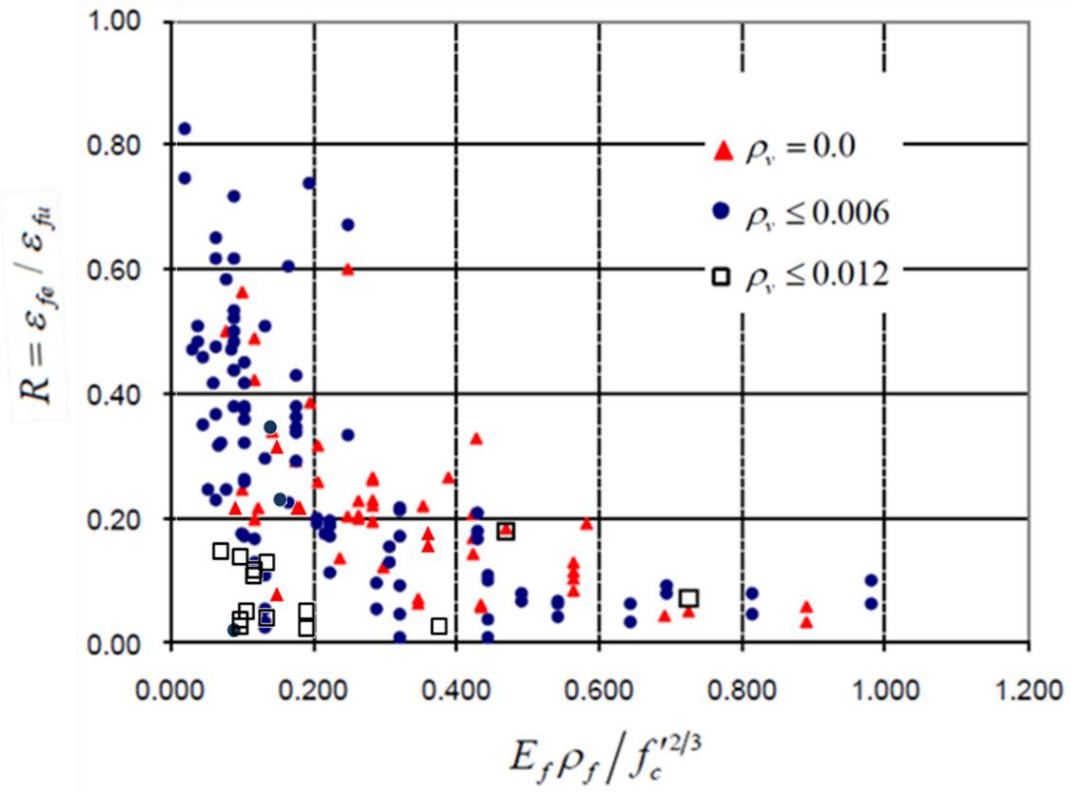

Fig. 2.5 Ratio of Effective FRP Strain to Ultimate FRP Strain, $R = \varepsilon_{fe} / \varepsilon_{fu}$, in Terms of $E_f \rho_f / \left(f_c^{'} \right)^{2/3}$ – Beams Failed by FRP Debonding (Adopted from NCHRP Report 678)

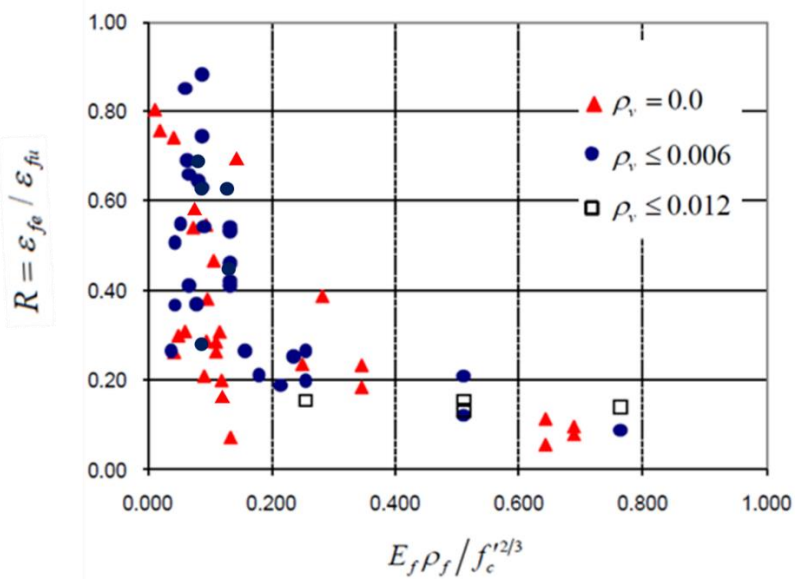

Fig. 2.6 Ratio of Effective FRP Strain to Ultimate FRP Strain, $R = \varepsilon_{fe} / \varepsilon_{fu}$, in Terms of $E_f \rho_f / \left(f_c^{'} \right)^{2/3}$ – Beams Failed by FRP Rupture (Adopted from NCHRP Report 678)

2.3 DEVELOPMENT OF TRUSS MODEL THEORIES

In this section, a summary of the development of the shear model based on truss model approach is addressed.

As one of the main approaches to study the shear behavior of the RC members, truss model concept was by Ritter (1899) and Morsch (1902). The model has a basic assumption the concrete was separated by diagonal cracks into several concrete "struts". The shear resistance mechanism includes the concrete strut that takes the compression and the internal steel reinforcement (longitudinal and transverse) that takes the tension. Due to the fact that the angle of the cracks were assumed to be 45 degrees to the beam axis, the model was called the "45-degree truss model".

Robinson and Demorieux (1968) are the first to realize that the concrete struts are subjected to biaxial tension-compression stress condition, which could have significant difference when subjected to uniaxial compression. They observed and discovered that the concrete becomes "softened" in compressive direction when there is tensile force applying on the perpendicular direction. They called this phenomenon "softening phenomenon". This phenomenon was essential for accurately predict the shear behavior using truss model approach. However, they could not evaluate the value of the softening coefficient.

Followed up their work, Vecchio and Collins (1981) studied the softening coefficient used the facility so-called "shear rig", and then developed the Compression Field Theory (CFT), which was able to predict the whole stress-strain curve of the specimen up to failure points. The main assumption of the CFT is that the direction of the principal stress is the same with the direction of the principal strain, also the crack direction is the direction of the principal direction of the concrete. The CFT satisfied the three

Navier's Principles, which are equilibrium, compatibility and material laws. It represents a major breakthrough in the shear modeling of RC element. The shortcoming of this model is the tensile contribution of the concrete was ignored, i.e., the concrete was assumed to take zero force in the tensile direction. By that time, several tests have proven that the concrete in tension (tension stiffening) exists and significantly affects the stiffness of the RC members in the post-cracking stage. By apply this into the CFT, Vecchio and Collins (1986) developed the modified compression field theory (MCFT). However, two deficiencies were pointed out by Hsu (1998). First, the MCFT violated the basic principle of mechanics by imposing concrete shear stresses in the principal directions. Second, it was found by several researchers (Okamura et al., 1985; Shima et al., 1987; Tamai et al., 1987; Belarbi and Hsu, 1994) that the tensile behavior of the embedded steel rebar is different than that of a bare rebar. A phenomenon called apparent yielding was observed in several tests.

The so-called Rotating-Angle Softened Truss Model (RA-STM) was developed at the University of Houston (Belarbi and Hsu, 1994 and 1995; Pang and Hsu, 1995). The model illustrates the inside of the softened truss model: the model is all based on smeared stress/strain concept, which means all the material laws used in the model should be smeared stress/strain relationships. In order to obtain the accurate "smeared" constitutive laws of the concrete and the steel in uniaxial tension and biaxial tension-compression, a Universal Panel Tester (UPT) was built at UH to test full-scale RC panel elements. New expressions of the constitutive laws of concrete in tension, in compression and steel in tension were proposed (Belarbi and Hsu, 1994 and 1994) and applied into the RA-STM (Pang and Hsu, 1995). Compared to the MCFT, the RA-STM has a clearer concept in

mechanics and is easier to apply into finite element analysis to further predict the shear behavior of the whole structure. Later on, Hsu modified the theory and proposed a new model called Fixed-Angle Softened Truss Model (FA-STM) for considering V_c, shear contribution of concrete. In this model, the direction of cracks is assumed to be the same as the direction of the principal direction of the whole member, which is fixed when the externally applied stresses increase proportionally.

Vecchio (2000 and 2001a) developed the Disturbed Stress Field Model (DSFM), which included shear slips along crack surfaces and requires a "crack check" as in the MCFT. Although the DSFM was more complicated when compared with the MCFT (Vecchio and Collins 1986), the predictions by DSFM and MCFT were found to be similar for most cases.

Belletti et al. (2001) proposed a fixed crack model considering the stress-strain relationships of concrete and steel, aggregate interlock, and dowel action. The softening coefficient ζ proposed by Pang and Hsu (1995) was adopted. The proposed model was used to predict the panel tests at the University of Toronto (Vecchio and Collins 1982 and 1986; Collins et al. 1985; Bhide and Collins 1989) and at the University of Houston (Belarbi and Hsu 1995; Pang and Hsu 1995 and 1996; Hsu and Zhang 1996). The prediction shows a good agreement with all these shear panel tests.

Although the previous models predicted well in the pre-peak stage, none of them can accurately capture the descending branch. The first model that can predict the whole stress strain curve was developed by Hsu and Zhu (2002). The model Softened Membrane Model (SMM) introduced the Hsu/Zhu ratio to describe the Poisson Effect of the RC members under biaxial loading, which is the key for predicting the descending portion. The

Hsu/Zhu ratio is applicable to RC element in pre- and post- cracking stages based on the smear stress/strain approaches. The evaluation of Hsu/Zhu ratio was conducted based on 12 panel tests (Zhu and Hsu, 2002). The SMM has been proven to be capable of predicting the entire stress strain curves including the descending portion.

2.4 DEVELOPMENT OF MATERIAL LAWS OF RC ELEMENT

2.4.1 Concrete in Compression

Softening phenomenon of concrete was first recognized by Robinson and Demorieux in 1968. They found the web concrete was softened due to its biaxial tension-compression stress state. The softening coefficient, ζ, was proposed to describe the softening phenomenon. Fig. 2.7 shows an example of stress strain relationship of concrete under compression considering the softening coefficient.

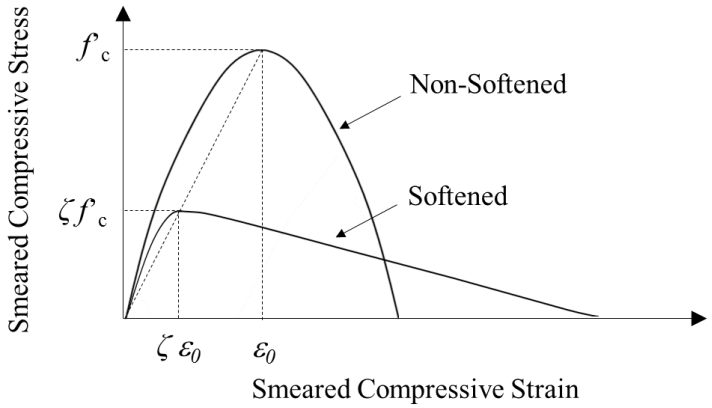

Fig. 2.7 Example of a Proposed Model for Softening Coefficient (Adopted from Hsu and Mo, 2010)

Several researchers have investigated the behavior through web crushing tests and biaxial membrane tests. Vecchio and Collins (1981) studied the softening coefficient by testing 17 reinforced concrete panels and a softened stress strain curve for concrete in compression was proposed. Later on in 1982, they modified the equation based on 13 extra

panel tests. In the equation they proposed, softening coefficient is only a function of the tensile strain. Miyahara et al. (1987) conducted experimental tests using hollow cylinders made of reinforced concrete. They proposed a bilinear equation for the stress strain curve. Based on same test data, Izumo et al. (1991) proposed a trilinear model. The models proposed by Miyahara and Izumo both have a constant value of softening coefficient ($\zeta = 0.6$) after a strain level, which seems unreasonable due to the fact that with an extremely large tensile strain, the softening coefficient should approach zero. In University of Houston, Belarbi and Hsu (1995) studied the effect of five variables on the softening coefficient, ζ by testing full scale RC panels. The variables include: 1) the principal tensile strain, 2) the presence of tensile stress at failure, 3) the loading path (sequential and proportional), 4) spacing of reinforcing, 5) the amount of main longitudinal reinforcement. They confirmed that the principal tensile strain is the dominant variable. The presence of tensile stress at failure has no effect on the softening coefficient. The load path, the spacing of reinforcing bars and the amount of longitudinal reinforcement have a small effect, but can be neglected for simplicity. Pang and Hsu (1996) studied the behavior of 2-D elements subjected to pure shear. The test specimens were reinforced with various amounts of steel bars. The test results of 13 panel specimens confirmed the following equation for the softening coefficient:

$$\zeta = \frac{0.9}{\sqrt{1+400\varepsilon_1}} \quad \text{for Proportional Loading and} \tag{2-49}$$

$$\zeta = \frac{0.9}{\sqrt{1+250\varepsilon_1}} \quad \text{for Sequential Loading.} \tag{2-50}$$

Later on, many panel tests and analytical studies have been conducted by other researchers (Zhang and Hsu, 1998; Wang, 2006), different parameters were then included in the equation for softening coefficient. The parameters that proved to be effective are namely: concrete strength f'_c, and the deviation angle β. So the equation of calculating ζ is expressed as

$$\zeta = \left(\frac{5.8}{\sqrt{f_c^{'}}} \le 0.9 \right) \left(\frac{1}{\sqrt{1+250\varepsilon_1}} \right) \left(1 - \frac{|\beta|}{24^\circ} \right). \tag{2-51}$$

In 2010, Moslehy (2010) investigated the softening coefficient considering the contribution of FRP reinforcement with 8 full-scale panel tests experimentally. The extra variable studied was FRP reinforcement ratio. It was observed from the tests that the softening coefficient increased with the existence of FRP reinforcement. By regression of the test data, a new term which represents the contribution of FRP is added into Eq. (2-34):

$$\zeta_f = \left(\frac{5.8}{\sqrt{f_c^{'}}} \le 0.9 \right) \left(\frac{1}{\sqrt{1+250\varepsilon_1}} \right) \left(1 - \frac{|\beta|}{24^\circ} \right) f_4\left(FRP\right) \text{ and} \tag{2-52}$$

$$f_4\left(FRP\right) = \begin{cases} \left(1 + \dfrac{E_f \varepsilon_1 t_f^{\frac{2}{3}}}{50,000} \right) \left(1.12 - 16\varepsilon_1 \right) & \text{with FRP} \\ 1 & \text{without FRP.} \end{cases} \tag{2-53}$$

By far, this is the only research study related to the softening coefficient of concrete in FRP RC elements. More tests are needed to validate and evaluate this effect.

2.4.2 Concrete in Tension

The stress strain relationship of plain concrete in tension was considered as a linear elastic curve followed by a brittle failure. For a long period of time, the descending branch or softening portion of the stress strain diagram could not be observed mostly due to the limitation of test facilities (Belarbi, 1994). Immediately after the first cracking occurs, the stress decreases suddenly and drops to zero, which was a challenging task for researchers to monitor the sudden release of the absorb elastic energy due to cracking. After modification of the test machines conducted by researchers (Hughes and Chapman, 1966; Evans and Marathe, 1968; Gopalaratnam and Shah, 1985), the descending portion of the stress-strain curve was obtained, this portion of the behavior is also known as tension softening curve, see Fig. 2.8.

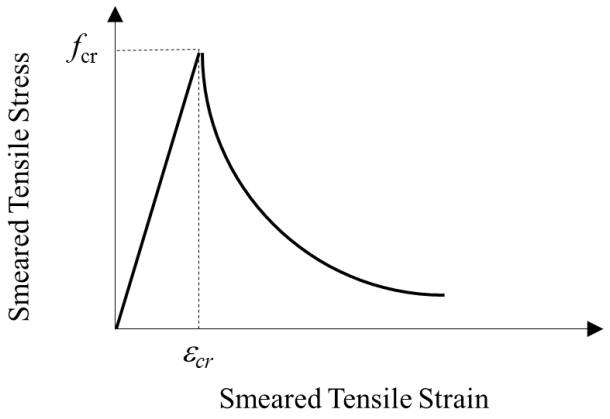

Fig. 2.8 Tensile Stress Strain Curve of Concrete

For RC members under tension load, the stress strain curve is linear in the pre-cracking stage. After crack occurs, the entire tensile stress is carried by the reinforcements at cracking section. However, the concrete continues to carry tensile stresses between the cracks due to the existing bond between the rebar and the concrete, which effectively

stiffens the member response and reduces deflections. The phenomenon, commonly known as tension stiffening, is the contribution of the concrete to stiffness of the member. The tension stiffening effect allows the stress transfer from the reinforcement to the surrounding concrete through the interface bond stress slip property (τ−δ). Hence, the concrete stress is gradually increasing due to this process. This stress transfer process continues until the tensile capacity of the concrete is reached after each cracks occur.

Based on 22 full size panel tests result, Belarbi and Hsu (1994) proposed a model including a linear portion before cracking, followed by a descending portion. The equation can be expressed as

$$\sigma_1 = E_c \varepsilon_1 \qquad \text{when } \varepsilon_1 \le \varepsilon_{cr} \text{ and} \tag{2-54}$$

$$\sigma_1 = f_{cr} \left(\frac{\varepsilon_{cr}}{\varepsilon_1} \right)^{0.4} \qquad \text{when } \varepsilon_1 > \varepsilon_{cr} . \tag{2-55}$$

To date, there are very few available studies on the tension stiffening of concrete in FRP RC element. Ueda et al. (2002), Ceroni et al. (2004), and Farah and Sato (2011) studied the tension stiffening by testing prismatic specimens under uniaxial tension load. Their studies show that the presence of FRP significantly alters the crack patterns, which explicitly influence the tension stiffening of the member. It was also observed that a proper amount of FRP reinforcement will enhance the tension stiffening of concrete, but with the increase of the FRP ratio, this effect tends to become insignificant (Farah and Sato, 2011). However, a rational analytical model has not been developed for calculating tension stiffening in FRP RC element considering this effect. These studies will be review in detail in other sections of this chapters.

2.4.3 Steel Reinforcement in Tension

The tension stiffening of a reinforced concrete member is usually obtained by superimposing the average stiffness of the concrete and that of the steel. The tensile behavior of the steel rebar embedded in concrete, especially in cracked concrete, tends to be different than that of the bare rebar. For a cracked reinforced concrete specimen under tension, at the location of the crack, the strain of the steel rebar is the maximum, this strain will decrease along the rebar due to the bond stress between the steel and concrete. As a result, the average strain of the steel is smaller than the strain at crack. Once the strain of steel at the cracks reaches the yield strain, the steel rebar will perform like yielding, see Fig. 2.9. At this point, the average strain is still smaller than the yield strain. Consequently, a definition of "apparent yielding point" was introduced to describe the "yielding" point in this case.

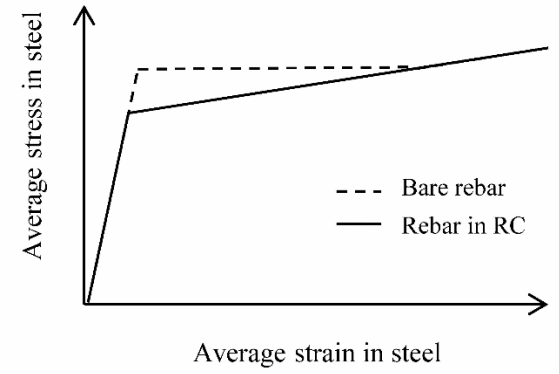

Fig. 2.9 Tensile Stress Strain Curve of Steel

Many researchers have investigated the post-yield behavior of the steel by uniaxial tension test of RC element (Okamura et al., 1985; Shima et al., 1987; Tamai et al., 1987). Belarbi and Hsu (1994) proposed a model based on the 22 full-scale panel tests. The mathematical expressions were proposed based on the results. The simplified bi-linear model proposed is

$$f_s = E_s \varepsilon_s \qquad \varepsilon_s < \varepsilon_y^{'}, \tag{2-56}$$

$$f_s = \left(0.91 - 2B\right) f_y + \left(0.02 + 0.25B\right) E_s \varepsilon_s \qquad \varepsilon_s \geq \varepsilon_y^{'}, \tag{2-57}$$

$$\varepsilon_y^{'} = f_y^{'} / E_s, \qquad f_y^{'} = \left(0.93 - 2B\right) f_y, \tag{2-58}$$

$$B = \frac{1}{\rho_s}\left(\frac{f_{cr}}{f_y}\right)^{1.5}, \qquad f_{cr} = 0.31\sqrt{f_c^{'}\left(\text{MPa}\right)}, \text{ and } \quad \rho_s \geq 0.15\%, \tag{2-59}$$

where B is a factor for calculating apparent yielding stress considering the effect of concrete strengthen and steel reinforcement ratio.

Same as tension stiffening of RC, there are very few available studies on the tensile behavior of the steel reinforcement in FRP RC element. Available data show that the apparent yielding stress become closer to that of bare rebar with the existence of FRP (Ueda et al., 2002; Ceroni et al., 2004, Farah and Sato, 2011). However a rational analytical model has not been developed to calculate the apparent yielding stress for FRP RC element considering this effect.

2.4.4 Shrinkage Effect on Material Laws

Although most frequently neglected by researchers, shrinkage of concrete is identified as another important factor that affects the tension stiffening of RC structures (Kaklauskas, 2001; Bischoff, 2001; Kaklauskas et al., 2009; Kaklauskas and Gribniak, 2011). It was found by Kaklauskas et al. (2009) that most of the previous tension stiffening models are derived based on the test results of specimen that already experienced shrinkage. As a result, the calculated tension stiffening curve has an unexpected "negative" portion when it reaches a certain strain level. As an example, an RC element with cross

section of 10.125 in × 7 in, A_s = 0.4 in^2, E_s = 30,000 ksi, E_c = 2,500 ksi, f_y = 60 ksi, f_{cr} = 200 psi has a shrinkage strain of 200 μm/m, the comparison between the calculated tensile behavior of tension with and without considering the shrinkage effect is presented in Fig.2.10. It can be seen that the effect of shrinkage is significant and should be carefully considered. A numerical approach to obtain a shrinkage-free relationship is proposed and the negative portion of the softening curves has disappeared after shrinkage was eliminated. In the proposed study, shrinkage has been considered in the derivation of the tension stiffening equations.

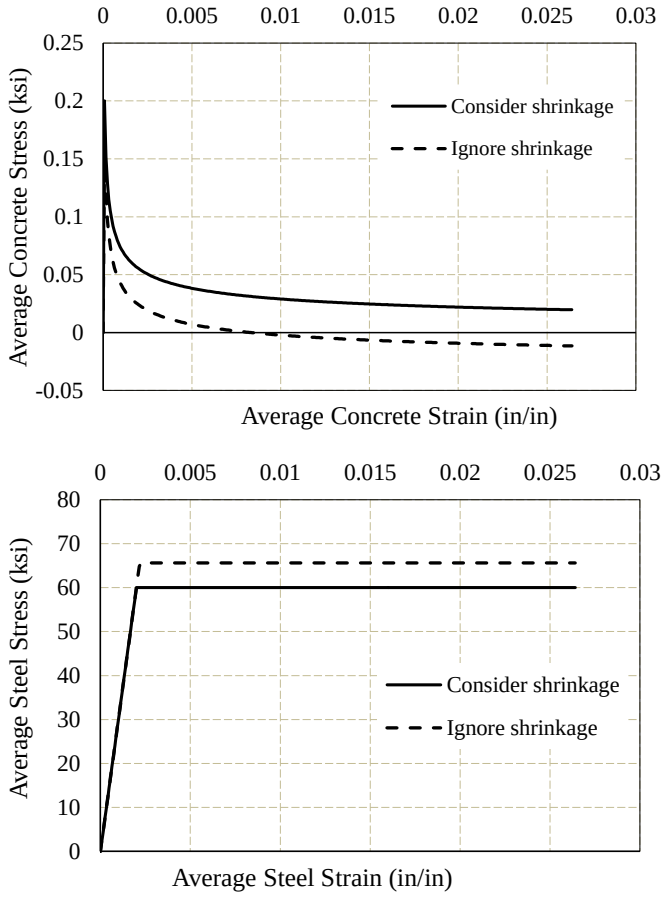

Fig. 2.10 Comparison of a Case Considering Shrinkage and Ignoring Shrinkage

The short-term (creep effect insignificant) shrinkage effect was considered using the approach proposed by Kaklauskas and Gribniak (2011). A fictitious axial force was proposed to evaluate the effect of the shrinkage on the specimen. Based on this approach, the shrinkage strains in the concrete and steel can be expressed as

$$\varepsilon_{c,sh} = \frac{\varepsilon_{sh} E_s A_s}{E_c A_c + E_s A_s} \text{ and} \tag{2-60}$$

$$\varepsilon_{s,sh} = \frac{\varepsilon_{sh} E_c A_c}{E_c A_c + E_s A_s}, \tag{2-61}$$

where ε_{sh} is the shrinkage strain in a plain concrete specimen. Gribniak (2009) suggested to calculate the initial shrinkage strain ε_{sh} of concrete by *Eurocode 2* method. The same approach was applied in this study to account for the effect of shrinkage for each specimen.

2.4.5 Hsu/Zhu Ratio

The Poisson ratio is known in mechanics to describe the strain change in one direction due to the change of the strain in the perpendicular direction. The definition of Poisson ratio is only valid for continuous isotropic materials. By utilizing smeared crack concept, Hsu and Zhu (2002) proposed so-called Hsu/Zhu ratio to describe the similar effect for cracked reinforced concrete, see Fig. 2.11.

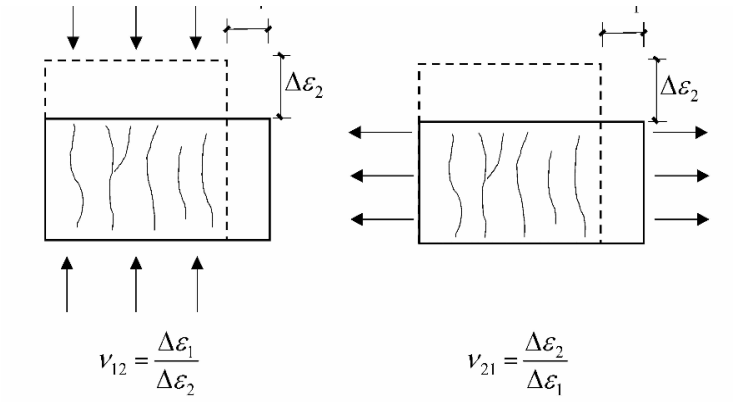

Fig. 2.11 Hsu/Zhu Ratio ν_{12} and ν_{21} under Biaxial Loading

The significance of the Hsu/Zhu ratio is that the SMM can predict the descending portion of the stress-strain behavior of the RC under shear stress. Twelve full-scale panel tests were conducted by Zhu and Hsu to study the Hsu/Zhu ratio. They proposed the equations from the test results as

$$\upsilon_{12} = 0.2 + 850\varepsilon_{sf} \qquad \varepsilon_{sf} \le \varepsilon_y , \tag{2-62}$$

$$\upsilon_{12} = 1.9 \qquad \varepsilon_{sf} > \varepsilon_y , \text{ and} \tag{2-63}$$

$$\upsilon_{21} = \begin{cases} 0.2 & \text{Before cracking} \\ 0 & \text{After cracking.} \end{cases} \tag{2-64}$$

It should be noted that for the cracked RC element in the post-yielding stage, the Hsu/Zhu ratio is higher than 0.5, which is the maximum value of Poisson ratio for continuous solid materials. The reason is that the smeared tensile strain of cracked RC element includes not only the strain of the material, but also the opening of cracks. By considering the cracked RC element as continuous material, the Hsu/Zhu ratio could then be significantly high (equals to 1.9). Due to the additionally bond action created by the externally bonded FRP sheets, the Hsu/Zhu ratio is expected to be smaller than that in RC element. No similar research has been identified in the literature to evaluate Hsu/Zhu ratio for FRP RC element.

2.5 STUDIES ON THE MATERIAL LAWS OF FRP RC ELEMENT

Up to date, there are limited investigations regarding the constitutive laws of FRP RC elements under uniaxial tension load. In this section, these available investigations are briefly reviewed and the main conclusions are summarized.

2.5.1 Experimental Investigations

Ueda (2002) tested 14 prismatic FRP RC specimens under tension. Two types of specimens with different width of CFRP sheets and different strain gage arrangements were tested to study the constitutive laws of concrete, steel and FRPs as well as the bond behavior among them. The test specimen is 50 in long with a testing zone of 47 in. The load was applied through the reinforcing bars at the end. Additional stirrups and confinement plates were used to strengthening the edges of the specimen. The details of the specimen is shown in Fig. 2.12.

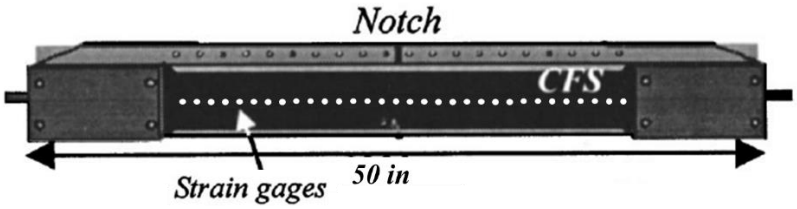

a) Specimen and Strain Gauge on CFS

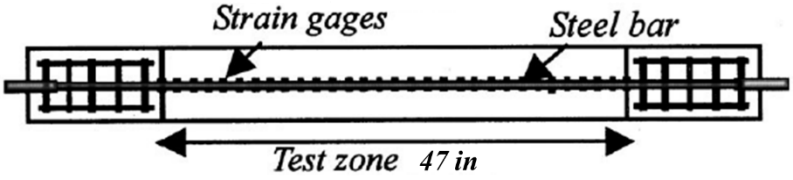

b) Specimen and Strain Gauge on Steel Bar

Fig. 2.12 Test Specimen for Ueda et al. (2002)

Strain gages were mounted on the rebars and on the FRP sheets to capture the strain variation along the material. Different FRP and steel reinforcement ratios were chosen. The main findings of this study includes: a) CFRP sheets reduced the crack spacing. As a result, the average bond stresses on the steel reinforcing bar became smaller; b) The apparent yielding stress of the reinforcing bar increased with both the CFRP ratios and the steel reinforcing bar ratio; c) The average concrete stress without CFRP sheets was smaller than

that in the specimen with CFRP sheets but became smaller as the CFRP reinforcement ratio increased.

Ceroni et al. tested three series of four tie specimens by applying a tensile force using the test setup shown in Fig. 2.13. The test specimen was a 47 in long prism with a square cross section of 3.9 in ×3.9 in. Each series includes one reference specimen and three specimens externally strengthened with FRP sheets. The FRP sheets contains GFRP and CFRP. The internal steel reinforcement includes one reinforcing bar with a diameter of 0.39 or 0.55 in.

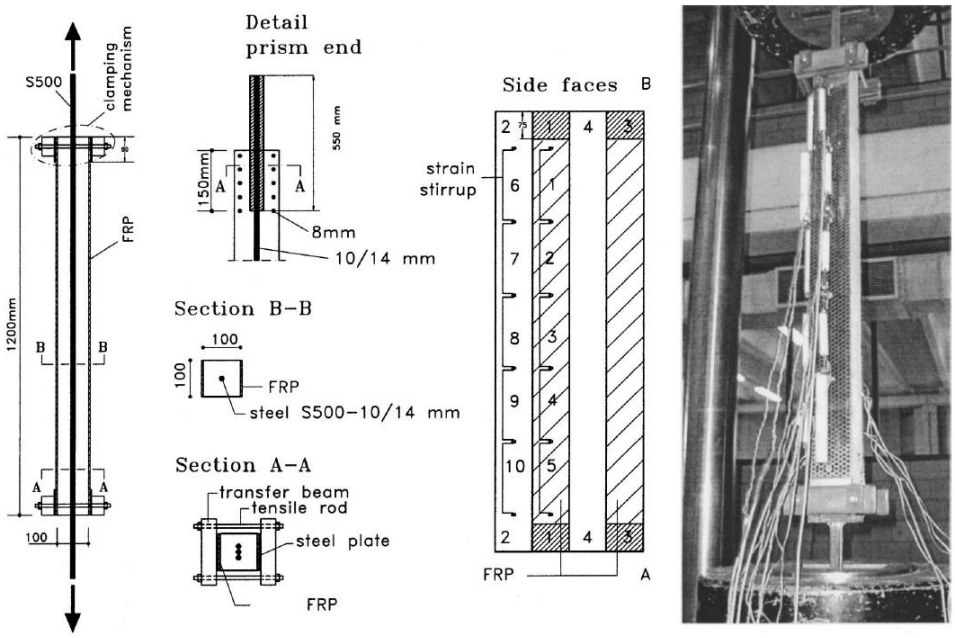

Fig. 2.13 Test Setup for Ceroni et al. Tests (2004) (25.4 mm=1 in)

The test parameters include FRP type (CFRP, GFRP), FRP reinforcement ratio (layers of sheets), steel reinforcement ratio (bar size), as well as the concrete strength. The main findings of this study are: a) The effect of FRP on the tension stiffening is relevant when comparing the experimental results at the same load level, but negligible when considering the same steel stresses, which means FRP may not affect the tension stiffening

behavior of the steel bar; b) The FRP has an effect on the variation of crack spacing and crack widths.

2.5.2 Analytical Investigations

Based on the test data of Ceroni et al. (2002), Pecce and Ceroni (2004) proposed a model to analyze the tensile behavior of the RC ties strengthened with FRP laminates. The approach is one dimensional but allows introducing any nonlinear constitutive relationship for materials and bond laws. The constitutive law of steel is considered before and after steel yields; The FRP constitutive law is linear; for the bond behavior at the steel and concrete interface, the well-known model developed by Eligehausen et al. (1983) is introduced, considering the bond degradation near cracks; and for the bond behavior between FRP and concrete, nonlinear behavior is considered without degradation near cracks. The model showed a good prediction of load-strain curve when compared with the experimental results.

Based on the test results of Ueda et al. (2002), Farah and Sato (2011) proposed a 2-D nonlinear numerical model by using the rigid body spring method (RBSM). In the code, different constitutive laws were used for different material components and the interface between FRP/steel and concrete was defined by different bond-slip relationships. Since the constitutive laws are the main research domain in this study, the constitutive modeling of the proposed method is reviewed.

As previously presented in the review of the experimental tests, the tension stiffening has been found to be greater in FRP RC element than that in RC element. The following expression was proposed as

$$\frac{\overline{\sigma_c}}{f_{ct}} = E_c \times \frac{\varepsilon}{f_{ct}} \qquad \varepsilon \le \varepsilon_{cr}$$

$$\frac{\overline{\sigma_c}}{f_{ct}} = \left[1 + \left(c_1 \frac{\varepsilon}{\varepsilon_{ct}}\right)^3\right] \exp\left(-c_2 \frac{\varepsilon}{\varepsilon_{cr}}\right) + c_3 \frac{\varepsilon}{\varepsilon_{cr}} \qquad \varepsilon > \varepsilon_{cr} \tag{2-65}$$

$$\varepsilon_{cr} = \frac{f_{ct}}{E_c}.$$

The parameters c_1, c_2 and c_3 are defined as a function of the internal reinforcement ratio ρ_s, external reinforcement ratio ρ_f, the steel-to-concrete modular ratio and the CFS-to-concrete modular ratio. These parameters are calibrated using the test data of Ueda et al. (2002). The calibrated model shows an acceptable agreement with the test results, see Fig. 2.14.

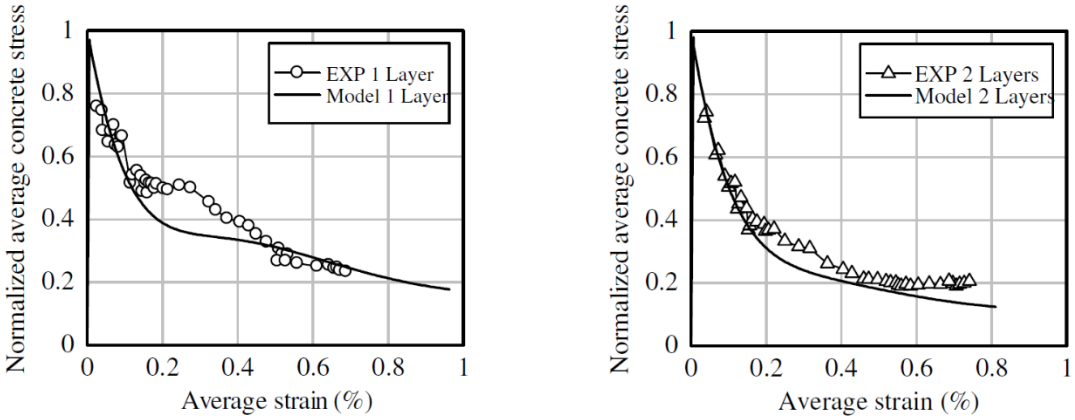

a) Specimen (S-1-1) (ρ_s=0.5%) (ρ_f=0.07%) b) Specimen (S-1-2) (ρ_s=0.5%) (ρ_f=0.13%)

Fig. 2.14 Comparison of Stress-strain Curve of Concrete between the Proposed Model (Farah and Sato., 2011) and Experimental Results (Ueda et al., 2002)

The stress-strain relationship of a deformed steel bar is usually assumed to be elastic and then perfectly plastic. It was observed that the apparent yielding stress is greater in the strengthened members than in the un-strengthened member. To account for this, the following expressions were proposed as

$$\overline{f_s} = E_s \varepsilon_s \quad \text{for } \overline{f_s} \le f_n^* \qquad \overline{f_s} = f_o^* + E_p \varepsilon_s \quad \text{for } \overline{f_s} > f_n^*$$

$$f_n^* = c_4 f_y \qquad E_p = c_5 E_s \qquad f_o^* = \frac{E_s - E_p}{E_s} f_n^* \qquad \text{and} \qquad (2\text{-}66)$$

$$f_o^* = c_4 (1 - c_5) f_y$$

$$\overline{f_s} = E_s \varepsilon_s \quad \text{for } \overline{f_s} \le c_4 f_y$$
$$\overline{f_s} = c_4 (1 - c_5) f_y + c_5 E_s \varepsilon_s \quad \text{for } \overline{f_s} \le c_4 f_y. \qquad (2\text{-}67)$$

The values of the parameters were also calibrated by regression of the test results. The model had a good prediction of the stress-strain curve of the rebar, see Fig. 2.15.

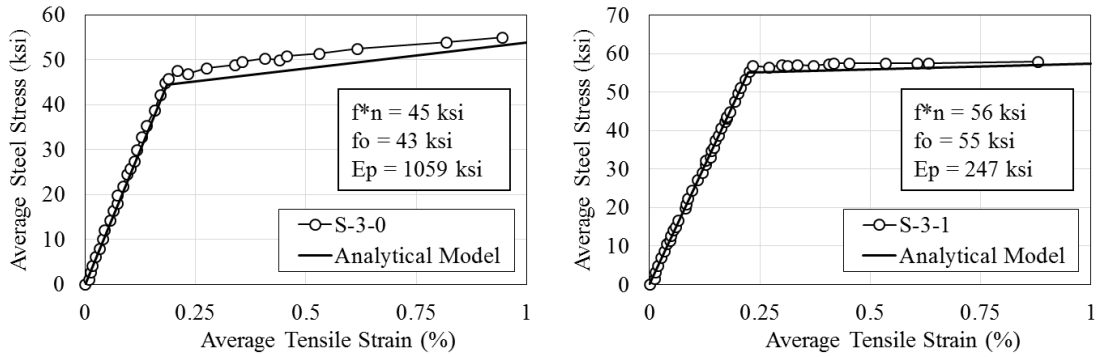

a) Specimen (S-3-0) (ρ_s=1.27%) (ρ_f=0%) b) Specimen (S-3-1) (ρ_s=1.27%) (ρ_f=0.12%)

Fig. 2.15 Comparison of the Stress-strain Curve for steel in tension between the Proposed Model (Farah and Sato, 2011) and Experimental Results (Ueda et al., 2002)

2.6 LITERATURE GAPS AND SUMMARY

In this chapter, a comprehensive literature review is conducted on the shear strengthening of RC structures with externally bonded FRP sheets. The state-of-art analytical and experimental investigations have been briefly reviewed and the development truss model theory was introduced. Previous research studies have shown that to rationally predict the shear behavior of FRP RC element using truss model approach, the constitutive laws of each components and the interaction between them have to be carefully

investigated (Farah and Sato, 2011). Up to date, only few studies have been conducted on constitutive modeling of the components in FRP RC elements. The results of these studies show that with the existence of externally bonded FRP sheets, the constitutive laws of concrete and steel will be altered when compared with the un-strengthened RC members. To validate this phenomenon and evaluate these changes of constitutive laws, more tests need to be conducted. In this study, both uniaxial and biaxial constitutive laws of different components in FRP RC elements are investigated, and the results is expected to fill the gap.

Moreover, several other gaps related to the shear strengthening using FRP are also addressed here in this section. In general, most of the current conducted test are rectangular and small scale as shown in Table 2.1 in the former section. Also, several parameters that have been found to have an effect on the shear behavior was not fully understood and there is no sufficient data to carefully investigate these factors:

a) Scale Factor: For RC beam without shear reinforcement, the shear resistance decreases as the beam size increases. The phenomenon was found also in FRP RC beams that shear strengthening showed a tendency for a decrease in the shear gain due to FRP as the height of the specimen increased (Bousselham and Chaallal, 2004; Leung et al., 2007). Fig. 2.16 showed that this phenomenon is more evident in the specimen that failed in debonding. However, the predictive models are largely based on test results which are mostly obtained from small-scale testing.

b) Pre-Loading/Cracking: Externally strengthening with FRP is most suitable for existing in-service structures that often are pre-cracked. The very few investigations carried out on RC beams that were pre-cracked prior to their strengthening indicate that pre-loading does not affect the shear performance of retrofitted beams (Czaderski, 2002;

Carolin and Taljsten, 2005a, Hassan Dirar et al., 2006; Belarbi et al., 2012; Murphy et al., 2012; and Dong et al., 2013). However, this finding may need to be confirmed by further tests.

c) Shear Fatigue Load: As shear fatigue behavior of RC beams has been studied since 50s, but it has not been well studied for FRP RC element. Only limited test has been done, and among these tests, most of them are flexural fatigue. The shear fatigue tests that have been done show a very limited degradation of shear behavior of FRP RC beams under fatigue load compared to static load.

d) Prestressing: The only available study on PC beams strengthened in shear with FRP was conducted by Hutchinson and Rizkalla (1999). The study reported that the prediction by the shear equations proposed by the authors based on ACI 318 was in good agreement with the test results of seven prestressed concrete beams strengthened with CFRP strips. Because most bridge girders are made of prestressed concrete, further studies dealing with prestressed concrete are needed. Recently in 2012, four tests were conducted on 54 in.-deep pre-stressed I girders in UT Austin, but prestressing is not investigated as a parameter in this study.

In this chapter, a comprehensive review has been presented on the knowledge related to the shear strengthening of RC using FRP sheets. The development of truss model approach and the constitutive modeling are emphasized. The literature review indicates that a huge gap exists in experimental and analytical investigations in constitutive modeling of FRP RC element under various stress fields. To fill this gap, the experimental and analytical investigations on the constitutive modeling in this study will be presented in detail in the following chapters.

CHAPTER 3 UNIVERSAL PANEL TESTER

3.1 INTRODUCTION

The experimental tests in this research were carried out with the Universal Panel Tester (UPT) at the University of Houston (Hsu, Belarbi, and Pang, 1995). The UPT was built in 1980s and has been used by the UH research group to develop several analytical models related to shear and torsion. The UPT is capable of applying various combination of in-plane and out-of-plane stresses to the test specimen. It is a powerful tool to study the in-plane and out-of-plane behavior of RC elements. To control all the 40 in-plane jacks and 10 out-of-plane jacks, the UPT is equipped with a sophisticated servo control hydraulic system. To better understand the loading procedure, test setup and the load/strain control methods in the experimental program, this chapter presents the information of the UPT in terms of the machine setup and the principles of the servo controller and hydraulic systems. Finally, the servo controller arrangement in the test program is also presented.

3.2 GENERAL DESCRIPTION

The test specimens for test panel tester are 55 in. × 55 in. and the thickness can be up to 16 in. Reinforced concrete panels with full-size steel reinforcement can be tested. Fig. 3.1 shows the north and south view of the UPT.

The UPT is capable of applying varies combination of in-plane and out-of-plane loads to the specimen through 37 in-plane jacks (with a capacity of 200 Kips/jack in tension and 250 Kips/jack in compression) and 3 in-plane rigid links, as well as 7 out-of-plane jacks (with a capacity of 120 Kips/jack in tension and 150 Kips/jack in compression) and 3 out-of-plane rigid links. Fig. 3.2 shows the illustration of the load application for in-plane and

out-of-plane jacks. The 40 in-plane jacks are fixed onto a 15.7 ft. × 15.7 ft. steel reaction frame by two layers. The specimen was first mounted onto the connector yokes by threaded bolts, and the yokes then connects with the hydraulic jacks by cylindrical pins.

a) North View b) South View

Fig. 3.1 North and South View of the UPT

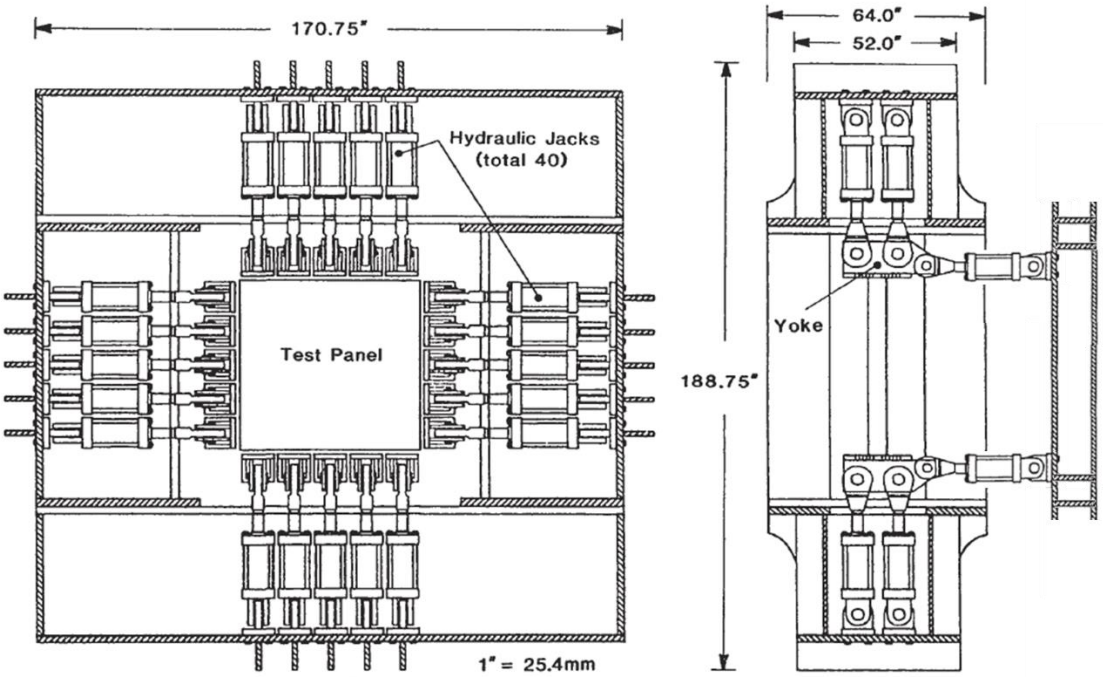

a) Front Section b) Side Section

Fig. 3.2 Illustration of the Load Application for Jacks (Adopted from Belarbi, 1991)

The UPT was originally designed to test specimen using only load control mode. Later in 1993, a closed-loop servo-control system was designed specifically for the UPT to conduct test using strain control mode (Hsu, Zhang and Gomez, 1995). By using the strain control mode, the post-yielding behavior can be captured more accurately. Up to date, the UPT is unique in the world that can be used to test the full-size RC panel using both load control and strain control modes.

3.3 SERVO-CONTROLLED HYDRAULIC SYSTEM

In order to better understand the control method used in this research, the principle of the closed-loop servo control for hydraulic system is presented in this section. This system was originally designed and installed in 1993, and the schematic diagram is shown in Fig. 3.3 (Hsu, Zhang, and Gomez, 1995). The hydraulic system can be controlled by two controllers, namely the manual controller and the servo-controller. The manual control mode is designed for specimen installation. Using the manual control mode, each jack can be controlled individually by strain control mode. When the specimen is in position, each of the hydraulic jack can be extended or contracted to fit position of the pin connections between the yokes and the jacks. The valves of the manual switch can control the jack to be in tension, in compression, or in holding status. The suggested oil pressure under the manual control mode is 500 psi. For the servo-controller mode, the forces/load are controlled by the servo system. The servo-control system contains ten channels, each including a servo controller and a servo-valve package. Each servo-valve package includes a servo-valve, a manifold with 10 pairs of outlets, and a pair of Delta P pressure transducers. For each channel, different oil pressure can be applied for different test purposes. These different oil pressure can be applied to any jack by connecting the jack with the manifold

using the specially designed Quick-Disconnected connections. A pair of flexible hoses is connected to the pair of jack terminals which is connected to the jack. By using this setup, various combination of loading along the side of the specimen can be applied as designated. These ten manifolds are controlled by ten servo boxes. The servo boxes receive command from the programmer computer and the feedback from either Delta P transducers (load control) or LVDTs (strain control), compare them and send a signal to the servo valve on the manifold to adjust the oil pressure accordingly. The detail of the close-loop system is discussed in the following section.

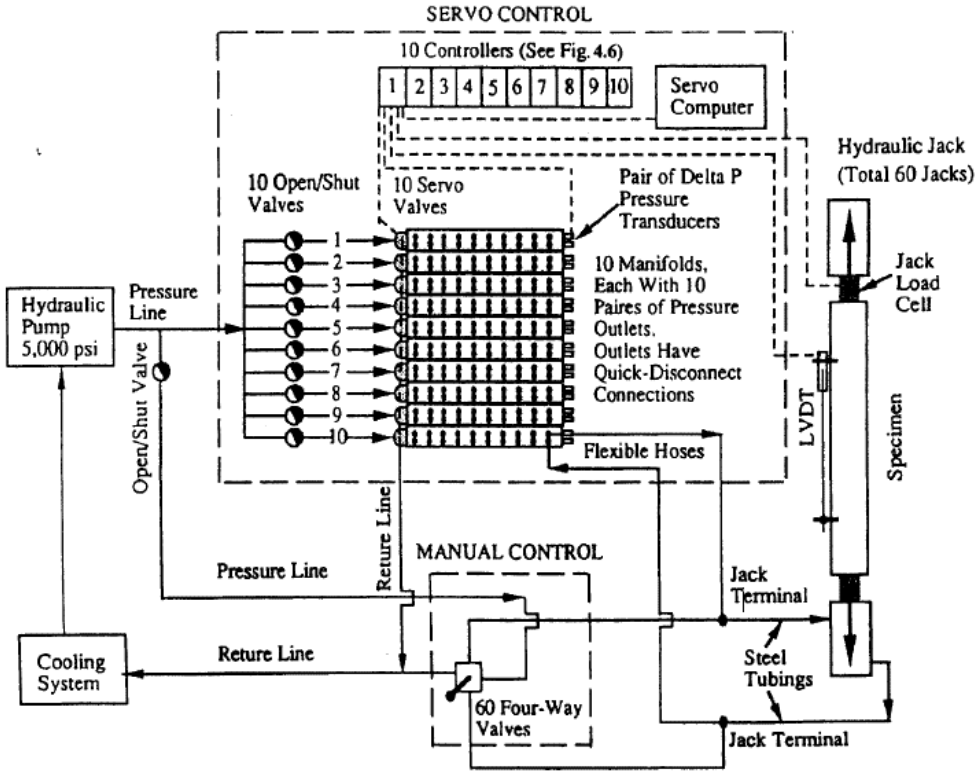

Fig. 3.3 Schematic Diagram of Control System

The basic principle of the closed-loop servo-control system is shown in Fig. 3.4 (Hsu, Zhang, and Gomez, 1995). It can be seen that two feedback selections are available in the system. The first selection (signal condition #1) is for load control mode. In this condition, the feedback is the loading read from the Delta P transducers attached on the ten

manifolds. The second selection (signal condition #2) is for displacement/strain control. In this case the feedback signals come from the average values of the horizontal/vertical LVDTs on each side of the specimen. All the experimental feedbacks are in voltage. The feedback values will be compared with the pre-assigned program signal in a voltage comparator unit. If there exists a difference in voltage, an error signal will activate the servo-valve to adjust the oil pressure in the manifold so that the desired condition for load/strain is achieved. This procedure will continue throughout the whole tests.

Prior to 1995, the servo control system can only conduct the test use either load control or strain control, there could be no switch between these two modes during the tests. In 1995, a new software was installed so that the mode can be switched during the test as needed.

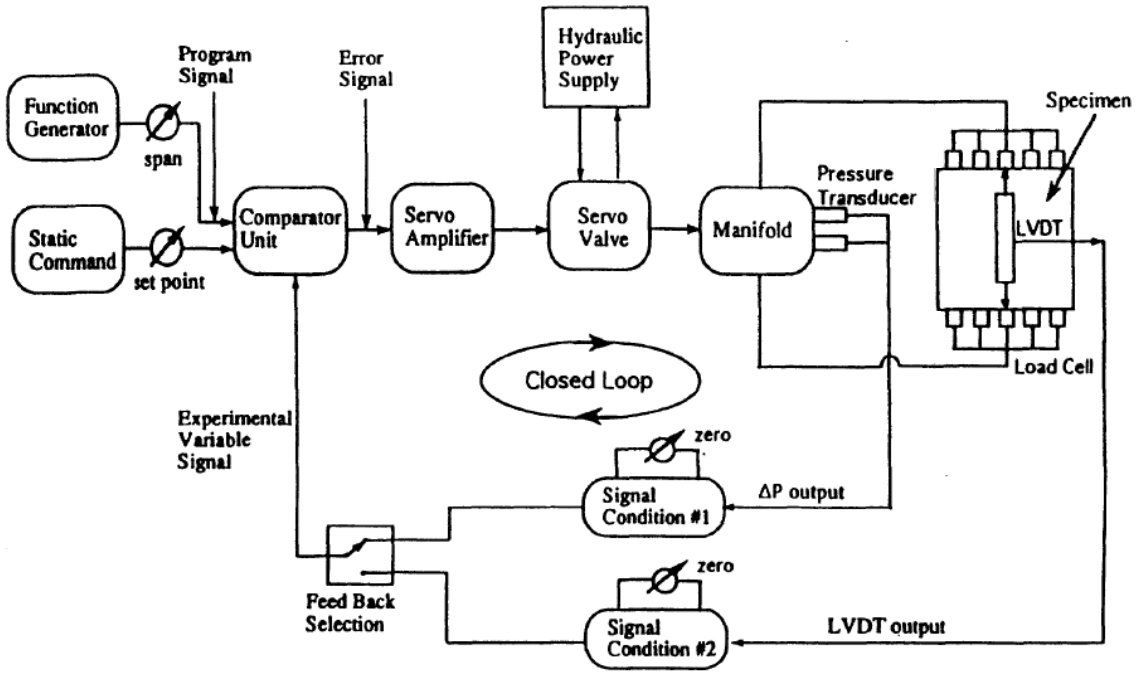

Fig. 3.4 Details of the Closed-loop Servo-control System

3.4 STRAIN MEASUREMENT

From the 30 years of panel test experiences at the University of Houston, a total of 20 LVDTs were proposed to measure the average strain on each side of the specimen. Twelve female 3/8 in. (9.5 mm) in diameter threaded LVDT anchors with couple nuts were pre-cast in the panel. Later on these anchors were used to securely fasten the LVDTs to the panel. Before a test, these 20 LVDTs were arranged symmetrically on both sides of the panel as shown in Fig. 3.5. They were arranged to measure the strains in four directions: horizontal, vertical, and two diagonals. Eight LVDTs with 1/2 in. range were used to measure the compressive strains in the vertical direction, and eight LVDTs with 2 in. range were used to measure the tensile strains in the horizontal direction. Four LVDTs with 1 in. range were used for the measurement in the diagonal directions. These 20 LVDTs were held by 4 pairs of corner brackets and 8 pairs of L-shape brackets. The brackets were fastened securely to prevent any movement of the measuring point.

The gage length is 31.5 in. for the horizontal/vertical LVDTs and 44.5 in. for the diagonal LVDTs. The initial values of the LVDTs were zeroed mechanically by adjusting the position of the rods (sensor attached), then electronically zeroed by the servo-boxes before the test started.

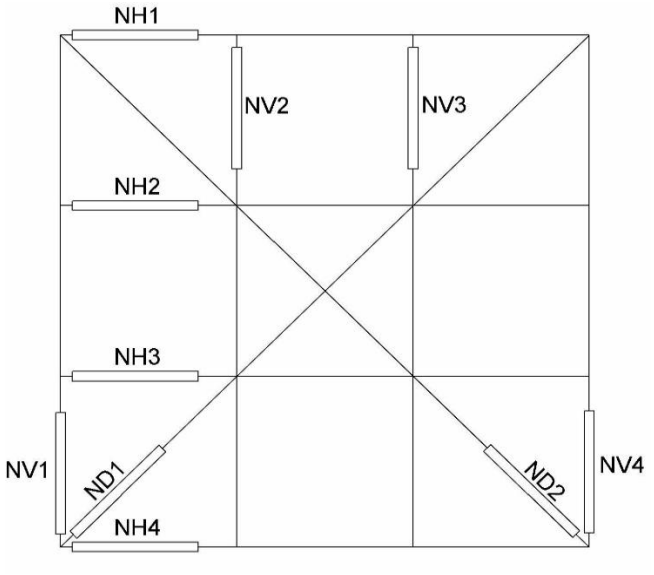

a) North Side

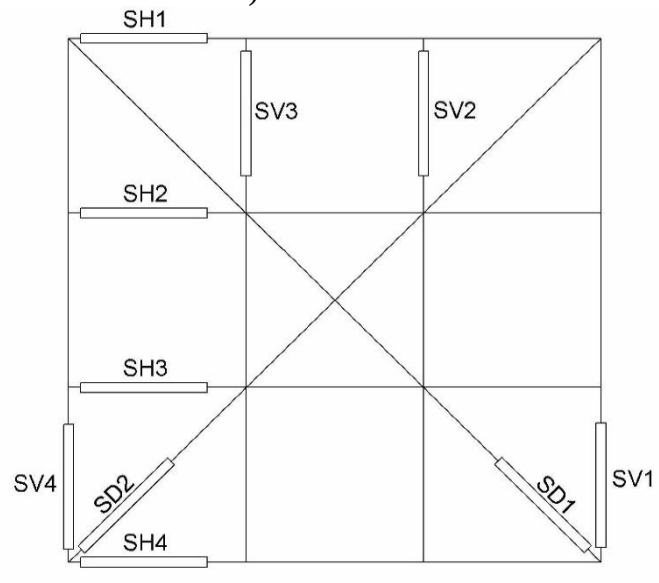

b) South Side

Fig. 3.5 LVDT Arrangement for the Panel Test

3.5 CONTROL ARRANGEMENT

In this research project, two different control arrangements were designed for different test purposes. The following section shows the details of the control arrangements used in this research.

3.5.1 Uniaxial Tension Test

Since there are only four jacks that were used to apply the tension load to the specimen in the uniaxial tension test, two manifolds and two servo control boxes were designed to conduct the test. No. 10 and No. 16 jacks on the north and south sides were chosen as the loading jacks. In order to maintain the same applied load on the left and right sides of the panel, the two jacks on one side (North/South) of the panel were controlled by the same manifold, i.e., the oil pressure in these two jacks were kept the same at all time. The jacks on north side were connected to manifold 10 and controlled by Box 10 while the ones on the south side were connected to manifold 4 and controlled by Box 4, as shown in Fig. 3.6. The aforementioned control method was achieved by the cable arrangements shown in Fig. 3.7.

The test was designated to start with load control mode till cracking, then switched to strain control mode till failure of the specimen. In the load control mode, the feedback from the pressure transducers attached on the manifold. In the strain control mode, the LVDT readings were used as feedback. On each side of the test specimen, there is one LVDT attached on the surface of the specimen, details of the instrumentation of uniaxial test are presented in the experiment section. The reading of strain values goes into control Box 10 and Box 4 as input to compare with the given command strain, then a proper command signal will be sent to the servo valve to control the load to achieve the target strain.

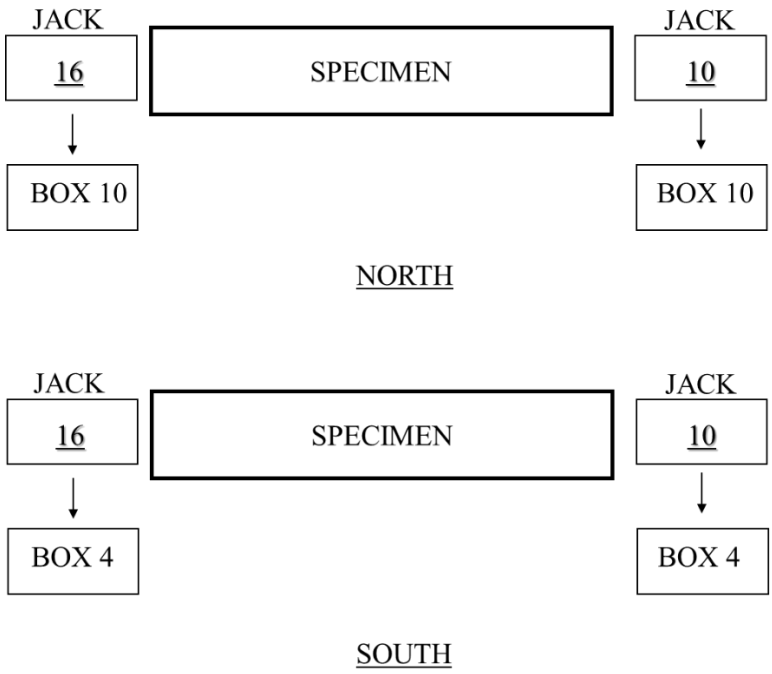

Fig. 3.6 Control Arrangement for the Uniaxial Tension Test

3.5.2 Biaxial Tension-Compression Test

For the biaxial tension-compression test in this project, eight oil pressures in the 8 servo valve manifolds were each controlled by a servo valve which, in turn, was monitored by a controller. On each manifold, up to 10 jacks could be connected by flexible hoses and fixed steel tubing. Of the 8 controllers, four are called programming controllers, No. 3, 4, 8, and 10. These can be directly controlled by the programming computer to achieve the expected load levels. The other four controllers can be controlled by the signals from these four programming controllers or by the signals from the in-plane rigid links. Three in-plane rigid links were installed to supply reactions from the jacks and to fix the test panel in space.

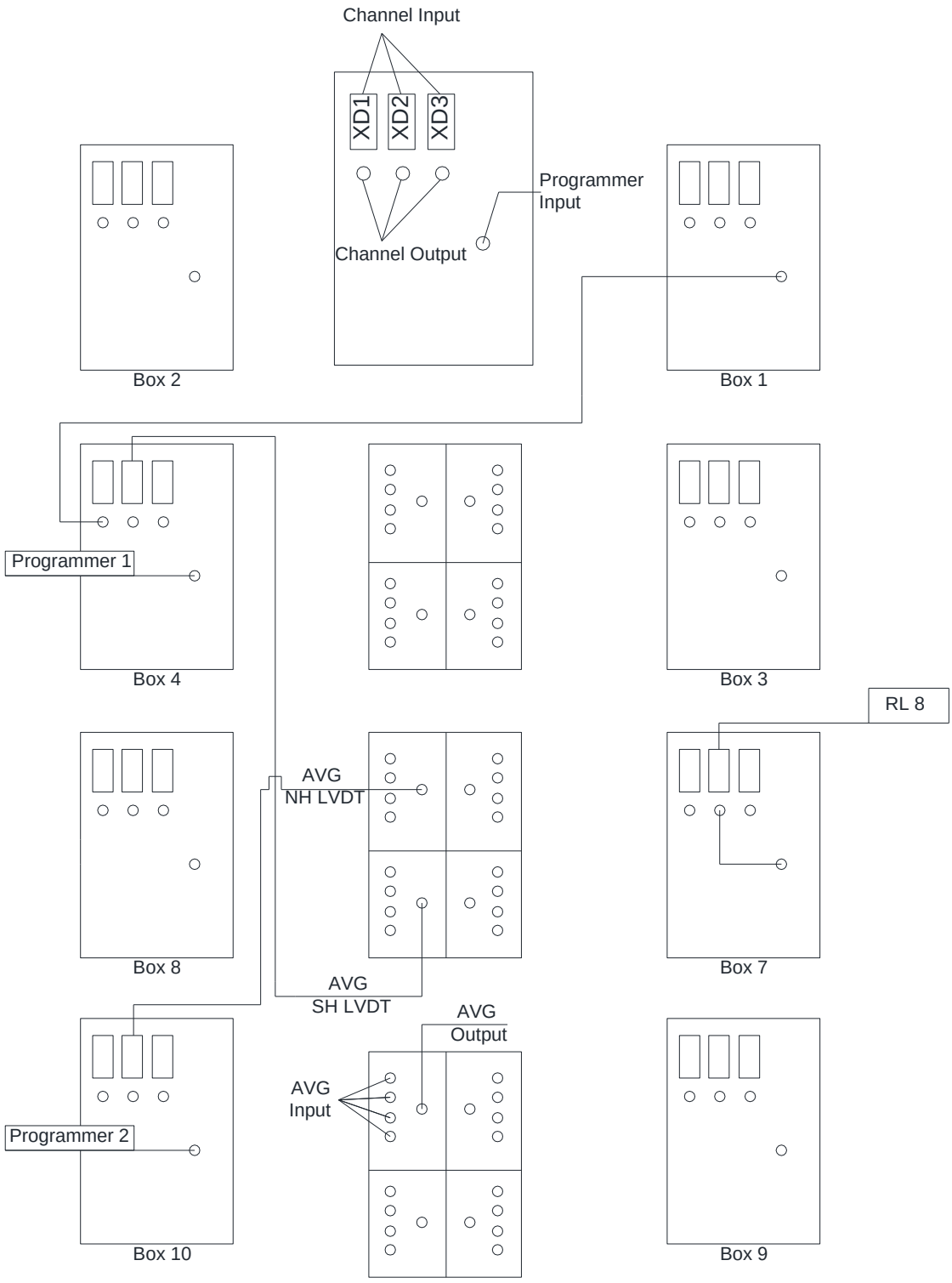

Fig. 3.7 Cable Arrangement for the Uniaxial Tension Test

Fig. 3.8 and 3.9 shows the servo control system and the cable arrangement of the biaxial tension-compression tests. In the north side, jacks N11 and N15 are actually the rigid links to fix the test panel in the vertical direction. Jack N8 is the rigid link to fix the test panel in the horizontal direction. During a test, all the unbalanced forces would be taken by the rigid links. The load cells readings in the rigid links were sent as input signals to the controllers. For the panel tests in this research the 20 jacks in the south side and the 17 jacks in the north side were controlled individually to make the strains on both faces of a panel more uniform. Controllers 3, 4, 8, and 10 were controlled directly by the programming computer. Controllers 1 and 2 were controlled by controllers 4 and 3, respectively. Controller 7 was controlled by the signal from the rigid link N8; and controller 9 was controlled by the average signal from rigid link N11 and N15.

On the south face, the jacks at the bottom, to the west, at the top, and to the east were supplied by manifolds 3, 4, 2, and 1, respectively. On the north face, the five jacks at the bottom and to the west were supplied by manifolds 8 and 10, respectively. The four jacks N6, N7, N9, and N10 were controlled by manifold 7; and the three jacks N12, N13 and N14 by manifold 9. After yielding, the strain-control mode was used. The average value of four vertical LVDT signals on both south and north faces of the panels were sent to controllers 3 and 8, respectively, as vertical strain feedbacks. In a similar way, the average values of four horizontal LVDT signals on both south and north faces were sent as horizontal strain feedbacks to controller 4 and 10, respectively.

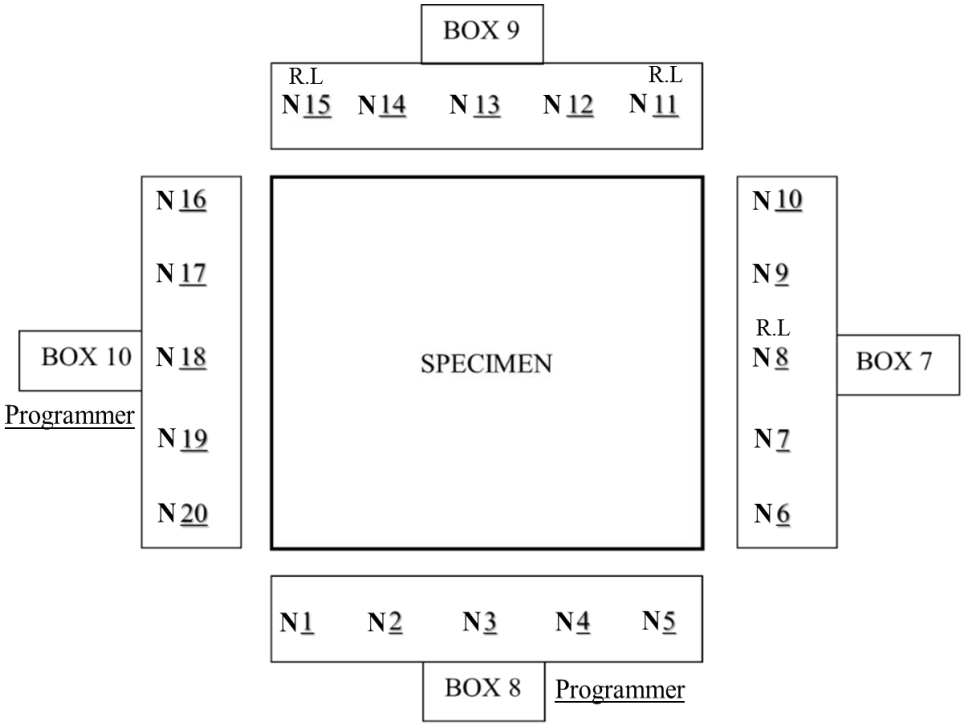

a) North Side

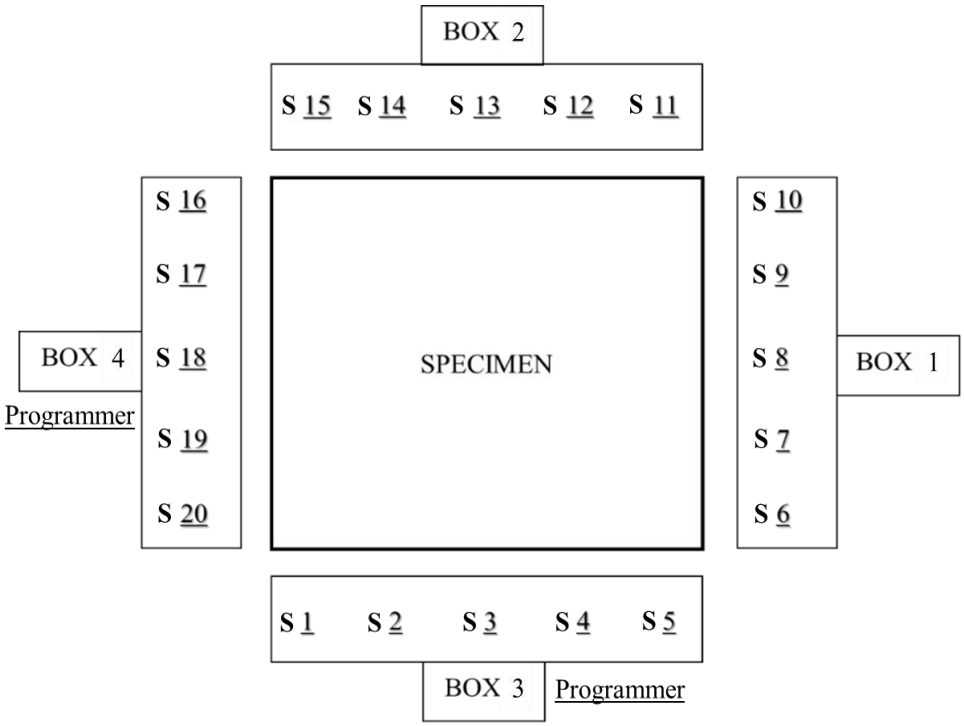

b) South Side

Fig. 3.8 Control Arrangement for the Biaxial Tension-compression Test

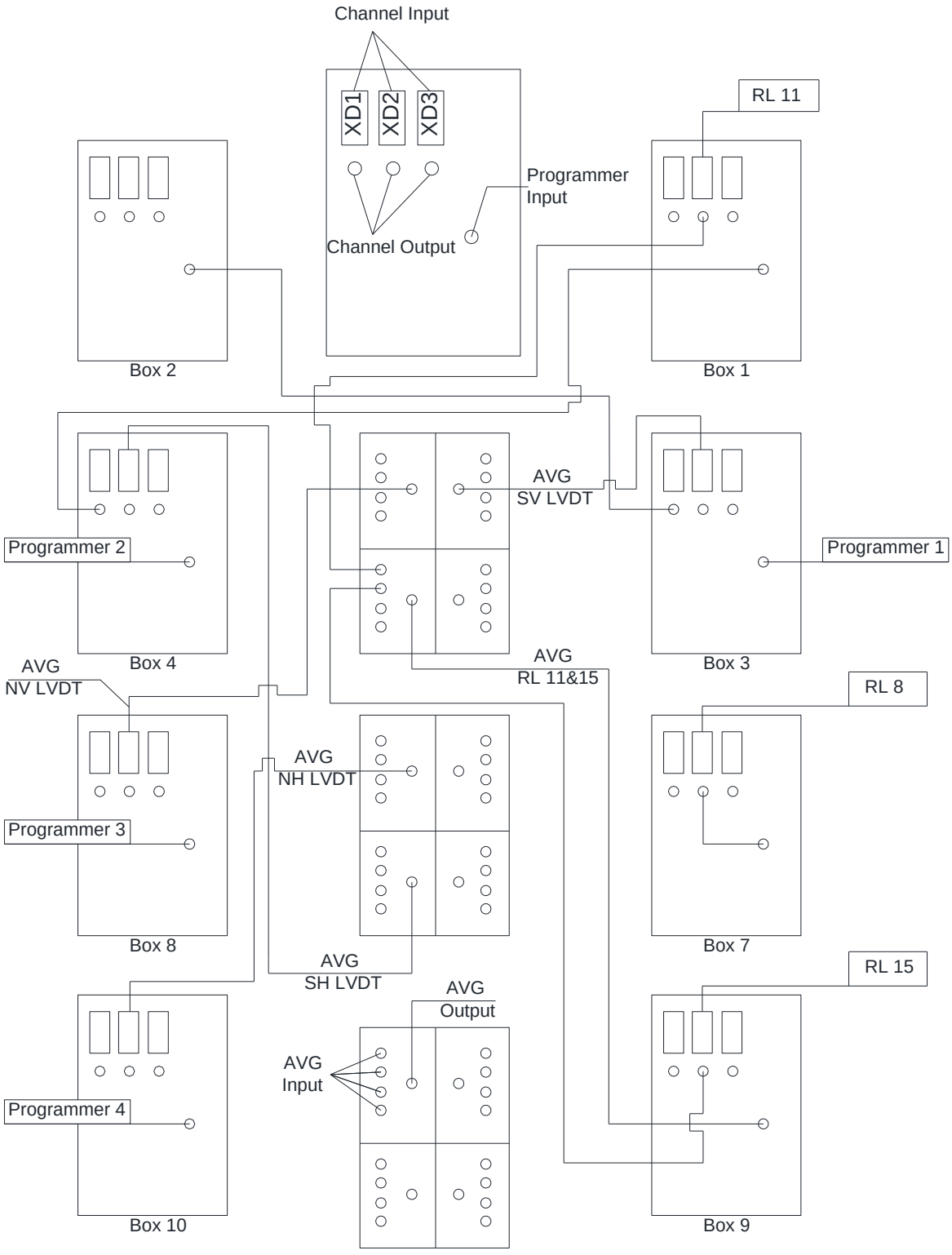

Fig. 3.9 Cable Arrangement for the Biaxial Tension-compression Test

The aforementioned control method was achieved by arranging the electric cables at the back of the servo-boxes (Fig. 3.9). In the softening test, both load control and strain control were used, but in the Hsu/Zhu ratio test, only load control was used. Thus, the control arrangement for softening test can be applied to the Hsu/Zhu ratio test.

3.6 SUMMARY

To better understand the loading procedure, test setup and the load/strain control methods in the experimental program, this chapter presents the information of the Universal Panel Tester with details, including the setup, the principles of the servo-control and hydraulic systems. In next chapter, the details of the experimental program will be presented.

CHAPTER 4 EXPERIMENTAL PROGRAM

4.1 GENERAL DESCRIPTION

To fulfill the research objectives and investigate parameters that affect the various material laws of FRP RC elements, large-scale tests were conducted. The experimental program was designed to study the following material laws: (1) concrete in tension; (2) steel in tension; (3) softening coefficient; (4) modified Hsu/Zhu ratios. The main variables investigated are steel reinforcement ratio, FRP reinforcement ratio and wrapping schemes of FRP sheets.

Fig. 4.1 shows the outline of the experimental program. It includes uniaxial tension tests of prismatic members and biaxial tension-compression tests of square panels. The results of uniaxial tension tests were used to develop the constitutive laws of concrete and steel in tension; the results of biaxial tension-compression tests were used to develop softening coefficient and modified Hsu/Zhu ratios. For the uniaxial tension test, thirteen prismatic specimens with a cross section of 7 in. $\times 10^{1}/_{8}$ in. and a length of 55 in. were tested; for the biaxial tension-compression tests, six full-scale square panels (55 in. $\times$ 55 in.) with a thickness of 7 in. were tested. In the following section, the details of the test program are given, which includes objective of the experimental program, material and fabrication of specimen, experimental setup, instrumentation method and loading procedures of each test.

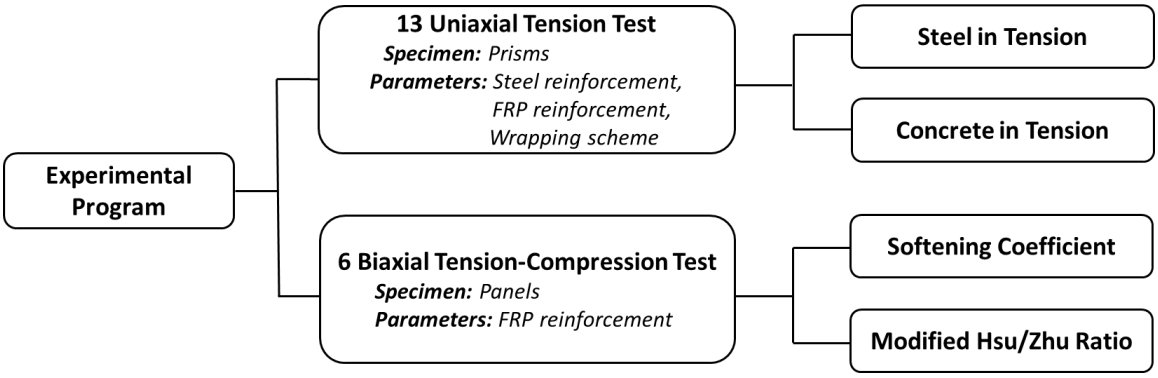

Fig. 4.1 Outline of the Experimental Program

4.2 MATERIAL

The same type of concrete, steel rebars and FRP sheets were used for uniaxial tension tests and biaxial tension-compression tests. The concrete strength was designed to be close to 6000 psi; Grade 60 deformed rebars with different sizes (No. 3, 4 and 5) were chosen as the internal steel reinforcements; two thicknesses (0.025 in and 0.04 in) of CFRP sheets were used as the externally bonded FRP reinforcements. In the following section, details of these materials are presented.

4.2.1 Concrete

A cylinder compressive strength of 6000 psi (41.4MPa) was chosen to be the target strength of the concrete in the test program. The mix ratio (based on weight) for cement, aggregate, sand was 1:2.02:1.19. The water-cement ratio was chosen to be approximately 0.48. The workability was controlled by the slump test with a desired value of 8 in. Type III high-early-strength Portland cement was used. The sand satisfies the requirements per ASTM C33. The graded limestone aggregate had a maximum size of ¾ in.

For the uniaxial tension test, five specimens were cast at one time and each cast contains two batches of mixing. For the panel test, each panel requires two batches of mixing. For each batch of mixing in this program, three 6 in×12 in cylinders and one 6 in×20 in beam were cast. The cylinders and beams were cured in the same environmental conditions as the specimens and were removed from the formwork at same time as the specimen. The specimens as well as the cylinders and beams were cured with saturated burlap covering on top beneath a plastic sheet in the air-conditioned lab temperature. The cylinders were tested on a Tinius Olsen Universal testing machine. The cylinder test satisfies the ASTM C39. The compressive stress and strain were recorded up to the peak point. Fig. 4.2 shows the typical compressive stress-strain curve and the parabolic simulation. It can be seen that the parabolic curve can well simulated the compressive stress-strain curve of concrete. The Young's Modulus E_c for the concrete can be decided using ACI method, which was developed by Pauw (1960). In this method, E_c was defined as the slope of the line drawn from zero to the point when stress is equal to 0.45 f'_c. All the cylinders were tested at the same day as the specimen. The beam was cast to test the pull-off strength of the FRP-concrete interface. The details of the pull-off test are shown in the section 4.2.3.

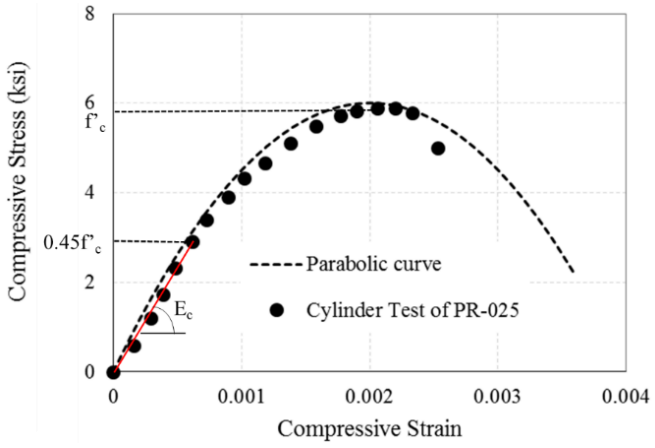

Fig. 4.2 Typical Stress-strain Curve from Concrete Cylinder Compression Test

4.2.2 Steel Reinforcements

Grade 60 deformed reinforcing bars of different sizes were used as the steel reinforcements. The stress strain characteristics of the rebars were determined by coupon tests. The manufacturer provided the steel rebar in several batches, for each batch and each size of the rebar, three 16 in coupons were cut as samples. The coupons were tested with the Tinius Olsen Universal testing machine. The tensile strain of the coupon test was measured by an extensometer with a gage length of 2 in. The load was captured by a calibrated load cell on the hydraulic cylinder.

The test setup of the specimen requires welding at the end of the rebar. And the excessive heat generated in the steel from the welding could cause early failure at the edge of the specimen (Belarbi, 1991). Therefore, weldable high ductility rebars were used in the test. The rebars used in this particular test program were ASTM A706 low-alloy steel deformed bars. This type of rebar is specially made for structure steel that requires welding. The ultimate strains from the conducted coupon tests were all greater than 20%. Typical stress strain curves for all rebars are shown in Fig. 4.3. It can be seen that only No. 3 rebar has the yielding plateau, the No.4 and 5 have no clear yielding plateau. This behavior affects the constitutive laws of the materials developed in this research, the details will be addressed in the analytical investigations. The material properties of the rebar are shown in Table 4.1, the modulus of elasticity is between 27359 ksi and 28326 ksi. The yield strength is between 66.5 ksi and 68 ksi. The yield strength for #4 and #5 is obtained using 0.2% strain offset method, the elasticity modulus are determined by the slope of the linear portion of the stress-strain curve, as shown in Fig. 4.4.

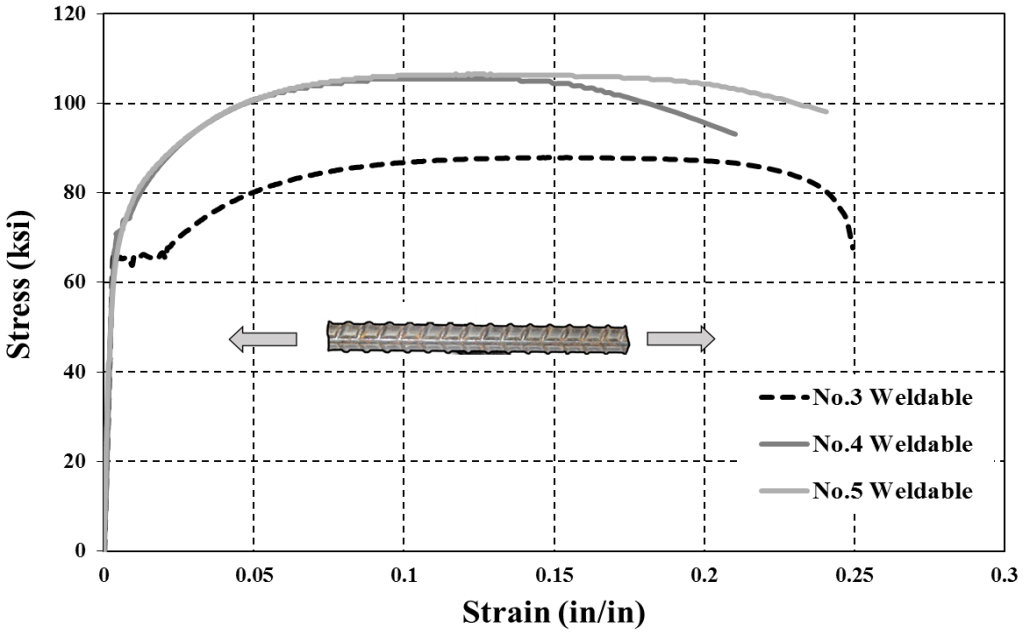

Fig. 4.3 Typical Stress-strain Curves of the Rebars

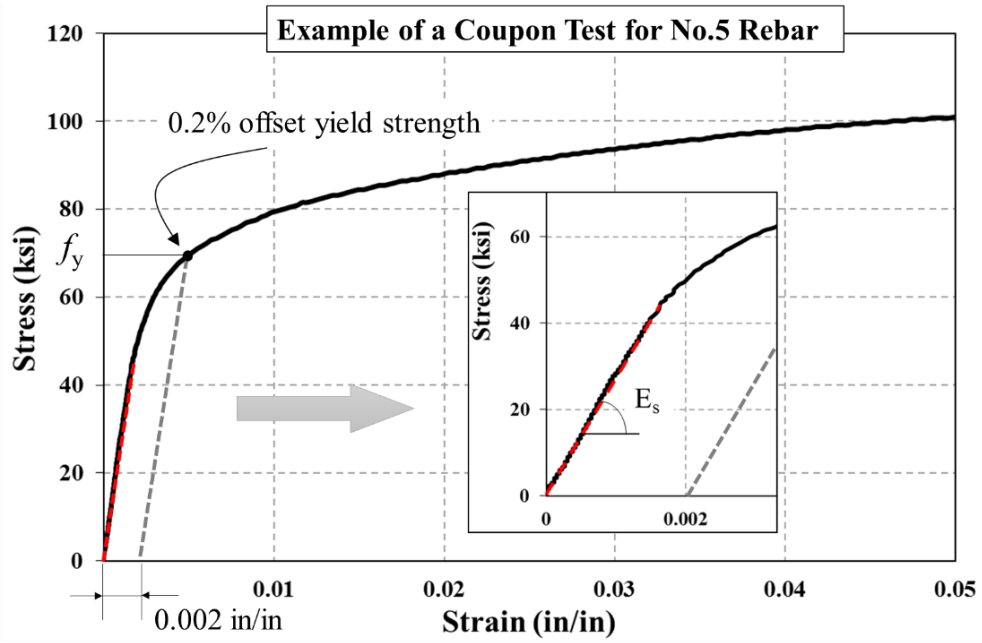

Fig. 4.4 Method of Calculating E_s and f_y for No. 4 and No. 5 Rebar

Table 4.1 Mechanical Properties of the Rebars

Rebar Size	f_y (ksi)	f_u (ksi)	E_s (ksi)	ε_u
No.3	66.5	87.4	27,359	0.245
No.4	67.0	106.2	27,565	0.212
No.5	68.0	107.1	28,326	0.240

4.2.3 FRP Sheets

In the experimental program, two types of FRP sheets were used, namely Tyfo® SCH-11UP and Tyfo® SCH-41S. The manufacturer Fyfe Co. suggests to use the Tyfo® S Epoxy as the adhesive for the application of these two FRP sheets. The Epoxy has two components A and B, which are mixed by a ratio (by volume) of 100:42 for 5 minutes at a mixer speed of 400-600 RPM until uniformly blended. And the curing time of the epoxy was suggested to be at least 72 hours. To have a quality control of the bond strength of the FRP-concrete interface, the standard pull-off tests were carried out by using the Dyna Z16 pull-off tester. The test follows the requirements of ASTM D7522. Before the pull-off test, several 2 in diameter cores were cut by a core drill, then the 2 in diameter aluminum disks were attached onto the FRP sheets by Devcon high strength epoxy, with manufacture tested strength of 1500 psi, see Fig. 4.5a). The strength of the epoxy has to be greater than the epoxy used for the FRP sheets to guarantee the failure happened inside the concrete. When testing, the disk was attached to the pull-off tester and the pull-off load was applied by the manual crank, see Fig. 4.5b). The ultimate load was captured by the load indicator and used to calculate the pull-off strength. Fig. 4.5c) shows a typical failure mode. As per ACI 440.2R-08, the minimum bond stress $f_{pull\text{-}off}$ required for the FRP-concrete interface is 200 psi. The details of the pull-off test results are presented in the Table 4.2 of the following section. The test results showed that the bond strength satisfies the ACI requirements. Coupon tests for the FRP composites were conducted by Moslehy (2010) and the results gathered from coupon tests showed a close correlation (within 5% difference for both Young's Modulus E_f and ultimate stress f_{fu}) with those shown as test results by the

manufacturer. The material properties of the FRP sheets were presented in Table 4.2 in the following sections.

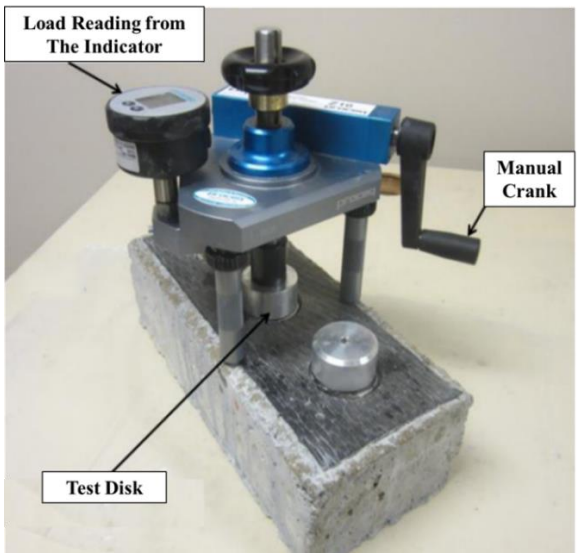

b) Setup of Pull-off Test

a) Disk Attached to Core

c) Typical Failure Mode

Fig. 4.5 Pull-off Tests for the FRP-concrete Interface

4.3 UNIAXIAL TENSION TEST

4.3.1 General Introduction

The tensile constitutive laws of steel and concrete are required in the modified softened truss model theory. Uniaxial tension tests were designed to study these constitutive laws. As mentioned in the literature review, there exists a high interaction between the components that constituting the composites when subjected to tension. Thus, different combinations of FRP/steel reinforcement ratios were designed in the research. Also, as a key issue affecting the behavior of FRP strengthened RC members, the effect of different wrapping scheme was also studied. Three most commonly used wrapping methods were chosen, namely fully wrap, side bonding, and U-wrap with anchors. The details of the three wrapping schemes are shown in the following sections.

The test specimens were prisms with a cross section of $10^{1}/_{8}$ in. × 7 in., and 55 in. in length. The FRP sheets were applied on two opposite sides of the specimen. The FRP sheets are 8 in. wide and applied using the wet layup method. To prevent the local failure in the loading zone at the specimen end, additional confinement plates were installed through threaded rods. The reinforcing bars were welded onto a pre-embedded connector inserts that were connected to the loading actuators. Fig. 4.6 shows the details of the specimen. The test matrix of the uniaxial tension test is shown in Table 4.2. The specimens are identified by steel rebar sizes (#3, #4 and #5), FRP thicknesses (0.025 in and 0.040 in), and wrapping schemes (Fully Wrap, Side Bond, U-wrap with FRP Anchor). As an example: S4-025-SB stands for the specimen with #4 rebar, 0.025 in thick FRP sheet and Side Bond (SB) wrapping scheme method. REF-R3, REF-R4, and REF-R5 stand for RC reference specimens with #3, #4 and #5 rebars, repectively.

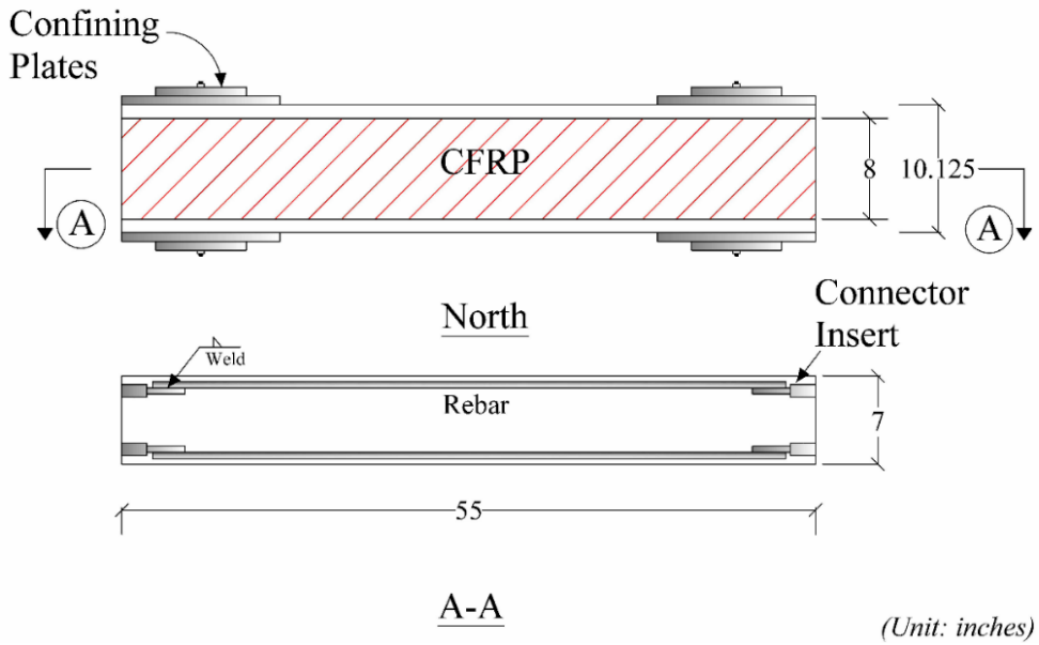

Fig. 4.6 Specimen of the Uniaxial Tension Test

Table 4.2 Material Properties of the Uniaxial Tension Test

Specimen Name	f'_c (psi)	ρ_s (%)	f_y (ksi)	E_s (ksi)	ρ_f (%)	$f_{u,FRP}$ (ksi)	E_f (ksi)	$f_{pull\text{-}off}$ (psi)
REF-R3	6,119	0.31	66.5	27,359	0	NA	NA	NA
REF-R4	6,119	0.55	67.0	27,565	0	NA	NA	NA
REF-R5	6,119	0.87	68.0	28,326	0	NA	NA	NA
S3-025-FA	6,699	0.31	66.5	27,359	0.56	120	12,000	610
S3-040-FA	6,699	0.31	66.5	27,359	0.90	127	10,500	610
S4-025-FA	6,971	0.55	67.0	27,565	0.56	120	12,000	680
S4-040-FA	6,699	0.55	67.0	27,565	0.90	127	10,500	610
S5-025-FA	6,699	0.87	68.0	28,326	0.56	120	12,000	610
S5-040-FA	6,971	0.87	68.0	28,326	0.90	127	10,500	680
S4-025-SB	6,119	0.55	67.0	27,565	0.56	120	12,000	550
S4-040-SB	6,971	0.55	67.0	27,565	0.90	127	10,500	680
S4-025-FW	6,119	0.55	67.0	27,565	0.56	120	12,000	550
S4-040-FW	6,971	0.55	67.0	27,565	0.90	127	10,500	680

For the test matrix, it can been see that the main parameters studied are steel reinforcement ratio, FRP reinforcement ratio and wrapping schemes. Several other parameters were kept constant, as shown Table 4.3.

Table 4.3 Constants and Studied Variables in Uniaxial Tension Test

Constants	Variables
Concrete strength Concrete thickness Cover length Spacing of rebar FRP Configuration	Steel reinforcement FRP reinforcement Wrapping Schemes

4.3.2 Fabrication of the Specimen

4.3.2.1 Casting

The formwork used to cast the prismatic specimen was developed using the formwork for panels, see Fig. 4.7. Six 3/8 in thick high strength steel plates were welded onto the formwork to create the required sizes of the prism specimen. As shown in Fig. 4.8, five specimens were cast at one time. Extra bars (12 in long) were welded at the end zone to prevent the local damage of the specimen. Ten PVC tubes were pre-embedded inside the

formwork for the bolts of the confinement plates. The U-shape hooks were pre-embedded for the handling during the removal of the panel after cured.

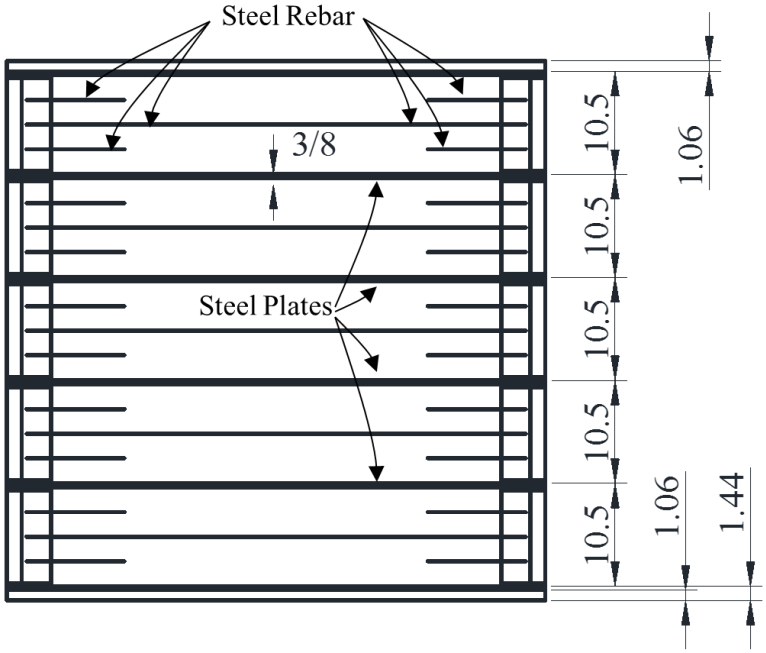

Fig. 4.7 Layout of the Formwork for Uniaxial Tension Test

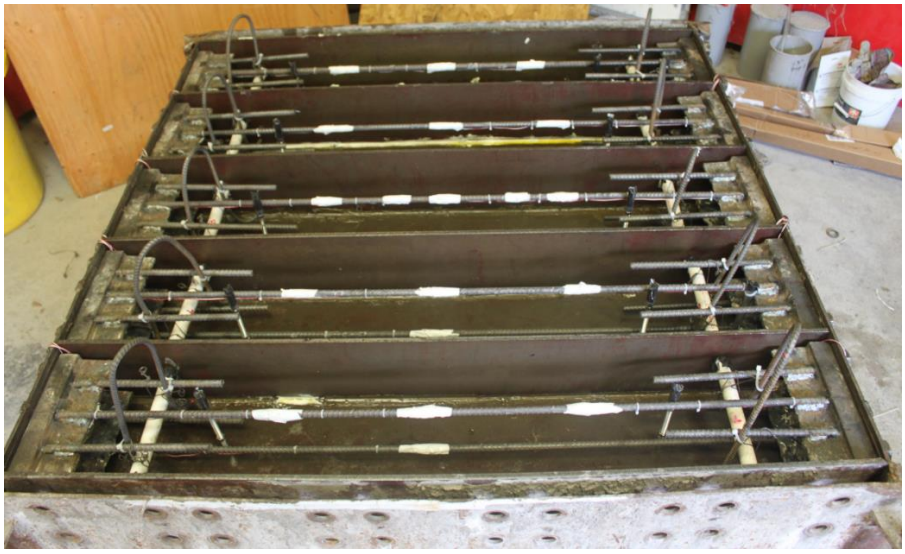

Fig. 4.8 Formwork for the Prismatic Specimen

4.3.2.2 Application of the FRP Sheets

The wet lay-up system was used for installation of FRP sheets. The specimen was first grinded, sandblasted and power washed to provide proper concrete surface conditions that would develop the necessary bond strength between the concrete and FRP sheets. The grinding was to smoothen the concrete surface to ensure a full contact with FRP sheets. The sandblasting and power washing was to remove all the loose parts on the surface. As suggested by the manufacturer, putty was applied to fill the small holes on the surface. During application, primer (a thin layer of the same epoxy used as adhesive) was applied first on the surface and waited for 30 minutes, then the FRP sheets were then impregnated by epoxy resin and applied in-situ. Rollers were used to ensure a good contact between FRP sheets and concrete surface, extra epoxy was also removed. Specimens were then cured in the air-conditioned lab temperature at least 72 hours before testing.

Three different wrapping schemes were used, including Fully Wrap (FW), Side Bond (SB) and U-wrap with FRP Anchors (FA), as shown in Fig. 4.9a)-c), respectively. For simplicity, U-wrap with FRP anchor was referred to as FRP Anchor (FA) in this document.

The FRP anchor provides a new way of anchoring the composite to the RC structure. After it was invented in Japan (Jinno and Tsukagishi, 1998), there have been several investigations regarding the design recommendation (Eshwar et al, 2003 and 2008; Orton, 2007; Niemtz, 2008). The considered parameters when designing the FRP anchor include anchor diameter, anchor amount and anchor length. The FRP anchor used in this research was Tyfo® SCH Composite Anchor manufactured by Fyfe. Co. As shown in Fig. 4.9c), the anchor has a diameter of 0.5 in and length of 24 in. The contact length of 8.5 in was

adequate to cover the whole width of the FRP sheets with 0.25 in extra on both sides, which satisfies the recommended length by Kobayashi et al. (2001). The edge of the anchor hole needs to be grinded to avoided the stress concentration, in this research, the corner was grinded with a diameter of 0.5in, which is recommended by ACI 440. The FRP anchor was fabricated by a bundle of the same carbon fiber as the FRP sheets to provide compatibility between the materials used. After saturating the FRP anchor into epoxy resin, one end of the anchor was inserted through a pre-drilled hole on the concrete surface, and the extra fibers from both sides were then fanned out on top of the FRP sheet, then another small piece of saturated FRP sheets was applied on top of the anchorage area. The details of a typical FRP anchor application are shown in Fig. 4.10.

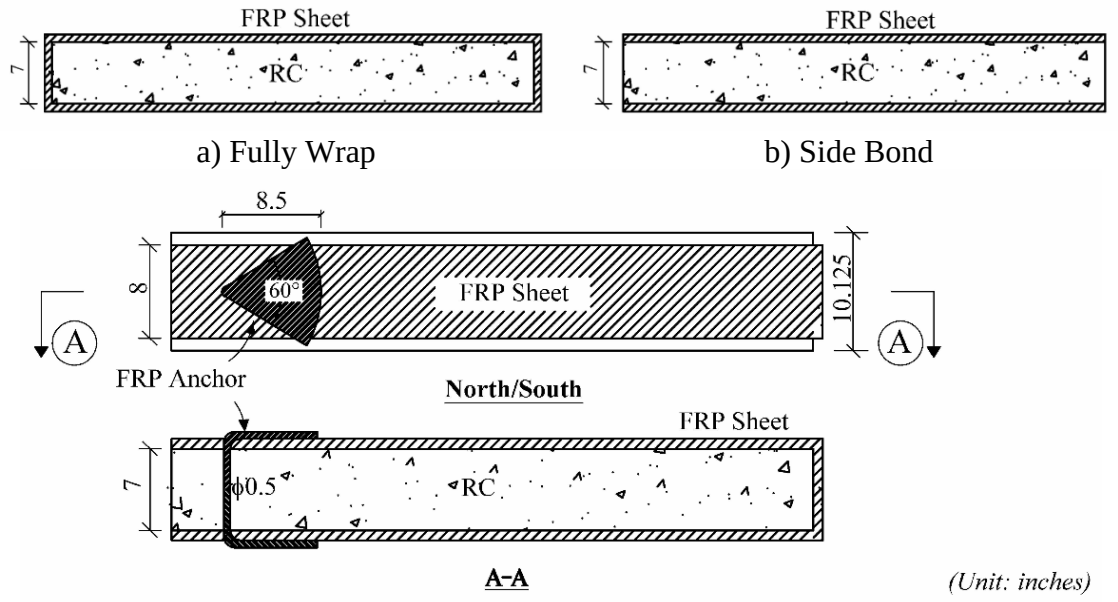

c) U Wrap with FRP Anchor

Fig. 4.9 Wrapping Scheme and FRP Anchor Details

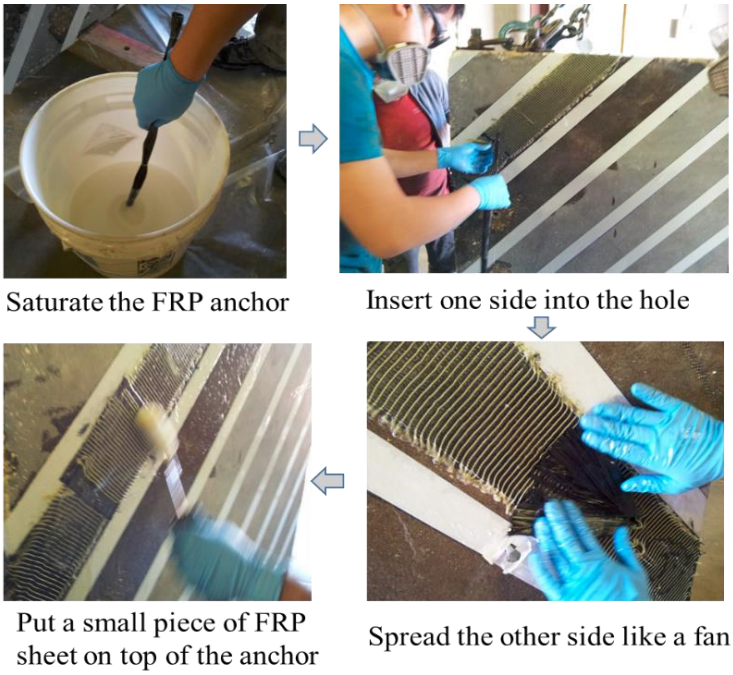

Fig. 4.10 Typical Procedure of FRP Anchor Application

4.3.3 Experimental Setup

The test setup for uniaxial tension test is shown in Fig. 4.11. At each end of the specimen, two hydraulic actuators with a total tension capacity of 400 Kips were used to apply tensile loading to the specimens through the pin connections on the connector yokes. To create a reaction against the gravity, two rollers were installed underneath the connector yokes. Fig. 4.12 shows the typical setup of a tested specimen REF-3 (reference specimen with #3 Rebar). The height of the roller support is adjusted to make sure the specimen is perfectly aligned with the hydraulic actuators. For the test procedure, load control was first used until the cracks occurs, after that the displacement control mode was used until the failure of the specimen. In the loading control mode, tensile load was applied at an increment of 0.5 kips/jack/min. For the displacement control steps in the post-cracking stage, the increment of the strain is set to 0.0001 (in/in)/min.

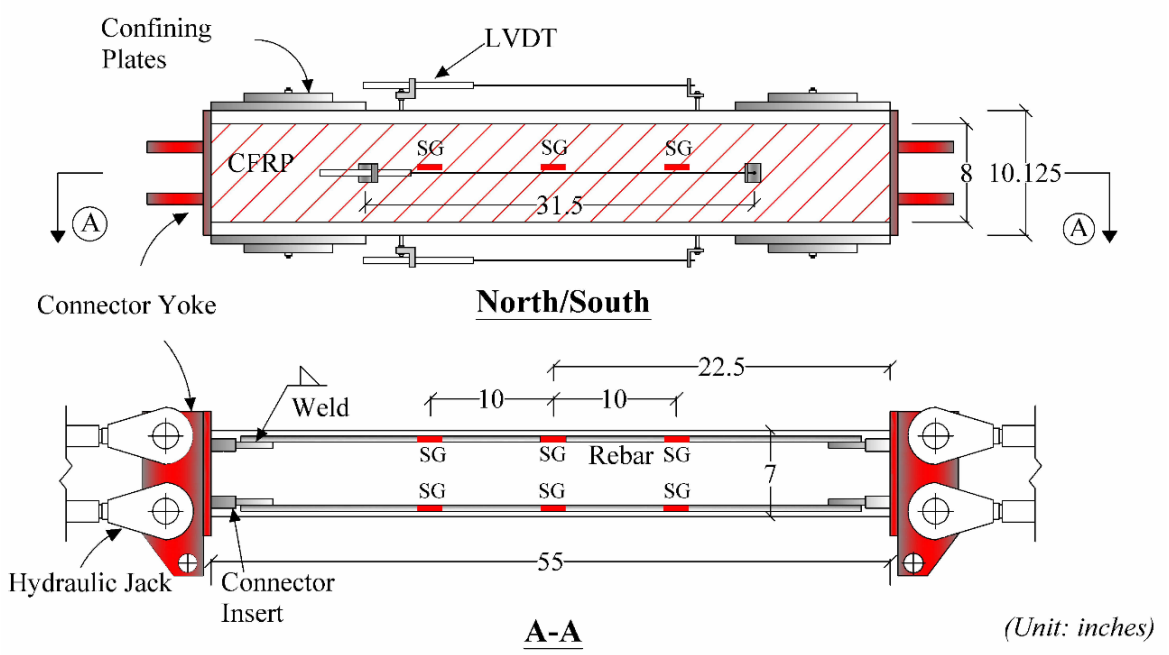

Fig. 4.11 Test Setup of the Uniaxial Tension Test

Fig. 4.12 Typical Setup for Uniaxial Tension Test

4.3.4 Instrumentation

For the uniaxial tension test, several instruments were used: the load was measured by the load cells installed on each actuator; the average strain was measured by the two LVDTs attached to the specimen; the local strains on the rebar and FRP were measured by the strain gauges; A digital image correlation (DIC) system, ARAMIS (GOM MbH., Germany) was used to capture the strain field on one side of the specimen.

4.3.4.1 Measurement Instrumentation

Each of the actuators has a calibrated load cell installed, the total tension load on each side of the specimen was taken as the summation of the two actuators on this side, and the tension load used in the derivation of the material laws is taken as the average of the total tension loads on each side.

As previous shown in Fig. 4.11, two LVDTs with a range of 2 in were installed on North and South side to measure the average deformations of the specimen. The measured length is 31.5 inches, which provides a sufficient distance of 11.75 inches away from the edge to avoid the stress non-uniformity at the end zone. Since the specimens were hold horizontally during the test, before the test started, the specimen was carefully adjusted to make sure the applied tension loads were perfectly aligned with the specimen. In order to monitor the effect of bending during the test, two additional LVDTs were installed on the top and bottom surface of the specimen. Strain Gauges (SG) were applied on the rebar and FRP sheets to monitor the local strains along these materials.

4.3.4.2 DIC system

A digital image correlation (DIC) system, ARAMIS (GOM MbH., Germany, 2011) was used in the test to obtain the displacement and deformation field on the South side of the specimen. DIC systems are well known techniques of non-contact optical measurement of deformations and strains. A suitable pattern with equal area of black-white spots should be achieved to ensure the accuracy of the measurements, see Fig. 4.13. The camera has a built-in coordinate system so that the position of the black-white dots can be recorded as (x,y,z) for different loading stages. Full field strain of a specimen were captured by

collecting digital images in the test and comparing them with the initial images (undeformed specimen).

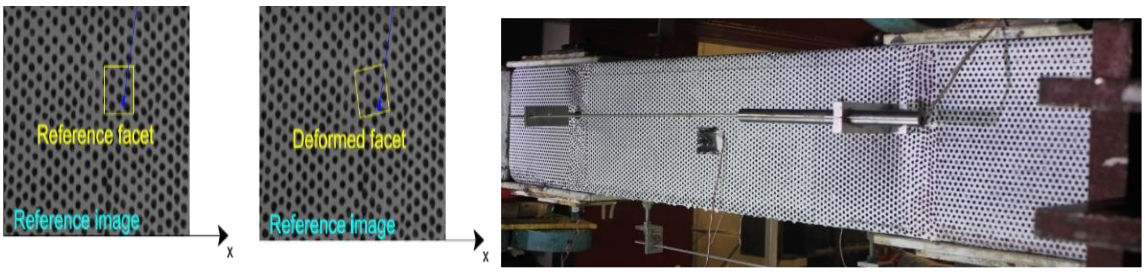

Fig. 4.13 Pattern on the Concrete Surface

Two cameras were used to capture a stereographic image of the specimen in a 3D measurement (Fig. 4.14). The position of the cameras was determined by system calibration. Calibration is performed by taking pictures of a calibration panel through a set range of motions within the volume where the measurement is being captured. The ARAMIS DIC-3D software by GOM was used in the post-processing. By post-processing the images, the software (i.e., GOM mbH, 2011) will recognize the dots in the pattern and locate them in a pre-defined coordinate system. A facet is used because it has a wider variation in gray levels which can be uniquely identified from other facets in the deformed image (Gencturk et al., 2014). Typically increasing the facet size increases the accuracy of the measurements but lowers the spatial resolution which is defined by the facet size (Ghiassi et al., 2013).

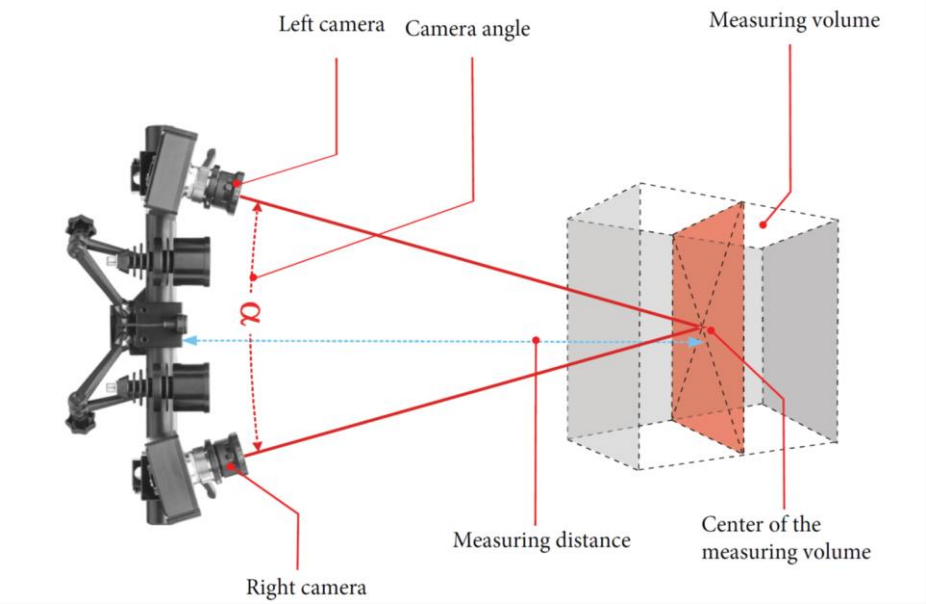

Fig. 4.14 ARAMIS 3D Sensor Setup

The specimens in the research program were prepared by applying a speckle pattern as shown in Fig. 4.13. A thin layer of white flat paint was first applied on the surface, covered by black dots using spray paint. In the test set-up, the DIC system was positioned facing the South surface of the specimen. A laser pointer in front of the camera was used to guarantee the correct alignment of the camera to the specimen. The measurement distance for the tests was set to be approximately 80 in. The aperture of the lens was f/11 and the shutter time was set to 55 msec. Several light sources was adjusted to maintain a bright and uniform light condition. In order to avoid statistically correlated measurements, the facet step was set to be 15×15 pixels and the facet size was 19×19 pixels according to the User Manual.

4.4 BIAXIAL TENSION-COMPRESSION TEST

4.4.1 Introduction

The biaxial tension-compression tests were conducted to study two topics: the softening coefficient of the concrete and the Hsu/Zhu ratio in FRP RC element. The specimens for these two tests were similar. But the loading procedures were quite different. In the following section, the details of the tests are presented.

The specimens of these two tests were square panels with the 90° steel reinforcement layout, as shown in Fig. 4.15. The specimen was 55 inches × 55 inches and had a thickness of 7 inches. The spacing of the reinforcement was 10.5 inches. The FRP sheets used in this test was 8 inches wide which were applied the same direction as the horizontal reinforcements.

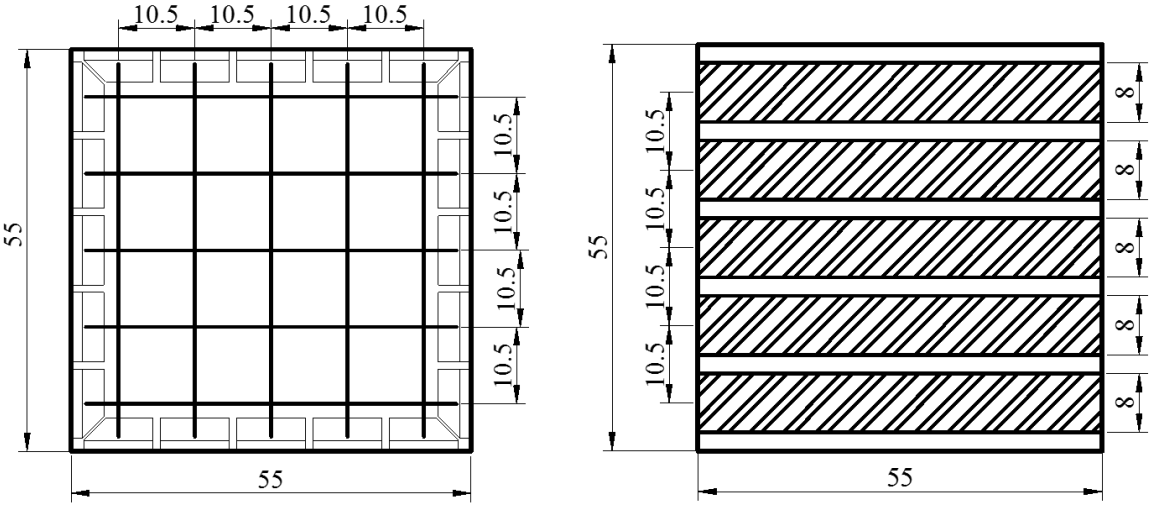

Fig. 4.15 Layout of the Panels

The test matrix of the biaxial tension-compression test is shown in Table 4.4. For softening test, F2 stands for Fiber type 2, which is Tyfo® SCH-41S; and P stands for Panel, the specimen number at the end of the name is numbered continuously after test conducted

by Moslehy (2010). For the Hsu/Zhu ratio test, PR stands for Poisson Ratio, and followed by the thickness of the FRP used for this specimen. As an example, PR-025 stands for the specimen with 0.025 in. thick FRP sheets. For the softening test, the main test parameters, average tensile strain ε_1, is also listed.

Table 4.4 Material Properties of the Biaxial Tension-Compression Test

Test	Specimen Name	f'_c (psi)	ρ_s (%)	f_y (ksi)	E_s (ksi)	ρ_f (%)	$f_{u,FRP}$ (ksi)	$f_{pull\text{-}off}$ (psi)	E_f (ksi)	ε_1
Softening Test	F2P-5	5,471	0.51	67	27,565	0.83	127	530	10,500	0.0025
	F2P-6	6,237	0.51	67	27,565	0.83	127	640	10,500	0.0055
	F2P-7	5,742	0.51	67	27,565	0.83	127	640	10,500	0.0075
Hsu/Zhu Ratio Test	PR-025	5,934	0.51	67	27,565	0.52	120	760	12,000	NA
	PR-040	5,334	0.51	67	27,565	0.83	127	680	10,500	NA
	PR-080	6,023	0.51	67	27,565	1.66	127	790	10,500	NA

4.4.2 Fabrication of Test Specimens

The formwork of the biaxial testing panels is shown in Fig. 4.16. Two layers of steel rebars were welded on to the connector inserts which were fastened onto the formwork by threaded bolts. Some threaded bolts with coupling nuts on both sides were fastened onto the base of the formwork for the LVDT installation later on. Premature edge failures of the panel in tension have been reported by Molslehy (2010) and confinement plates were suggested to be installed to prevent the local failure. Several PVC tubes were pre-embedded along the tension side in the formwork, later on steel plates were fastened by threaded bolts through these pre-embedded holes.

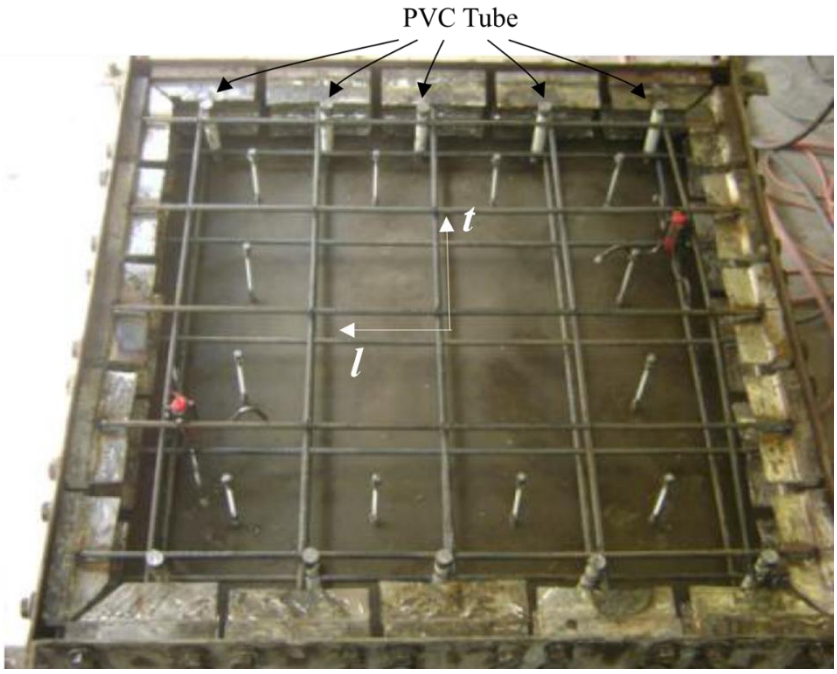

Fig. 4.16 Formwork of the Panels

4.4.3 Experimental Setup

The biaxial tension-compression tests were conducted by the UPT. As shown in Fig. 4.17, in total of 37 in-plane jacks and 3 rigid links were used to apply the biaxial loading. The specimen was first lifted using the 10-ton crane to a proper height, then fasten onto the two trolleys by threaded bolts. The trolley itself was attached onto two out-of-plane beams on the test frame. The crane was then removed and the specimen was pulled inside the machine. Each jack was then adjusted by using the manual control mode. Forty 4 in. diameter pins were installed to connect the yokes and the heads of the jacks. To ensure the stability of the specimen and the uniformity of the applied forces, two rigid links on the top and one rigid link on the East side were used. Three out-of-plane rigid links were also used to avoid the out-of-plane movement.

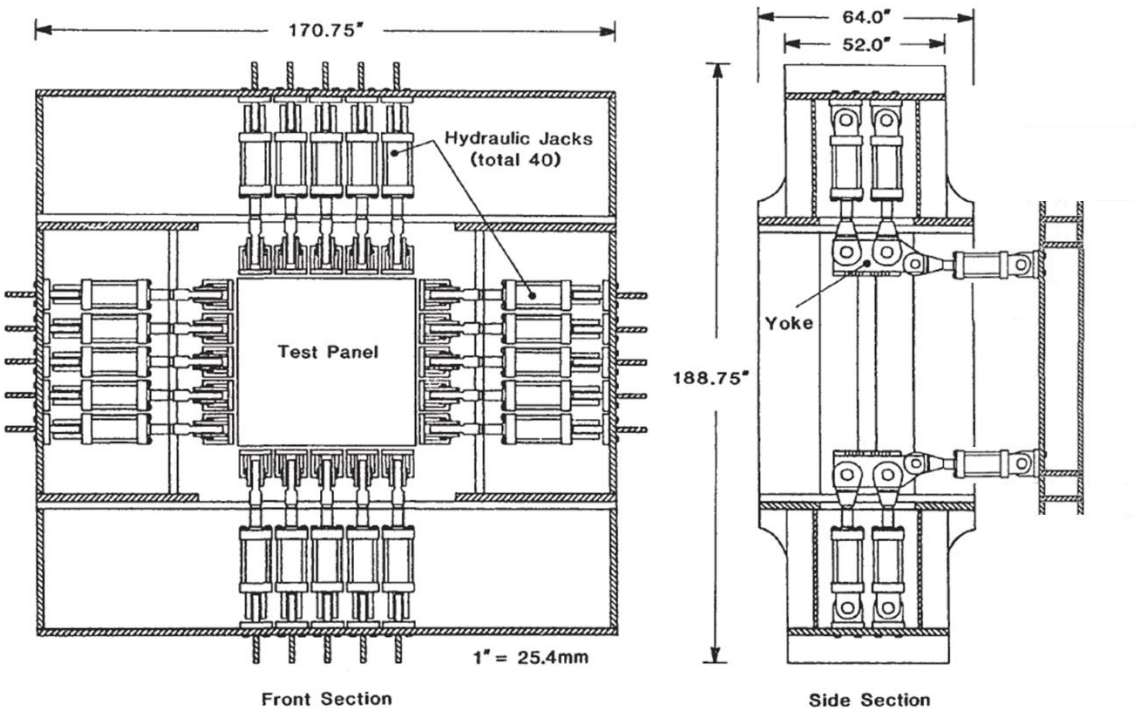

Fig. 4.17 Test Frame for the Biaxial Tension-compression Test

4.4.4 Instrumentation Methods

The strains of the specimen in the horizontal, vertical and diagonal direction were measured by a total of 20 LVDTs attached on both side of the specimen. The LVDT measurements were also used as feedback when using strain control. In this test, strain gauges were also used to measure the localized strain of the specimen, as shown in Fig. 4.18.

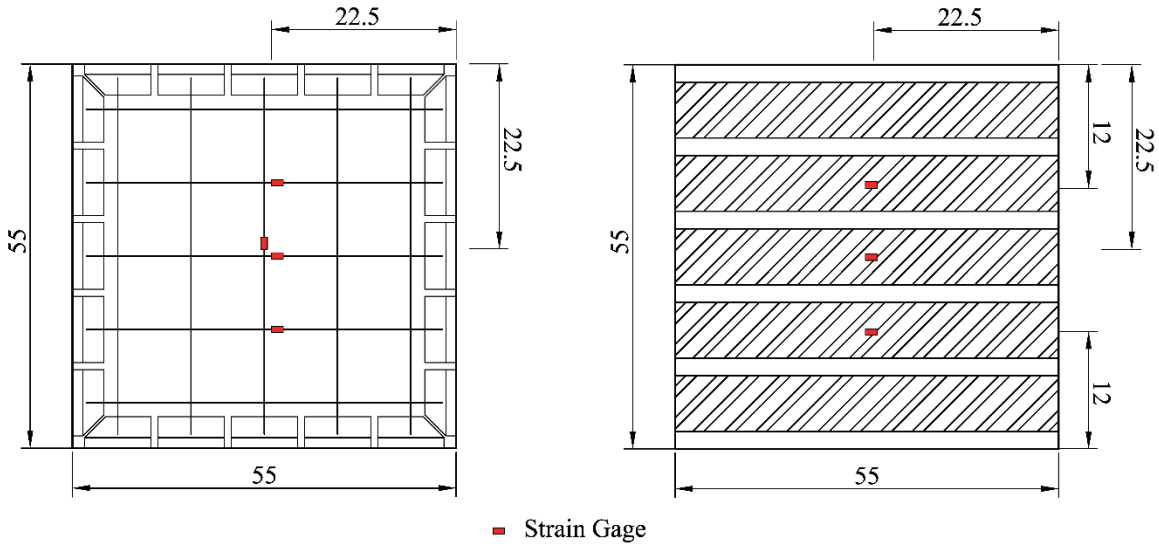

Fig. 4.18 Strain Gage Layout of the Test Panels

4.4.5 Loading Procedures

4.4.5.1 Softening Test

The softening test has two phases of loading: tension stage and compression stage. In the tension stage, tension load was applied to the specimen in the horizontal direction by load control until the yielding of the reinforcements, after that strain control was used till the designated strain level was reached, and then the strain was kept constant; in the compression stage, the compression load was applied using load control till the failure of the specimen in the vertical direction while the tensile strain in the horizontal direction was kept constant. Fig. 4.19 shows the load pattern.

4.4.5.2 Hsu/Zhu Ratio Test

The loading step includes two types: compression step and tension step. The load was sequential in tension-compression. For the compression step, compressive load was applied while tensile load was held constant and vice versa, see Fig. 4.20. Forty Kips increment was used in each step. Load control was used throughout the test.

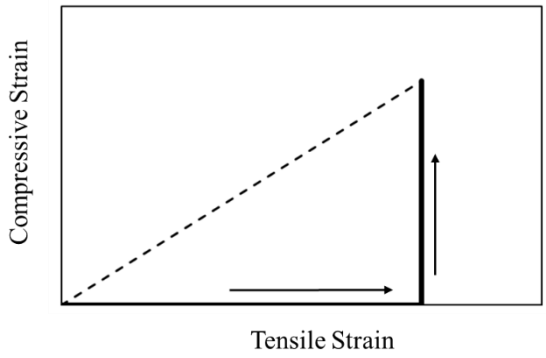

Fig. 4.19 Load Pattern for the Softening Test

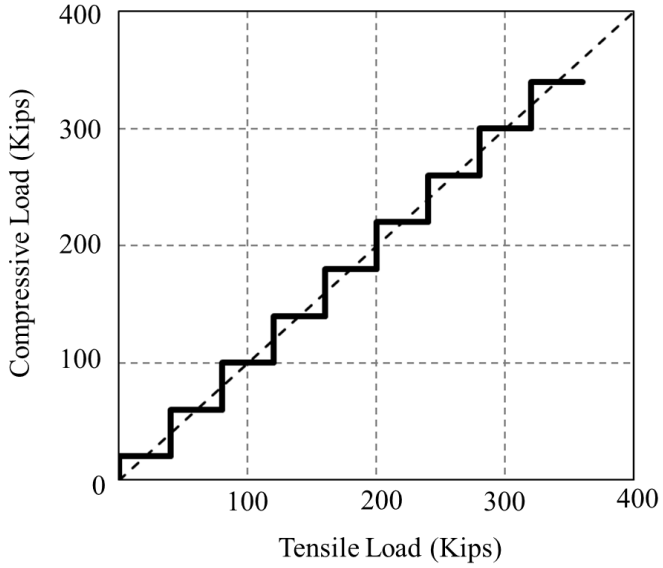

Fig. 4.20 Load Pattern for the Hsu/Zhu Ratio Test

4.5 SUMMARY

This chapter presents the detail of the experimental tests conducted in the research. The details of the test specimen, test setup, instrumentation method and the loading procedure are introduced. In the following chapter, the experimental and analytical results will be presented in detail.

CHAPTER 5 ANALYSIS OF THE TEST RESULTS

5.1 GENERAL

Softened truss model theory have been developed and widely used to predict the behavior of RC element under in-plane shear stress field. In the past three decades, the UH research group has proposed a series of softened truss models to predict the shear behavior of RC members (Pang and Hsu, 1996; Zhang and Hsu, 1998; Hsu and Zhu, 2002), of which the most recent one is the Softening Membrane Model (SMM). The SMM has been proven to be able to predict the whole stress-strain curve of the RC member under in-plane pure shear stress field (Hsu and Mo, 2010). The SMM requires three equilibrium equations, three compatibility equations, and a set of constitutive laws that links stress and strain. The SMM model was developed for RC element, but the concept can be applied onto FRP RC element. Fig. 5.1 shows the stress diagram for an FRP RC element under in-plane stresses. The FRP RC element (Fig 5.1a) was subjected to in-plane stresses. This element contains several material components, namely concrete element (Fig. 5.1b), steel grid element (Fig. 5.1c) and FRP strip element (Fig. 5.1d). In SMM, the cracks were assumed to occur along the principal direction 2. After cracking, the concrete became several struts that carries compression stress σ_2 in 2 direction, also the tension σ_1 in 1 direction (due to tension stiffening effect), see Fig. 5.1e)-f). The equilibrium equations can be developed along the *l* and *t* directions by the stress transformation equations:

$$\begin{aligned}
\sigma_l &= \sigma_1^c \cos^2\alpha_1 + \sigma_2^c \sin^2\alpha_1 - \tau_{12}^c 2\sin\alpha_1\cos\alpha_1 + \rho_l f_l + \rho_{fl} f_{fl} \\
\sigma_t &= \sigma_1^c \sin^2\alpha_1 + \sigma_2^c \cos^2\alpha_1 + \tau_{12}^c 2\sin\alpha_1\cos\alpha_1 + \rho_t f_t + \rho_{ft} f_{ft} \\
\tau_{lt} &= (\sigma_1^c - \sigma_2^c)\sin\alpha_1\cos\alpha_1 + \tau_{12}^c(\cos^2\alpha_1 - \sin^2\alpha_1).
\end{aligned} \tag{5-1}$$

It should be noted that besides the contributions of concrete and steel, two additional terms $\rho_{fl} f_{fl}$ and $\rho_{ft} f_{ft}$ were added into the equation to include the tensile contribution of FRP in the *l* and *t* directions.

Same as RC element, the strain variables in FRP RC element must satisfy the strain compatibility equations in the *l* and *t* directions:

$$\varepsilon_l = \varepsilon_1 \cos^2 \alpha_1 + \varepsilon_2 \sin^2 \alpha_1 - \frac{\gamma_{12}}{2} 2 \sin \alpha_1 \cos \alpha_1$$

$$\varepsilon_t = \varepsilon_1 \sin^2 \alpha_1 + \varepsilon_2 \cos^2 \alpha_1 + \frac{\gamma_{12}}{2} 2 \sin \alpha_1 \cos \alpha_1 \qquad (5\text{-}2)$$

$$\frac{\gamma_{lt}}{2} = (\varepsilon_1 - \varepsilon_2) \sin \alpha_1 \cos \alpha_1 + \frac{\gamma_{12}}{2} (\cos^2 \alpha_1 - \sin^2 \alpha_1).$$

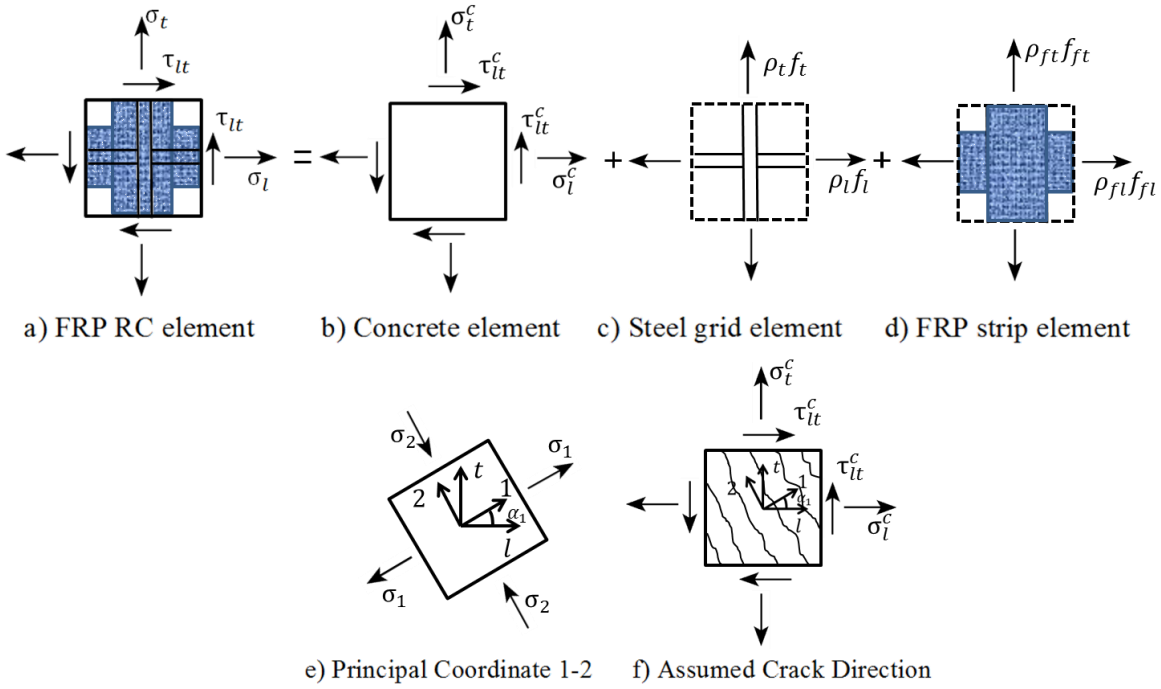

Fig. 5.1 Stress Diagram for FRP RC Element Subjected to In-plane Stresses

Besides the equilibrium and compatibility equations, a set of stress-strain relationships have to be provided to link the stress and strain variables. For concrete element in Fig. 5.1f), the stress-strain relationships are needed in the principal tensile

direction 1 and the principal compressive direction 2. Therefore the constitutive laws of concrete in tension (in principal direction 1) and concrete in compression (in principal direction 2) are required. For the steel element, since no dowel action is considered, only constitutive law of steel in tension (in *l* and *t* direction) is required. Similar to the steel reinforcement, the constitutive laws of FRP in tension (in *l* and *t* direction) is needed. As shown in Fig. 5.1, once the biaxial principal strains ε_1 and ε_2 along the crack direction are evaluated, the Poisson Ratios of cracked concrete are required to derive the equivalent uniaxial strains. In order to use the SMM to predict the behavior of the FRP RC element under in-plane shear stress field, new constitutive laws for each material component in FRP RC element have to be established. The material laws of SMM for FRP RC elements includes: concrete in tension, steel in tension, FRP in tension, concrete in compression and Hsu/Zhu ratios. These materials laws were modified based on the tests results in this research. By updating these constitutive laws, the new model SMM-FRP can be developed to predict the FRP RC element under in-plane shear stress field. The modified constitutive laws of concrete in tension, steel in tension, were determined from uniaxial tension tests for 13 FRP RC prims specimen; the modified softening coefficient and Hsu/Zhu ratios were investigated by biaxial tension-compression tests of six full-size FRP RC panels. The studied variables in uniaxial tension tests are steel reinforcement ratio, FRP reinforcement ratio and wrapping schemes; the studied variable in biaxial tension-compression tests is FRP reinforcement ratios.

In the following sections, the modifications of these constitutive laws are presented based on the test results. The derivations and validation of the proposed equations are also given.

5.2 CONCRETE IN TENSION

For un-strengthened RC members under uniaxial tension load, both concrete and steel exhibit an elastic behavior in the pre-cracking stage. After crack occurs, the entire tensile force is carried by the reinforcements at cracking section. However, the concrete continues to carry tensile stresses between the cracks through the bond actions between concrete and steel reinforcements, which effectively increases the stiffness of the member and reduces deflections. The phenomenon, also known as tension stiffening, is the contribution of the concrete to stiffness of the member. The concept of tension stiffening has been widely used in predicting the behavior of reinforced concrete members under service load. It is not only important in controlling the deflection of beams but also used for predicting multiple crack spacing and crack widths (Bischoff et al., 2003; Kong et al., 2007; Wu et al., 2009). The tension stiffening effect allows the stress transferring from the reinforcement to the surrounding concrete through the interface bond stress. For the tension stiffening in FRP RC element, the bond characteristics are different. The bonds that transfer the stress includes not only the bond between steel and concrete, but also the bond between FRP and concrete. Consequently, the tension stiffening behavior in FRP RC element was found to be altered. In the following sections, the behavior of concrete in tension is discussed in two stages: the behavior prior to cracking and the behavior after cracking. The analytical expressions were proposed for both stages.

5.2.1 Prior to Cracking

The test specimen is subjected to a tensile force P, oriented in the longitudinal direction of the specimen. The applied force is resisted by concrete, longitudinal internal

steel reinforcement and external bonded FRP sheets. Before cracking, steel, FRP sheets, and concrete are in the elastic range and the equilibrium equation can written as

$$P = A_s\sigma_s + A_f\sigma_f + A_c\sigma_c, \tag{5-3}$$

where σ_s, σ_f, and σ_c are the average stresses in steel, FRP, and concrete, respectively; A_s, A_f, and A_c are the areas of steel, FRP, and concrete, respectively.

The cracking stress is then determined by

$$f_{cr} = \frac{P_{cr}}{A_c} - \rho_s E_s \varepsilon_{cr} - \rho_f E_f \varepsilon_{cr}, \tag{5-4}$$

where ρ_s and ρ_f are the reinforcement ratios of steel and FRP, respectively; E_s and E_f are the modulus of elasticity of steel and FRP, respectively; ε_{cr} is the strain at cracking and P_{cr} is the force at cracking. The cracking strength and cracking strain were measured in the test and modulus of elasticity of concrete was then calculated. Table 5.1 lists the computed cracking strength f_{cr}, the observed cracking strains ε_{cr} and the corresponding modulus of elasticity of concrete E_c for each specimen. The specimens are identified by steel rebar sizes (#3, #4 and #5), FRP thicknesses (0.025 in and 0.040 in), and wrapping schemes (Fully Wrap, Side Bond, U-wrap with FRP Anchor). REF-R3/R4/R5 stands for RC reference specimens with #3/#4/#5 rebars. It was found that the expressions proposed by Belarbi and Hsu (1994) for RC fit very well with the test results. It was found that the extra bond stress from FRP did not help postpone the cracking, the cracking strength and modulus of elasticity were found to be similar to that of RC. The result seems rational because in the pre-cracking stage, the load is mainly taken by concrete due to its much

greater area compared to FRP and steel, so FRP and steel did not contributed too much in tension before cracking. The test data fits the expression

$$f_{cr} = 3.75\sqrt{f_c^{'}(\text{psi})} \text{ and} \tag{5-5}$$

$$E_c = 47,000\sqrt{f_c^{'}(\text{psi})} \,. \tag{5-6}$$

The comparisons between 13 experimental results and predictions of Eqns. (5-5) and (5-6) are plotted in Fig. 5.2. The ratio of experimental to predicted f_{cr} has a mean value of 1.015 and a coefficient of correlation of 40.2 %, and the ratio of experimental to predicted E_c has a mean value of 0.967 and a coefficient of correlation of 38.8%. The expression has a good agreement with test results. It should be noted that ACI 318-14 (2014) used the square root expression with a coefficient of 3.5 for shear cracking in beams, which is very close to the 3.75 proposed in this study.

Table 5.1. Test Results for Specimens at Cracking Stage

Specimen	f'c (psi)	f_{cr} (psi)	ε_{cr} ($\times 10^{-6}$)	E_c (ksi)
REF-R3	6,118	326	80	4,078
REF-R4	6,118	291	83	3,511
REF-R5	6,118	278	81	3,437
S3-025-FA	6,697	265	85	3,122
S3-040-FA	6,697	293	83	3,529
S4-025-FA	6,969	357	98	3,640
S4-040-FA	6,697	307	83	3,704
S5-025-FA	6,697	313	83	3,773
S5-025-FA	6,969	309	78	3,960
S4-025-SB	6,118	267	89	2,998
S4-040-SB	6,969	274	76	3,606
S4-025-FW	6,118	264	81	3,258
S4-040-FW	6,969	312	80	3,897

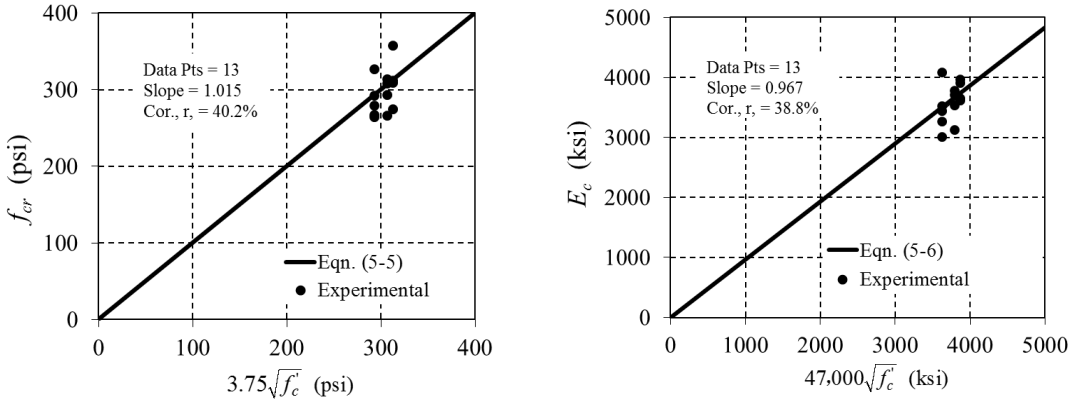

Fig. 5.2 Comparison of the Test Results and Eqn. (5-5) & (5-6)

5.2.2 Post-cracking Behavior

After cracking occurs, the stress distribution along the length of the member becomes non-uniform. At the crack location, the tensile stress is carried by steel rebar and FRP sheets. Between the cracks, the tensile stress will be transferred to concrete gradually through the bond actions. The bond actions in FRP RC element contain two components: bond action on the interface between concrete and internal steel rebar and bond action between interface between concrete and externally bonded FRP sheets. Fig. 5.3 shows the schematic distribution of stresses, strains, and forces between two cracks along the length of the tested FRP RC member. The maximum strains for FRP and steel are assumed to be the same at the crack location, and gradually reduce due to the bond action on the interface. For simplicity, the strain distributions for FRP and steel are assumed to be the same along the length of the member. The concrete stress is zero at the crack location but increases by the bond stress and reaches maximum at the center between two cracks, the strains for concrete, steel and FRP at the center between two cracks were assumed to be the same.

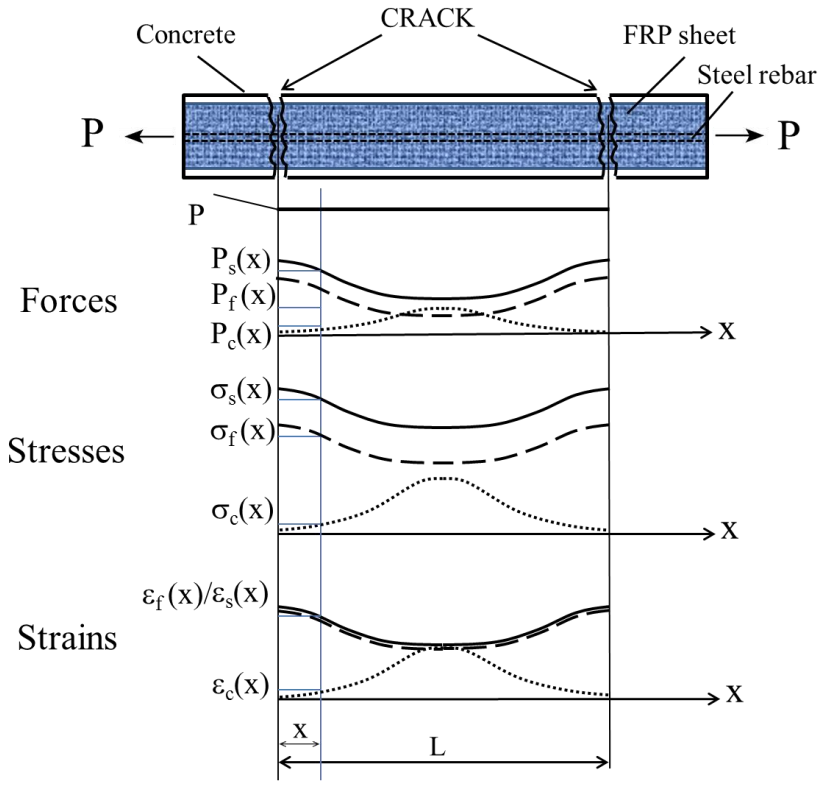

Fig. 5.3 Schematic Distribution of Force, Stress and Strain for Cracked FRP RC under Unaxial Tension Stress Field (adopted from Belarbi and Hsu, 1994)

The average stress of the steel and FRP can be obtained by

$$\sigma_s = \frac{1}{L}\int_0^L \sigma_s(x)\,dx \text{ and} \tag{5-7}$$

$$\sigma_f = \frac{1}{L}\int_0^L \sigma_f(x)\,dx, \tag{5-8}$$

where σ_s and σ_f are the average stresses in steel and FRP; $\sigma_s(x)$ and $\sigma_f(x)$ are the stresses in steel and FRP at a distance x along the length measured from a crack and L is the distance between two adjacent cracks.

Since the concrete cracked at a lower level of strain, the steel and FRP are still in the elastic range and therefore the calculations of average stresses are given as

$$\sigma_s = E_s \frac{1}{L}\int_0^L \varepsilon_s(x)\,dx = E_s\varepsilon_1 \text{ and} \tag{5-9}$$

$$\sigma_f = E_f \frac{1}{L}\int_0^L \varepsilon_f(x)\,dx = E_f\varepsilon_1, \tag{5-10}$$

where σ_s and σ_f are the average stresses of steel and FRP, respectively; $\varepsilon_s(x)$ and $\varepsilon_f(x)$ are the local strains for steel and FRP at a distance x from a crack, respectively. The average strain ε_1 is given as

$$\varepsilon_1 = \int_0^L \varepsilon_s(x)\,dx = \int_0^L \varepsilon_f(x)\,dx. \tag{5-11}$$

Hence Eqn. (5-1) becomes

$$P = A_s E_s \varepsilon_1 + A_f E_f \varepsilon_1 + A_c \sigma_c. \tag{5-12}$$

Stress in concrete can be calculated from Eqn. (5-12) as

$$\sigma_c = \frac{\mathrm{P}}{A_c} - \rho_s E_s \varepsilon_1 - \rho_f E_f \varepsilon_1. \tag{5-13}$$

Although Eqn. (5-13) and Eqn. (5-4) have the same form for calculating average stress of concrete before and after cracking, the right hand side represents two different concepts: Before crack occurs, the strain distributions of concrete, steel and FRP are uniform, thus the "average" strain ε_1 also equals to the "local" strain at any location along the length of the specimen. However, in the post-crack stage, the average strain ε_1, also known as smeared strain, includes not only the deformation of the material but also the crack widths. The concept of smeared stress/strain is applied herein so that the cracked FRP RC element can be considered as a homogeneous material. Using Eqn. (5-13), the average stress-strain curve of concrete in tension can be obtained.

Before presenting the tensile stress strain curves of concrete in tension, it should be noted that most of the study related to tension stiffening failed to consider the effect of shrinkage (Sato and Vecchio, 2003). It was found by Kaklauskas et al. (2009) that most of the tension stiffening models were derived based on the test results of specimens that already experienced shrinkage. This shrinkage contains short-term shrinkage and long-term shrinkage (related to creep). Viktor et al. (2014) conducted a statistical analysis of all the available tests related to tension stiffening in literature and concluded that if the shrinkage is not considered, the tension stiffening curve will have an unexpected "negative" portion and thus be underestimated. To eliminate the effect of shrinkage on the behavior of the concrete in tension, the shrinkage strains were calculated for all the tested specimens. In the following section, the method of calculating the shrinkage is presented.

5.2.3 Shrinkage

In the study, since all the tests were conducted within 40 days, only the short-term (creep insignificant) shrinkage effect was considered using the approach proposed by Kaklauskas et al. (2008). When the concrete starts shrinking, compression is developed in the rebar while tension is developed in the concrete. In this approach, a fictitious axial force was proposed to evaluate the effect of the shrinkage on the specimen. The strains in the concrete and steel due to shrinkage were proposed as

$$\varepsilon_{c,sh} = -\frac{\varepsilon_{sh} E_s A_s}{E_c A_c + E_s A_s} \text{ and} \tag{5-14}$$

$$\varepsilon_{s,sh} = \frac{\varepsilon_{sh} E_c A_c}{E_c A_c + E_s A_s}, \tag{5-15}$$

where ε_{sh} is the shrinkage strain of a plain concrete specimen with same material, size and curing conditions as the test specimen. Viktor et al. (2014) calculated the shrinkage strain ε_{sh} of concrete using an approach based on *Eurocode 2* (2004). In this study, same approaches were applied to account for the effect of shrinkage for each specimen. The total shrinkage strain ε_{sh} is composed of two components, namely the drying shrinkage strain ε_{cd} and the autogenously shrinkage strain ε_{ca}:

$$\varepsilon_{sh} = \varepsilon_{cd} + \varepsilon_{ca}. \tag{5-16}$$

The details of the equations for calculating the drying shrinkage strain and autogenously shrinkage strain are available in Annex B of *Eurocode 2 EN 1992-1-1* (2004). The calculation for the shrinkage strains in this study is presented in Appendix II. The relative humidity (RH), specimen sizes, material properties, and curing time required in the calculation were measured and presented in detail in Appendix II. Table 5.2 lists all the results for the shrinkage strain in each specimen.

Table 5.2 Shrinkage Stress and Strain for the Test Specimen

Specimen	ε_{sh}	E_c	E_s	$\varepsilon_{c,sh}$	$\varepsilon_{s,sh}$	$\sigma_{c,sh}$	$\sigma_{s,sh}$
	μ in/in	ksi		μ in/in		ksi	
REF-R3	-157.80	4,070	27,352	3.22	-154.58	0.0131	-4.23
REF-R4	-152.97	3,931	27,558	5.68	-147.29	0.0223	-4.06
REF-R5	-142.81	3,670	28,319	8.98	-133.83	0.0330	-3.79
S3-025-FA	-144.35	3,429	27,352	3.48	-140.86	0.0119	-3.85
S3-040-FA	-159.00	4,280	27,352	3.09	-155.91	0.0132	-4.26
S4-025-FA	-150.25	4,350	27,558	5.06	-145.19	0.0220	-4.00
S4-040-FA	-188.10	4,298	27,558	6.41	-181.70	0.0275	-5.01
S5-025-FA	-163.62	4,225	28,319	9.02	-154.61	0.0381	-4.38
S5-040-FA	-223.19	4,350	28,319	11.96	-211.23	0.0520	-5.98
S4-025-SB	-162.47	3,666	27,558	6.45	-156.02	0.0236	-4.30
S4-040-SB	-180.87	4,445	27,558	5.96	-174.91	0.0265	-4.82
S4-025-FW	-166.99	4,350	27,558	5.62	-161.37	0.0245	-4.45
S4-040-FW	-199.00	4,350	27,558	6.70	-192.30	0.0291	-5.30

5.2.4 Effect of Different Parameters on Concrete in Tension

In the following section, the effects of different parameters on the stress strain curve of concrete in tension were investigated. The studied parameters includes: a) steel reinforcement ratio; b) FRP reinforcement ratio; c) wrapping schemes. For ease of comparison, the average stress of concrete in tension was normalized by the tensile strength of the specimen. Table 5.3 lists all the variables and the test specimens that were tested to study them. The test specimens were divided by three groups to study three variables.

Table 5.3 Test Specimens and the Variables Studied for Concrete in Tension

Group	Test Specimen	Constants	Variables
I	S3-025-FA, S4-025-FA, S5-025-FA S3-040-FA, S4-040-FA, S5-040-FA	FRP Reinforcement Wrapping Schemes	Steel reinforcement
II	REF-R3, S3-025-FA, S3-040-FA REF-R4, S4-025-FA, S4-040-FA REF-R5, S5-025-FA, S5-040-FA REF-R4, S4-025-SB, S4-040-SB REF-R4, S4-025-FW, S4-040-FW	Steel reinforcement Wrapping Schemes	FRP Reinforcement
III	S4-025-SB, S4-025-FA, S4-025-FW S4-040-SB, S4-040-FA, S4-040-FW	Steel reinforcement FRP Reinforcement	Wrapping Schemes

5.2.4.1 Effect of Steel Reinforcement Ratio

Fig. 5.4 shows the stress strain curves of concrete in tension for specimens with same FRP reinforcement ratio and wrapping scheme but various steel reinforcement ratios. This figure shows that the tension stiffening effect tends to be greater in the specimen with higher steel reinforcement ratio.

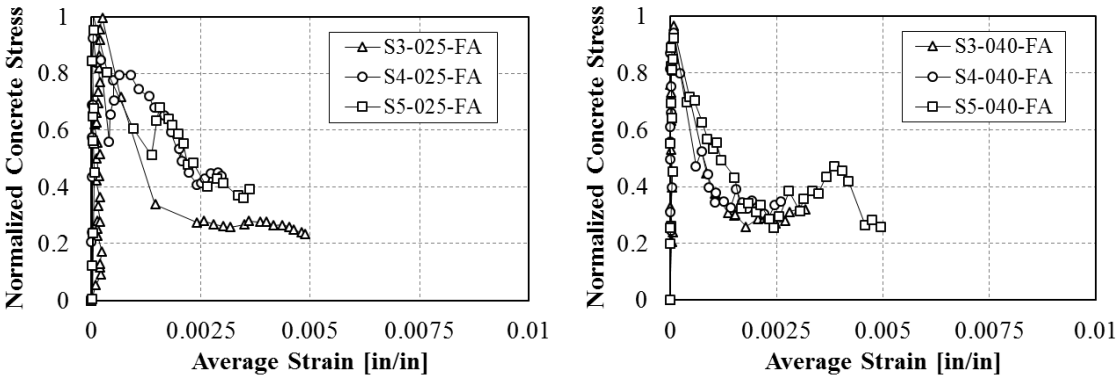

a) Specimen (ρ_f = 0.56%, FRP Anchors) b) Specimen (ρ_f = 0.90%, FRP Anchors)

Fig. 5.4 Tension Stiffening for Specimens with Various Steel Reinforcement Ratios

This phenomenon can be explained by the change of the bond characteristics in specimen with different steel reinforcement ratios. Bentz (2005) conducted a comparison of different tension stiffening equations in literature (Vecchio and Collins, 1982; Collins and Mitchell, 1987; Tamai et al., 1987; Vecchio et. al., 1994; Belarbi and Hsu, 1994; Pang and Hsu, 1995). He concluded that the most important factor that affects the tension stiffening is the ratio of the concrete cross-section area to the average bond area of the reinforcement. This so-called bond parameter *M* was proposed as

$$M = \frac{A_c}{\sum d_b \pi}, \tag{5-17}$$

and the tension stiffening of concrete is given as

$$f_1 = \frac{f_t}{1 + \sqrt{3.6M \cdot \varepsilon_1}}, \tag{5-18}$$

where f_1 is the average tensile stress in concrete and f_t is the cracking strength.

A smaller ratio M indicates stronger bonding condition, and consequently a greater tension stiffening effect. The conclusion of this study was verified with several test results in database and the proposed equation can predict the test data well in general. The conclusion of this study can be used to explain the phenomenon observed in this test that

with the increase in rebar size, the bonding area increases and consequently the tension stiffening effect becomes more significant.

5.2.4.2 Effect of FRP Reinforcement Ratio

Fig. 5.5 shows results for specimens with same steel reinforcement ratio and wrapping scheme but various FRP reinforcement ratios. It can be observed that compared with un-strengthened reference specimen (REF-R4), the specimen with FRP exhibited a greater tension stiffening effect. Also, when compared the specimen wrapping with different thickness of FRP sheets, it was found that the specimens strengthened with thinner FRP sheets (smaller FRP reinforcement ratio), trend to have a greater tension stiffening effect.

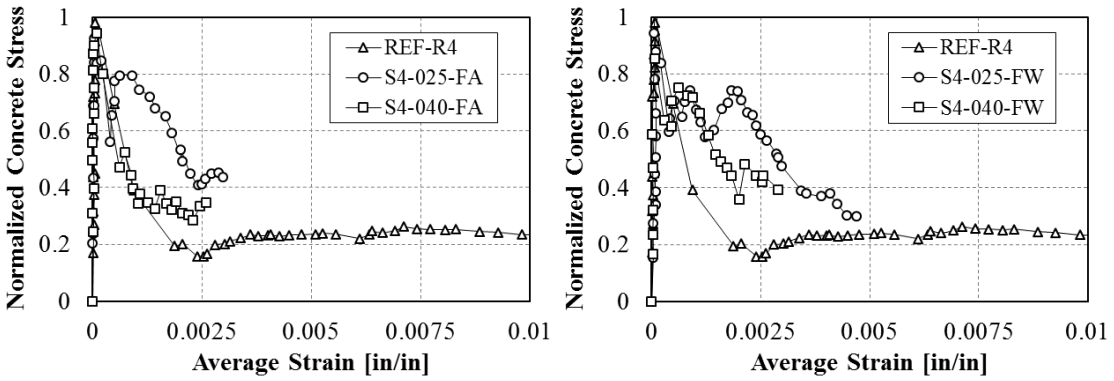

a) Specimen (ρ_s = 0.55%, FRP Anchors) b) Specimen (ρ_s = 0.55%, Fully Wrap)

Fig. 5.5 Tension Stiffening for Specimens with Various FRP Reinforcement Ratios

Same conclusions were also put forward by other researchers (Ueda et al., 2002; Farah and Sato, 2011). In the tests conducted by Ueda et al. (2002), strain gauges were applied on the steel rebar at a 1.6 in spacing and on the FRP sheets at a 0.8 in spacing. The whole strain distribution along the rebar and FRP sheets was captured for different loading steps, and the bond stresses between concrete and FRP/steel along the specimen were calculated based on the strain distribution profile. Explanation for this phenomenon was

given as follows. The average concrete stress is developed by two bond actions, namely the bond between concrete and steel rebar, and the bond between concrete and FRP sheets. As an example, Fig. 5.6 shows the tensile stress strain curve for S-3 series (Farah and Sato, 2011), in which, the same RC specimens were strengthened with different layers of FRP sheets, and Fig 5.7 shows the average bond stress with respect to average tensile strain. It can be observed that, with the increase of FRP stiffness, the bond between steel and concrete decreases dramatically while the bond between FRP and concrete increases slightly. Consequently, the decrease of the bond stress between steel and concrete is dominant, and the combination of these two bond actions decreases, which leads to a decrease of the tension stiffening effect.

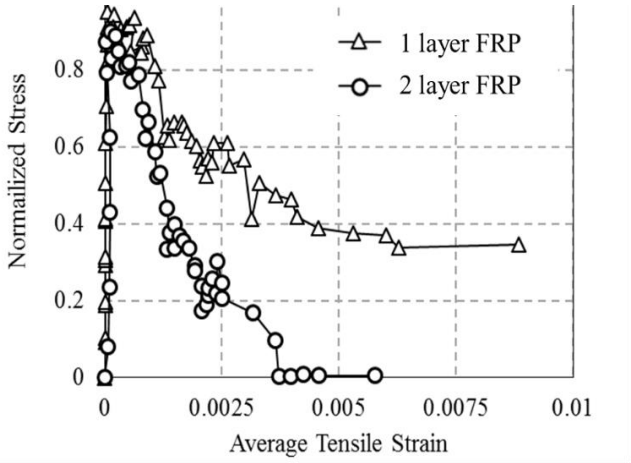

Fig. 5.6 Tension Stiffening for S-3 Series (Farah and Sato, 2011)

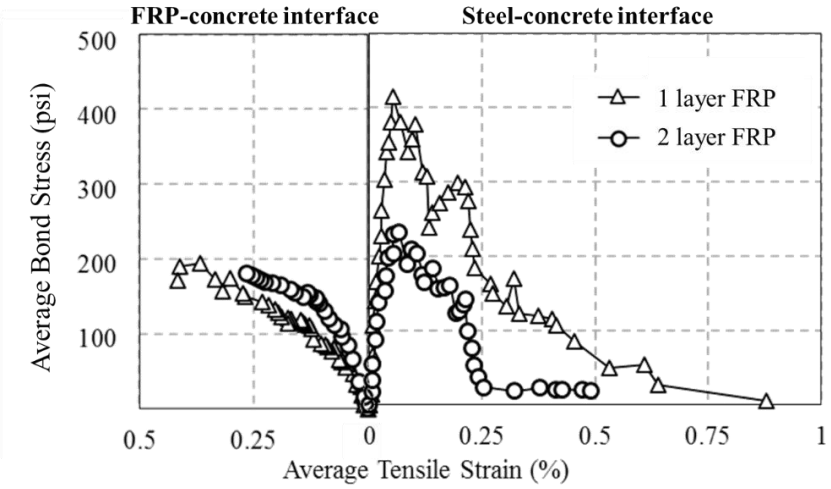

Fig. 5.7 Average Bond Stress for S-3 Series (Farah and Sato, 2011)

5.2.4.3 Effect of Wrapping Scheme

Fig. 5.8 shows the results for the average stress strain curve of concrete in tension for specimen with same FRP and steel reinforcement ratio but using different wrapping schemes. It can be observed that the tension stiffening is more evident in specimens strengthened using the fully wrap and FRP anchor method than those using side bonding methods. A great number of test results have indicated a better bond performance on the concrete-FRP interface using fully wrap or U-wrap with a proper anchorage system rather than side bonding (Uji, 1992; Sato et al., 1996; Khalifa and Nanni, 2002; Beber, 2003; Monti and Liotta, 2005; Sim et al., 2005; Bukhari et al., 2010; Panigrahi et al., 2014). The greater tension stiffening effect for the fully wrap and FRP anchor can also be attributed to the greater performance of the bond action due to these wrapping methods.

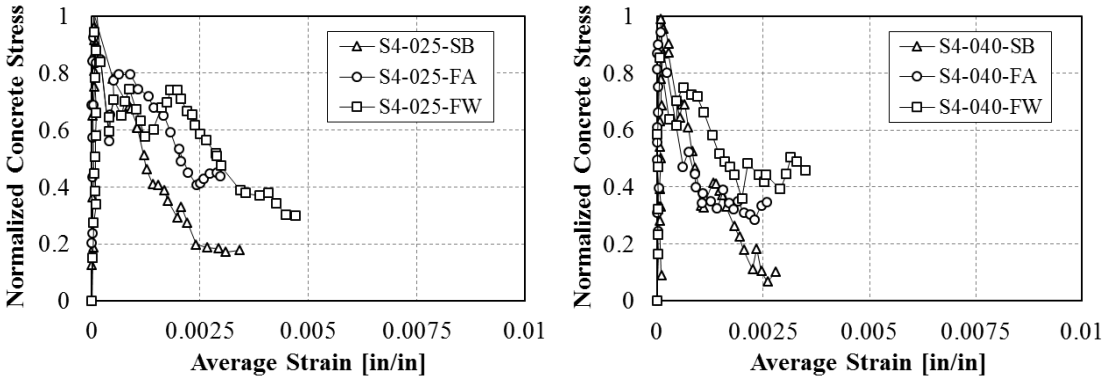

a) Specimen (ρ_s = 0.55%, ρ_s = 0.56%) b) Specimen (ρ_s = 0.55%, ρ_s = 0.90%)

Fig. 5.8 Tension Stiffening for Specimen with Different Wrapping Schemes

Numerical study was conducted by Dai et al. (2006) to analyze the full-range strain distribution on FRP-concrete interface. Bond-slip model was proposed in this study. The interfacial facture energy G_f and interfacial ductility index B in the bond-slip model were calibrated and upper and lower bounds of G_f and B were proposed for different bond conditions (fully wrapping, proper mechanical anchors, and side bonding). These models were used to investigate the tension stiffening effect for different bonding conditions (Dai et al., 2012). The results showed similar conclusion that the tension stiffening effect of concrete tends to become weaker for a weaker bonding method, such as side bonding method.

5.2.5 Proposed Equations

The chosen format of the tension stiffening model is

$$\sigma_c = E_c \varepsilon_1 \qquad \text{when } \varepsilon_1 \le \varepsilon_{cr} \text{ and} \tag{5-19}$$

$$\sigma_c = f_{cr}\left(\frac{\varepsilon_{cr}}{\varepsilon_1}\right)^c \qquad \text{when } \varepsilon_1 > \varepsilon_{cr}. \tag{5-20}$$

The chosen form of the tension stiffening model was first proposed by Okamura et al. (1985) and later on modified by Tamai et al. (1987). Belarbi and Hsu (1994) proposed c equals to 0.4 based on test results of 17 large scale RC panels. The coefficient c was originally proposed as a constant depending on the bond characteristics in RC element. In the proposed equation, this concept can be applied to describe the bond characteristics in FRP RC elements. To account for the effects of FRP reinforcement, steel reinforcement, and the wrapping schemes, the coefficient *c* is proposed as

$$c = K_w K_{f/s}\,, \tag{5-21}$$

where K_w and $K_{f/s}$ are two factors considering the effects of wrapping scheme and the ratio of FRP and steel stiffness, respectively.

By the mathematical regression of the test results using the given format in Eqn. (5-20), the experimental values $c_{\exp}$ were obtained. The relationships between $c_{\exp}$ and the wrapping scheme as well as the ratio of FRP and steel stiffness are shown in the Fig. 5.9 and Fig 5.10, respectively. Fig. 5.9 indicates that the fully wrap and U-wrap with FRP anchors have very close values of $c_{\exp}$. For simplicity, factor K_w for fully wrap and FRP anchors were assumed equal to 1, thus the factor K_w for side bonding wrapping scheme was normalized to be 1.6 by regression of the test data as below.

For full anchorage (rupture failure expected): fully wrap or U-wrap with anchors,

$$K_w = 1, \tag{5-22a}$$

and for other anchorage (non-rupture failure more likely): side bond or U-wrap,

$$K_w = 1.6\,. \tag{5-22b}$$

It should be noted that the expression for K_w is based on different anchorage conditions. For fully anchorages, it means the FRP sheets are fully wrapped or U-wrapped with proper anchorage system so that the rupture failure are more likely to occur rather than other failure modes. The proposed value of 1 is based on test results of specimen with the fully wrap and U-wrap with the particular FRP anchor used in this research, the details of FRP anchors was presented in Chapter 4. For the other anchorages like U-wrap without anchors or side bonding, non-rupture failure, such as debonding of FRP sheets, is more likely to occur. This factor was proposed to be 1.6 based on the test result for specimen with side bonding.

For $K_{f/s}$, a linear relationship between the coefficient $c_{\exp}$ and $\rho_f E_f / \rho_s E_s$ was observed with coefficient of determination of 0.82. The equation for $K_{f/s}$ is shown as

$$K_{f/s} = 0.25\left(\frac{\rho_f E_f}{\rho_s E_s}\right) + 0.15 . \tag{5-23}$$

The comparison between the $c_{\exp}$ and the proposed expression is shown in Fig. 5.11. The prediction and the test results show an acceptable agreement with coefficient of determination of 0.70.

The proposed equation was based on the regression of test data with $\rho_f E_f / \rho_s E_s$ between 0.25 and 1.11. However, the verification of the lower and upper bound values for the proposed equation requires more test results. Fig 5.12 shows the comparison of average stress strain curve of concrete in tension between the test results and the proposed models. An acceptable level of agreement was observed.

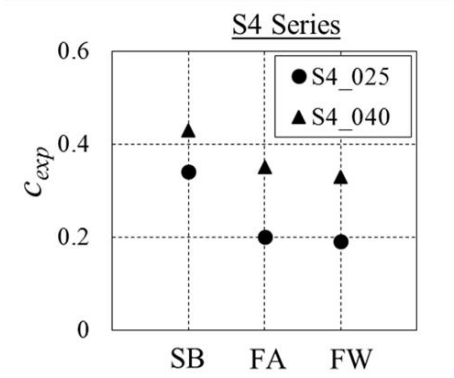

Fig. 5.9 Relationships between c_{exp} and the Wrapping Scheme

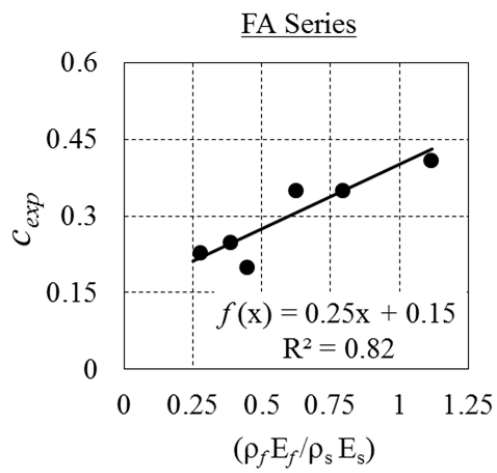

Fig. 5.10 Relationships between c_{exp} and the Ratio of FRP and Steel Stiffness

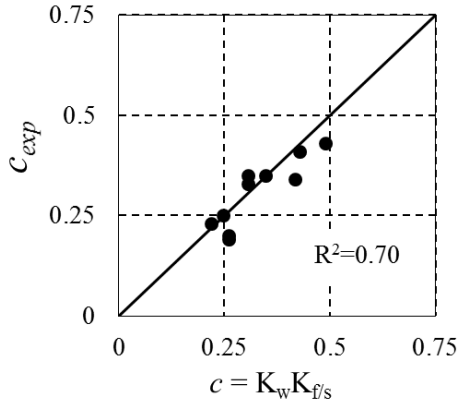

Fig. 5.11 Comparison between the Proposed Equation for c_{exp} and Experimental Results

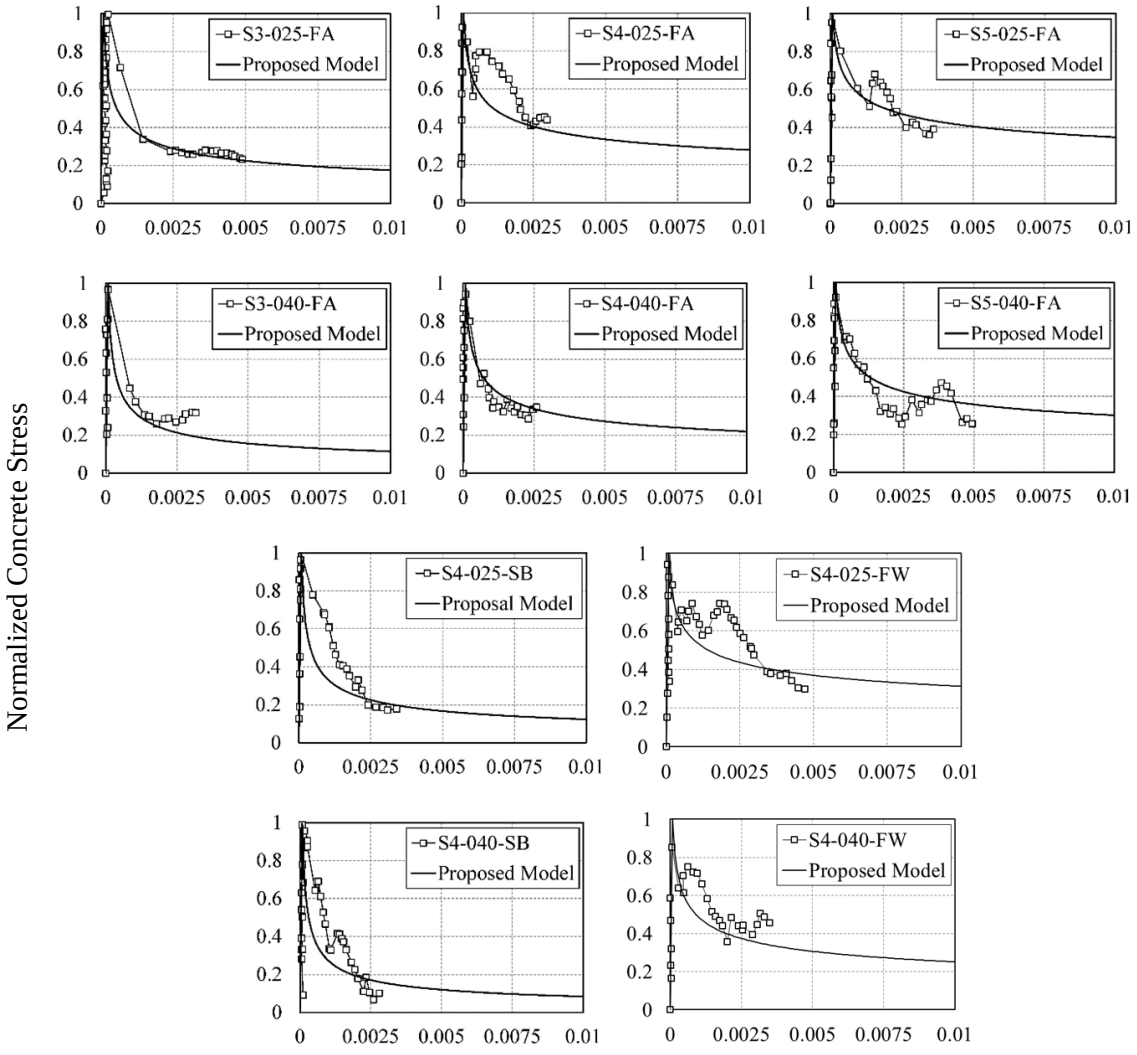

Fig. 5.12 Comprasion of Stress-strain Curve for Concrete in Tension between the Experimental Results and Eqns. (5-19)-(5-23)

5.2.6 Verification of Proposed Equations

The proposed equations were used to predict the tension stiffening curves of Farah and Sato (2011) to verify the accuracy. It should be noted that in their test, two confinement plates were fastened onto the FRP sheets to avoid the debonding failure at the end zone of the specimen, thus the wrapping scheme is assumed to be fully wrap, i.e., K_w is assumed to be 1. Also, Farah and Sato (2010) have considered the shrinkage effect in the analysis.

The comparison was conducted for the six specimens with the ratio of $\rho_f E_f / \rho_s E_s$ between 0.18-1.68. Fig 5.12 shows the comparison between the proposed model and the results from Farah and Sato's tests. A well agreement can be observed between them.

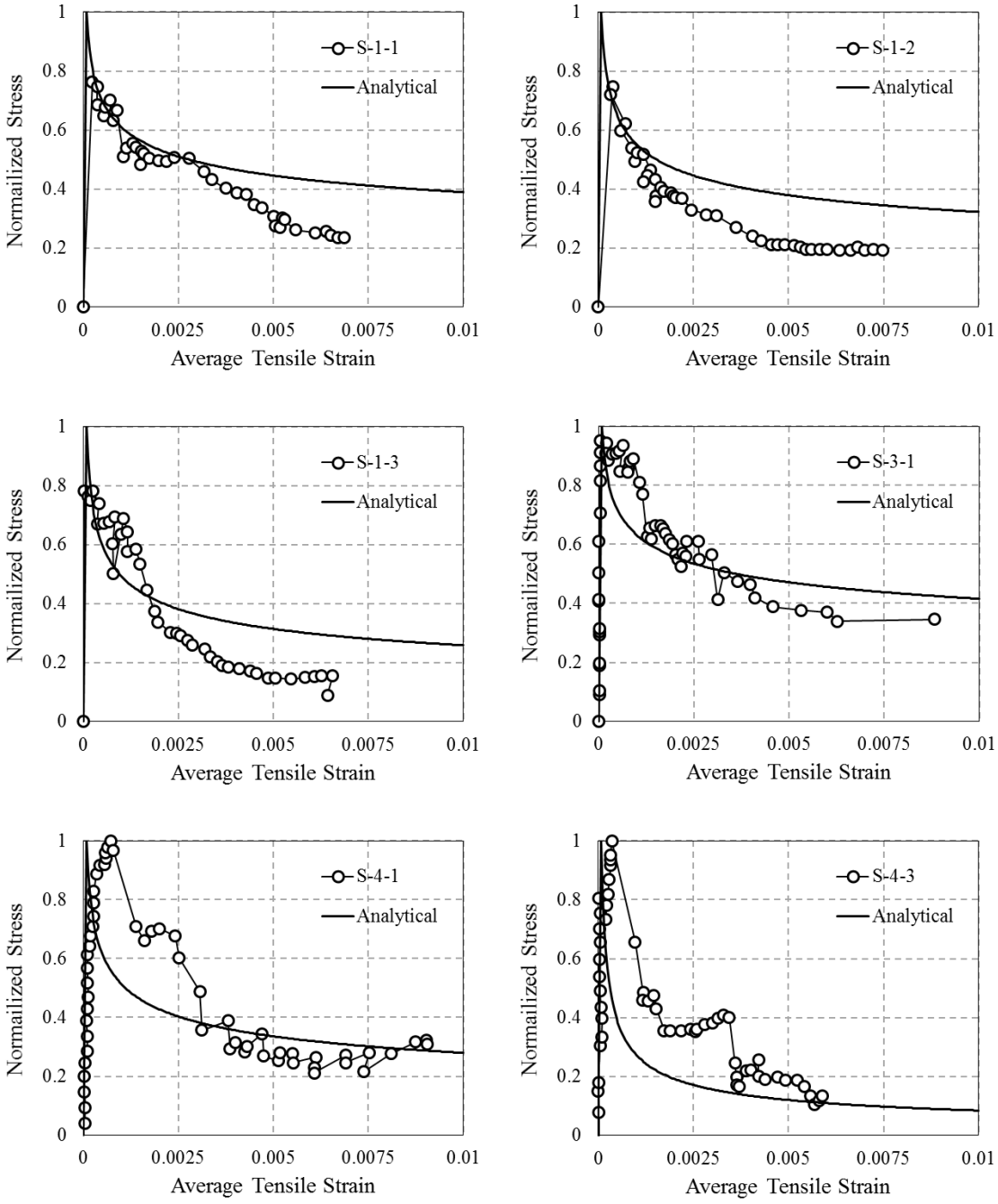

Fig. 5.13 Comprasion of Proposed Model and Test Results by Farah and Sato (2011)

5.3 STEEL IN TENSION

5.3.1 Apparent Yielding Point

Before crack occurs, the strain distributions for concrete, steel, and FRP are uniform along the specimen, therefore the stress strain relationship of steel is elastic. After crack occurs, the strain distribution becomes nonlinear as previously shown in Fig. 5.3. At a high strain level, the stress strain curve of the steel embedded in concrete is quite different than that of a bare rebar, a reduction of yielding stress was observed by several researchers (Okamura, 1985; Shima, 1987; Tamai, 1987; Belarbi and Hsu, 1994). This new yielding point in the average stress strain curve is called apparent yielding point. The phenomenon of apparent yielding was also observed for steel in FRP RC element.

The comparison between the stress strain relationships of steel in FRP RC element and those of bare rebars is shown in Fig. 5.14 a)-c). The results showed that the apparent yielding stress was altered due to the existence of the externally bonded FRP sheets. It can be observed that the apparent yield stress increases with the increase of FRP stiffness, especially for S3 series. This phenomenon can be explained by the crack characteristics of the specimen. Fig. 5.15 shows the crack patterns for different specimens in S3 series at the same strain level of 0.002. It can be observed that in the specimen strengthened with externally bonded FRP sheets, crack spacing is smaller compare to un-strengthened RC members. At the same strain level, smaller crack spacing indicates that the average crack width is smaller. This is attributed to the additional bond action on the FRP-concrete interface. This bond action reduces the crack width compared to un-strengthened RC. As a result, the local yielding of the rebar at the crack location was postponed, which leads to an increase of the apparent yield stress. Fig. 5.15 also shows that as the increase of the FRP

thicknesses, the crack width becomes smaller. This explains the phenomenon that with the increase of FRP thickness, the apparent yielding stress increases.

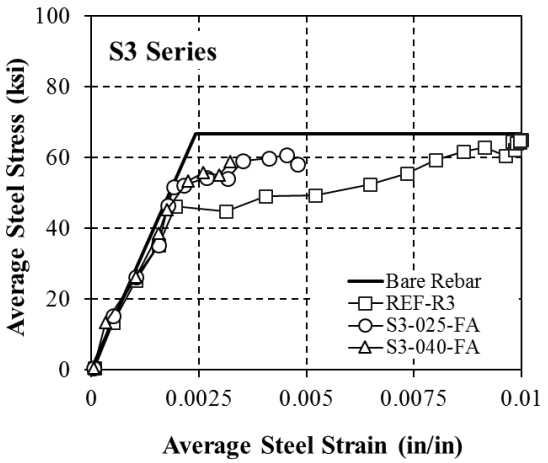

a) S3 Series (ρ_s = 0.31%, FRP Anchors)

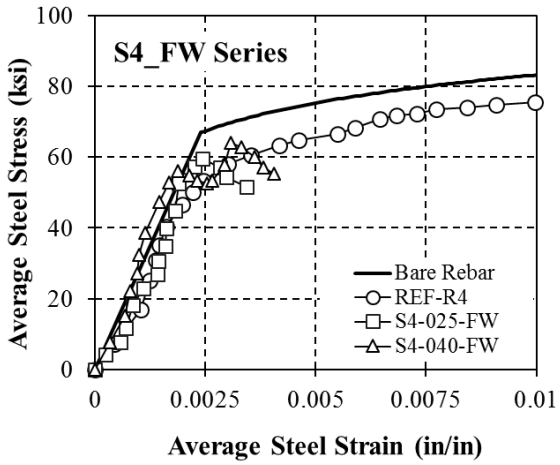

b) S4 Series (ρ_s = 0.55%, Fully Wrap)

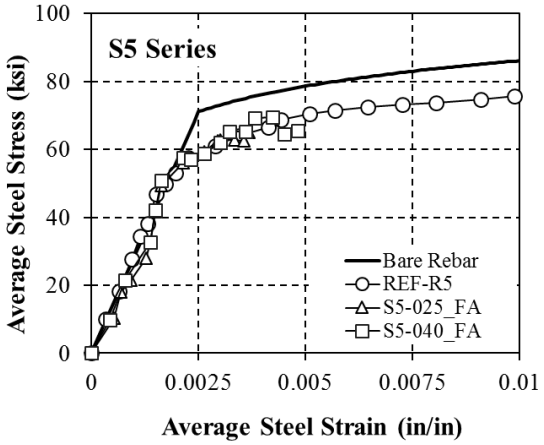

c) S5 Series (ρ_s = 0.87%, FRP Anchor)

Fig. 5.14 Average Stress Strain Curve of Steel in Tension

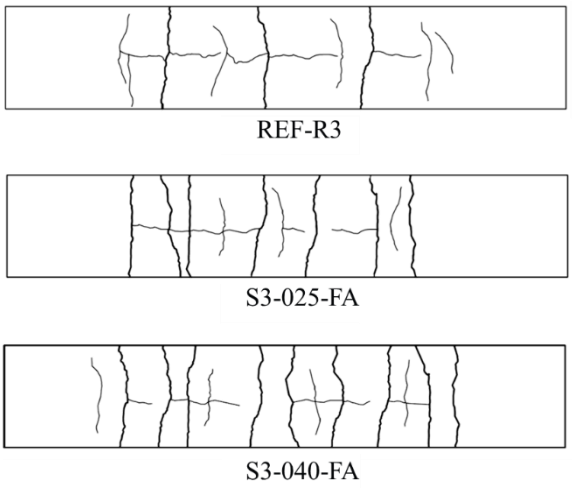

Fig. 5.15 Crack Patterns for S3 Series at Average Tensile Strain of 0.002

5.3.2 Proposed Equations

A bilinear expression was proposed by Belarbi and Hsu (1994) to predict the tensile behavior of steel in RC element. The apparent yielding stress $f_y^{'}$ was proposed to describe the reduction of yielding stress. The equations are

$$f_s = E_s \varepsilon_s \qquad \varepsilon_s < \varepsilon_y^{'}, \tag{5-24}$$

$$f_s = (0.91 - 2B)\, f_y + (0.02 + 0.25B) E_s \varepsilon_s \qquad \varepsilon_s \geq \varepsilon_y^{'}, \tag{5-25}$$

$$\varepsilon_y^{'} = f_y^{'} / E_s, \qquad f_y^{'} = (0.93 - 2B)\, f_y, \tag{5-26}$$

$$B = \frac{1}{\rho_s}\left(\frac{f_{cr}}{f_y}\right)^{1.5}, \tag{5-27}$$

$$f_{cr} = 3.75\sqrt{f_c^{'}\,(psi)}, \quad \text{and} \quad \rho_s \geq 0.15\%. \tag{5-28}$$

For the given equations, the apparent yielding stress will increase as the increase of the steel reinforcement ratio. This is due to fact that more reinforcement at the crack location tends to prevent the cracking from opening, which reduces the local stress concentration

on the rebar, and consequently increases the apparent yielding stress. The same idea can be applied onto the externally bonded FRP sheets. The externally bonded FRP sheets also helps preventing the cracks from opening and reduce the stress concentration. In this study, it is assumed that the strain distribution of FRP and steel are the same along the specimen. Based on this assumption, the FRP reinforcement can be transferred to the "equivalent" steel reinforcement. Based on the test result, the effect of FRP reinforcement on the behavior of the steel in tension is described by introducing a new parameter called Equivalent Reinforcement Ratio ρ_e. The following equations were proposed for ρ_e:

$$\rho_e = \rho_s + n_{f/s}\rho_f \text{ and} \tag{5-29}$$

$$n_{f/s} = \frac{E_f}{E_s}. \tag{5-30}$$

Fig. 5.16 shows the comparison between the proposed equations and the test results. Since #4 and #5 rebar have no clear yielding plateau, the stiffness of the post-yielding portion for the specimen with #4 and #5 rebar was set to be equal to the post-yielding stiffness of the respective bare rebar. Fig. 5.16 shows an acceptable level of agreement between the proposed model and the test results.

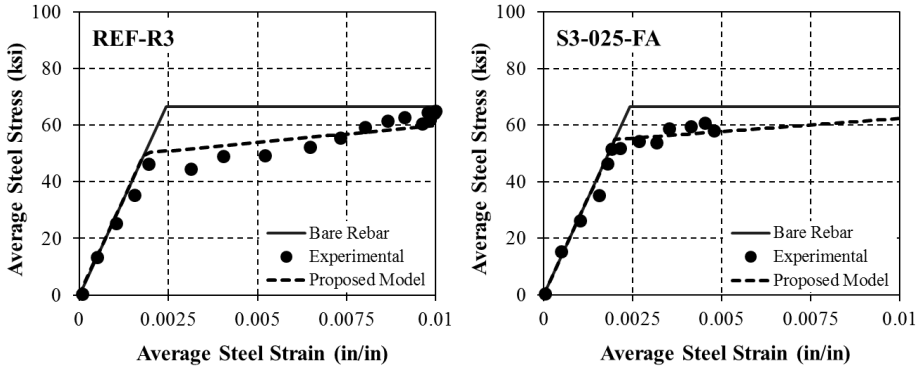

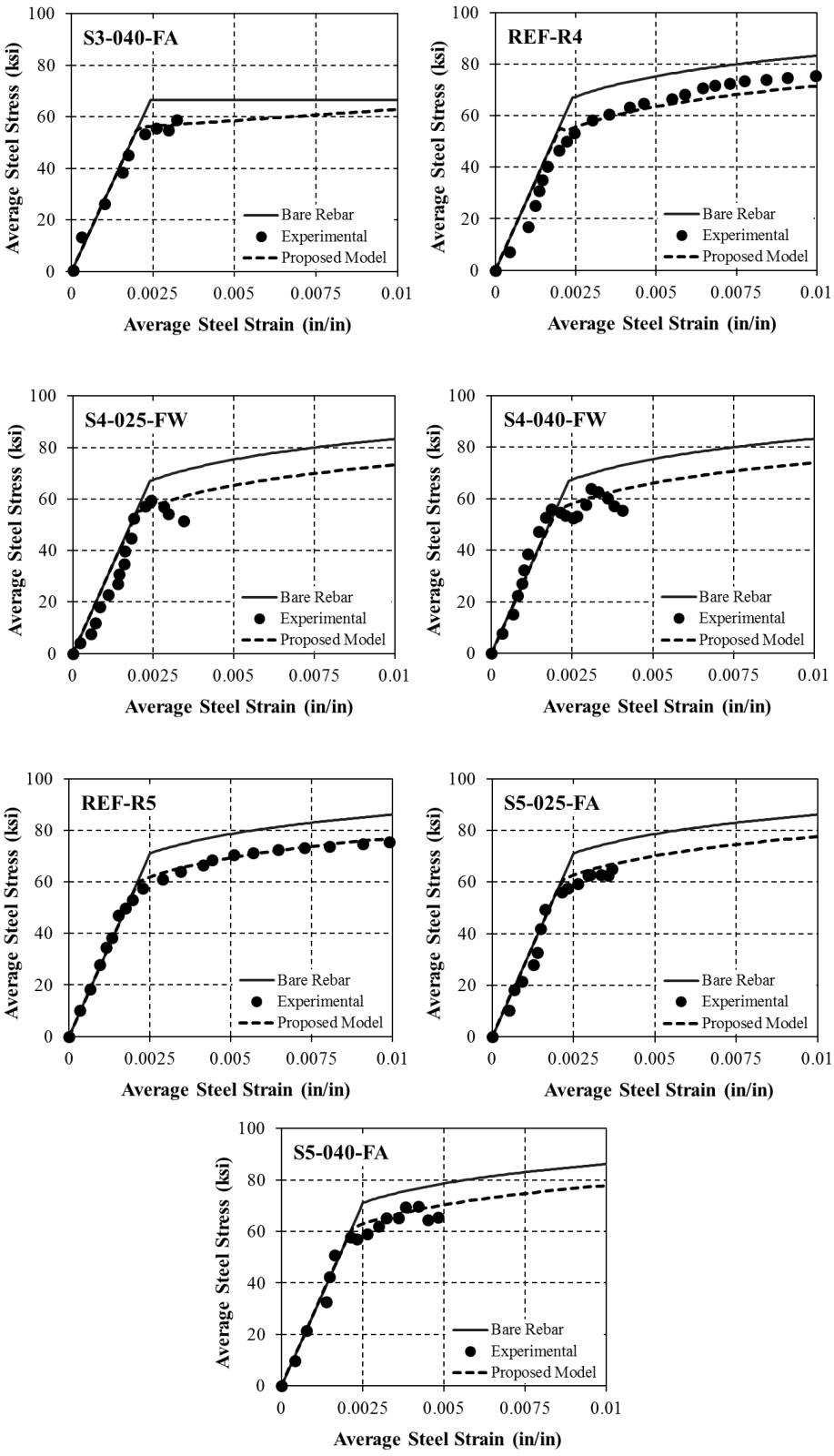

Fig. 5.16 Comparison of Proposed Equations and Test Results for the Stress-strain Relationships in Steel

5.3.3 Verification of Proposed Equations

The prediction from the proposed equations were compared with the test results of Farah and Sato (2011). Fig. 5.17 shows the steel stress strain curve for S-1 Series. The specimen name S-1-1/2/3 stands for the S1 series of specimen with $\rho_s = 0.5\%$ and 1/2/3 layers of FRP, i.e., $\rho_f = 0.07\%, 0.13\%,$ and 0.20% respectively. Similar phenomenon was observed that with the increase of the FRP reinforcement ratio, the apparent yielding stress increases. Fig. 5.18 shows the comparison between the proposed equation and the experimental results. It can be observed that the prediction has a very good agreement with the experimental test results.

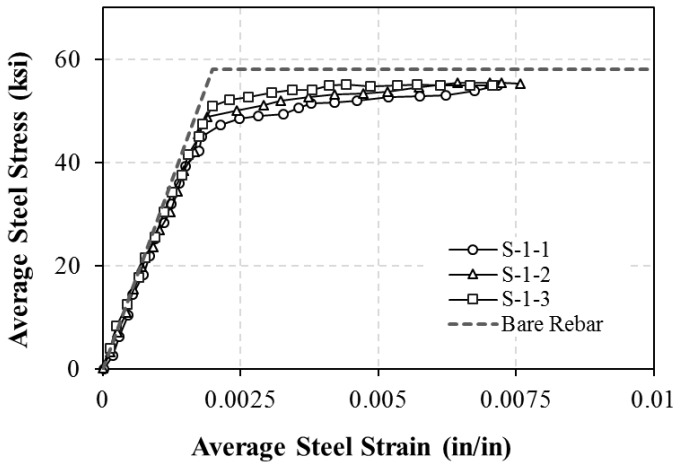

Fig. 5.17 Stress-strain Relationships for Steel in Tension (Farah and Sato, 2011)

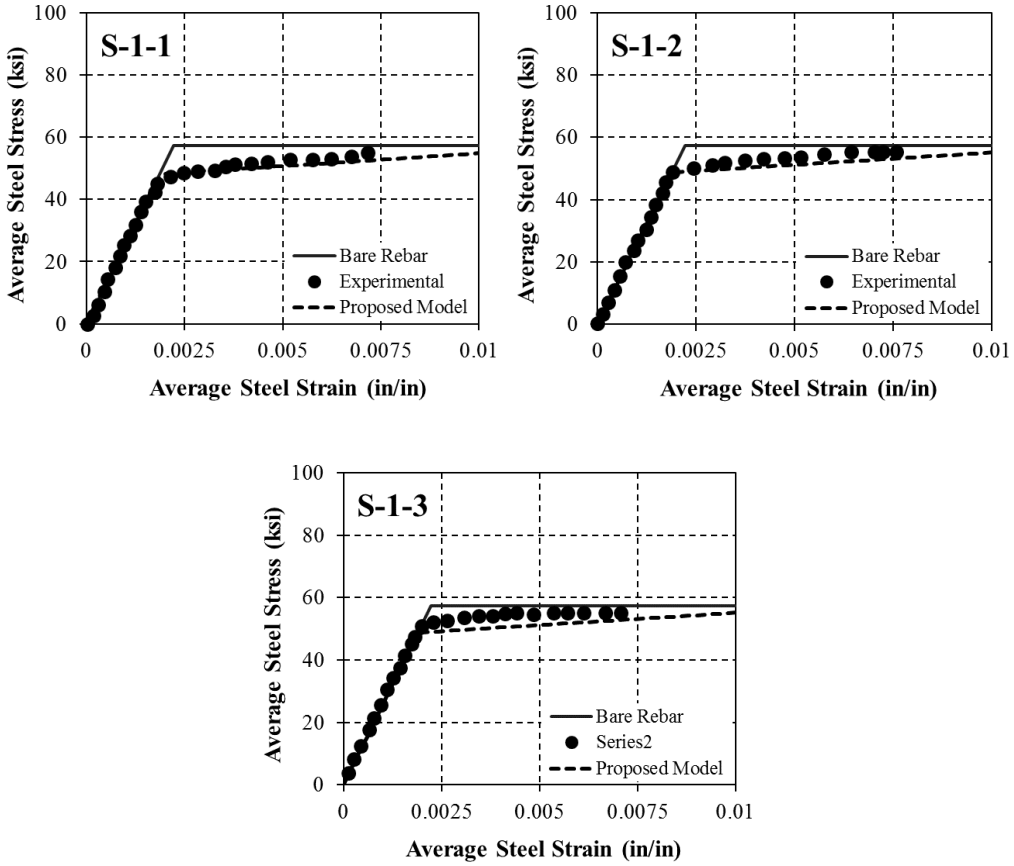

Fig. 5.18 Comparison of the Stress-strain Relationships in Steel between Proposed Equations and Test Results by Farah and Sato (2011)

5.4 RESULTS FROM DIC SYSTEM

As introduced in Chapter 4, DIC system was used to capture the strain variation on one side of the specimen. Fig. 5.19 shows a typical strain variation of the tested specimen S5-025-FA. The red area on the strain fields indicates the location of the cracks. The white area at the center of the specimen are the areas blocked by the LVDTs and cables so that no results can be obtained for them. The debonding of the FRP at the ultimate stage was also captured by the DIC system, as shown in Fig. 5.20.

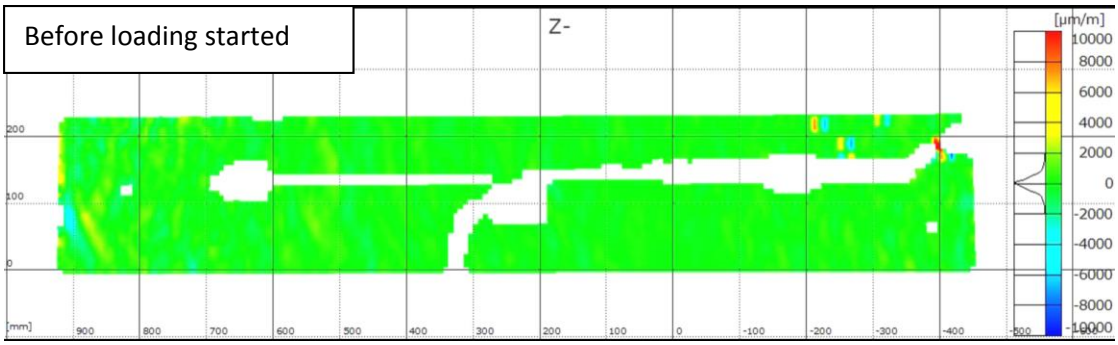

Load: 0 Kips Avg. Strain: 0 in./in.

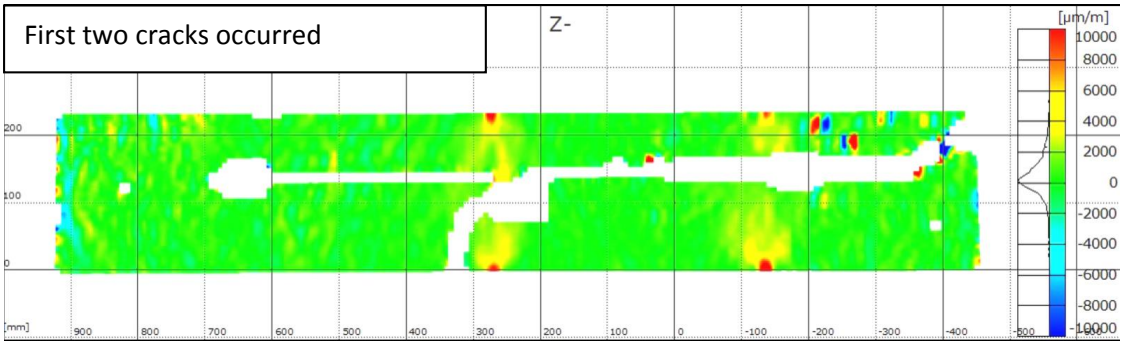

Load: 32 Kips Avg. Strain: 0.0003 in./in.

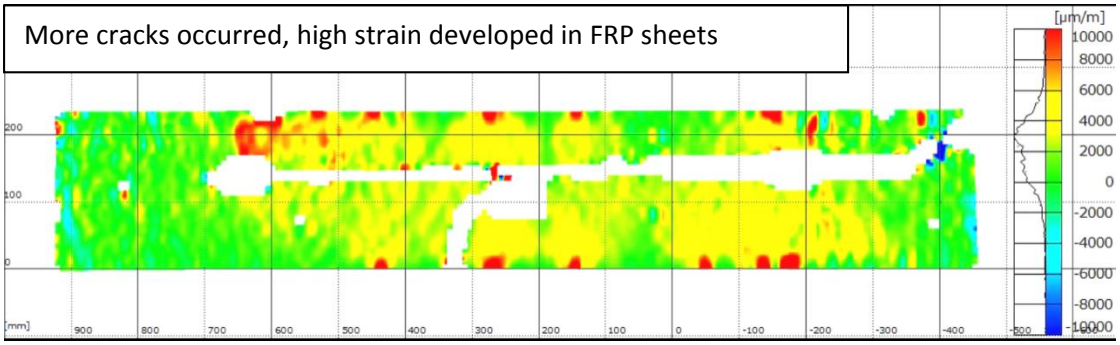

Load: 55 Kips Avg. Strain: 0.0018 in./in.

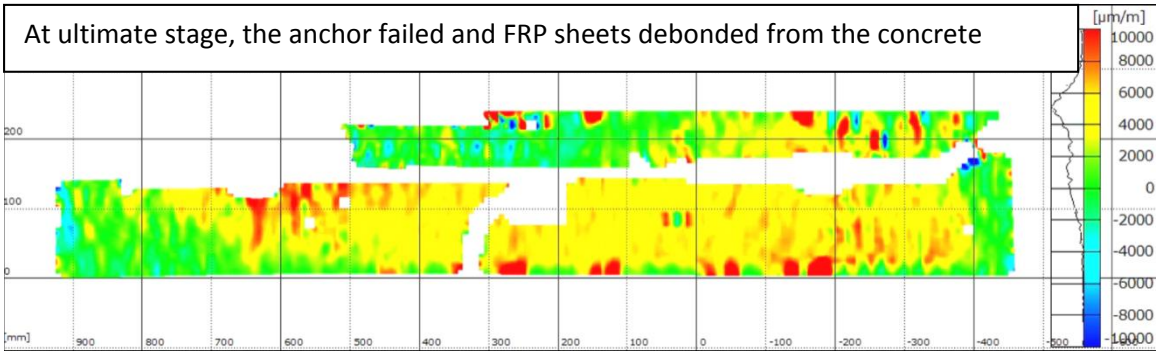

Load: 73 Kips Avg. Strain: 0.0038 in./in.

Fig. 5.19 Tensile Strain Field from DIC for Specimen S5-025-FA

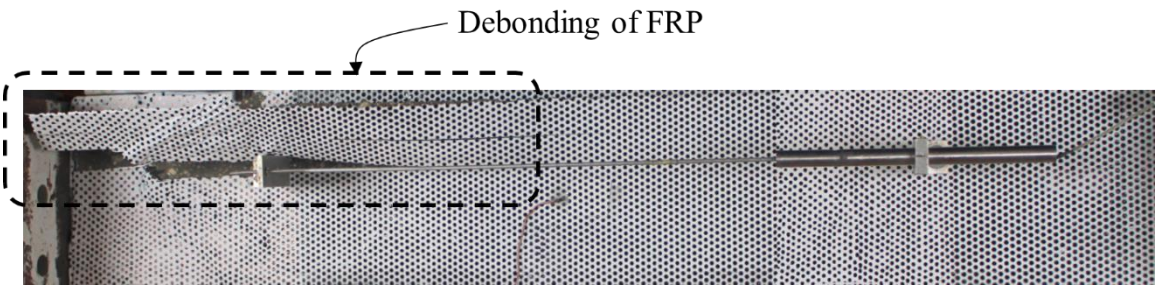

Fig. 5.20 Debonding of FRP Sheets at Ultimate Stage

5.5 CONCRETE IN COMPRESSION

5.5.1 General

As shown in Fig. 5.21, the softening coefficient was defined as

$$\zeta_f = \frac{\sigma_p}{f_c'}, \tag{5-31}$$

where σ_p is the compressive strength of concrete in biaxial tension-compression.

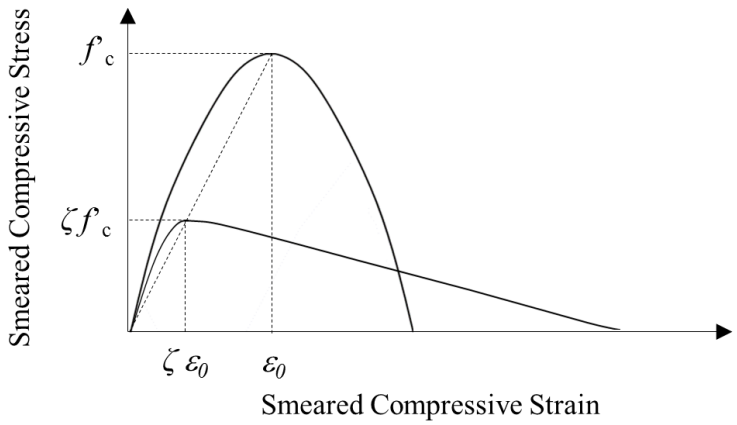

Fig. 5.21 Example of a Proposed Model for Softening Coefficient (Adopted from Hsu and Mo, 2010)

Several researchers have investigated the softening coefficient by various experimental tests (Vecchio and Collins, 1981; Miyahara et al., 1987; Izumo et al., 1991). In University of Houston, Belarbi and Hsu (1995) studied the effect of five variables on

the softening coefficient ζ by testing 22 full scale RC panels. The variables include: 1) the principal tensile strain, 2) the presence of tensile stress at failure, 3) the loading path (sequential and proportional), 4) spacing of reinforcing, 5) the amount of main longitudinal reinforcement. They confirmed that the principal tensile strain is the dominant variable. The presence of tensile stress at failure has no effect on the softening coefficient. The load path, the spacing of reinforcing bars and the amount of longitudinal reinforcement have a small effect, but can be neglected for simplicity. Pang and Hsu (1996) studied the behavior of 2-D elements subjected to pure shear. The test specimens were reinforced with various amounts of steel bars. The test results of 13 panel specimens confirmed the following equation for the softening coefficient:

$$\zeta = \frac{0.9}{\sqrt{1+400\varepsilon_1}} \quad \text{for proportional Loading and} \tag{5-32}$$

$$\zeta = \frac{0.9}{\sqrt{1+250\varepsilon_1}} \quad \text{for sequential Loading.} \tag{5-33}$$

Later on, many panel tests and analytical studies have been conducted by other researchers (Zhang and Hsu, 1998; Chintrakarn, 2001; Wang, 2006), different parameters were then included in the equation for softening coefficient. The parameters that proved to be effective are namely: concrete strength f'_c, and the deviation angle β. So the equation of calculating ζ is expressed as

$$\zeta = \left(\frac{5.8}{\sqrt{f'_c}} \le 0.9\right)\left(\frac{1}{\sqrt{1+250\varepsilon_1}}\right)\left(1-\frac{|\beta|}{24°}\right). \tag{5-34}$$

In the following section, the modification of Eqn. (5-36) is presented based on the results of the softening tests. The studied parameter is FRP reinforcement ratios.

5.5.2 Test Results

For the test in this study, the loading procedure is sequential. Tension was applied onto the panel in the horizontal direction up to a tensile strain level, then the tensile strain in horizontal direction was kept constant using the strain control mode and the compression load was applied in the vertical direction until the failure of the specimen. The failure strength σ_p was obtained and plugged in Eqn. (5-33) to obtain the softening coefficient for each test specimen.

Fig. 5.22 shows the comparison between the test data for FRP RC and the test data for RC (Belarbi and Hsu, 1995). Fig. 5.22 indicates that the test data for RC is more scattered compared to the test data for FRP RC. It can be seen that the softening coefficient is greater for FRP RC than in RC. The prediction for RC element underestimated the softening coefficient in FRP RC element. Fig. 5.23 shows the result for FRP RC when compared to ±15% of the model for RC. The softening coefficient of FRP RC shows 10% increase for specimen with ρ_f = 0.56% and 18 % increase for specimen with ρ_f = 0.90% when compared to the prediction for RC. This increase of softening coefficient is attributed to the confinement provided by the FRP sheets. Also, by comparing the result for specimen with different FRP reinforcement ratios, it can be concluded that as the increase of the FRP reinforcement ratio, the confinement effect is more significant, and consequently the softening coefficient is greater.

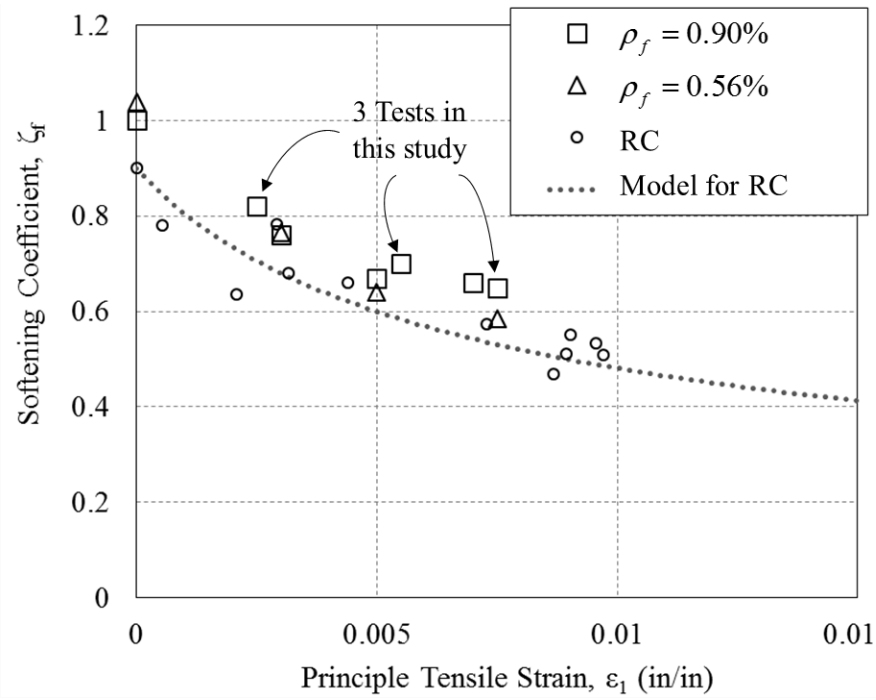

Fig. 5.22 Comparison between the Softening Coefficients for RC (Belarbi and Hsu, 1995) and FRP RC

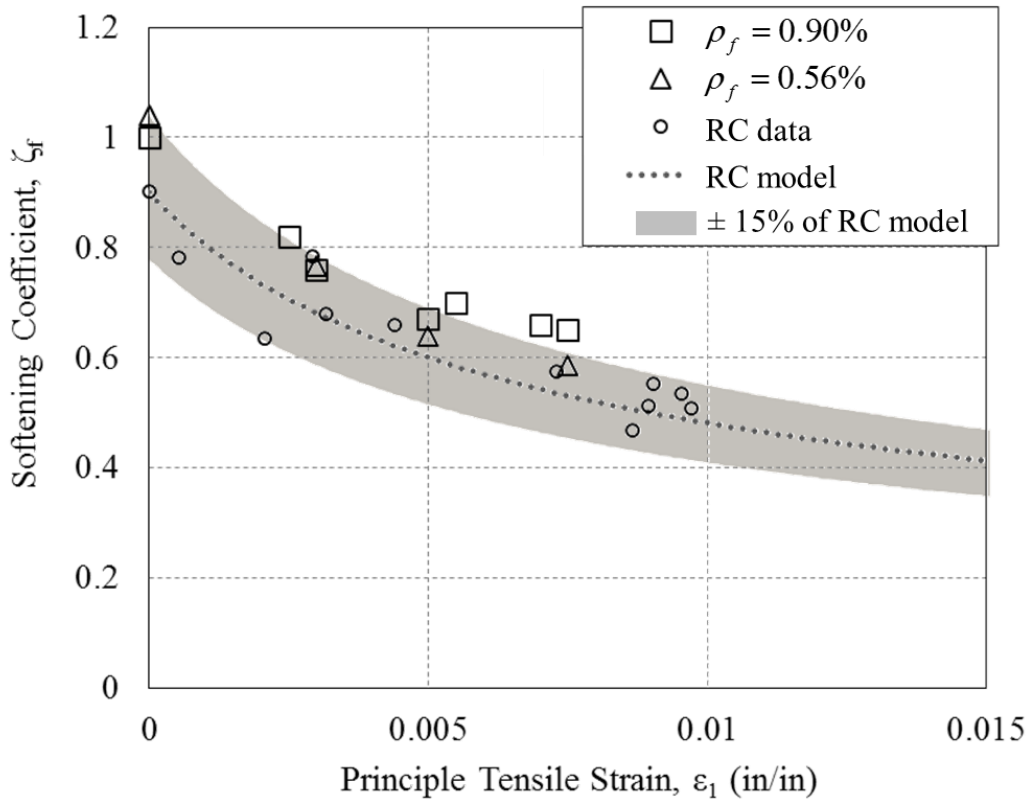

Fig. 5.23 Comparison between the Softening Coefficients for RC (Belarbi and Hsu, 1995) with Envelop of Test Data and FRP RC

5.5.3 Proposed Equations

Moslehy (2010) investigated the softening coefficient by investigating the effect of FRP reinforcement. By regression of the test data, equations for the softening coefficient were proposed as

$$\zeta_f = \left(\frac{5.8}{\sqrt{f_c'}} \le 0.9\right)\left(\frac{1}{\sqrt{1+250\varepsilon_1}}\right)\left(1-\frac{|\beta|}{24°}\right) f_4\left(FRP\right) \text{ and} \tag{5-35}$$

$$f_4\left(FRP\right) = \begin{cases} \left(1+\dfrac{E_f \varepsilon_1 t_f^{\frac{2}{3}}}{50,000}\right)\left(1.12-16\varepsilon_1\right) & \text{with FRP} \\ 1 & \text{without FRP.} \end{cases} \tag{5-36}$$

The first three terms on the right hand side of Eqn. (5-37) are the same as the softening coefficient for RC by other researchers at University of Houston (Belarbi and Hsu, 1994; Pang and Hsu, 1996; Zhang and Hsu, 1998; Wang, 2006). Fig. 5.24 shows the prediction of these equations and the test results. However, this proposed model contains a shortcoming that the concrete area A_c was not considered, i.e., large or small concrete structures strengthened with same amount of FRP will end up with same softening coefficient, which seems against the expectation.

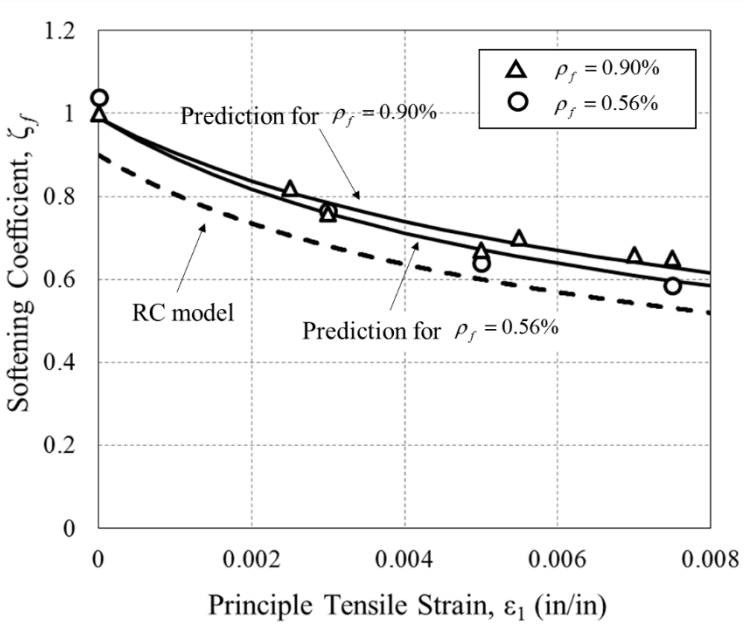

Fig. 5.24 Comparison of the Softening Coefficient between Model Proposed by Moslehy (2010) and Test Data

To account for the aforementioned shortcoming of model of Moslehy (2010). In this study, $\rho_f E_f$, instead of $E_f t_f$ was used in the expression of $f_4(FRP)$ so the effect of concrete area is taken into account. The derivation of the equation still follows the method of regression of test data. Fig 5.25 shows the comparison between all the test data for ζ and the FRP stiffness $\rho_f E_f$. The test data fits well to the expression

$$f_4(FRP) = 1 + 0.02\sqrt{\rho_f E_f} \ . \tag{5-37}$$

In the proposed equation, $\rho_f E_f$ instead of $E_f t_f$ were adopted to account for the area of the concrete. It should be noticed that the proposed equation converges to the result of RC when $\rho_f E_f$ equals to zero, in which case f_4(FRP) equals to 1 and the expression will be the same as model for RC. Fig 5.26 shows the comparison between the proposed equation and the test data and a good agreement can be observed.

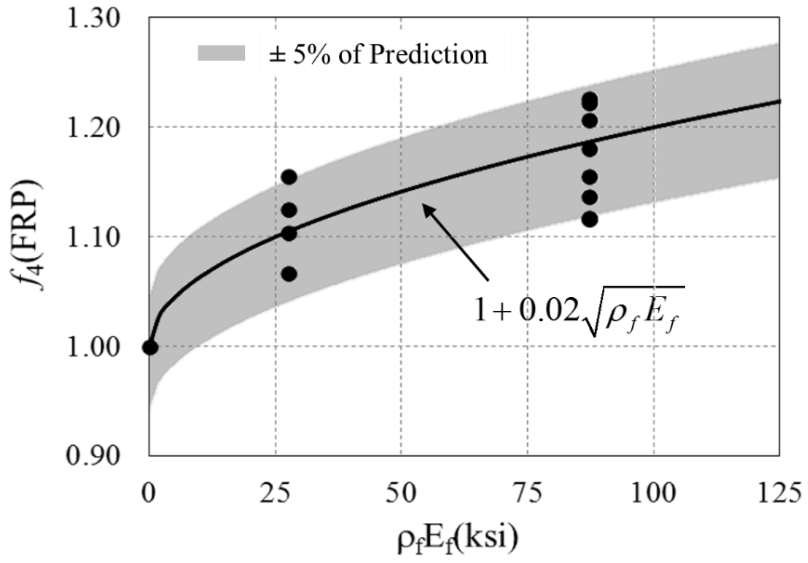

Fig. 5.25 Regression of Test Data for f_4(FRP)

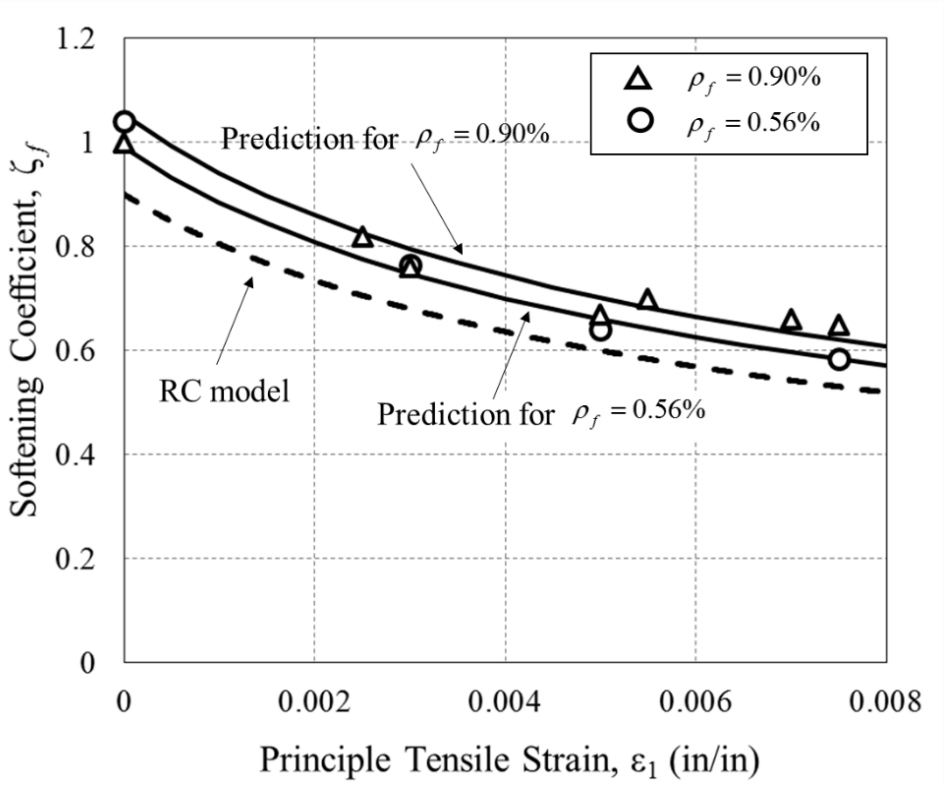

Fig. 5.26 Comparison of the Softening Coefficient between the Proposed Eqn. (5-37) and Test Data

5.6 MODIFIED HSU/ZHU RATIO

5.6.1 General

The Poisson ratio is known in mechanics to describe the strain change in one direction due to the change of the strain in the perpendicular direction. The definition of Poisson ratio is only valid for continuous isotropic materials. By utilizing smeared crack concept, Hsu and Zhu (2002) proposed so-called Hsu/Zhu ratio to describe the similar effect for cracked reinforced concrete. The Hsu/Zhu ratio ν_{12} and ν_{21} is defined as shown in Fig. 5.27.

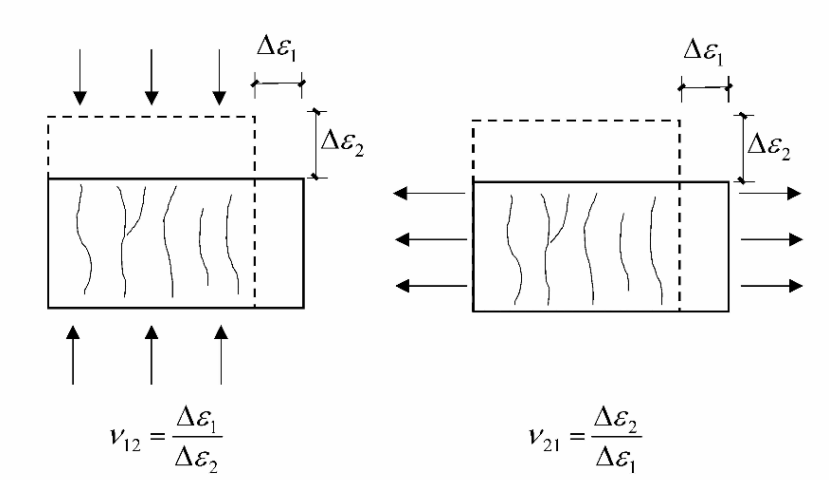

Fig. 5.27 Illustrative Plot for Hsu/Zhu Ratio ν_{12} and ν_{21}

The Poisson effect have to be considered in the softened truss model theory since all the material laws were developed based on uniaxial test (Hsu and Zhu, 2002), but the stress condition in the shear element is biaxial, therefore in order to be used these material laws in the SMM model, the biaxial strain have to be transferred into uniaxial strain by involving the Poisson ratio, see Eqn. (5-38)-(5-39).

$$\bar{\varepsilon}_1 = \frac{1}{1-\upsilon_{12}\upsilon_{21}}\varepsilon_1 + \frac{\upsilon_{12}}{1-\upsilon_{12}\upsilon_{21}}\varepsilon_2 \text{ and} \tag{5-38}$$

$$\bar{\varepsilon}_2 = \frac{\upsilon_{21}}{1-\upsilon_{12}\upsilon_{21}}\varepsilon_1 + \frac{1}{1-\upsilon_{12}\upsilon_{21}}\varepsilon_2 . \tag{5-39}$$

Moreover, in Finite Element Analysis, the Hsu/Zhu ratio υ_{12} and υ_{21} are applied to consider the Poisson effect. The constitutive laws of concrete can be expressed as

$$\begin{Bmatrix} \sigma_2^c \\ \sigma_1^c \\ \tau_{21}^c \end{Bmatrix} = \begin{bmatrix} E_2^c & \nu_{21}E_2^c & 0 \\ \nu_{12}E_2^c & E_1^c & 0 \\ 0 & 0 & G_{21}^c \end{bmatrix} \begin{Bmatrix} \varepsilon_2 \\ \varepsilon_1 \\ \gamma_{21} \end{Bmatrix}. \tag{5-40}$$

Hsu/Zhu ratio was input in the material stiffness matrix to considering the Poisson Effect. By introducing the Hsu/Zhu ratio, the biaxial strains in the equations can be transferred into uniaxial strains. The Hsu/Zhu ratio is applicable to RC element in pre- and post-cracking stages based on the smear stress/strain approaches. The evaluation of Hsu/Zhu ratio was conducted based on 12 panel tests (Zhu and Hsu, 2002). They proposed the equations from the test results as

$$\upsilon_{12} = 0.2 + 850\varepsilon_{sf} \qquad \varepsilon_{sf} \le \varepsilon_y , \tag{5-41}$$

$$\upsilon_{12} = 1.9 \qquad \varepsilon_{sf} > \varepsilon_y \text{ and} \tag{5-42}$$

$$\upsilon_{21} = \begin{cases} 0.2 & \text{Before cracking} \\ 0 & \text{After cracking} \end{cases} , \tag{5-43}$$

where ε_{sf} is the strain in the reinforcement. The results for the Hsu/Zhu ratio υ_{12} and υ_{21} and comparison with the proposed model are shown in Fig. 5.28a)-b), respectively.

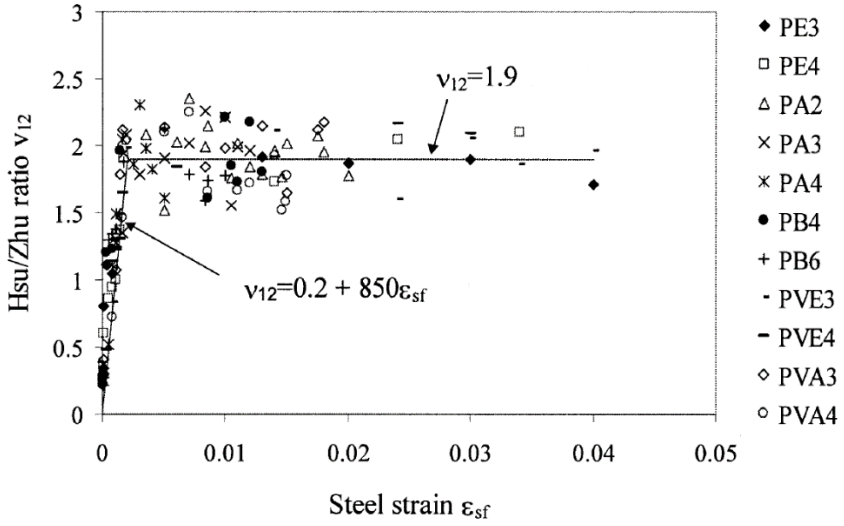

a) Test Data and Proposed Model for ν_{12}

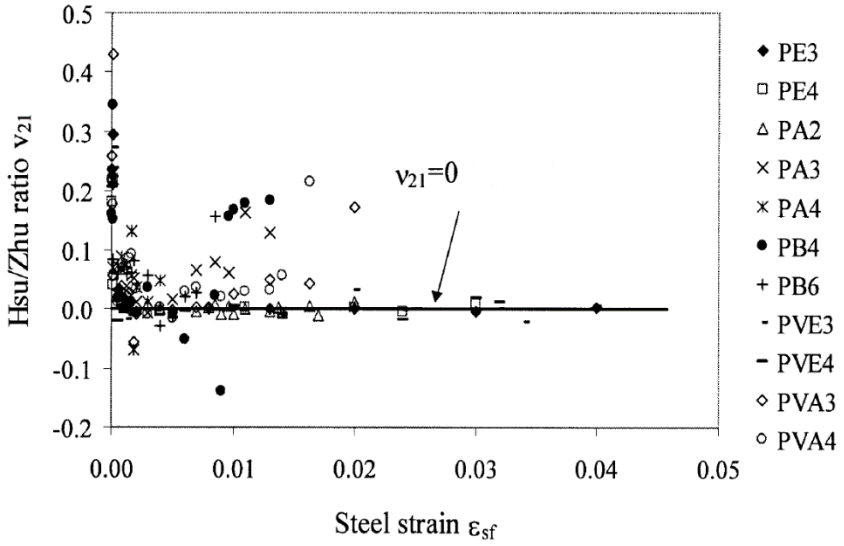

b) Test Data and Proposed Model for ν_{21}

Fig. 5.28 Hsu/Zhu Ratios for RC (Adopted from Zhu and Hsu, 2002)

It can be observed from 5.28a) that the model for υ_{12} is bilinear curve: before yielding of the reinforcement, the ratio was found to increase from 0.2 linearly to 1.9 and then kept constant. It should be noted that for the cracked RC element in the post-yielding stage, the Hsu/Zhu ratio is higher than 0.5, which is the maximum value of Poisson ratio for continuous solid materials. The reason is that the smeared tensile strain of cracked RC

element includes not only the strain of the material, but also the opening of cracks. By considering the cracked RC element as continuous material, the Hsu/Zhu ratio could then be significantly high (equals to 1.9). It can be observed from 5.28b) that υ_{21} is around 0.2 before cracking of concrete, and suddenly dropped to zero once the crack occurs. Due to the additionally bond action created by the externally bonded FRP sheets, the Hsu/Zhu ratio is expected to be altered in RC element.

5.6.2 Data Analysis Method

As discussed in the chapter 4, small step-wise increments loading procedure was applied so that the Hsu/Zhu ratio can be determined at each loading step. As an example, the loading procedure for specimen PR-025 is shown in Fig. 5.29.

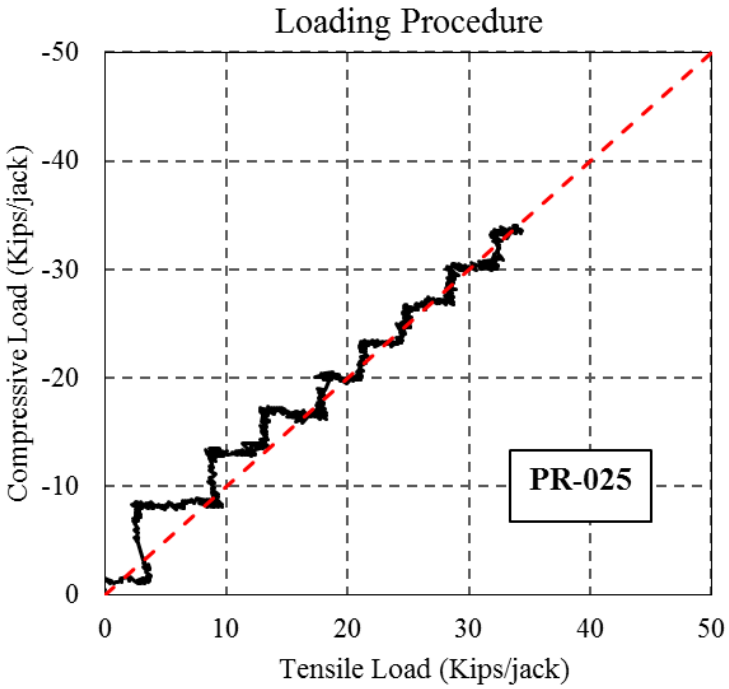

Fig. 5.29 Loading Procedure for PR-025

The tensile strains $\Delta\varepsilon_1$ is obtained by averaging the 8 horizontal LVDTs attached on the specimen, and the compression $\Delta\varepsilon_2$ is obtained by averaging the 8 vertical LVDTs

attached on the specimen. According to Zhu (2000), the load in actuators would fluctuate slightly due to frictions and electrical noise, the minimum step increment was set to be 4 kips/jack. To increase the accuracy and stability of the test data, $\Delta\varepsilon$ for each step was calculated using the average strains of five points for the initial and final strain, as shown in Fig. 5.30. This method guarantees the stability of the data and reduces the error due to the fluctuation of the data, especially for the compression step in which the strain increment is fairly small (in the scale of 0.00005).

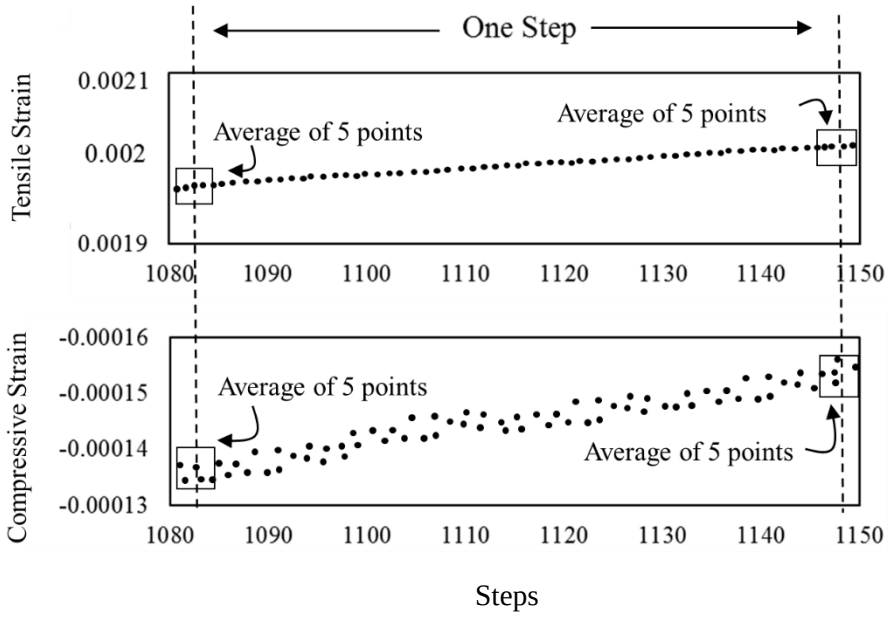

Fig. 5.30 Method of Data Collection in Hsu/Zhu Ratio Test

5.6.3 Effect of FRP Reinforcement Ratio on ν_{21}

The Hsu/Zhu ratio ν_{21} obtained from the tests is shown in Fig. 5.31. It can be observed that the Hsu/Zhu ratio ν_{21} is around 0.25 before crack occurs. After crack occurs, it decreased rapidly to zero. This trend is the same for the RC specimen tested by Zhu and Hsu (2002), as previously shown in Fig. 5.28b).

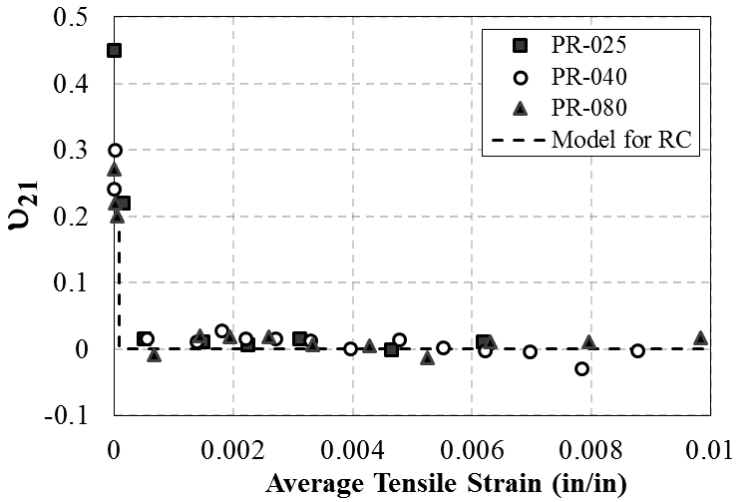

Fig. 5.31 Hsu/Zhu Ratio ν_{21} in This Study

This phenomenon can be explained as follows. In the post-cracking stage, the increase of the tensile strain is mainly attributed to the opening of the cracks the decrease of strain in the compression direction is almost negligible.

5.6.4 Effect of FRP Reinforcement Ratio on ν_{12}

The test data for the ν_{12} and the comparison with RC test data (with envelop) are shown in Fig. 5.32. It can be observed that the Hsu/Zhu ratio ν_{12} for un-strengthened RC members is much larger than that for the cases with FRP sheets, which means the for the same compressive strain increment, the increase of tensile strain is much smaller for specimen with FRP than the un-strengthened RC members. This can be attributed to the confinement the FRP provides, which stiffens the specimen in the tensile direction. Another fact that can be observed from the figure is that as the increase of the FRP stiffness, the Hsu/Zhu ratio ν_{12} decreases. This can be explained that as the FRP stiffness increases, a better confinement is provided and the specimen becomes stiffer in the tensile direction.

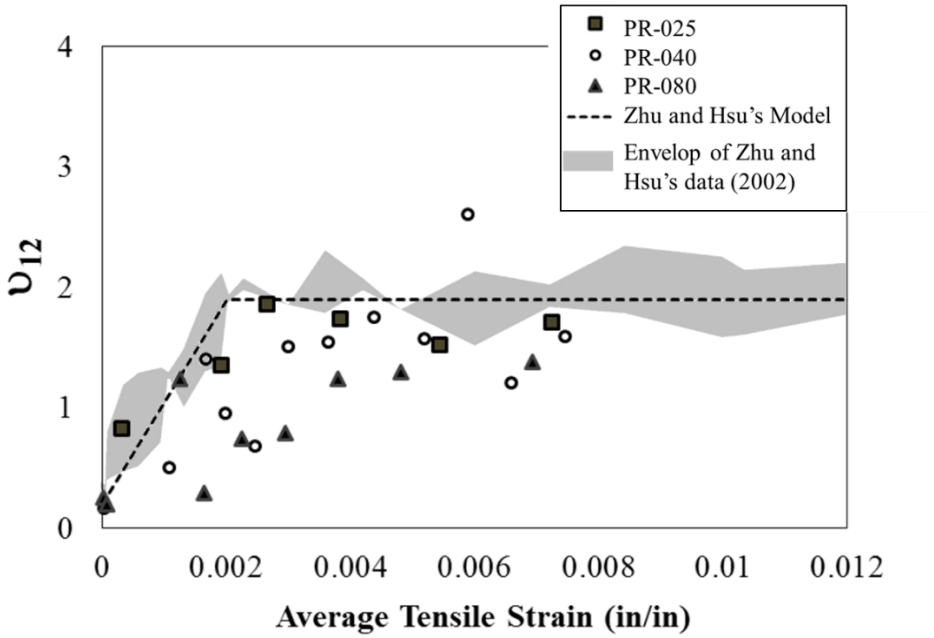

Fig. 5.32 Comparison of Hsu/Zhu Ratio ν_{12} between FRP RC and RC

The reason ν_{12} is significantly larger than ν_{21} is that when the specimen is under compression stress field, the cracked concrete struts between cracks are not regularly shaped, as shown in Fig. 5.33. The compression applied with eccentricity could cause bending and makes the struts push each other in the tensile direction. Also, when the steel yielded, the resistance to the expansion in the tensile direction becomes much smaller. These two effects combines and leads to a great value of ν_{12}.

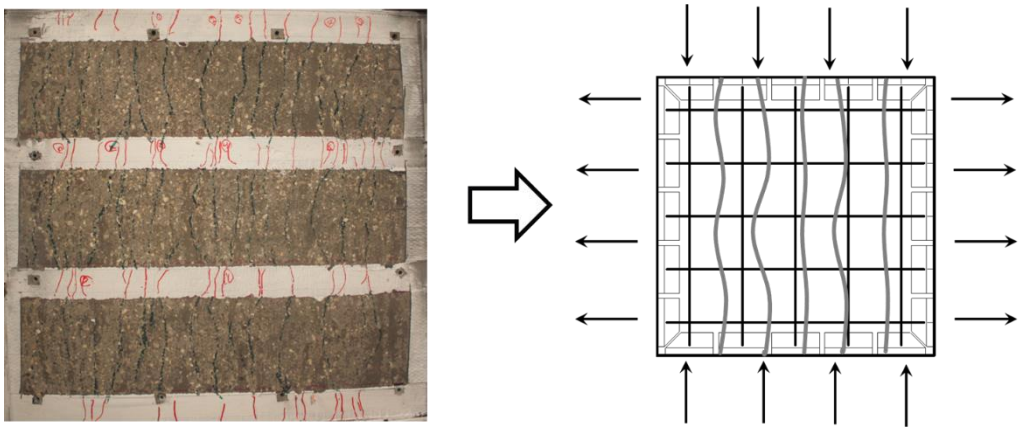

Fig. 5.33 Bending Effect on the Cracked Specimen in the Hsu/Zhu Ratio Test

5.6.5 Proposed Equations

As explained in the previous section, the Hsu/Zhu ratio is affected mainly by the post-yielding stiffness in the tensile direction. In this research, $\rho_f E_f$ was chosen as the parameter to describe the FRP contribution to the post-yielding stiffness. For the FRP RC element, the average value of ν_{12} after the yielding strain ($\varepsilon_y = 0.0024$) is listed in Table 5.4. Fig. 5.34 shows the relationship between ν_{12} and FRP stiffness $\rho_f E_f$. A good linear relationship was observed.

Table 5.4 Test Results for υ_{12} at Post-yielding Stage

Specimen	$\rho_f E_f$ (ksi)	Post-yielding υ_{12} (AVG)
RC	0	1.9
PR-025	62.4	1.7
PR-040	87.15	1.56
PR-080	174.3	1.18

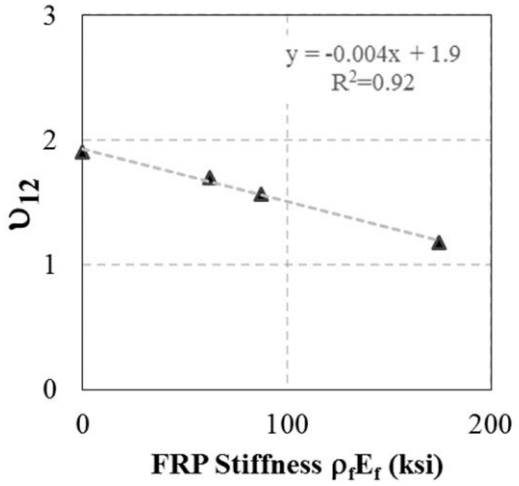

Fig. 5.34 Relationship between ν_{12} and FRP Stiffness

The proposed equations for calculating the Hsu/Zhu ratio ν_{12} and ν_{21} are

$$\nu_{12} = 0.2 + k\varepsilon_{sf} \qquad \varepsilon_{sf} \le \varepsilon_y , \tag{5-44}$$

where $k = \dfrac{1.7 - 0.004\rho_f E_f}{\varepsilon_y}$. (5-45)

$$\nu_{12} = 1.9 - 0.004\rho_f E_f \qquad \varepsilon_{sf} > \varepsilon_y, \tag{5-46}$$

$$\nu_{21} = \begin{cases} 0.2 & \text{Before cracking} \\ 0 & \text{After cracking} \end{cases}, \tag{5-47}$$

where ε_{sf} is average strain along the FRP and steel reinforcement.

The comparison between the prediction of the proposed equation and the experimental results for ν_{21} is shown in Fig. 5.35. A good agreement is observed between the proposed models and the test data.

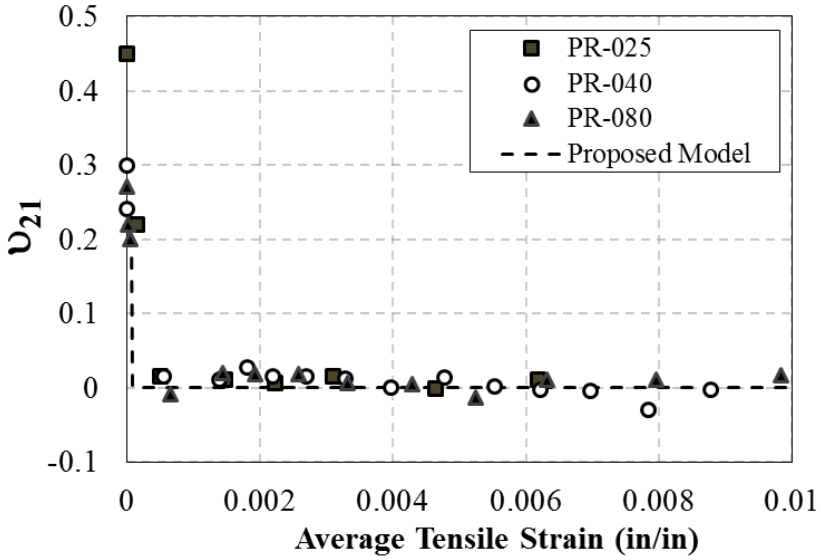

Fig. 5.35 Comparison of ν_{21} between Experimental Data and Prediction of Eqn. (5-47)

For ν_{12}, the proposed equation converges to RC when $\rho_f E_f$ equals to zero. And as the increase of the FRP reinforcement ratio, the ratio ν_{12} decreases. Fig. 5.36 shows the comparison between the prediction and experimental results for ν_{12}. It can be observed

that the tendency of ν_{12} with respect to FRP stiffness $\rho_f E_f$ is reasonably captured. The prediction shows a good agreement with the experimental results.

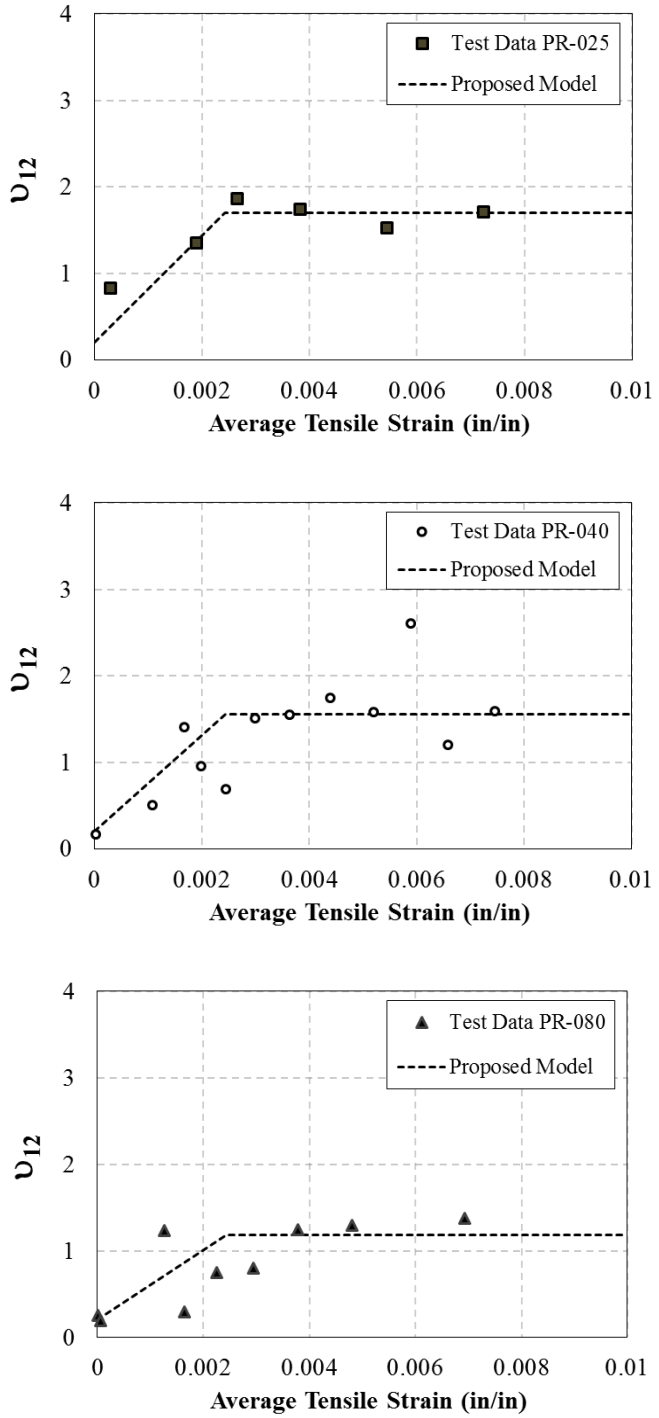

Fig. 5.36 Comparison of ν_{12} between Experimental Data and Prediction of Eqns. (5-44)-(5-46)

5.7 CASE STUDY OF SMM WITH MODIFIED CONSITUTIVE LAWS

In the previous sections, all the analysis of the test data and proposed modified constitutive laws of concrete and steel in tension, concrete in compression as well as Poisson ratios (Hsu/Zhu ratios) are presented. It can be observed that the proposed expressions have a good agreement with the test result in this study and results from other researchers (Ueda et al., 2002; Farah and Sato, 2011). To further verify the proposed equations, the constitutive laws developed in this research were incorporated with the SMM model to predict the behavior of FRP RC elements under pure shear load. The results of the prediction are compared with two pure shear test results conducted by Zomorodian in the second phase of the researcher project.

The panel tests were conducted by the state-of-art Universal Panel Tester (Hsu et al. 1995). As shown in Fig. 5.37, the panel 55 in × 55 in with a thickness of 7 in. FRP sheets with a width of 5.7 in was applied using full wrap method. No. 4 rebar was used as steel reinforcement along the longitudinal (l) direction and transverse (t) direction and the reinforcement ratios $\rho_l = \rho_t = 0.77\%$; two different thicknesses (0.025 in and 0.040 in) of the FRP sheets were used along transverse direction with reinforcement ratio $\rho_f = 0.54\%$ and 0.87%, respectively. The concrete strength is approximately 40 MPa. Both FRP sheets and steel rebar are the same type as used in the uniaxial tensile tests in this paper. The proportional tension-compression load was applied at the principal directions 1 and 2 to simulate the pure shear stress condition. The details of the pure shear test setup, specimen and the test results will be presented elsewhere by Zomorodian.

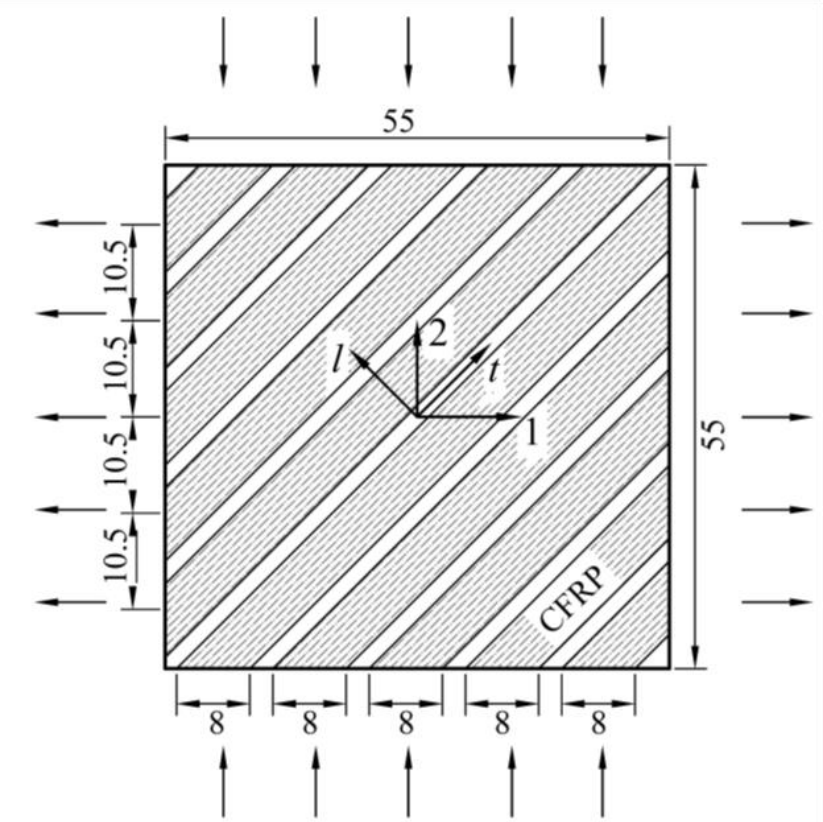

Fig. 5.37 Pure Shear Test Specimen Layout

SMM model provides a rational theory of reinforced concrete membrane elements. The theory satisfies Navier's three principles of mechanics of materials, known as: stress equilibrium, strain compatibility, and the constitutive laws of materials. Fig. 5.38 shows the FRP RC element subjected to in-plane stress. For the conducted pure shear test, FRP sheets were applied the same direction as the transverse steel reinforcement. And the stress in the FRP strip (Figure 5.38d) was considered similar to the steel reinforcement (Figure 5.38c). The crack was assumed to occur along the principal direction 2 for applied stresses.

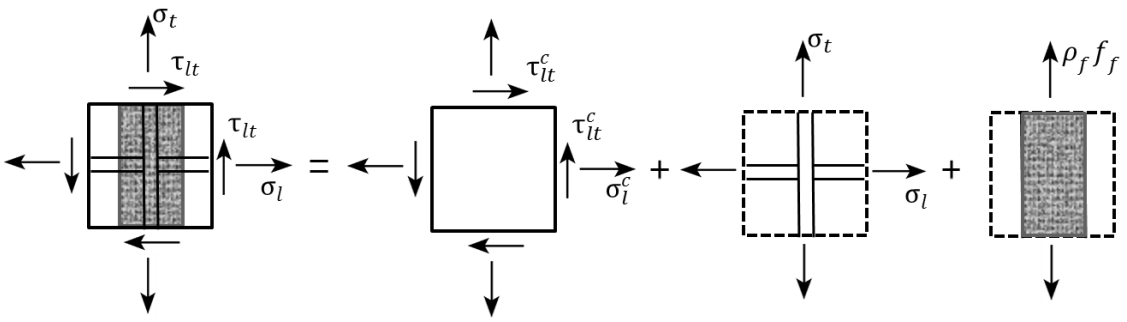

a) FRP RC element b) Concrete c) Steel grid d) FRP sheets

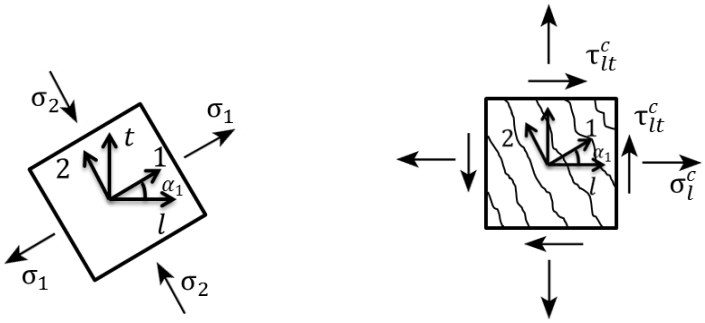

e) Principal Coordinate 1-2 f) Assumed Crack Direction

Fig. 5.38 FRP RC Element under In-plane Stress

It can be observed that the new equilibrium for FRP RC elements requires a new term $\rho_f E_f$ as

$$\begin{aligned}
\sigma_l &= \sigma_1^c \cos^2\alpha_1 + \sigma_2^c \sin^2\alpha_1 - \tau_{12}^c 2\sin\alpha_1\cos\alpha_1 + \rho_l f_l \\
\sigma_t &= \sigma_1^c \sin^2\alpha_1 + \sigma_2^c \cos^2\alpha_1 + \tau_{12}^c 2\sin\alpha_1\cos\alpha_1 + \rho_t f_t + \rho_{ft} f_{ft} \\
\tau_{lt} &= (\sigma_1^c - \sigma_2^c)\sin\alpha_1\cos\alpha_1 + \tau_{12}^c(\cos^2\alpha_1 - \sin^2\alpha_1).
\end{aligned} \tag{5-48}$$

The FRP RC element still satisfies the strain compatibility equation as

$$\begin{aligned}
\varepsilon_l &= \varepsilon_1 \cos^2\alpha_1 + \varepsilon_2 \sin^2\alpha_1 - \frac{\gamma_{12}}{2} 2\sin\alpha_1\cos\alpha_1 \\
\varepsilon_t &= \varepsilon_1 \sin^2\alpha_1 + \varepsilon_2 \cos^2\alpha_1 + \frac{\gamma_{12}}{2} 2\sin\alpha_1\cos\alpha_1 \\
\frac{\gamma_{lt}}{2} &= (\varepsilon_1 - \varepsilon_2)\sin\alpha_1\cos\alpha_1 + \frac{\gamma_{12}}{2}(\cos^2\alpha_1 - \sin^2\alpha_1).
\end{aligned} \tag{5-49}$$

The modified constitutive laws were incorporated into the SMM model. The stress strain relationship for concrete in tension is calculated as

$$\sigma_c = E_c \varepsilon_1 \qquad \text{when } \varepsilon_1 \le \varepsilon_{cr}, \text{ and} \tag{5-50}$$

$$\sigma_c = f_{cr}\left(\frac{\varepsilon_{cr}}{\varepsilon_1}\right)^c \qquad \text{when } \varepsilon_1 > \varepsilon_{cr}, \tag{5-51}$$

$$\text{where } c = K_w K_{f/s}. \tag{5-52}$$

The factor K_w is to describe the effect of wrapping schemes to the tensile behavior of concrete. In the case study, fully wrap method was used, therefore

$$K_w = 1, \tag{5-53}$$

The factor K_f is to describe the effect of FRP/steel stiffness ratio to the tensile behavior of concrete. It was calculated as

$$K_f = 0.25\left(\frac{\rho_f E_f}{\rho_s E_s}\right) + 0.15, \tag{5-54}$$

where ε_1 is the average tensile strain of concrete, σ_c are the average compressive stress in concrete, ρ_s and ρ_f are the reinforcement ratios of steel and FRP, respectively, E_s and E_f are the modulus of elasticity of steel and FRP, respectively; ε_{cr} and f_{cr} are the strain and stress at cracking, K_w and $K_{f/s}$ are two factors considering the effect of wrapping schemes and FRP/steel stiffness ratio.

The stress strain relationship for steel in tension is calculated as

$$f_s = E_s \varepsilon_s \qquad \varepsilon_s < \varepsilon_y', \tag{5-55}$$

$$f_s = (0.91 - 2B) f_y + (0.02 + 0.25B) E_s \varepsilon_s \qquad \varepsilon_s \ge \varepsilon_y', \tag{5-56}$$

$$\varepsilon_y^{'} = f_y^{'} / E_s, \qquad f_y^{'} = (0.93 - 2B)\, f_y, \tag{5-57}$$

$$B = \frac{1}{\rho_e}\left(\frac{f_{cr}}{f_y}\right)^{1.5}, \tag{5-58}$$

$$f_{cr} = 3.75\sqrt{f_c^{'}(\text{psi})}\ , \tag{5-59}$$

$$\rho_e = \rho_s + n_{f/s}\rho_f \text{ and } n_{f/s} = \frac{E_f}{E_s}, \tag{5-60}$$

where f_s is the average tensile stress of steel, f_y and $f_y^{'}$ are the yielding stress and the apparent yielding stress, respectively, $\varepsilon_y^{'}$ is the average tensile strain at apparent yielding point, and ρ_e is the proposed equivalent reinforcement ratio.

For the softening coefficient, ζ_f, the proposed expression in this study is for the sequential loading condition, however, in the pure shear test, the biaxial loading applied on the concrete strut is actually proportional. The detail study on the softening coefficient ζ_f for the proportional loading will be conducted in the second phase of the project. For this case study, it is decided to used the original equation in SMM for the constitutive laws of concrete in compression.

The equations for calculating the modified Hsu/Zhu ratios ν_{12} and ν_{21} in FRP RC element are

$$\upsilon_{12} = 0.2 + k\varepsilon_{sf} \qquad \varepsilon_{sf} \le \varepsilon_y, \tag{5-61}$$

$$\text{where } k = \frac{1.7 - 0.004\rho_f E_f}{\varepsilon_y} \tag{5-62}$$

$$\nu_{12} = 1.9 - 0.004\rho_f E_f \qquad \varepsilon_{sf} > \varepsilon_y, \text{ and} \tag{5-63}$$

$$\upsilon_{21} = \begin{cases} 0.2 & \text{Before cracking} \\ 0 & \text{After cracking} \end{cases}, \tag{5-64}$$

where ε_y is the yielding strain for steel, *1* direction is the principal tensile direction, and *2* direction is the principal compressive direction, the crack occurs along *1* direction.

To solve all the stress equilibrium, strain compatibility, and stress-strain relationships, iteration method is applied. Details of the solution algorism is presented in another publication of the author (Yang et al., 2013). Fig. 5-39a)-b) show the comparison of the shear stress τ and shear strain γ curve between the experimental tests and two different SMM. One is the SMM with the original constitutive laws of concrete and steel in tension for un-strengthened RC members; the other one is the SMM with the proposed modified constitutive laws. P4-025-FW and P4-040-FW stand for the specimen with ρ_f = 0.54% and 0.87%, respectively. It can be seen that the original model underestimated the tension stiffening effect of concrete, while the SMM with modified constitutive laws shows a much better prediction, especially for the pre-yielding portion of the behavior, this can be attributed to the more accurate constitutive models proposed in this study.

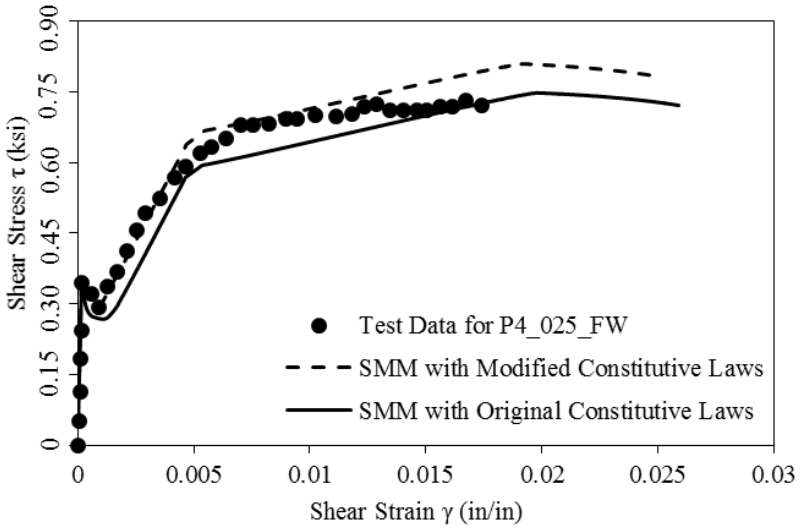

a) P4-025-FW

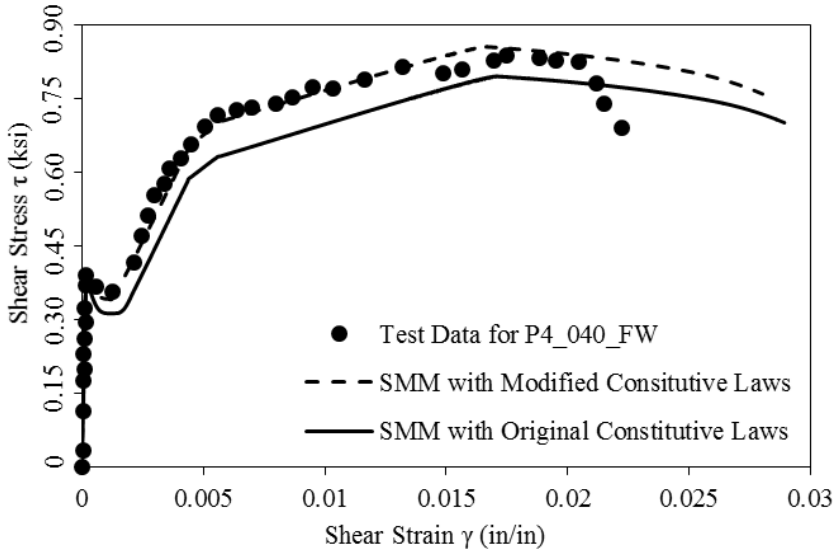

b) P4-040-FW

Fig. 5.39 Comparison between Test Results and SMM with Original and Modified Constitutive Laws

5.8 SUMMARY

The experimental and the analytical results are reported in detail in this chapter. The constitutive laws of concrete in tension, steel in tension were carefully investigated by analyzing the test data of uniaxial tension test. The softening coefficient and Hsu/Zhu ratio were investigated by analyzing the data of biaxial tension-compression test. Effect of different parameters such as steel reinforcement ratio, FRP reinforcement ratio and wrapping schemes were carefully investigated. The main findings includes:

1) It was found that the wrapping scheme, steel reinforcement ratio and FRP reinforcement ratio have an effect on the behavior of concrete in tension: first, compared to the un-strengthened RC element, the specimens strengthened with FRP exhibit a greater tension stiffening effect. Also, the tension stiffening effect tends to be more significant for the specimen with greater steel reinforcement ratio and lower FRP reinforcement ratios. Last but not the least, specimen strengthened by fully wrap and U-warp with FRP anchors tends to have a more significant tension stiffening effect than the specimen with side bond.

2) FRP reinforcement ratio was found to have an effect on the apparent yielding stress of the steel. As the increase of the FRP reinforcement ratio, the apparent yielding stress increases. This could be due to the effect of FRP on controlling the crack width. It was observed that with the increase of the FRP reinforcement ratio, the average crack width decreases, and consequently the local stress concentration for the rebar is reduced, which postponed the yielding of the steel.

3) The softening coefficient for FRP RC element was found to be greater than un-strengthened RC element. And the softening coefficient became greater with the increase of FRP reinforcement ratio. The additional compressive strength of concrete can be attributed to the confinement provided by the externally bonded FRP sheets. As the increase of the FRP reinforcement ratio, the confinement effect becomes stronger and consequently the softening coefficient is greater.

4) The existence of FRP was also found to alter the Hsu/Zhu ratios. While the Hsu/Zhu ratio ν_{21} for FRP RC element was the same as un-strengthened RC element, the Hsu/Zhu ratio ν_{12} was found to be much smaller in FRP RC element than for RC element, which means the for the same compressive strain increment, the increase of tensile strain is much smaller for specimen with FRP than the un-strengthened RC members. This can be attributed to the confinement the FRP provides, which stiffens the specimen in the tensile direction. Another fact that can be observed from the test results is that as the increase of the FRP stiffness, the Hsu/Zhu ratio decreases. This can be explained that as the FRP reinforcement ratio increases, a better confinement is provided and the specimen becomes stiffer in the tensile direction.

5) As case study, the modified constitutive laws was incorporated in SMM and used to predict the behavior of two FRP strengthened RC panels subjected to pure shear load. The prediction of SMM with modified constitutive laws shows a better agreement with experimental test compared to SMM with original constitutive laws, which indicates the accuracy of the modified constitutive laws proposed in this paper.

In next chapter, conclusion of this research will be given. Application and limitation for this study is also addressed. Future work is also given at the end.

CHAPTER 6 CONCLUSIONS AND RECOMMENDATIONS

6.1 GENERAL

Softened truss model theories have been developed and widely used to predict the behavior of RC element under in-plane shear stress fields. The softened truss model theory requires equilibrium equations, compatibility equations, and a set of constitutive laws that links stress and strain. In order to use the softened truss model theory to predict the behavior of the FRP RC element under in-plane shear stress fields, new constitutive laws for each material component in FRP RC element have to be re-established. The object of this research was to investigate the constitutive laws related to concrete in tension, steel in tension, the softening coefficient and the modified Hsu/Zhu ratios.

The modified constitutive laws of concrete in tension, steel in tension, were determined from uniaxial tension tests of 13 FRP RC prim specimens; the softened coefficient and Hsu/Zhu ratio were modified by biaxial tension-compression tests of six full-size FRP RC panels. The studied variables in uniaxial tension tests are steel reinforcement ratio, FRP reinforcement ratio and wrapping schemes; the studied variable in biaxial tension-compression tests is FRP reinforcement ratios. These newly developed material laws will be used to further develop models to predict the behavior of FRP strengthened RC elements subjected to shear and torsion. The results from both experimental and analytical studies in this research project will provide a promising contribution to the prediction of the behavior of FRP RC members under shear, which is expected to ultimately improve the accuracy of the available design guidelines.

As a summary, all these derived constitutive laws are presented in this chapter. The main findings and conclusions are addressed, and also, recommendations for future research are presented.

6.2 SUMMARY OF MODIFIED CONSTITUTIVE LAWS

6.2.1 Concrete in Tension

The stress strain relationship for concrete in tension was proposed as:

$$\sigma_c = E_c \varepsilon_1 \qquad \text{when } \varepsilon_1 \le \varepsilon_{cr}, \text{ and} \tag{6-1}$$

$$\sigma_c = f_{cr}\left(\frac{\varepsilon_{cr}}{\varepsilon_1}\right)^c \qquad \text{when } \varepsilon_1 > \varepsilon_{cr}, \tag{6-2}$$

$$\text{where } c = K_w K_{f/s}\,. \tag{6-3}$$

The factor K_w is to describe the effect of wrapping schemes to the tensile behavior of concrete. For full anchorage (rupture failure expected): fully wrap or U-wrap with anchors,

$$K_w = 1, \tag{6-4a}$$

and for other anchorage (non-rupture failure more likely): side bond or U-wrap

$$K_w = 1.6\,. \tag{6-4b}$$

The factor K_f is to describe the effect of FRP/steel stiffness ratio to the tensile behavior of concrete. It is proposed as

$$K_f = 0.25\left(\frac{\rho_f E_f}{\rho_s E_s}\right) + 0.15\,, \tag{6-5}$$

where ε_1 is the average tensile strain of concrete, σ_c are the average compressive stress in concrete, ρ_s and ρ_f are the reinforcement ratios of steel and FRP, respectively, E_s and

E_f are the modulus of elasticity of steel and FRP, respectively; ε_{cr} and f_{cr} are the strain and stress at cracking, K_w and $K_{f/s}$ are two factors considering the effect of wrapping schemes and FRP/steel stiffness ratio.

6.2.2 Steel in Tension

The stress strain relationship for steel in tension was proposed as:

$$f_s = E_s \varepsilon_s \qquad \varepsilon_s < \varepsilon_y^{'}, \tag{6-6}$$

$$f_s = (0.91 - 2B)\, f_y + (0.02 + 0.25B) E_s \varepsilon_s \qquad \varepsilon_s \geq \varepsilon_y^{'}, \tag{6-7}$$

$$\varepsilon_y^{'} = f_y^{'} / E_s, \qquad f_y^{'} = (0.93 - 2B)\, f_y, \tag{6-8}$$

$$B = \frac{1}{\rho_e}\left(\frac{f_{cr}}{f_y}\right)^{1.5}, \tag{6-9}$$

$$f_{cr} = 3.75\sqrt{f_c^{'}(\text{psi})}, \tag{6-10}$$

$$\rho_e = \rho_s + n_{f/s}\rho_f \text{ and } n_{f/s} = \frac{E_f}{E_s}, \tag{6-11}$$

where f_s is the average tensile stress of steel, f_y and $f_y^{'}$ are the yielding stress and the apparent yielding stress, respectively, $\varepsilon_y^{'}$ is the average tensile strain at apparent yielding point, and ρ_e is the proposed equivalent reinforcement ratio.

6.2.3 Softening Coefficient ζ_f

The softening coefficient, ζ_f, for concrete considering the effect of FRP sheets was proposed as

$$\zeta_f = \left(\frac{5.8}{\sqrt{f_c^{'}}} \le 0.9 \right) \left(\frac{1}{\sqrt{1+250\varepsilon_1}} \right) \left(1 - \frac{|\beta|}{24°} \right) f_4\left(FRP\right) \text{ and} \tag{6-12}$$

$$f_4\left(FRP\right) = 1 + 0.02\sqrt{\rho_f E_f}\ , \tag{6-13}$$

where β is the deviation angle, $f_c^{'}$ is the compressive strength of concrete from cylinder tests.

6.2.4 Modified Hsu/Zhu Ratios

The equations for calculating the modified Hsu/Zhu ratios ν_{12} and ν_{21} in FRP RC element were proposed as

$$\upsilon_{12} = 0.2 + k\varepsilon_{sf} \qquad \varepsilon_{sf} \le \varepsilon_y\ , \tag{6-14}$$

$$\text{where } k = \frac{1.7 - 0.004\rho_f E_f}{\varepsilon_y} \tag{6-15}$$

$$\nu_{12} = 1.9 - 0.004\rho_f E_f \qquad \varepsilon_{sf} > \varepsilon_y \text{, and} \tag{6-16}$$

$$\upsilon_{21} = \begin{cases} 0.2 & \text{Before cracking} \\ 0 & \text{After cracking} \end{cases}, \tag{6-17}$$

where ε_y is the yielding strain for steel, *1* direction is the principal tensile direction, and *2* direction is the principal compressive direction, the crack occurs along *1* direction.

6.3 CONCLUSIONS

The constitutive laws for concrete in tension and steel in tension were determined from 13 uniaxial tension tests of FRP RC prisms; the softening coefficient was determined from eight biaxial tension-compression panel tests conducted by Moslehy (2010) and three additional tests by the author; the modified Hsu/Zhu ratios were determined by three biaxial

tension-compression panel tests. The Effect of different parameters such as steel reinforcement ratio, FRP reinforcement ratio, and wrapping schemes were carefully investigated. The main findings in this research are discussed as follows:

a) It was found that the wrapping scheme, steel reinforcement ratio and FRP reinforcement ratio have an effect on the behavior of concrete in tension. First, compared to the un-strengthened RC element, the specimens strengthened with FRP exhibit a greater tension stiffening effect. Second, the tension stiffening effect tends to be more significant for the specimens with greater steel reinforcement ratio and lower FRP reinforcement ratios. Last but not the least, specimens strengthened by fully wrap and U-warp with FRP anchors tend to have a more significant tension stiffening effect than the specimens with side bond wrapping scheme.

b) The FRP reinforcement ratio was found to have an effect on the apparent yielding stress of the steel. With the increase of the FRP reinforcement ratio, the apparent yielding stress increases. This could be due to the effect of FRP on controlling the crack widths. It was observed that with the increase of the FRP reinforcement ratio, the average crack width decreases, and consequently the local stress concentration of the rebars at cracks decrease, which ultimately postponed the yielding of the steel.

c) The softening coefficient for FRP RC element was found to be greater than un-strengthened RC element. And also, the softening coefficient became greater with the increase of FRP reinforcement ratio. The additional compressive strength of concrete can be attributed to the confinement provided by the externally bonded FRP sheets. As the increase of the FRP reinforcement ratio, the confinement effect becomes stronger and consequently the softening coefficient will be greater.

d) The existence of FRP was also found to alter the Hsu/Zhu ratios. While the Hsu/Zhu ratio ν_{21} for FRP RC element was the same as un-strengthened RC element, the Hsu/Zhu ratio ν_{12} was found to be much smaller in FRP RC element than for RC element; which means for the same compressive strain increment in direction *2*, the increase of tensile strain in direction *1* is much smaller for the specimen with FRP than the un-strengthened RC members. This can be attributed to the additional confinement the FRP provides, which stiffens the specimen in the tensile direction. Another fact that can be observed from the test results is that with the increase of the FRP stiffness, the Hsu/Zhu ratio decreases. This can be explained in a sense that as the FRP reinforcement ratio increases, a better confinement is provided and the specimen becomes stiffer in the tensile direction.

6.4 UPCOMING WORK ON DEVELOPMENT OF SHEAR MODEL

The research work conducted by the author is part of an on-going NSF project with the aim of developing the analytical models for FRP strengthened RC elements under shear stress field including membrane stresses. Fig. 6.1 shows the work plan of the project and the contribution of the author. As the first step of developing a shear model of FRP RC elements, constitutive laws of each material component were studied through experimental and analytical investigations. The second phase of the research, which will be presented by another PhD candidate, will focus on using the newly developed material laws of the FRP RC members to predict the behavior of FRP RC member subjected to pure shear. The main objective of the second phase of the research will be developing an analytical model based on the softened membrane model to predict the behavior of FRP strengthened RC elements subjected to pure shear. In order to evaluate such behavior, a series of large scale FRP

strengthened RC panels were tested under pure shear by the Universal Panel Tester. The softening coefficients proposed here for FRP RC members will be modified based on pure shear tests. Specifically, the effect of deviation angle β will be investigated, which was not considered as an effecting parameter in the research done in this dissertation.

Furthermore, several design guidelines for FRP shear-strengthened reinforced concrete sections are currently being used around the world. Lack of basic understanding of the shear behavior in FRP strengthened members and also, inaccurate evaluation of the contribution of concrete (V_c) and transverse reinforcement (V_s) has led to the inaccuracy of the proposed models and guidelines. Unlike the models proposed by researchers, the selected relationships for V_f in design codes are expected to have considered a broader range of application and have been calibrated by a larger pool of test results. Previous studies revealed that, similar to the analytical models a large scatter was observed between the experimentally and code-derived shear strength values. This research work will lead to the basic understanding of the shear behavior. The existing shear design models for FRP strengthened members will be reviewed and assessed with the experimental tests proposed herein and possible refinements will be discussed.

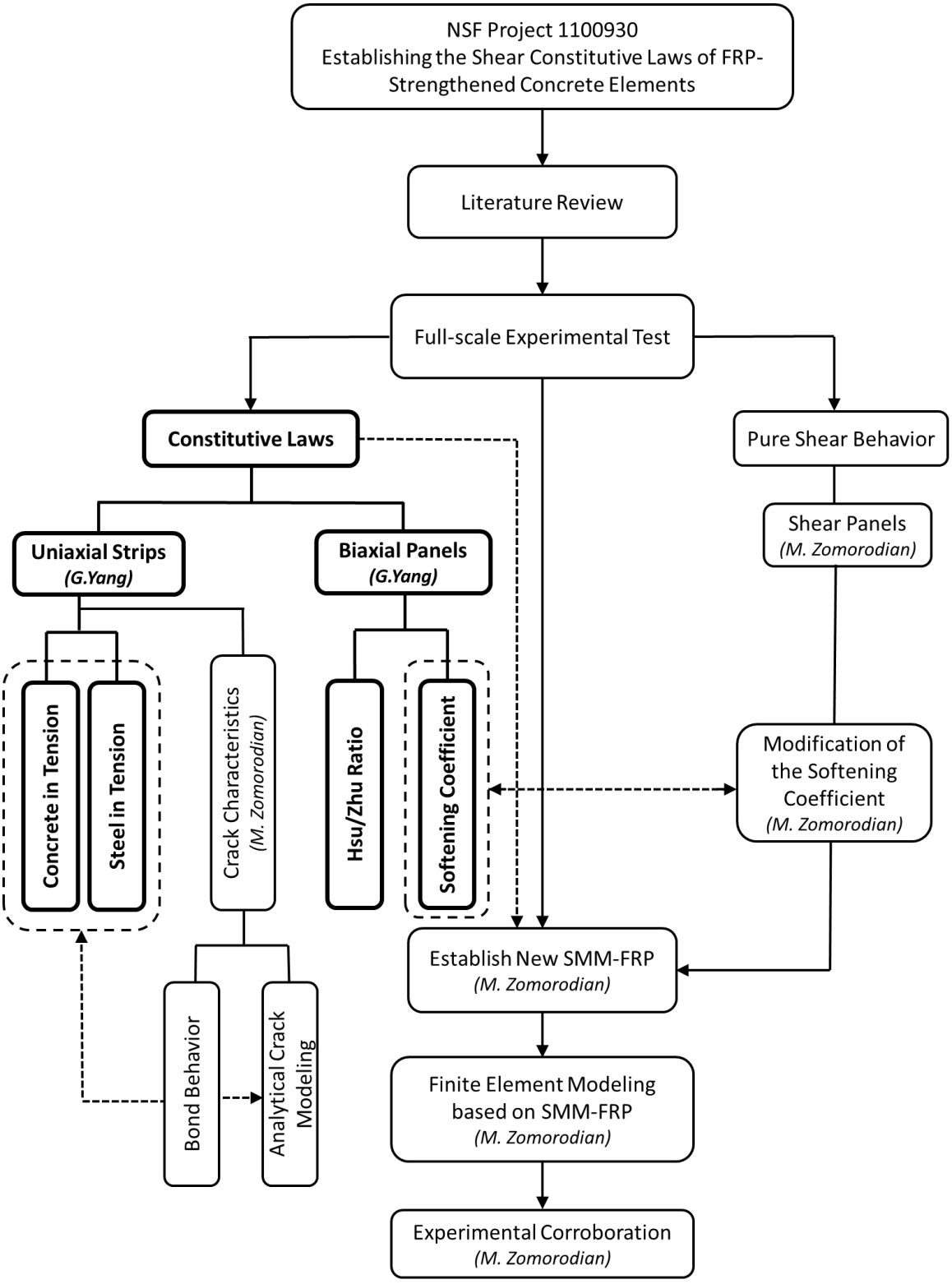

Fig. 6.1 Outline of the Whole Project

6.5 LIMITATIONS AND FUTURE WORK

6.5.1 Future Work on Shear Modeling of Beams

Due to the complexity of the shear behavior of FRP RC element, continuous research activity is still needed to fulfill the gaps in the literature. The following topics can be further studied in terms of the behavior of FRP RC element under shear stress fields:

a) Scale Factor: For RC beam without shear reinforcement, the shear resistance decreases as the beam size increases. Few test results indicate that this phenomenon was also observed in FRP RC beams; as the height of the specimen increased the shear gain due to FRP decreased. (Bousselham and Chaallal, 2004; Leung et al., 2007). More experiments can be conducted to investigate the effect of scale on the shear behavior of the FRP RC members.

b) Pre-Loading/Cracking: Externally strengthening with FRP is more suitable for existing in-service structures that often are pre-cracked. The very few investigations carried out on RC beams that were pre-cracked prior to their strengthening indicate that pre-loading does not affect the shear performance of retrofitted beams (Czaderski, 2002; Carolin and Taljsten, 2005a, and Hassan Dirar et al., 2006). However, this finding may need to be confirmed by further tests.

c) Shear Fatigue Load: As shear fatigue behavior of RC beams has been studied since 1950s, but it has not been well studied for FRP RC element. Only limited test has been done, and among these tests, most of them are flexural fatigue. The shear fatigue tests that have been done show a very limited degradation of shear behavior of FRP RC beams under fatigue load compared to static load. More tests are needed to further study the effect

of fatigue load since this loading condition exists widely in the bridge girders strengthened by externally bonded FRP sheets.

6.5.2 Limitations and Future Work on Constitutive Modeling

As for the constitutive modeling of the FRP RC element, different material laws were investigated in this study by full-scale tests of FRP RC specimens. The studied parameters in this study include the steel reinforcement ratio, FRP reinforcement ratio, and wrapping schemes. The effect of each parameters on various constitutive laws were carefully investigated. However, several other factors that might affect the constitutive laws are still in need of being investigated:

a) Effect of concrete strength and deviation angle β on the softening coefficient. The softening coefficient has been proven to be a function of concrete strength and deviation angle β for un-strengthened RC members. The derivation angle was defined as the difference between the principal directions of the un-cracked and cracked element. For FRP RC element, the effect of concrete strength and deviation angle β might be altered. In the proposed equation, this effect was not considered as a parameter.

b) Effect of loading pattern on the softening coefficient. In the proposed study, sequential loading was used. However, in the real shear loading stress condition, the stress is proportionally applied to the structure member. For un-strengthened RC members, loading patterns have been proven to be a factor that affects the behavior of concrete under compression, but similar research was not available for FRP RC elements. Therefore, research needs to be conducted to study the effect of the loading patterns on the softening coefficient for the FRP RC element.

c) Effect of wrapping scheme or anchorage system on the behavior of concrete in tension. In the proposed study, three different wrapping schemes were used, and their effects on the tension stiffening were investigated. However, there are various types of anchorage systems in the application of FRP. The proposed equation was derived based on one type of anchor only, more tests are needed to check the tension stiffening effect of specimen with other types of anchors. Also, the mechanism of different wrapping schemes, the bond behavior and crack characteristics for each wrapping schemes and anchorage systems need to be further studied to give a physical explanation for the change of the behavior due to different wrapping methods.

d) Boundary values for the effect of FRP/steel reinforcement ratios to the tension stiffening. The proposed equation was based on the regression of test data with $\rho_f E_f / \rho_s E_s$ between 0.25 and 1.11. However, the verification of the lower and upper boundary value for the proposed equation requires more test results.

e) Effect of specimen thickness to the constitutive laws. It has been observed from the beam tests (Murphy et al., 2012) that the thickness of the web will reduce after FRP debonding. The reduction of web thickness results in decrease of the shear strength. This phenomenon could also affect the material laws. In the softening test, decrease in concrete thickness could potentially cause sooner compression failure of concrete which will reduce the softening coefficient. This effect should be investigated by further tests.

REFERENCES

AASHTO (2012). *AASHTO LRFD Bridge design specifications*. Washington, DC: American Association of State Highway and Transportation Officials.

Al-Sulaimani, G. J., Shariff, A., Basanbul, I. A., Baluch, M. H, and Ghaleb, B. N. (1994). Shear repair of reinforced concrete by fiber glass plate bonding. *ACI Structural Journal*, *91*(4). 458–464.

ACI (2008). *Guide for the design and construction of externally bonded FRP systems for strengthening concrete structures*. Farmington Hills, MI: American Concrete Institute.

ACI (2008). *Building code requirements for structural concrete*. Farmington Hills, MI: American Concrete Institute.

ACI (2014). *Building code requirements for structural concrete*. Farmington Hills, MI: American Concrete Institute.

Antonopoulos, C. P. (1996). *Shear strengthening of reinforced concrete structures using composite materials* (Doctoral dissertation). Department of Civil Engineering, University of Patras, Patras, Greece.

Araki, N., Matsuzaki, Y., Nakano, K., Kataoka, T., and Fukuyama, H. (1997). Shear capacity of retrofitted RC members with continuous fiber sheets. *Proceedings of the 3rd International RILEM Symposium on Non-Metallic (FRP) Reinforcement for Concrete Structures (FRPRCS-3)*. Sapporo, Japan.

ASTM INTERNATIONAL C39/C39M-14a (2014). *Standard test method for compressive strength of cylindrical concrete specimens*. West Conshohocken: American Society for Testing and Materials.

ASTM INTERNATIONAL D30.04 (2014). *Standard test method for tensile properties of polymer matrix composite materials*. West Conshohocken, PA: American Society for Testing and Materials.

ASTM INTERNATIONAL D30.10 (2014). *Standard test method for pull-off strength for FRP bonded to concrete substrate*. West Conshohocken, PA: American Society for Testing and Materials.

Bakis, C. E., Bank, L. C., Brown, V. L., Cosenza, E., Davalos, J. F., Lesko, J. J., Machida, A., Rizkalla, S. H., and Triantafillou, T. C. (2002). Fiber-reinforced polymer composites for construction: State-of-the-art review. *Journal of Composites for Construction*, *6*(2), 73–87.

Balakrishnan, S. and Murray, D.W. (1988). Prediction of R/C panels and deep beam behavior by NLFEA. *Journal of Structural Engineering*, *114*(10), 2323–2342.

Belarbi, A., and Hsu, T. T. C. (1994). Constitutive laws of concrete in tension and reinforcing bars stiffened by concrete. *ACI Structural Journal*, *91*(4), 465–474.

Belarbi, A., and Hsu, T. T. C. (1995). Constitutive laws of softened concrete in biaxial tension compression. *ACI Structural Journal*, *92*(5), 562–573.

Belarbi, A., Bae, S., and Brancaccio, A. (2010). Behavior of full-scale RC T-beams strengthened in shear with externally bonded FRP sheets. *Construction Building Material*, *32*, 27–40.

Belarbi, A., Bae, S. W., Ayoub, A., Kuchma, D., Mirmiran, A., and Okeil, A. (2011). *NCHRP Report 678: Design of FRP systems for strengthening concrete girders in shear*. Washinton, DC: National Cooperative Highway Research Program.

Belarbi, A., Bae, S. W., Brancaccio, A. (2012). Behavior of full-scale RC T-beams strengthened in shear with externally bonded FRP sheets. *Construction and Building Materials*, *32*, 27-40.

Belarbi, A., Acun, B. (2013). FRP systems in shear strengthening of reinforced concrete structures. *Modern Building Materials, Structures and Techniques, 57*, 2–8.

Belletti, B., Cerioni, R. and Iori, I. (2001). Physical Approach for Reinforced-Concrete (PARC) membrane elements. *Journal of Structural Engineering*, *127*(12) 1412–1426.

Berset, J. D. (1992). S*trengthening of reinforced concrete beams for shear using FRP composites* (Master's thesis). Retrieved from DSpace@MIT.

Bischoff, P. H. (2001). Effects of shrinkage on tension stiffening and cracking in reinforced concrete. *Canadian Journal of Civil Engineering*, *28*(3), 363–374.

Bischoff, P. H. (2003). Tension stiffening and cracking of steel fiber-reinforced concrete. *Journal of Materials in Civil Engineering*, *15*(2), 174–182.

Bischoff, P. H. (2005). Reevaluation of deflection prediction for concrete beams reinforced with steel and Fiber Reinforced Polymer bars. *Journal of Structural Engineering, 131*(5), 752–767.

Bousselham, A., and Chaallal, O. (2004). Shear strengthening reinforced concrete beams with fiber-reinforced polymer: assessment of influencing parameters and required research. *ACI Structural Journal*, *101*(2), 219–227.

Bousselham, A., and Chaallal, O. (2006). Effect of transverse steel and shear span on the performance of RC beams strengthened in shear with CFRP. *Composites Part B: Engineering*, *37*(1). 37–46.

Bousselham A., and Chaallal O. (2008). Mechanisms of shear resistance of concrete beams strengthened in shear with externally bonded FRP. *Journal of Composite for Constructions, 12*(5), 499–512.

CAN/CSA S806-12 (2012). *Design and construction of building structures components with Fiber-Reinforced Polymers.* Rexdale, Ontario, Canada: Canadian Standard Association.

Cao, S. Y., Chen, J. F., Teng, J. G., Hao, Z., and Chen, J. (2005). Debonding in RC beams strengthened with complete FRP wraps. *Journal of Composites for Construction, 9*(5), 417–428.

Carolin, A., and Taljsten, B. (2005). Theoretical study of strengthening for increased shear bearing capacity. *Journal of Composites for Construction, 9*(6), 497–506.

Ceroni, F., Pecce M., and Matthys, S. (2004). Tension stiffening of RC ties strengthened with externally bonded FRP sheets. *Journal of Composites for Construction, 8*(1), 510–518.

Chaallal, O., Nollet, M. J., and Perraton, D. (1998). Strengthening of RC beams with externally bonded fiber-reinforced-plastic plates: design guidelines for shear and flexure. *Canadian Journal of Civil Engineers, 25*(4), 692–704.

Chaallal, O., Shahawy, M., and Hassan, M. (2002). Performance of reinforced concrete T-girders strengthened in shear with carbon fiber reinforced polymer fabrics. *ACI Structural Journal, 99*(3), 335–343.

Chajes, M. J., Jansuska, T. F., Mertz, D. R., Thomson, T. A., and Finch, W. W. (1995). Shear strength of RC beams using externally applied composite fabrics. *ACI Structural Journal, 92*(3), 295–303.

Chen G.M., Teng J.G., Chen J.F. (2010). Interaction between steel stirrups and shear-strengthening FRP strips in RC Beams. *Journal of Composite for Constructions, 14*(5), 498–509.

Chen, G., Teng, J., and Chen, J. (2013). Shear strength model for FRP-strengthened RC beams with adverse FRP-steel interaction. *Journal of Composites for Construction, 17*(1), 50–66.

Chen, J. F., and Teng, J. G. (2003a). Shear capacity of FRP strengthened RC beams: FRP debonding. *Construction Building Materials, 17*(1), 27–41.

Chen, J. F., and Teng, J. G. (2003b). Shear capacity of Fiber-Reinforced Polymer-strengthened reinforced concrete beams: Fiber Reinforced Polymer rupture. *Journal of Structural Engineering, 129*(5), 615–625.

Chintrakarn, R. (2001). *Minimum shear steel and failure modes diagram of reinforced concrete membrane elements* (Master's thesis). Department of Civil and Environmental Engineering, University of Houston, Houston, Texas, USA.

Colalillo, M. A., and Sheikh, S. (2014). Behavior of shear-critical reinforced concrete beams strengthened with Fiber-Reinforced Polymer—Analytical method. *ACI Structural Journal*, *111*(6), 1385–1396.

Colotti, V., and Swamy, R. N. (2011). Unified analytical approach for determining shear capacity of RC beams strengthened with FRP. *Engineering Structures, 33*, 827–842.

Concrete Society (2004). *Design guidance on strengthening concrete structures using fibre composite materials: Technical report 55*. London, UK: Concrete Society.

Crisfield, M.A. andWills, J. (1989). Analysis of R/C panels using different concrete models. *Journal of Engineering Mechanics*. *115*(3) 578–597.

Dai, J. G., Saito, Y., Ueda, T., and Sato, Y. (2005). Static and fatigue bond characteristics of interfaces between CFRP sheets and frost damage experienced concrete. *Proceedings of the 7th International RILEM Symposium on Non-Metallic (FRP) Reinforcement for Concrete Structures (FRPRCS-7)*. Kansas City, Missouri.

Deniaud, C., and Cheng, J. J. R. (2001). Shear behavior of reinforced concrete t-beams with externally bonded fiber-reinforced polymer sheets. *ACI Structural Journal, 98*(3). 386–394..

Deniaud, C., and Cheng, J. J. R. (2004). Simplified shear design method for concrete beams strengthened with fiber reinforced polymer sheets. *Journal of Composites for Construction, 8*(5), 425–433.

Denton, S. R., Shave, J. D., and Porter, A. D. (2004). Shear strengthening of reinforced concrete structures using FRP composites. *Proceedings of the International Conference on Advanced Polymer composites for Structural applications in Constructions*. Cambridge, UK.

Dolan, C. W., Rider, W., Chajes, M. J., and DeAscanis, M. (1992). Prestressed concrete beams using non-metallic tendons and external shear reinforcement. *ACI SP 138-29*. 475–495.

Eshwar, N., Nanni, A., and Ibell, T. (2003). CFRP strengthening of concrete bridges with curved soffits. *Proceedings of the International Conference on Structural Faults and Repairs*, Montreal, Quebec.

Eshwar, N., Nanni, A., and Ibell, T.J. (2008). Performance of two anchor systems of externally bonded Fiber-Reinforced Polymer laminates. *ACI Materials Journal, 105*(1), 72–80.

Eurocode-2 (2004). *Eurocode 2: Design of Concrete Structures-Part 1: General Rules and Rules for Buildings*. Brussels, Belgium: European Committee for Standardization.

Evans, R. H., and Marathe, M. S. (1968). Microcracking and stress-strain curves for concrete in tension. *Materials and Structures*, *1*(1), 61–64.

Farah, Y., and Sato, Y. (2011). Uniaxial tension behavior of reinforced concrete members strengthened with carbon fiber sheets. *Journal of Composites for Construction*, *15*(2), 215–228.

Fialkow, M. N. (1985). Design and capacity evaluation of reinforced concrete shell membranes. *ACI Structural Journal*, *82*(6), 844–852.

fib-TG9.3 (2001). *Design and Use of Externally Bonded Fiber Polymer Reinforcement (FRP EBR) for Reinforced Concrete Structures*. Lausanne, Switzerland: International Federation for Structural Concrete.

Funakawa, I., Shimono, K., Watanabe, T., Asada, S., and Ushijima, S. (1997). Experimental study on shear strengthening with continuous fiber reinforcement sheet and methyl methacrylate resin. *Proceedings of the 3rd International RILEM Symposium on Non-Metallic (FRP) Reinforcement for Concrete Structures (FRPRCS-3)*. Sapporo, Japan.

Ghiassi, B., Xavier, Oliveira, D., Lourenço, P. (2013). Application of digital image correlation in investigating the bond between FRP and masonry. *Composite Structures*, *106*, 340–349.

Gopalaratnam, V. S., and Shah, S. P. (1985). Softening response of plain concrete in direct tension. *ACI structural Journal*, *83*(3), 310-323.

Hsu T. T. C., Belarbi A., and Pang X. (1995). A universal panel tester. *Journal of Testing and Evaluation*, *23*(1), 41–49.

Hsu, C. T. T., Punurai, W., and Zhang, Z. (2003). Flexural and shear strengthening of RC beams using Carbon Fiber Reinforced Polymer laminate, *ACI SP 211-5*, 89–113.

Hsu, T. T. C. (1993). *Unified theory of reinforced concrete*. Boca Raton, FL: CRC Press Inc.

Hsu, T.T.C. and Zhang, L.X. (1996). Tension stiffening in reinforced concrete membrane elements. *Structural Journal of the American Concrete Institute*, *93*(1), 108–115.

Hsu, T. T. C., and Zhang, L. X. (1997). Nonlinear analysis of membrane elements by Fixed-Angle Softened-Truss Model. *Structural Journal of the American Concrete Institute*, *94*(5), 483–492.

Hsu, T.T.C., and Zhu, R. R. H. (2002). Softened Membrane Model for reinforced concrete elements in shear. *Structural Journal of the American Concrete Institute*, *99*(4), 460–469.

Hsu, C. T. T., Punurai, W., and Zhang, Z. (2003). Flexural and shear strengthening of RC beams using Carbon Fiber Reinforced Polymer Laminate. *ACI SP-211-5*, 89–113.

Hughes, B. P., and Chapman, G. P. (1966). The deformation of concrete and microconcrete in compression and tension with particular reference to aggregate size. *Magazine of Concrete Research*, *8*(54), 19–24.

Hutchinson, R. L., and Rizkalla, S. H. (1999). Shear strengthening of AASHTO bridge girders using carbon fiber reinforced polymer sheets. *ACI SP188*, 945–958.

ISIS Design Manual 4. (2001). *Strengthening reinforced concrete structures with externally-bonded fiber reinforced polymers*. Winnipeg, Canada: Intelligent Sensing for Innovative Structures.

Izumo, J., Shin H., Maekawa, K., and Okamura, H. (1991). An analytical model for RC panels subjected to in-plane stresses. *Proceedings of the International Workshop on Concrete Shear in Earthquake*. London, UK: Elsevier Science Publishers, Inc.

Jiang, D. H., Shah, S. P., and Andonian, A. T. (1984). Study of the transfer of tensile forces by bond, *ACI Journal Proceedings, 81*(3), 251–259.

Jinno, Y., and Tsukagishi, H. (1998). Structural properties of RC walls strengthened by Carbon Fiber Sheets, *Proceedings of Architectural Institute of Japan Annual Conference*, Fukuoka, Japan.

JSCE (2001). *Recommendations for upgrading of concrete structures with use of continuous fiber sheets*. Tokyo, Japan: Japan Society of Civil Engineers

Kachlakev, D. I, and Barnes, W. A. (1999). Flexural and shear performance of concrete beams strengthened with fiber reinforced polymer laminates. *Proceedings of the 4th International RILEM Symposium on Non-Metallic (FRP) Reinforcement for Concrete Structures (FRPRCS-4)*. Baltimore, Maryland.

Kage, T., Abe, M., Lee, H. S., Tomosawa F. (1997). Effect of CFRP sheets on shear strengthening of rc beams damaged by corrosion of stirrup. *Proceedings of the 3rd International RILEM Symposium on Non-Metallic (FRP) Reinforcement for Concrete Structures (FRPRCS-3)*. Sapporo, Japan.

Kaklauskas, G., and Gribniak, V. (2011). Eliminating shrinkage effect from moment-curvature and tension-stiffening relationships of reinforced concrete members, *Journal of Structural Engineering. 137*(12), 1460–1469.

Kaklauskas, G., Gribniak, V., Bacinskas, D. and Vainiunas, P. (2009). Shrinkage influence on tension stiffening in concrete members, *Engineering Structures*, *31*(6), 1305–12.

Kamiharako, A., Maruyama, K., Takada, K., and Shimomura, T. (1997). Evaluation of shear contribution of FRP sheets attached to concrete beams. *Non-Metallic (FRP) Reinforcement for Concrete Structures*, *1*, 467–474.

Kaufmann, W. and Marti, P. (1998). Structural concrete: cracked membrane model. *Journal of Structural Engineering*. *124*(12) 1467–1475.

Khalifa, A., and Nanni, A. (2002). Rehabilitation of rectangular simply supported RC beams with shear deficiencies using CFRP composite. *Construction and Building Materials*, *16*(1), 135–146.

Khalifa, A., Gold, W., Nanni, A., and Abdel Aziz, M. I. (1998). Contribution of externally bonded FRP to shear capacity of RC flexural members," *Journal of Composites for Construction*, *2*(4), 195–202.

Khalifa, A., Tumialan, G., Nanni, A., and Belarbi, A. (1999). Shear strengthening of continuous reinforced concrete beams using externally bonded Carbon Fiber Reinforced Polymer sheets. *Proceedings of 4th International RILEM Symposium on Non-Metallic (FRP) Reinforcement for Concrete Structures (FRPRCS-4)*, Baltimore, Maryland.

Kong, K. L., Beeby, A. W., Forth, J. P. and Scott, R. H. (2007). Cracking and tension zone behavior in reinforced concrete flexural members. *Proceedings of ICE: Structure and Buildings, 160*(3), 165–172.

Lee, G. Y., and Kim, W. (2008). Cracking and tension stiffening behavior of high strength concrete tension members subjected to axial load. *Advances in Structural Engineering, 11*(5), 127–137.

Maeda, T., Asano, Y., and Sato, Y. (1997). A study on bond mechanism of carbon fiber sheet. *Proceedings of the 3rd International RILEM Symposium on Non-Metallic (FRP) Reinforcement for Concrete Structures (FRPRCS-3).* Sapporo, Japan.

Malek, A. M., and Saadatmanesh, H. (1998). Analytical study of reinforced concrete beams strengthened with web-bonded fiber reinforced plastics or fabrics. *ACI Structural Journal*, *95*(3), 343–351.

Malvar, L. J. (1995). Tensile and bond properties of GFRP reinforcing bars. *ACI Materials Journal*, *92*(3). 276–285.

Miller, B. (1999). *Bond between carbon fiber reinforced polymer sheets and concrete* (Master's thesis), Department of Civil, Architectural, and Environmental Engineering, University of Missouri-Rolla, Rolla, MO.

Mitsui, Y., Murakami, K., Takeda, K., and Sakai, H. (1998). A study on shear reinforcement of reinforced concrete beams externally bonded with carbon fiber sheets. *Composites Interfaces*, *5*(4), 285–295.

Miyahara, T., Kawakami, T., and Maekawa, K. (1987). Nonlinear behavior of cracked reinforced concrete plate element under uniaxial compression. *Concrete Library of JSCE*, 131–144. (Translation from *Proceedings of JSCE*, No. 378N-6, Feb. 1987).

Mofidi, A. and Chaallal, O. (2014). Effect of steel stirrups on shear resistance gain due to externally bonded fiber-reinforced polymer strips and sheets. *ACI Structural Journal, 111*(2), 353–361.

Monti, G., and Liotta, M. A. (2005). FRP-strengthening in shear: tests and design equations. *Proceedings of 7th International RILEM Symposium on Non-Metallic (FRP) Reinforcement for Concrete Structures (FRPRCS-7).* Kansas City, Missouri.

Monti, G., and Liotta, M. A. (2005). FRP-strengthening in shear: tests and design equations. *Proceedings of the 7th International RILEM Symposium on Non-Metallic (FRP) Reinforcement for Concrete Structures (FRPRCS-7).* Kansas City, Missouri.

Moslehy, Y. (2010). *Constitutive relationships and smart aggregates-based damage evaluation of FRP retrofitted concrete membrane elements* (Doctoral dissertation). Department of Civil and Environmental Engineering, University of Houston, Houston, Texas.

Murphy, M., Belarbi, A., and Bae, S. W. (2012). Behavior of prestressed concrete I-girders strengthened in shear with externally bonded fiber-reinforced-polymer sheets. *PCI Journal*, 63-82.

Mutsuyoshi, H., Ishibashi, T., Okano, M., and Katsuki, F. (1999). New design method for seismic retrofit of bridge columns with continuous fiber sheet–Performance-based design. *Proceedings of the 4th International RILEM Symposium on Non-Metallic (FRP) Reinforcement for Concrete Structures (FRPRCS-4).* Baltimore, Maryland.

Nehdi, M., and Nikopour, H. (2010). Genetic algorithm model for shear capacity of RC beams reinforced with externally bonded FRP. *Materials and Structures*, *33*, 1249-1258.

Niemitz, C.W. (2008). *Anchorage of Carbon Fiber Reinforced Polymers to reinforced concrete in shear applications* (Master's thesis). Department of Civil and Environmental Engineering, University of Massachusetts-Amherst, Amherst, MA.

Oehlers, D. J., Liu. I. S. T., and Seracino, R. (2005). Shear deformation debonding of adhesively bonded plates. *Proceedings of the ICE - Structures and Buildings*, *158*(1), 77-84.

Ohuchi, H., Ohno, S., Katsumata, H., Kobatake, Y., Meta, T., Yamagata, K., Inokuma, Y., and Ogata, N. (1994). Seismic strengthening design technique for existing bridge columns with CFRP, *Proceedings of the 2nd International Workshop on Seismic Design and Retrofitting of Reinforced Concrete Bridges*. Queenstown, New Zealand.

Okamura, H., Maekawa, K., and Sivasubramaniyam, S. (1985). Verification of modeling for reinforced concrete finite element. *Proceedings of Japan-US Seminar on Finite Element Analysis of Reinforced Concrete Structures*, Tokyo, Japan.

Ono, K., Matsumura, M., Sakanishi, S., and Miyata, K. (1997). Strength improvement of rc bridge piers with carbon fiber sheet. *Proceedings of the 3rd International RILEM Symposium on Non-Metallic (FRP) Reinforcement for Concrete Structures (FRPRCS-3)*. Sapporo, Japan.

Orton, S.L. (2007). *Development of a CFRP system to provide continuity in existing reinforced concrete buildings vulnerable to progressive collapse* (Doctoral dissertation). Department of Civil, Architectural, and Environmental Engineering, University of Austin-Texas, Austin, Texas.

Pang, X. B., and Hsu, T. T. C. (1995). Behavior of reinforced concrete membrane elements in shear. *ACI Structural Journal*, *92*(6), 665–679.

Pang, X. B., and Hsu, T. T. C. (1996). Fixed-Angle Softened-Truss Model for reinforced concrete. *ACI Structural Journal, 93*(2), 197–207.

Park, S. Y., Naaman, A. E., Lopez, M. M., and Till, R. D. (2001).Shear strengthening effect of R/C beams using glued CFRP sheets. *Proceedings of the International Conference on FRP Composites in Civil Engineering*. Hong Kong, China.

Pellegrino, C., and Modena, C. (2002). Fiber Reinforced Polymer shear strengthening of reinforced concrete beams with transverse steel reinforcement, *Journal of Composites for Construction, 6*(2), 104–111.

Ritter, W. (1899). Die bauweise hennebique. *Schweizerische Bauzeitung*, *33*(7) 59–61.

Robinson, J. R. and Demorieux, J. M. (1968). Essai de Traction-Compression sur Modeles d'Ames de Poutre en Beton Arme. Compte Rendu Partiel I, U.T.I., Institut de Recherches Appliquees du Beton Arme, Paris, France.

Sato, Y., Ueda, T., Kakuta, Y., and Tanaka, T. (1996). Shear reinforcing effect of carbon fiber sheet attached to the side of reinforced concrete beams. *Proceedings of the 3rd International Conference on Advanced Composite Materials in Bridges and Structures*. Montreal, Canada.

Shima, H., Chou, L., and Okamura, H. (1987). Micro and macro models for bond in reinforced concrete. *Journal of Facture Engineering. 39*(2), 133–194.

Sim, J., Kim, G., Park, C., and Ju, M. (2005). Shear strengthening effects with varying types of FRP materials and strengthening methods. *Proceedings of the 7th International RILEM Symposium on Non-Metallic (FRP) Reinforcement for Concrete Structures (FRPRCS-7)*. Kansas City, Missouri.

Somayaji, S., and Shah, S.P. (1981). Bond stress versus slip relationship and cracking response of tension members. *ACI Journal Proceedings*, *78*(3), 217–225.

Taerwe, L., Khalil, H., and Matthys, S. (1997). Behavior of rc beams strengthened in shear by external cfrp sheets. *Proceedings of the 3rd International RILEM Symposium on Non-Metallic (FRP) Reinforcement for Concrete Structures (FRPRCS-3)*. Sapporo, Japan.

Taljsten, B. (1997). Strengthening of concrete structures for shear with bonded CFRP fabrics. *Proceedings of the US-Canada-Europe Workshop on Bridge Engineering*. Zurich, Switzerland.

Tamai, S., Shima, H., Izumo, J. and Okamura, H. (1987). Average stress-strain relationship in post yield range of steel bar in concrete. *Concrete Library of JSCE, 11*, 117-129.

Tastani, S. P., and Pantazopoulou, S. J. (2010). Direct tension pullout bond test: experimental test. *Journal of Structural Engineering*, *136*(6), 731–743.

Teng, J. G., Lam, L., and Chen J. F., (2004). Shear strengthening of RC beams with FRP composites. *Progress in Structural Engineering and Materials*, *6*(1), 173–184.

Triantafillou, T. C. (1997). Shear strengthening of concrete members using composites. *Proceedings of the 3rd International RILEM Symposium on Non-Metallic (FRP) Reinforcement for Concrete Structures (FRPRCS-3)*. Sapporo, Japan.

Triantafillou, T. C. (1998), Shear strengthening of reinforced concrete beams using epoxy-bonded FRP composites. *ACI Structural Journal*, *95*(2), 107–115.

Triantafillou, T. C., and Antonopoulos, C. P. (2000). Design of concrete flexural members strengthened in shear with FRP, *Journal of Composites for Construction, 4(*4), 198–205.

Ueda, T., Yamaguchi, R., Shoji, K., and Sato, Y. (2002). Study on behavior in tension of reinforced concrete members strengthened by carbon fiber sheet. *Journal of Composite for Construction*, *6*(3), 168–174.

Uji, K. (1992). Improving the shear capacity of existing reinforced concrete members by applying carbon sheets. *Transactions of the Japan Concrete Institute*, *14*(1). 253–266.

Umezu, K., Fujita, M., Nakai, H., and Tamaki, K. (1997). Shear behavior of RC beams with aramid fiber sheet. *Proceedings of the 3rd International RILEM Symposium on Non-Metallic (FRP) Reinforcement for Concrete Structures (FRPRCS-3)*. Sapporo, Japan.

Vecchio, F. J., and Collins, M. P. (1981). Stress-strain characteristic of reinforced concrete in pure shear. *Advanced Mechanics of Reinforced Concrete*, Final Report, International Association of Bridge and Structural Engineering, Zurich, Switzerland, 221–225.

Vecchio, F. J., and Collins, M. P. (1986). The Modified Compression-Field Theory for reinforced concrete elements subjected to shear. *ACI Structural Journal*, *83*(2), 219–231.

Vecchio, F. J. (2000). Disturbed stress field model for reinforced concrete: formulation. *Journal of Structural Engineering*. *126*(9) 1070–1077.

Vecchio, F. J. (2001). Disturbed stress field model for reinforced concrete: Implementation. *Journal of Structural Engineering*, *127*(1) 12–20.

Wang, J., (2006). *Constitutive relationships of prestressed concrete membrane elements* (Doctoral Thesis). Department of Civil and Environmental Engineering, University of Houston, Houston, Texas.

Wu, H. Q., and Gilbert, R. I. (2008). An experimental study of tension stiffening in reinforced concrete members under short term and long term loads, *Report No. R-449*, University of New South Wales, Sydney, Australia.

Wu, H. Q., and Gilbert, R. I. (2009). Modelling short-term tension stiffening in reinforced concrete prisms using a continuum-based finite element model. *Engineering Structures*, *31*(10), 2380–2391.

Zararis, P. D. (2003). Shear strength and minimum shear reinforcement of reinforced concrete slender beams. *ACI Structural Journal*, *100*(2), 203–214.

Zhang, L. X., and Hsu, T. T. C. (1998). Behavior and analysis of 100-MPa concrete membrane elements. *Journal of Structural Engineering*, *124*(1), 24–34.

Zhang, Z., and Hsu, C. T. (2005). Shear strengthening of reinforced concrete beams using Carbon-Fiber-Reinforced Polymer laminates, *Journal of Composites for Construction*, *9*(2), 158–169.

Zhu, R. R. H., and Hsu, T. T. C. (2002). Poisson effect in reinforced concrete membrane elements. *ACI Structural Journal*, *99*(5), 631–640.

APPENDIX I ANALYZED DATA OF TEST SPECIMENS

List of Notations

NH	=	average tensile load on the north side (kips/jack)
SH	=	average tensile load on the south side (kips/jack)
NV	=	average compressive load on the north side (kips/jack)
SV	=	average compressive load on the south side (kips/jack)
NH 1~2	=	No. 1~2 horizontal LVDT readings on the north side
SH 1~2	=	No. 1~2 horizontal LVDT readings on the south side
NH lvdt	=	Average of 4 horizontal LVDT readings on the north side
SH lvdt	=	Average of 4 horizontal LVDT readings on the south side
NV lvdt	=	Average of 4 vertical LVDT readings on the north side
SV lvdt	=	Average of 4 vertical LVDT readings on the south side
ND lvdt	=	Average of 2 diagonal LVDT readings on the north side
SD lvdt	=	Average of 2 diagonal LVDT readings on the south side

Group I

Uniaxial Tensile Test

Prism REF-R3

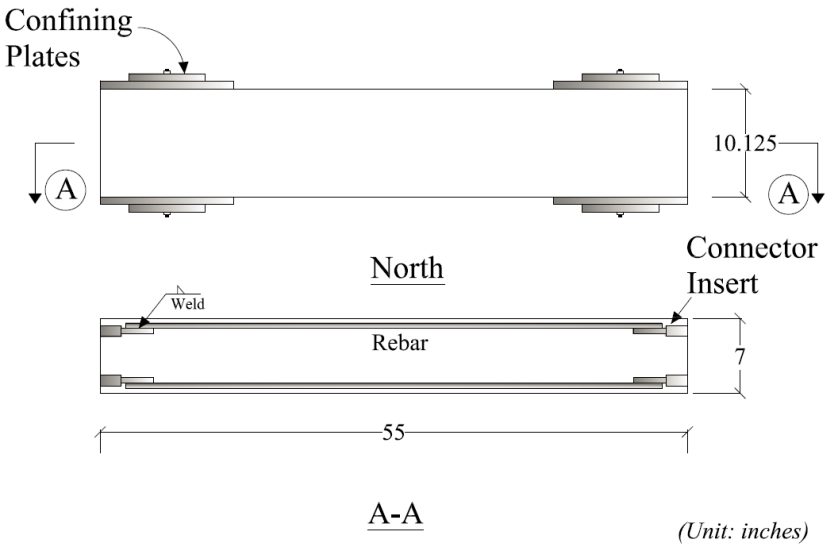

Casting Date: Dec. 01, 2013

Testing Date: Dec. 10, 2013

Materials:

Concrete

f'c=6,119 psi (1st batch: 6449psi; 2nd batch: 5,789 psi)

Steel Reinforcements

2 #3 rebar, ρs = 0.31%, *fy* = 66.5 ksi

FRP Reinforcements

No FRP

Test Data_REF-R3				
	NH	SH	NH1	SH1
1	0.00	0.05	0.000000	0.000000
2	0.06	0.15	0.000083	0.000017
3	0.10	0.20	0.000017	0.000067
4	0.15	0.50	0.000035	0.000031
5	0.20	0.75	0.000017	0.000020
6	4.50	1.60	0.000013	0.000010
7	4.05	2.80	0.000013	0.000019
8	4.20	4.75	0.000010	0.000002
9	4.15	6.65	0.000050	0.000067
10	6.60	8.05	0.000033	0.000033
11	8.55	10.25	0.000052	0.000083
12	10.65	11.15	0.000079	0.000077
13	8.40	6.85	0.004850	0.003228
14	7.65	6.50	0.012434	0.009124
15	2.50	2.05	0.008465	0.008856
16	0.80	-1.25	0.005984	0.008106
17	1.65	0.50	0.006598	0.008290
18	3.75	2.75	0.007432	0.008606
19	6.35	4.85	0.008582	0.009058
20	8.10	5.50	0.009701	0.009455
21	9.15	6.70	0.010165	0.009855
22	9.05	7.25	0.011051	0.010654
23	10.35	6.75	0.012184	0.011753
24	10.25	6.90	0.013399	0.012835
25	11.85	6.90	0.014516	0.013953
26	11.20	6.25	0.015218	0.014650
27	6.70	4.85	0.016332	0.015684
28	10.10	5.90	0.017101	0.016498
29	12.35	11.15	0.017884	0.017397
30	11.90	11.15	0.018749	0.018331
31	12.05	10.60	0.019501	0.019112
32	11.70	11.55	0.020416	0.020030
33	12.15	12.30	0.021001	0.020677
34	8.00	10.05	0.017399	0.021445
35	5.45	6.35	0.015368	0.019497

Prism REF-R4

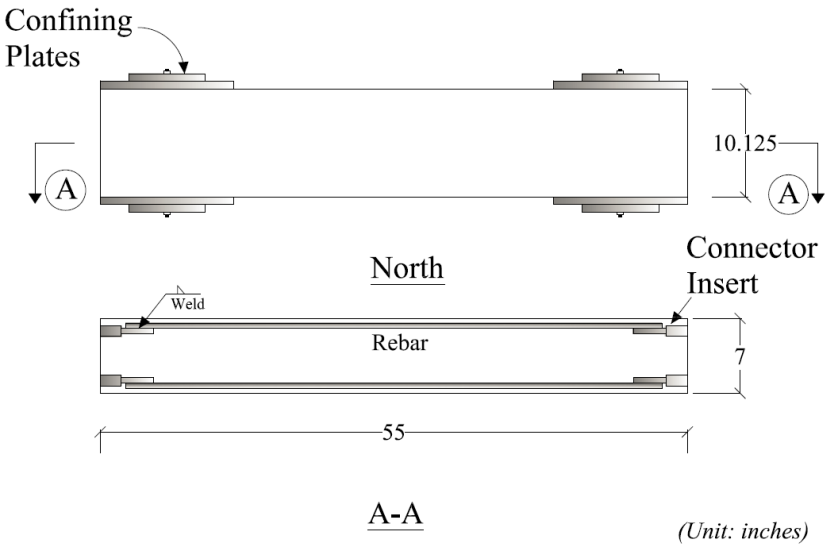

Casting Date: Dec. 01, 2013

Testing Date: Dec. 09, 2013

Materials:

Concrete

f'c=6,119 psi (1st batch: 6449psi; 2nd batch: 5,789 psi)

Steel Reinforcements

2 #4 rebar, ρs = 0.55%, *fy* = 67.0 ksi

FRP Reinforcements

No FRP

Test Data_REF-R4				
	NH	SH	NH1	SH1
1	0.00	0.00	0.000000	0.000000
2	0.40	0.30	0.000008	0.000035
3	3.15	4.90	0.000083	0.000033
4	7.45	8.60	0.000035	0.000031
5	9.20	9.40	0.000052	0.000031
6	10.90	11.00	0.000048	0.000033
7	11.15	12.80	0.000067	0.000085
8	13.10	9.40	0.001681	0.001265
9	11.15	9.60	0.001965	0.001848
10	3.00	2.50	0.000533	0.001332
11	6.20	4.20	0.000981	0.001201
12	5.20	4.40	0.000833	0.001165
13	7.55	6.30	0.001031	0.001415
14	9.65	8.30	0.001315	0.001715
15	11.25	10.20	0.001631	0.001850
16	13.35	11.50	0.001931	0.002164
17	14.85	10.80	0.002167	0.002416
18	15.15	13.20	0.002531	0.002797
19	16.65	14.90	0.003248	0.003363
20	16.60	15.20	0.003834	0.003929
21	16.65	15.40	0.004300	0.004412
22	17.05	16.40	0.005134	0.005128
23	17.20	16.80	0.005848	0.005944
24	18.05	16.20	0.006367	0.006460
25	18.35	17.10	0.007250	0.007193
26	18.45	16.40	0.008267	0.008108
27	18.75	17.70	0.009551	0.009341
28	20.30	17.50	0.011415	0.011039
29	19.40	16.50	0.013099	0.012639
30	19.35	17.90	0.014632	0.014055
31	18.90	18.30	0.016568	0.016000
32	19.60	19.00	0.018516	0.017751
33	19.65	17.60	0.020201	0.019547
34	19.85	18.70	0.021551	0.020912
35	13.80	14.30	0.020268	0.021331

Prism REF-R5

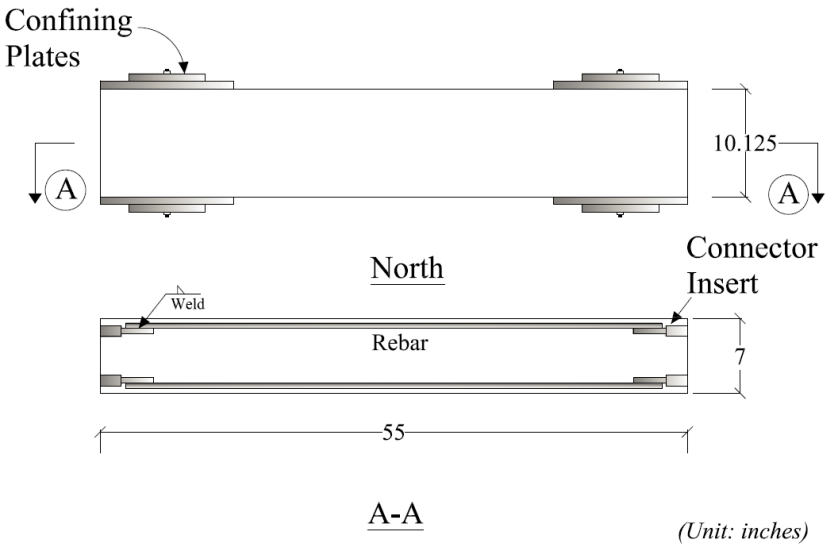

Casting Date: Dec. 01, 2013

Testing Date: Jan. 07, 2013

Materials:

Concrete

f'c=6,119 psi (1st batch: 6449psi; 2nd batch: 5,789 psi)

Steel Reinforcements

2 #5 rebar, ρs = 0.87%, *fy* = 68.0 ksi

FRP Reinforcements

No FRP

Test Data_REF-R5				
	NH	SH	NH1	SH1
1	0.00	0.00	0.000000	0.000001
2	0.55	0.15	0.000065	0.000035
3	6.20	8.30	0.000055	0.000065
4	8.50	13.60	0.000790	0.000086
5	8.80	7.25	0.001133	0.000098
6	1.35	1.55	0.000433	0.000266
7	1.65	1.35	0.000367	0.000298
8	3.85	3.90	0.000533	0.000381
9	3.25	1.55	0.000331	0.000081
10	0.52	0.13	0.000365	0.000081
11	0.85	0.60	0.000315	0.000114
12	12.30	13.70	0.000567	0.000583
13	13.20	14.00	0.000783	0.000785
14	15.65	17.90	0.001302	0.001101
15	18.45	20.45	0.001783	0.001548
16	21.45	19.30	0.002169	0.002233
17	19.10	22.15	0.002583	0.002550
18	20.55	22.50	0.003100	0.002916
19	21.20	22.95	0.003767	0.003863
20	21.45	22.45	0.004469	0.004364
21	22.70	23.80	0.005000	0.004964
22	23.10	24.15	0.005669	0.005644
23	23.45	23.75	0.006502	0.006427
24	23.40	22.65	0.007267	0.007143
25	24.00	23.25	0.008036	0.007961
26	24.10	23.70	0.008553	0.008527
27	22.80	23.75	0.010067	0.009923
28	23.55	24.30	0.011717	0.011522
29	24.10	25.40	0.013451	0.012904
30	25.05	24.65	0.015270	0.014454
31	25.55	24.80	0.017701	0.017052
32	26.50	25.00	0.021603	0.020848
33	26.20	26.95	0.025285	0.024827
34	30.55	24.85	0.029102	0.028690
35	2.95	4.15	0.027468	0.026525

Prism S3-025-FA

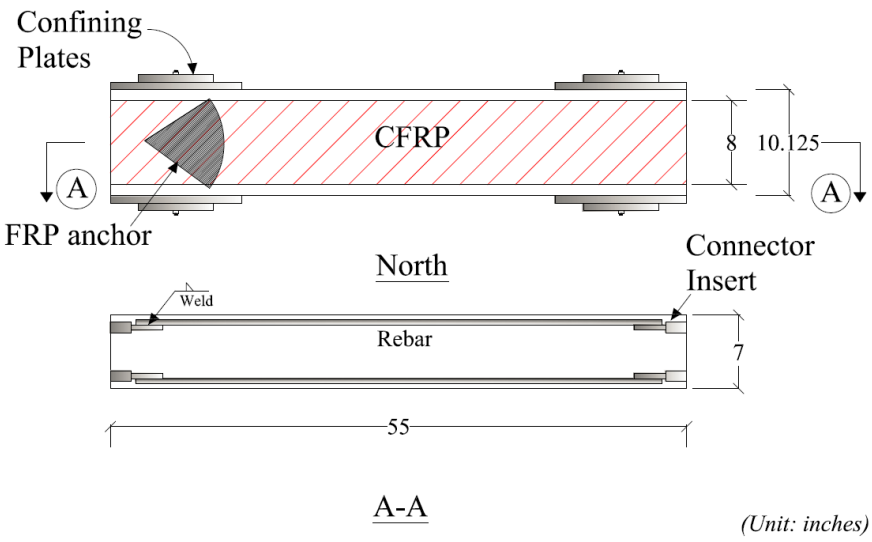

Casting Date: Dec. 29, 2013

Testing Date: Jan. 04, 2014

Materials:

Concrete

f'c=6,699 psi (1st batch: 6,826 psi; 2nd batch: 6,572 psi)

Steel Reinforcements

2 #3 rebar, ρs = 0.31%, *fy* = 66.5 ksi

FRP Reinforcements

One layer with FRP anchor, ρf = 0.56%, *fu* = 120 ksi

Test Data_S3-025-FA				
	NH	SH	NH1	SH1
1	0.00	0.00	0.000017	0.000004
2	0.05	1.65	0.000008	0.000014
3	4.25	6.00	0.000021	0.000013
4	6.45	9.85	0.000035	0.000021
5	9.20	10.85	0.000068	0.000031
6	10.90	12.60	0.000048	0.000043
7	11.15	13.30	0.000065	0.000091
8	13.10	10.55	0.001681	0.001265
9	11.15	17.40	0.001965	0.001848
10	3.00	9.45	0.000533	0.001332
11	6.20	10.90	0.000981	0.001201
12	5.20	12.15	0.000833	0.001165
13	7.55	11.55	0.001031	0.001415
14	9.65	14.95	0.001315	0.001715
15	11.25	17.30	0.001631	0.001850
16	13.35	18.45	0.001931	0.002164
17	14.85	16.80	0.002167	0.002416
18	15.15	21.40	0.002531	0.002797
19	16.65	22.75	0.003248	0.003363
20	16.60	23.40	0.003834	0.003929
21	16.65	23.10	0.004300	0.004412
22	17.05	24.25	0.005134	0.005128
23	17.20	25.00	0.005848	0.005944
24	18.05	22.80	0.006367	0.006460
25	18.35	24.20	0.007250	0.007193
26	18.45	23.10	0.008267	0.008108
27	18.75	25.30	0.009551	0.009341
28	20.30	24.70	0.011415	0.011039
29	19.40	19.90	0.013099	0.012639
30	19.35	24.80	0.014632	0.014055
31	18.90	24.40	0.016568	0.016000
32	19.60	24.70	0.018516	0.017751
33	19.65	25.90	0.020201	0.019547
34	19.85	24.55	0.021551	0.020912
35	13.80	21.40	0.020268	0.021331

Prism S3-040-FA

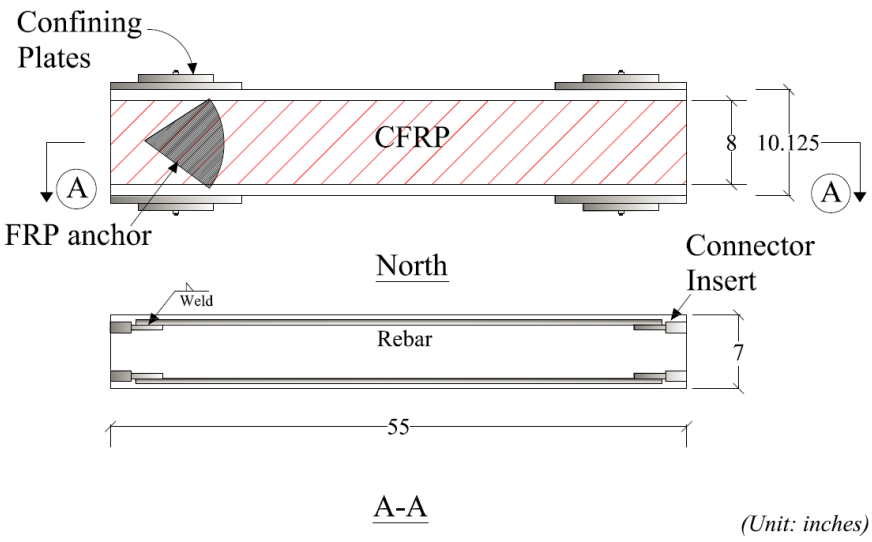

Casting Date: Dec. 29, 2013

Testing Date: Jan. 07, 2014

Materials:

Concrete

f'c=6,699 psi (1st batch: 6,826 psi; 2nd batch: 6,572 psi)

Steel Reinforcements

2 #3 rebar, ρs = 0.31%, *fy* = 66.5 ksi

FRP Reinforcements

One layer with FRP anchor, ρf = 0.90%, *fu* = 105 ksi

Test Data_S3-040-FA				
	NH	SH	NH1	SH1
1	0.00	0.00	0.000000	0.000000
2	0.38	0.25	0.000017	0.000015
3	1.25	0.85	0.000019	0.000015
4	2.36	1.52	0.000021	0.000017
5	4.30	3.25	0.000015	0.000033
6	7.10	8.25	0.000065	0.000069
7	10.60	7.90	0.000065	0.000067
8	14.10	12.45	0.000075	0.000073
9	17.75	15.00	0.000082	0.000067
10	14.70	13.25	0.001615	0.001996
11	6.50	5.35	0.000548	0.001498
12	6.00	3.55	0.000431	0.001032
13	5.15	3.65	0.000383	0.001199
14	7.65	5.35	0.000515	0.001249
15	8.60	6.00	0.000715	0.001297
16	11.30	6.60	0.000848	0.001265
17	12.70	7.70	0.001100	0.001299
18	13.60	9.50	0.001165	0.001397
19	14.40	10.10	0.001250	0.001397
20	16.45	11.25	0.001233	0.001665
21	15.35	11.50	0.001381	0.001715
22	17.65	12.70	0.001500	0.001946
23	19.00	14.00	0.001431	0.002115
24	14.95	14.15	0.001631	0.002314
25	20.35	15.75	0.001815	0.002595
26	20.60	17.80	0.002067	0.002728
27	21.80	18.70	0.002333	0.002962
28	25.50	19.40	0.002665	0.003213
29	25.90	19.45	0.002800	0.003397
30	26.15	21.90	0.003081	0.003711
31	28.55	22.80	0.003234	0.003844
32	0.85	-0.40	0.003000	0.004229
33	8.40	2.00	0.002931	0.004179
34	6.35	2.30	0.002965	0.004227
35	2.70	1.35	0.002998	0.004194

Prism S4-025-FA

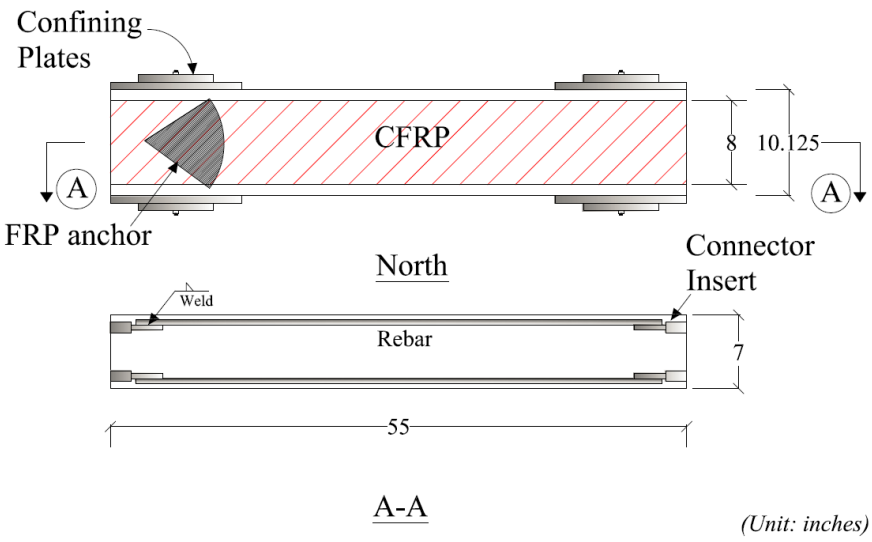

Casting Date: Apr. 15, 2014

Testing Date: Apr. 23, 2014

Materials:

Concrete

f'c=6,971 psi (1st batch: 6,810 psi; 2nd batch: 7,132 psi)

Steel Reinforcements

2 #4 rebar, ρs = 0.55%, *fy* = 67.0 ksi

FRP Reinforcements

One layer with FRP anchor, ρf = 0.56%, *fu* = 120 ksi

Test Data_S4-025-FA				
	NH	SH	NH1	SH1
1	0.00	0.00	0.000000	0.000000
2	0.00	0.25	0.000003	0.000004
3	0.35	1.20	0.000012	0.000002
4	1.02	1.45	0.000019	0.000032
5	2.75	2.82	0.000029	0.000039
6	5.75	3.40	0.000041	0.000051
7	8.75	8.20	0.000066	0.000017
8	10.05	12.30	0.000056	0.000054
9	13.75	11.10	0.000081	0.000073
10	12.80	14.10	0.000153	0.000330
11	7.75	9.95	0.000068	0.000379
12	4.25	4.60	0.000082	0.000172
13	2.90	0.00	0.000100	-0.000017
14	12.15	13.50	0.000578	0.000519
15	8.95	10.95	0.000374	0.000588
16	7.00	9.25	0.000238	0.000500
17	9.75	11.70	0.000136	0.000709
18	12.30	14.15	0.000170	0.000828
19	13.25	15.75	0.000323	0.000897
20	15.65	17.00	0.000372	0.001086
21	16.85	17.85	0.000510	0.001069
22	16.65	16.45	0.000882	0.001138
23	18.95	18.45	0.001020	0.001241
24	19.45	18.25	0.001222	0.001345
25	19.25	19.20	0.001394	0.001535
26	20.05	20.95	0.001477	0.001744
27	20.90	21.35	0.001513	0.001862
28	21.30	21.55	0.001664	0.002054
29	21.95	21.85	0.001868	0.002106
30	22.90	23.90	0.002329	0.002330
31	23.70	24.15	0.002564	0.002431
32	23.25	24.20	0.002581	0.002623
33	24.70	24.90	0.002751	0.002690
34	24.50	26.40	0.002974	0.002897
35	23.95	17.75	0.003312	0.003362

Prism S4-040-FA

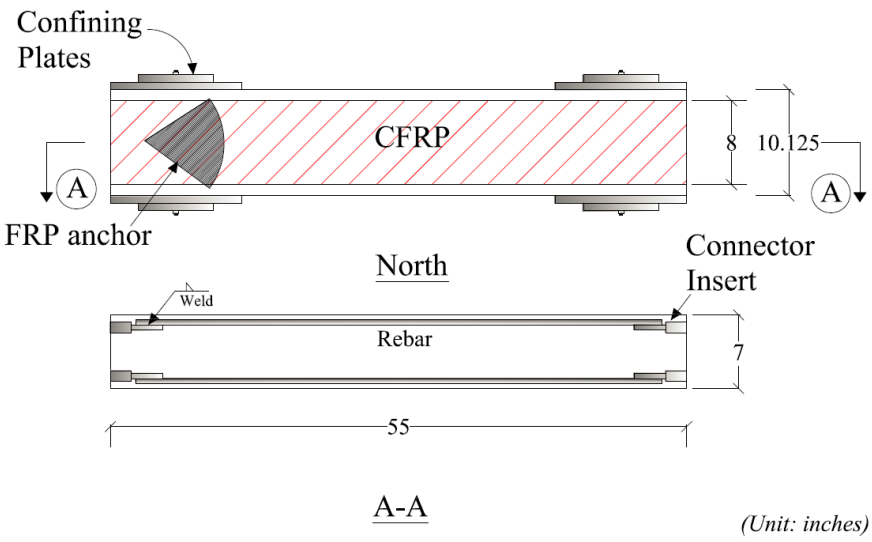

Casting Date: Dec. 29, 2013

Testing Date: Jan. 14, 2014

Materials:

Concrete

f'c=6,699 psi (1st batch: 6,826 psi; 2nd batch: 6,572 psi)

Steel Reinforcements

2 #4 rebar, ρs = 0.55%, *fy* = 67.0 ksi

FRP Reinforcements

One layer with FRP anchor, ρf = 0.90%, *fu* = 105 ksi

Test Data_S4-040-FA				
	NH	SH	NH1	SH1
1	0.00	0.00	0.000000	0.000004
2	0.20	0.21	0.000002	0.000001
3	0.15	0.31	0.000010	0.000016
4	0.63	0.89	0.000012	0.000018
5	2.10	3.40	0.000026	0.000039
6	2.25	2.55	0.000031	0.000041
7	5.25	9.70	0.000050	0.000048
8	7.55	11.75	0.000055	0.000048
9	10.05	11.80	0.000052	0.000047
10	10.85	14.20	0.000068	0.000047
11	12.95	16.75	0.000076	0.000057
12	14.90	16.75	0.000083	0.000069
13	17.15	18.35	0.000467	0.000050
14	4.60	12.35	0.000283	0.000050
15	0.40	6.95	0.000152	0.000133
16	3.30	9.65	0.000533	0.000183
17	1.55	7.10	0.000450	0.000266
18	1.60	6.10	0.000435	0.000183
19	2.55	7.60	0.000433	0.000248
20	4.00	10.45	0.000417	0.000266
21	9.50	12.45	0.000500	0.000350
22	10.20	12.85	0.000533	0.000431
23	11.00	15.65	0.000619	0.000581
24	15.00	17.00	0.000733	0.000714
25	13.00	14.45	0.000850	0.000882
26	11.35	13.45	0.000985	0.000997
27	14.30	16.35	0.001100	0.001130
28	15.15	8.85	0.001302	0.001513
29	20.10	18.60	0.001652	0.001632
30	20.15	18.65	0.001900	0.001896
31	22.45	19.65	0.002100	0.002062
32	23.40	21.45	0.002300	0.002262
33	26.20	24.70	0.002536	0.002514
34	22.20	24.95	0.002700	0.002745
35	17.50	18.25	0.002817	0.002947

Prism S4-025-FW

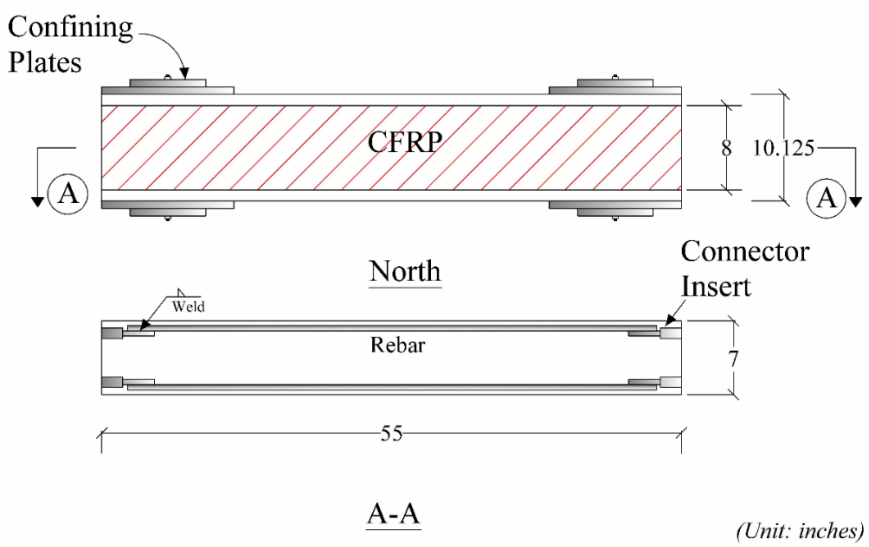

Casting Date: Dec. 1, 2013

Testing Date: Dec 12, 2013

Materials:

Concrete

f'c=6,119 psi (1st batch: 6449psi; 2nd batch: 5,789 psi)

Steel Reinforcements

2 #4 rebar, ρs = 0.55%, *fy* = 67.0 ksi

FRP Reinforcements

One layer with Fully Wrap method, ρf = 0.56%, *fu* = 120 ksi

Test Data_S4-025-FW				
	NH	SH	NH1	SH1
1	0.00	0.13	0.000000	0.000003
2	0.53	0.35	0.000019	0.000000
3	1.10	0.69	0.000005	0.000053
4	2.60	1.15	0.000100	0.000015
5	5.30	3.10	0.000017	0.000098
6	9.35	6.60	0.000041	0.000065
7	13.20	6.30	0.000052	0.000091
8	13.35	9.60	0.000085	0.000100
9	8.50	5.20	0.000202	0.000233
10	3.60	3.10	0.000150	0.000098
11	7.25	5.10	0.000433	0.000233
12	8.40	9.30	0.000435	0.000283
13	8.75	8.30	0.000350	0.000481
14	8.70	9.55	0.000285	0.000549
15	12.40	12.20	0.000383	0.000664
16	12.50	12.50	0.000602	0.000714
17	14.10	14.00	0.000850	0.000749
18	18.55	17.45	0.001133	0.001163
19	17.50	18.45	0.001483	0.001432
20	19.75	21.90	0.001819	0.001732
21	21.85	25.10	0.001983	0.002046
22	24.10	26.25	0.002252	0.002364
23	23.35	28.25	0.002619	0.002762
24	18.55	20.85	0.003167	0.003328
25	19.60	22.00	0.003667	0.003744
26	24.90	31.10	0.004067	0.003994
27	23.85	31.95	0.004502	0.004427
28	25.10	32.10	0.004884	0.004729
29	21.60	17.50	0.005517	0.005459
30	25.15	21.15	0.006017	0.006009
31	26.65	23.00	0.006484	0.006394
32	22.15	16.20	0.006686	0.006793
33	3.75	-0.05	0.006000	0.005859
34	-6.20	-10.50	0.005384	0.004543
35	-2.45	-6.45	0.005417	0.004495

Prism S4-040-FW

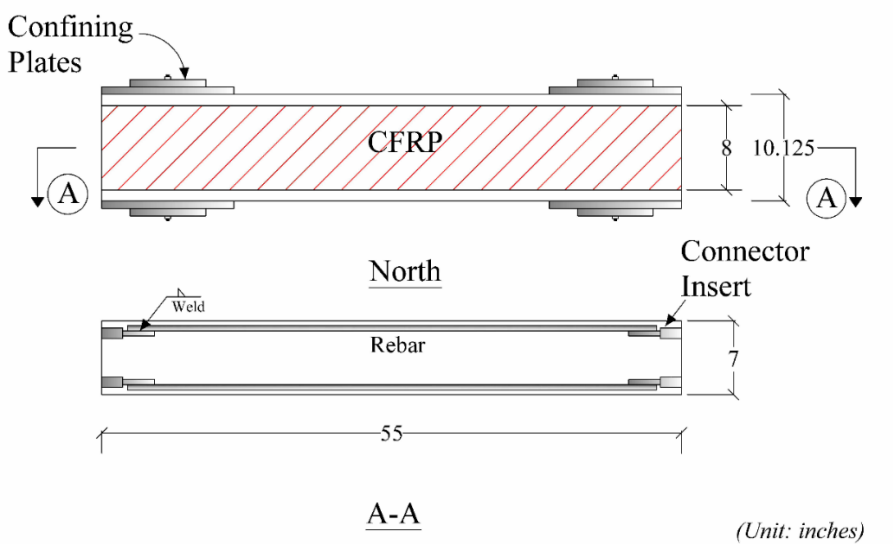

Casting Date: Apr. 15, 2014

Testing Date: May. 05, 2014

Materials:

Concrete

$f'c$=6,971 psi (1st batch: 6,810 psi; 2nd batch: 7,132 psi)

Steel Reinforcements

2 #4 rebar, ρs = 0.55%, fy = 67.0 ksi

FRP Reinforcements

One layer with Fully Wrap method, ρf = 0.90%, fu = 105 ksi

Test Data_S4-040-FW				
	NH	SH	NH1	SH1
1	0.00	0.00	0.000000	0.000010
2	0.75	0.36	0.000013	0.000019
3	1.00	3.12	0.000026	0.000037
4	3.55	5.70	0.000032	0.000050
5	5.35	10.25	0.000070	0.000123
6	6.15	9.60	0.000061	0.000066
7	1.60	1.30	0.000014	0.000035
8	10.80	9.15	0.000304	0.000466
9	6.80	7.60	0.000083	0.000399
10	6.35	7.10	0.000083	0.000466
11	10.20	9.60	0.000100	0.000074
12	12.30	12.50	0.000100	0.000535
13	10.60	10.60	0.000202	0.000623
14	13.30	12.95	0.000423	0.000675
15	15.75	15.15	0.000712	0.000916
16	17.30	17.45	0.001137	0.001485
17	18.65	18.00	0.001545	0.001793
18	22.75	21.35	0.001986	0.002259
19	22.35	22.20	0.002343	0.002606
20	21.35	23.45	0.002734	0.003106
21	22.95	23.50	0.003229	0.003690
22	26.80	26.85	0.003669	0.004104
23	22.45	25.15	0.004162	0.004759
24	29.10	28.85	0.004621	0.005175
25	31.55	31.30	0.005286	0.005776
26	27.05	29.60	0.005811	0.006380
27	-2.85	2.90	0.006289	0.006983
28	27.90	31.40	0.006729	0.007434
29	28.55	33.45	0.007323	0.008052
30	25.85	29.15	0.008258	0.008742
31	31.45	36.30	0.008870	0.009604
32	30.60	34.55	0.009890	0.010692
33	27.30	23.90	0.010878	0.011846
34	33.85	29.15	0.012473	0.013434
35	16.45	19.75	0.013699	0.014158

Prism S4-025-SB

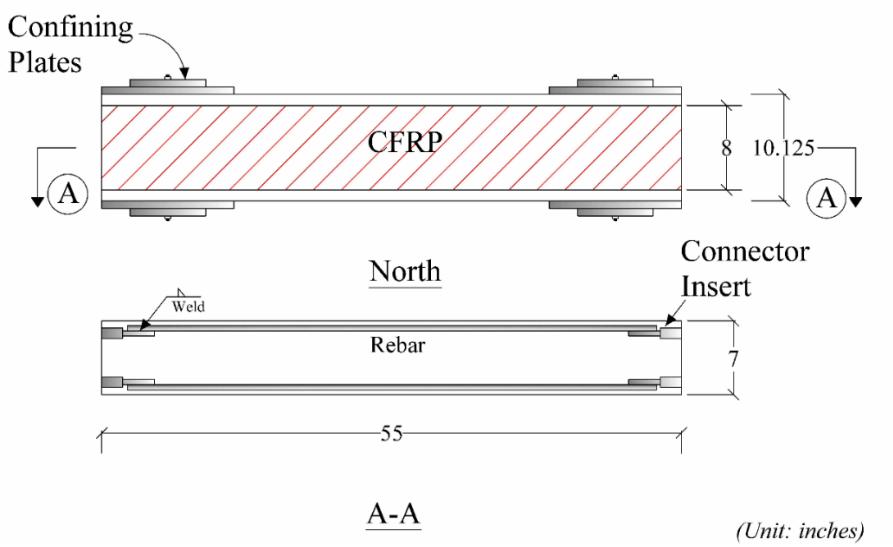

Casting Date: Dec. 01, 2013

Testing Date: Dec. 11, 2013

Materials:

Concrete

$f'c$=6,119 psi (1st batch: 6449psi; 2nd batch: 5,789 psi)

Steel Reinforcements

2 #4 rebar, ρs = 0.55%, fy = 67.0 ksi

FRP Reinforcements

One layer with Side Bond method, ρf = 0.56%, fu = 120 ksi

Test Data_S4-025-SB				
	NH	SH	NH1	SH1
1	0.00	0.00	0.000003	0.000005
2	0.58	0.17	0.000010	0.000010
3	0.82	1.10	0.000031	0.000017
4	1.90	2.50	0.000038	0.000017
5	3.30	5.80	0.000031	0.000048
6	5.10	7.20	0.000051	0.000051
7	9.00	12.00	0.000065	0.000081
8	5.20	6.40	0.000200	0.000350
9	0.10	2.50	0.000031	0.000248
10	8.00	6.30	0.000548	0.000181
11	0.10	0.90	0.000165	0.000133
12	0.40	1.40	0.000081	0.000150
13	1.40	1.80	0.000033	0.000117
14	2.10	2.90	0.000035	0.000348
15	1.90	3.50	0.000002	0.000283
16	2.10	6.10	0.000065	0.000400
17	3.80	7.30	0.000133	0.000283
18	5.60	7.30	0.000300	0.000248
19	3.70	6.90	0.000367	0.000431
20	6.60	10.60	0.000350	0.000647
21	8.10	9.90	0.000481	0.000714
22	7.70	10.20	0.000665	0.000882
23	8.20	13.20	0.000898	0.000997
24	10.20	10.50	0.001081	0.001182
25	10.00	11.60	0.001267	0.001330
26	12.50	12.40	0.001517	0.001563
27	13.20	13.60	0.001715	0.001696
28	14.80	15.50	0.002031	0.001981
29	15.40	16.90	0.002315	0.002331
30	16.90	17.20	0.002717	0.002564
31	18.10	18.00	0.002867	0.002814
32	18.90	18.50	0.003248	0.003130
33	20.20	19.10	0.003565	0.003478
34	14.30	17.80	0.003884	0.003827
35	-0.50	-6.80	0.004248	0.003644

Prism S4-040-SB

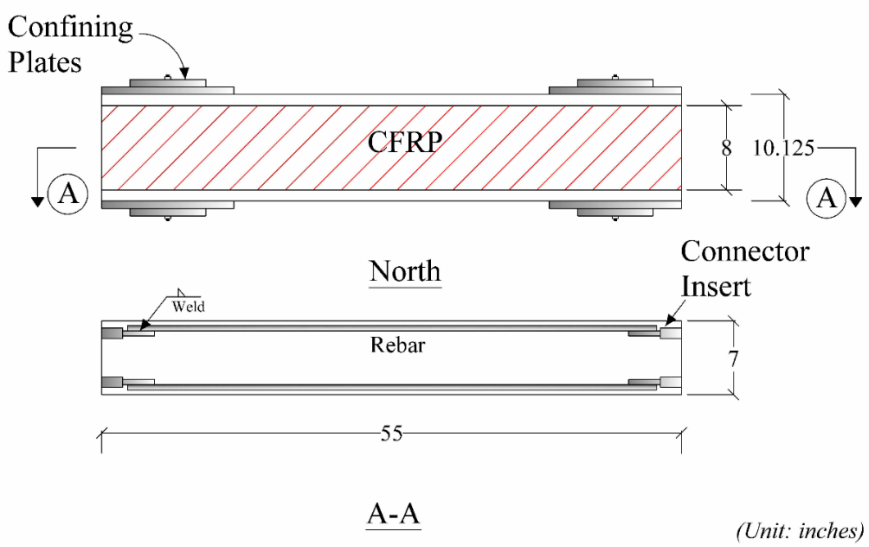

Casting Date: Apr. 15, 2014

Testing Date: Apr. 30, 2014

Materials:

Concrete

$f'c$=6,971 psi (1st batch: 6,810 psi; 2nd batch: 7,132 psi)

Steel Reinforcements

2 #4 rebar, ρs = 0.55%, fy = 67.0 ksi

FRP Reinforcements

One layer with Side Bond method, ρf = 0.90%, fu = 105 ksi

Test Data_S4-040-SB				
	NH	SH	NH1	SH1
1	0.10	0.20	0.000000	0.000002
2	0.22	0.35	0.000015	0.000002
3	1.25	1.40	0.000053	0.000017
4	3.30	1.80	0.000034	0.000067
5	3.75	2.25	0.000034	0.000053
6	7.10	5.05	0.000042	0.000063
7	8.25	6.80	0.000057	0.000052
8	9.45	7.90	0.000062	0.000069
9	11.05	10.60	0.000063	0.000069
10	13.75	12.35	0.000074	0.000081
11	11.20	10.00	0.000374	0.000241
12	9.20	4.45	0.000355	0.000071
13	2.20	1.35	0.000236	0.000103
14	7.25	7.90	0.000204	0.000276
15	3.75	6.10	0.000219	0.000226
16	5.10	5.50	0.000202	0.000172
17	5.60	5.80	0.000151	0.000175
18	7.40	5.85	0.000204	0.000209
19	9.55	10.55	0.000236	0.000278
20	11.50	12.30	0.000253	0.000313
21	13.45	13.40	0.000372	0.000364
22	13.00	14.40	0.000389	0.000433
23	16.90	14.65	0.000406	0.000450
24	8.65	11.40	0.000440	0.000552
25	13.15	13.55	0.000510	0.000554
26	13.75	13.55	0.000593	0.000672
27	15.90	15.35	0.000729	0.000690
28	16.40	15.50	0.000763	0.000830
29	18.00	17.80	0.000865	0.000914
30	17.90	17.75	0.000899	0.000966
31	18.85	18.40	0.001054	0.001052
32	18.95	19.40	0.001154	0.001140
33	20.20	19.10	0.001156	0.001259
34	15.80	17.40	0.001428	0.001724
35	-3.00	-4.55	0.001103	0.001172

Prism S5-025-FA

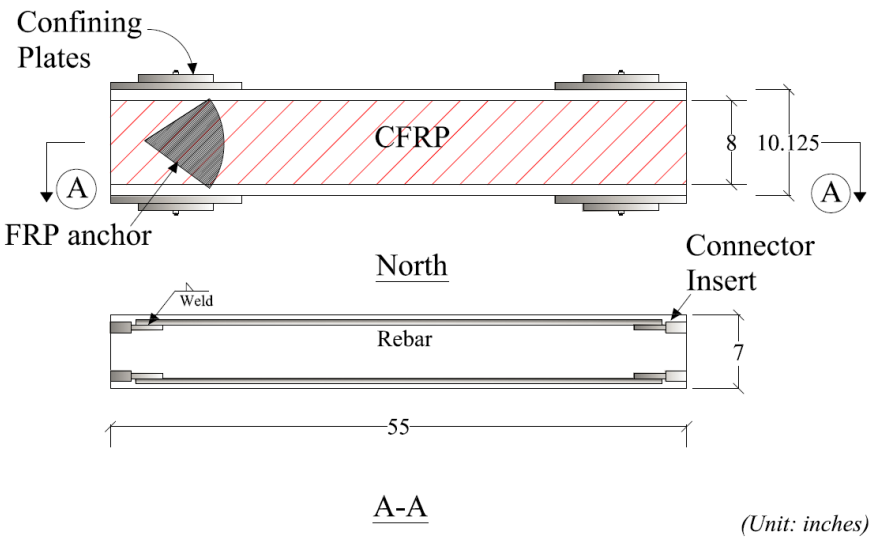

Casting Date: Dec. 29, 2013

Testing Date: Jan. 08, 2014

Materials:

Concrete

f'c=6,699 psi (1st batch: 6,826 psi; 2nd batch: 6,572 psi)

Steel Reinforcements

2 #5 rebar, ρs = 0.87%, *fy* = 68.0 ksi

FRP Reinforcements

One layer with FRP anchor, ρf = 0.56%, *fu* = 120 ksi

Test Data_S5-025-FA				
	NH	SH	NH1	SH1
1	0.08	0.00	0.000000	0.000003
2	1.52	0.85	0.000023	0.000006
3	1.89	1.53	0.000019	0.000010
4	2.85	1.96	0.000029	0.000050
5	3.65	4.75	0.000063	0.000062
6	4.50	9.40	0.000079	0.000063
7	5.95	11.55	0.000064	0.000083
8	10.05	14.40	0.000069	0.000091
9	14.05	15.85	0.000083	0.000089
10	16.35	15.80	0.000515	0.000314
11	4.90	7.40	0.000200	0.000283
12	13.40	13.90	0.000483	0.000566
13	8.05	10.15	0.000283	0.000499
14	9.40	13.20	0.000183	0.000547
15	9.30	12.85	0.000215	0.000549
16	11.90	14.95	0.000181	0.000566
17	12.40	16.70	0.000283	0.000633
18	14.60	17.30	0.000367	0.000699
19	10.10	11.70	0.000481	0.000683
20	13.75	14.55	0.000633	0.000783
21	17.05	17.65	0.000731	0.000799
22	18.25	18.60	0.001081	0.001014
23	18.85	19.55	0.001150	0.001197
24	21.15	22.55	0.001298	0.001415
25	26.40	26.85	0.001531	0.001563
26	27.65	29.65	0.001648	0.001848
27	28.60	31.25	0.001915	0.002048
28	29.65	32.00	0.002165	0.002212
29	31.00	33.00	0.002365	0.002495
30	32.05	33.65	0.002667	0.002695
31	33.85	35.75	0.002934	0.002978
32	31.45	33.85	0.003184	0.003280
33	33.75	37.05	0.003434	0.003528
34	24.25	27.65	0.003665	0.003777
35	18.05	18.55	0.003217	0.002962

Prism S5-040-FA

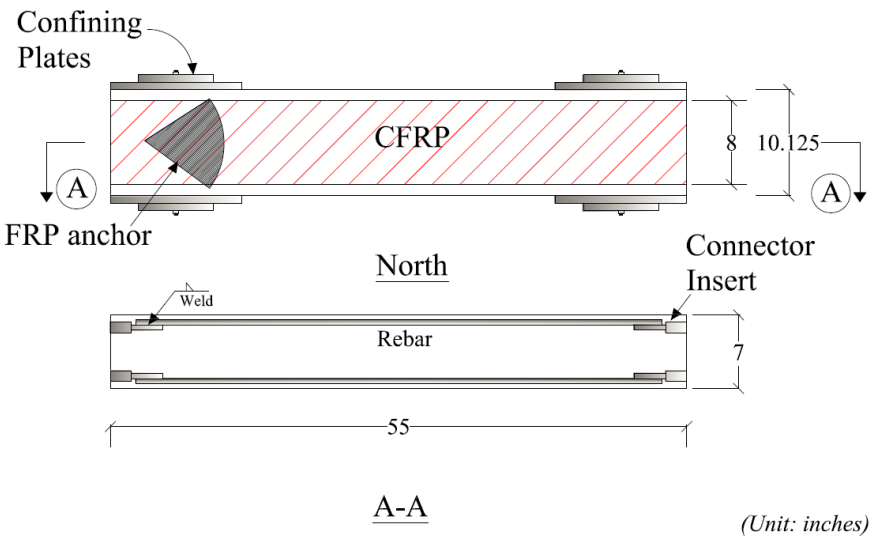

Casting Date: Apr. 15, 2014

Testing Date: May. 13, 2014

Materials:

Concrete

f'c=6,971 psi (1st batch: 6,810 psi; 2nd batch: 7,132 psi)

Steel Reinforcements

2 #5 rebar, ρs = 0.87%, *fy* = 68.0 ksi

FRP Reinforcements

One layer with FRP anchor, ρf = 0.90%, *fu* = 105 ksi

Test Data_S5-040-FA				
	NH	SH	NH1	SH1
1	0.07	0.00	0.000003	0.000002
2	1.18	1.07	0.000029	0.000020
3	2.25	2.53	0.000026	0.000029
4	3.08	3.62	0.000031	0.000033
5	3.58	4.32	0.000033	0.000039
6	8.14	8.80	0.000053	0.000069
7	14.30	10.56	0.000088	0.000077
8	8.86	8.47	0.000272	0.000261
9	3.69	3.74	0.000000	0.000244
10	15.40	9.35	0.000442	0.000244
11	8.53	4.73	0.000289	0.000328
12	11.61	10.01	0.000240	0.000330
13	10.34	10.23	0.000306	0.000362
14	12.76	13.48	0.000323	0.000414
15	14.25	13.42	0.000323	0.000468
16	6.93	17.00	0.000493	0.000588
17	12.27	10.12	0.000682	0.000810
18	14.41	11.00	0.000631	0.000847
19	17.55	15.62	0.000699	0.000916
20	19.80	18.15	0.000969	0.001175
21	21.40	19.53	0.001107	0.001364
22	20.08	19.31	0.001411	0.001657
23	23.60	21.01	0.001736	0.001916
24	24.53	22.99	0.001974	0.002155
25	25.08	26.40	0.002195	0.002483
26	29.43	29.54	0.002448	0.002709
27	31.68	32.40	0.002773	0.002983
28	40.10	33.00	0.003008	0.003207
29	41.20	34.32	0.003246	0.003655
30	43.56	37.24	0.003586	0.004054
31	46.42	37.24	0.003843	0.004207
32	42.68	34.43	0.004115	0.004569
33	44.83	35.97	0.004455	0.004845
34	46.64	36.30	0.004759	0.005140
35	28.82	17.88	0.004997	0.005089

Group II

Softening Test

Panel F2P-5

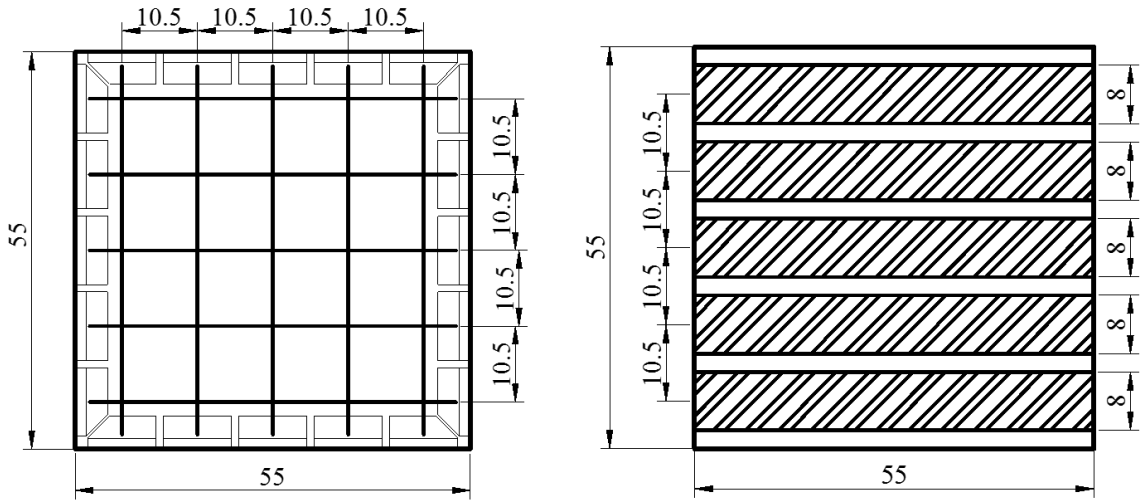

Casting Date: Oct. 04, 2012

Testing Date: Apr. 25, 2012

Materials:

Concrete

f'c=5,471 psi (1st batch: 5,587 psi; 2nd batch: 5,355psi)

Steel Reinforcements

Horizontal direction : #4 rebar, ρs = 0.51%, *fy* = 67.0ksi

Vertical direction : #4 rebar, ρs = 0.51%, *fy* = 67.0 ksi

FRP Reinforcements

One layer with Fully Wrap method, ρf = 0.83%, *fu* = 105 ksi

Target Tensile Strain:

1 = 0.0025

	NV	SV	NH	SH	NV lvdt	SV lvdt	NH lvdt	SH lvdt
1	-0.11	-0.08	-0.67	-0.17	0.000021	0.000002	-0.000021	-0.000065
2	-2.41	-3.10	-0.75	4.08	0.000310	-0.000079	-0.000251	0.000236
3	-2.83	-3.32	4.19	9.50	0.000403	-0.000086	-0.000300	0.000679
4	-2.54	-3.07	4.11	9.54	0.000439	-0.000089	-0.000235	0.000619
5	-2.54	-3.11	10.06	11.04	0.000436	-0.000092	0.000002	0.000743
6	-2.70	-3.32	12.58	15.17	0.000464	-0.000097	0.000116	0.000872
7	-2.51	-3.03	15.69	16.00	0.000504	-0.000099	0.000152	0.001077
8	-2.58	-3.05	18.00	18.63	0.000515	-0.000101	0.000307	0.001130
9	-2.53	-2.97	20.03	20.58	0.000550	-0.000107	0.000422	0.001436
10	-2.45	-2.93	22.81	23.04	0.000593	-0.000094	0.000737	0.001512
11	-2.60	-3.04	24.92	25.46	0.000668	-0.000097	0.000892	0.001617
12	-2.64	-3.08	27.47	26.71	0.000746	-0.000089	0.001063	0.001937
13	-2.66	-3.25	29.78	29.63	0.000820	-0.000084	0.001295	0.001960
14	-2.62	-3.14	31.39	31.13	0.000834	-0.000070	0.001408	0.002130
15	-2.66	-3.20	31.42	29.54	0.000876	-0.000069	0.001442	0.002169
16	-2.70	-3.25	30.58	30.63	0.000920	-0.000066	0.001494	0.002118
17	-2.92	-3.59	31.31	30.13	0.000924	-0.000068	0.001606	0.002183
18	-2.83	-3.35	31.61	30.71	0.000973	-0.000069	0.001534	0.002143
19	-4.84	-5.74	31.64	30.79	0.000939	-0.000113	0.001555	0.002158
20	-19.81	-22.14	31.17	30.04	0.000831	-0.000373	0.001542	0.002195
21	-36.47	-38.19	35.17	30.54	0.000501	-0.000533	0.001697	0.002141
22	-52.30	-53.73	33.61	30.71	0.000154	-0.000643	0.001821	0.002194
23	-64.74	-65.82	32.14	29.75	-0.000050	-0.000734	0.001813	0.002283
24	-73.31	-74.52	35.06	31.83	-0.000239	-0.000807	0.002024	0.002285
25	-85.38	-86.65	32.25	28.54	-0.000321	-0.000881	0.002011	0.002399
26	-97.60	-98.55	31.53	26.00	-0.000473	-0.000966	0.002110	0.002235
27	-109.55	-110.38	28.28	22.33	-0.000683	-0.001040	0.002048	0.002284
28	-122.10	-122.18	24.25	18.50	-0.000779	-0.001129	0.002011	0.002352
29	-131.61	-131.49	22.64	19.42	-0.000880	-0.001186	0.002152	0.002338
30	-139.04	-138.34	14.42	14.17	-0.000930	-0.001243	0.001889	0.002430
31	-146.64	-146.35	17.64	16.54	-0.000989	-0.001312	0.002008	0.002430
32	-154.75	-153.86	17.39	15.17	-0.001055	-0.001375	0.002072	0.002313
33	-163.21	-162.06	13.17	12.88	-0.001163	-0.001439	0.002153	0.002304
34	-171.22	-169.51	10.72	12.33	-0.001320	-0.001502	0.002112	0.002430
35	-180.05	-177.44	1.31	6.38	-0.001416	-0.001561	0.002201	0.002481

Panel F2P-6

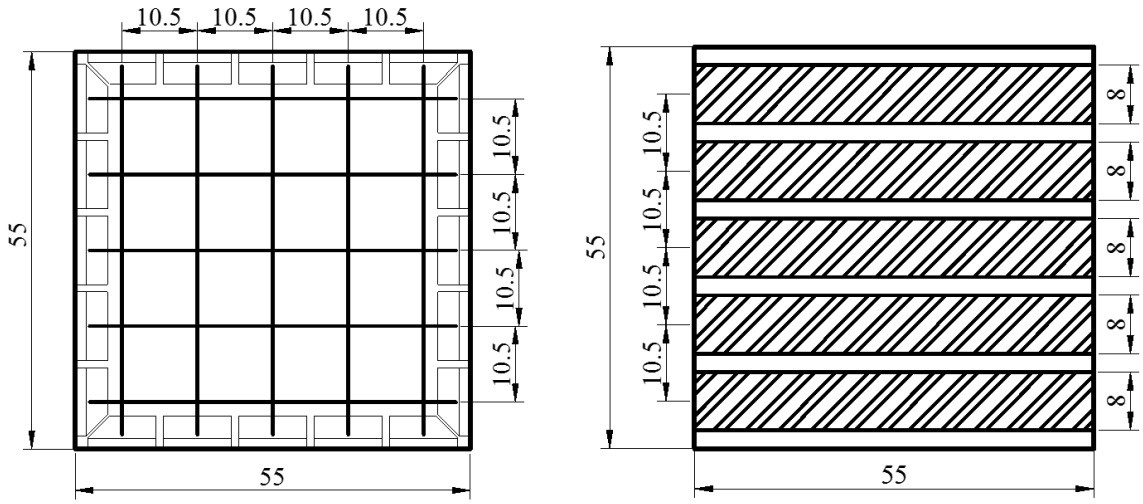

Casting Date: May. 23, 2012

Testing Date: Jun. 18, 2012

Materials:

Concrete

f'c=6,237 psi (1st batch: 6,888 psi; 2nd batch: 5,586 psi)

Steel Reinforcements

Horizontal direction : #4 rebar, ρs = 0.51%, *fy* = 67.0ksi

Vertical direction : #4 rebar, ρs = 0.51%, *fy* = 67.0 ksi

FRP Reinforcements

One layer with Fully Wrap method, ρf = 0.83%, *fu* = 105 ksi

Target Tensile Strain:

1 = 0.0055

	NV	SV	NH	SH	NV lvdt	SV lvdt	NH lvdt	SH lvdt
1	3.55	-0.28	0.43	0.00	-0.000025	0.000010	0.000000	0.000052
2	0.57	-3.17	-1.25	0.00	0.000133	-0.000038	0.000000	0.000114
3	0.77	-3.03	-0.70	0.00	0.000148	-0.000048	0.000000	0.000059
4	1.21	-2.49	5.98	3.16	0.000165	-0.000052	0.000368	0.000358
5	0.31	-2.75	10.43	6.76	0.000184	-0.000043	0.000846	0.000877
6	0.46	-2.73	12.53	8.30	0.000201	-0.000042	0.001276	0.001270
7	-0.18	-2.46	16.67	12.74	0.000238	-0.000041	0.001660	0.001710
8	-0.17	-3.14	17.08	13.50	0.000280	-0.000037	0.002105	0.002107
9	-0.66	-3.54	21.35	18.42	0.000337	-0.000048	0.002520	0.002684
10	-1.14	-3.83	25.28	20.68	0.000395	-0.000049	0.002954	0.003160
11	-0.97	-3.61	27.63	22.96	0.000423	-0.000046	0.003383	0.003539
12	-0.99	-3.74	29.45	24.78	0.000454	-0.000035	0.003695	0.003791
13	-0.97	-2.82	31.78	26.32	0.000504	-0.000039	0.003984	0.004117
14	-1.96	-3.04	32.58	27.94	0.000522	-0.000031	0.004335	0.004484
15	-1.63	-3.17	32.87	27.04	0.000550	-0.000023	0.004694	0.004757
16	-9.24	-13.86	32.55	27.50	0.000564	-0.000139	0.004685	0.004871
17	-14.94	-21.91	31.72	27.46	0.000679	-0.000244	0.004706	0.004872
18	-25.92	-32.80	32.08	27.02	0.000619	-0.000351	0.004693	0.004828
19	-36.96	-43.34	32.28	26.82	0.000439	-0.000440	0.004654	0.004845
20	-47.63	-53.92	32.55	26.06	0.000352	-0.000519	0.004647	0.004829
21	-58.37	-64.68	31.37	24.38	0.000232	-0.000610	0.004653	0.004899
22	-65.58	-72.69	31.43	25.98	0.000116	-0.000661	0.004738	0.004933
23	-75.06	-82.04	31.07	22.52	-0.000009	-0.000741	0.004997	0.005041
24	-82.21	-91.48	31.30	20.26	-0.000015	-0.000812	0.005258	0.005025
25	-93.65	-102.15	30.37	20.32	-0.000076	-0.000902	0.005244	0.005041
26	-103.91	-112.33	30.82	18.92	-0.000111	-0.000995	0.005308	0.005023
27	-114.46	-122.16	28.95	21.46	-0.000202	-0.001082	0.005316	0.005077
28	-120.85	-127.99	28.13	20.86	-0.000287	-0.001122	0.005368	0.005014
29	-127.60	-132.72	27.55	15.62	-0.000452	-0.001148	0.005320	0.005034
30	-135.17	-137.61	27.33	15.96	-0.000648	-0.001175	0.005385	0.005050
31	-141.64	-142.32	27.02	15.52	-0.000814	-0.001197	0.005421	0.005085
32	-148.50	-147.07	27.25	15.76	-0.000985	-0.001200	0.005410	0.005068
33	-155.80	-152.46	27.08	18.10	-0.001151	-0.001224	0.005527	0.005164
34	-162.07	-156.70	25.67	16.24	-0.001245	-0.001228	0.005637	0.005171
35	-165.70	-156.15	18.75	10.44	-0.001407	-0.001691	0.005820	0.005230

Panel F2P-7

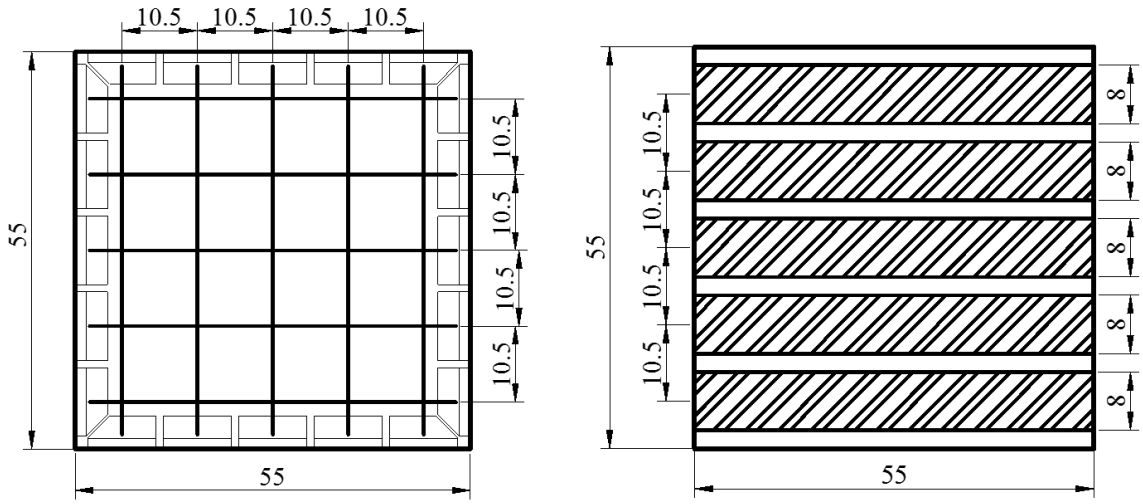

Casting Date: Jun. 10, 2012

Testing Date: Aug. 21, 2012

Materials:

Concrete

f'c=5,742 psi (1st batch: 5549 psi; 2nd batch: 5,935 psi)

Steel Reinforcements

Horizontal direction : #4 rebar, ρs = 0.51%, *fy* = 67.0ksi

Vertical direction : #4 rebar, ρs = 0.51%, *fy* = 67.0 ksi

FRP Reinforcements

One layer with Fully Wrap method, ρf = 0.83%, *fu* = 105 ksi

Target Tensile Strain:

1 = 0.0075

	NV	SV	NH	SH	NV lvdt	SV lvdt	NH lvdt	SH lvdt
1	-0.96	-0.01	0.44	0.35	0.000019	0.000002	0.000015	0.000025
2	-2.54	-2.34	1.03	0.36	0.000276	-0.000071	0.000013	0.000044
3	-3.01	-2.59	2.02	2.35	0.000359	-0.000078	0.000236	0.000073
4	-2.83	-2.47	6.12	3.74	0.000391	-0.000080	0.000497	0.000520
5	-2.61	-2.45	10.68	8.00	0.000389	-0.000082	0.001119	0.001249
6	-2.81	-2.66	12.83	9.82	0.000414	-0.000087	0.001678	0.001802
7	-2.47	-2.44	17.06	15.08	0.000449	-0.000089	0.002176	0.002419
8	-2.54	-2.30	17.48	15.98	0.000459	-0.000091	0.002755	0.002977
9	-2.37	-2.12	21.85	21.80	0.000490	-0.000096	0.003295	0.003788
10	-2.18	-2.01	25.87	24.47	0.000528	-0.000085	0.003859	0.004456
11	-2.37	-2.17	28.28	27.17	0.000595	-0.000088	0.004416	0.004989
12	-2.41	-2.18	30.14	29.32	0.000665	-0.000080	0.004822	0.005343
13	-2.42	-2.57	32.53	31.15	0.000731	-0.000076	0.005198	0.005800
14	-2.15	-2.41	33.34	33.06	0.000743	-0.000063	0.005654	0.006317
15	-2.27	-2.44	33.63	32.00	0.000781	-0.000062	0.006121	0.006700
16	-0.48	0.08	33.31	32.54	0.000820	-0.000060	0.006109	0.006861
17	0.67	1.67	32.46	32.49	0.000824	-0.000061	0.006136	0.006861
18	3.40	4.52	32.83	31.97	0.000867	-0.000062	0.006119	0.006799
19	4.03	4.66	33.04	31.74	0.000837	-0.000102	0.006069	0.006824
20	-8.38	-9.20	33.31	30.84	0.000741	-0.000335	0.006060	0.006801
21	-22.46	-22.67	32.10	28.85	0.000447	-0.000479	0.006067	0.006900
22	-36.56	-36.28	32.17	30.74	0.000137	-0.000578	0.006178	0.006948
23	-46.72	-46.13	31.79	26.65	-0.000045	-0.000660	0.006515	0.007099
24	-53.58	-52.56	32.03	23.97	-0.000213	-0.000727	0.006853	0.007076
25	-62.90	-62.13	31.08	24.05	-0.000286	-0.000793	0.006835	0.007098
26	-72.66	-71.59	31.54	22.39	-0.000421	-0.000870	0.006919	0.007073
27	-82.08	-81.06	29.63	25.39	-0.000609	-0.000936	0.006929	0.007149
28	-93.10	-91.46	28.79	24.68	-0.000694	-0.001016	0.006996	0.007061
29	-100.98	-99.64	28.19	18.48	-0.000785	-0.001067	0.006935	0.007088
30	-106.60	-105.31	27.97	18.89	-0.000829	-0.001118	0.007019	0.007111
31	-112.65	-112.19	27.65	18.37	-0.000882	-0.001180	0.007065	0.007161
32	-119.11	-118.56	27.89	18.65	-0.000941	-0.001237	0.007051	0.007136
33	-125.82	-125.47	27.72	21.42	-0.001037	-0.001295	0.007204	0.007272
34	-132.32	-131.90	26.27	19.22	-0.001177	-0.001352	0.007347	0.007282
35	-140.28	-139.97	19.19	12.35	-0.001263	-0.001405	0.007585	0.007364

Group III

Modified Hsu/Zhu Ratio Test

Panel PR-025

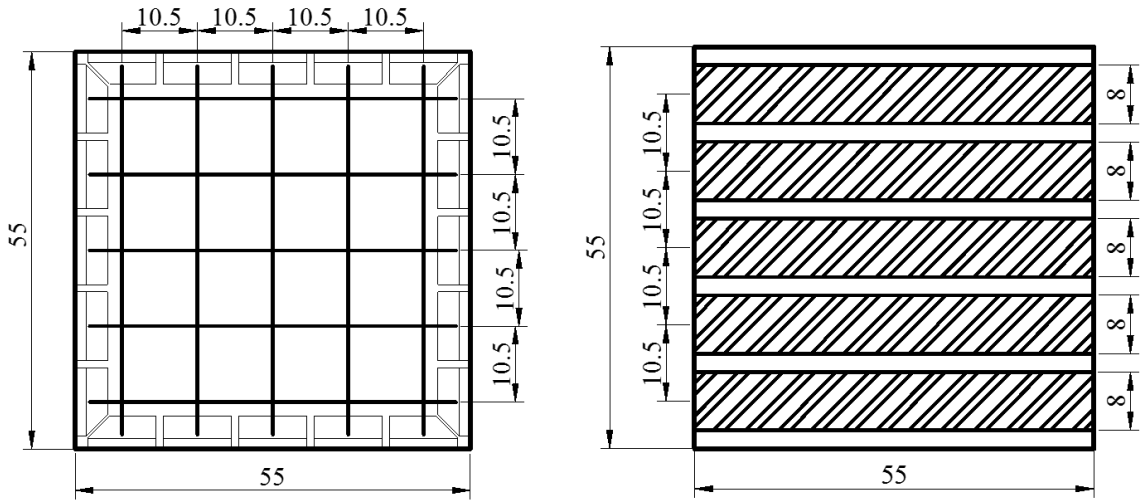

Casting Date: Jul. 24, 2014

Testing Date: Aug. 05, 2014

Materials:

Concrete

f'c=5,934 psi (1st batch: 5,677 psi; 2nd batch: 6,191 psi)

Steel Reinforcements

Horizontal direction : #4 rebar, ρs = 0.51%, *fy* = 67.0ksi

Vertical direction : #4 rebar, ρs = 0.51%, *fy* = 67.0 ksi

FRP Reinforcements

One layer with Fully Wrap method, ρf = 0.52%, *fu* = 120 ksi

	V	H	V lvdt	H lvdt
1	-0.54	-0.02	0.000009	-0.000037
2	-2.76	-3.50	-0.000004	-0.000136
3	-2.29	-3.13	0.000004	-0.000113
4	-1.81	-2.96	-0.000003	-0.000096
5	-1.88	-2.66	0.000003	-0.000078
6	-2.06	-1.96	0.000005	-0.000119
7	-1.99	-1.26	0.000002	-0.000087
8	-1.86	-1.06	-0.000009	-0.000104
9	-1.75	-0.81	-0.000010	-0.000092
10	-1.47	0.22	-0.000001	-0.000042
11	-1.35	0.62	-0.000004	-0.000086
12	-1.86	2.10	-0.000016	-0.000013
13	-1.37	3.07	-0.000012	0.000028
14	-1.58	3.23	-0.000017	-0.000012
15	-1.79	3.57	-0.000018	-0.000016
16	-2.50	3.33	-0.000020	-0.000008
17	-2.99	3.19	-0.000021	-0.000012
18	-2.83	3.58	-0.000024	-0.000034
19	-3.75	3.21	-0.000037	-0.000012
20	-6.17	2.51	-0.000054	-0.000012
21	-7.16	2.57	-0.000068	-0.000038
22	-8.18	2.43	-0.000086	-0.000011
23	-8.08	2.72	-0.000088	-0.000002
24	-8.48	2.85	-0.000081	0.000001
25	-9.39	2.61	-0.000081	0.000022
26	-9.07	2.68	-0.000085	0.000008

	V	H	V lvdt	H lvdt
27	-9.25	2.79	-0.000090	-0.000003
28	-9.60	2.50	-0.000086	-0.000026
29	-9.84	2.71	-0.000084	0.000011
30	-10.05	2.97	-0.000089	0.000012
31	-9.67	3.50	-0.000096	-0.000003
32	-9.95	3.59	-0.000087	0.000034
33	-9.37	4.77	-0.000093	0.000010
34	-9.51	5.19	-0.000092	0.000013
35	-10.04	5.22	-0.000101	0.000039
36	-9.68	5.76	-0.000108	0.000299
37	-10.15	6.45	-0.000095	0.000613
38	-10.08	6.94	-0.000102	0.000698
39	-10.35	8.00	-0.000095	0.000722
40	-10.13	8.46	-0.000097	0.000718
41	-9.94	8.79	-0.000093	0.000698
42	-10.08	8.93	-0.000111	0.000762
43	-10.18	8.89	-0.000106	0.000750
44	-10.23	8.23	-0.000087	0.000791
45	-10.16	9.23	-0.000100	0.000735
46	-10.37	9.03	-0.000101	0.000743
47	-10.25	9.13	-0.000105	0.000748
48	-11.07	8.84	-0.000104	0.000789
49	-11.45	8.90	-0.000113	0.000786
50	-12.31	8.54	-0.000121	0.000765
51	-12.79	8.95	-0.000122	0.000716

Panel PR-040

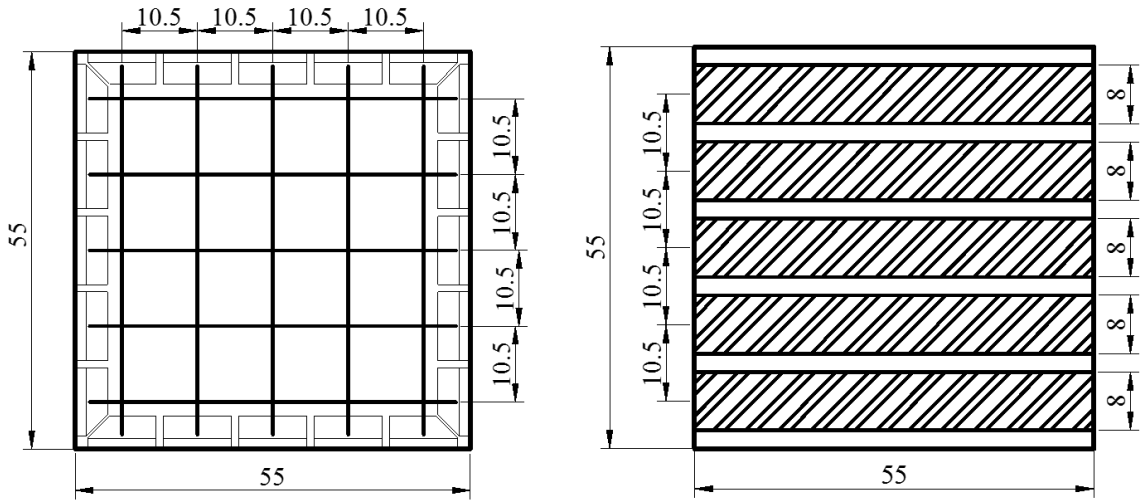

Casting Date: Jul. 13, 2014

Testing Date: Jul. 22, 2014

Materials:

Concrete

f'c=5,334 psi (1st batch: 5,000 psi; 2nd batch: 5,668 psi)

Steel Reinforcements

Horizontal direction : #4 rebar, ρs = 0.51%, *fy* = 67.0ksi

Vertical direction : #4 rebar, ρs = 0.51%, *fy* = 67.0 ksi

FRP Reinforcements

One layer with Fully Wrap method, ρf = 0.83%, *fu* = 105 ksi

	V	H	V lvdt	H lvdt
1	-0.54	-0.02	0.000009	-0.000037
2	-3.38	-3.53	0.000014	-0.000094
3	-3.20	-1.73	-0.000001	-0.000058
4	-3.47	0.89	-0.000012	-0.000018
5	-3.87	3.64	-0.000005	0.000045
6	-3.86	4.19	-0.000021	0.000039
7	-5.45	3.84	-0.000043	0.000039
8	-7.01	3.90	-0.000065	0.000029
9	-7.36	4.01	-0.000062	-0.000007
10	-7.36	7.08	-0.000057	0.000061
11	-7.11	8.28	-0.000073	0.000037
12	-8.87	8.59	-0.000091	0.000071
13	-11.31	9.50	-0.000109	0.000129
14	-11.26	12.65	-0.000124	0.001277
15	-11.09	14.31	-0.000140	0.002715
16	-14.30	14.05	-0.000163	0.002772
17	-16.19	13.71	-0.000173	0.002789
18	-16.53	16.45	-0.000180	0.003822
19	-16.80	16.76	-0.000193	0.004048
20	-16.86	17.18	-0.000197	0.004046
21	-17.64	17.06	-0.000209	0.004223
22	-19.02	16.92	-0.000222	0.004278
23	-19.90	17.42	-0.000227	0.004382
24	-19.96	18.28	-0.000226	0.004792
25	-20.84	19.32	-0.000244	0.004998
26	-21.47	19.09	-0.000256	0.005102

	V	H	V lvdt	H lvdt
27	-21.83	20.41	-0.000277	0.005339
28	-22.13	21.35	-0.000281	0.006073
29	-23.63	21.56	-0.000296	0.006351
30	-23.73	21.74	-0.000305	0.006456
31	-23.70	23.15	-0.000304	0.007338
32	-25.09	23.29	-0.000320	0.007573
33	-25.63	23.96	-0.000332	0.007961
34	-25.95	25.45	-0.000350	0.008959
35	-27.39	25.91	-0.000360	0.009373
36	-27.82	26.26	-0.000366	0.009773
37	-27.78	27.73	-0.000364	0.010807
38	-28.98	27.85	-0.000384	0.011211
39	-29.14	28.00	-0.000394	0.011391
40	-29.26	29.73	-0.000405	0.012558
41	-30.59	30.47	-0.000422	0.013141
42	-31.47	30.60	-0.000425	0.013448
43	-31.48	31.73	-0.000427	0.014215
44	-32.70	32.31	-0.000440	0.014811
45	-33.43	32.58	-0.000446	0.015021
46	-33.07	33.61	-0.000453	0.015963
47	-34.29	34.23	-0.000449	0.016628
48	-35.32	34.50	-0.000461	0.017020
49	-35.21	35.92	-0.000459	0.018255
50	-37.21	36.70	-0.000476	0.018868
51	-37.41	36.84	-0.000484	0.019124

Panel PR-080

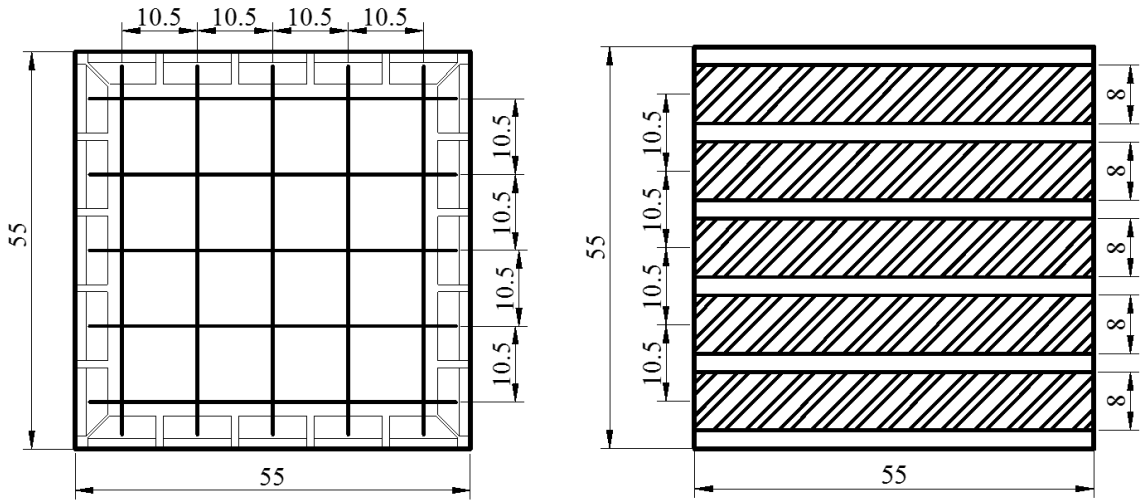

Casting Date: Sep. 20, 2014

Testing Date: Oct. 06, 2014

Materials:

Concrete

f'c=6,023 psi (1st batch: 6,010 psi; 2nd batch: 6,036 psi)

Steel Reinforcements

Horizontal direction : #4 rebar, ρs = 0.51%, *fy* = 67.0ksi

Vertical direction : #4 rebar, ρs = 0.51%, *fy* = 67.0 ksi

FRP Reinforcements

Two layer with Fully Wrap method, ρf = 1.66 %, *fu* = 105 ksi

	V	H	V lvdt	H lvdt
1	-0.54	-0.02	0.000009	-0.000037
2	-2.56	-4.18	-0.000004	-0.000064
3	-2.35	-0.12	0.000005	-0.000038
4	-2.45	0.46	-0.000006	-0.000060
5	-2.49	2.03	-0.000009	-0.000049
6	-2.73	2.40	-0.000006	0.000010
7	-4.96	2.43	-0.000029	0.000000
8	-7.99	2.23	-0.000046	0.000005
9	-9.00	4.11	-0.000066	0.000057
10	-9.48	7.11	-0.000075	0.000083
11	-9.73	7.13	-0.000078	0.000084
12	-13.06	6.78	-0.000092	0.000113
13	-15.31	7.00	-0.000108	0.000132
14	-15.15	10.52	-0.000133	0.000109
15	-15.37	12.50	-0.000122	0.000185
16	-20.27	12.36	-0.000174	0.000213
17	-21.61	15.12	-0.000171	0.001033
18	-21.38	19.73	-0.000162	0.003014
19	-23.20	19.91	-0.000176	0.003111
20	-26.46	19.71	-0.000203	0.003287
21	-26.20	22.46	-0.000212	0.003950
22	-29.69	23.00	-0.000240	0.004102
23	-31.26	25.37	-0.000241	0.004681
24	-31.27	28.54	-0.000251	0.005582
25	-36.70	28.52	-0.000290	0.005659
26	-37.38	28.58	-0.000297	0.005678

	V	H	V lvdt	H lvdt
27	-37.92	32.83	-0.000321	0.006962
28	-38.34	33.45	-0.000321	0.007324
29	-42.72	33.51	-0.000376	0.007432
30	-43.18	35.81	-0.000392	0.008168
31	-43.87	38.75	-0.000401	0.009375
32	-48.02	38.66	-0.000442	0.009608
33	-48.57	42.61	-0.000454	0.011113
34	-49.35	44.17	-0.000462	0.011932
35	-52.13	44.01	-0.000501	0.012118
36	-52.39	45.25	-0.000503	0.012478
37	-52.40	46.16	-0.000490	0.012885
38	-53.96	49.13	-0.000503	0.014547
39	-57.64	49.20	-0.000551	0.014833
40	-58.32	50.54	-0.000560	0.015187
41	-58.72	53.52	-0.000574	0.016918
42	-62.88	53.22	-0.000615	0.017400
43	-62.83	53.47	-0.000623	0.017614
44	-63.92	54.41	-0.000640	0.018017
45	-63.72	56.53	-0.000651	0.019162
46	-64.09	59.25	-0.000684	0.022403
47	-68.44	59.45	-0.000731	0.023080
48	-69.01	61.63	-0.000766	0.024362
49	-70.13	63.97	-0.000799	0.026503
50	-9.78	6.95	-0.000228	0.013321
51	-1.79	-0.85	0.000021	0.011097

APPENDIX II SHRINKAGE CALCULATION USING EUROCODE 2

The ε_{sh} is the shrinkage strain in a plain concrete specimen. Viktor et al. (2014) calculated the initial shrinkage strain ε_{sh} of concrete using the approach in *Eurocode 2.* Same approaches were applied in the proposed study to account for the effect of shrinkage for each specimen. In the following section, the details of the calculation are presented:

The total shrinkage strain is composed of two components, namely, the drying shrinkage ε_{cd} and the autogenously shrinkage strain ε_{ca}, the expressions are

$$\varepsilon_{sh} = \varepsilon_{cd} + \varepsilon_{ca},$$

$$\varepsilon_{cd}(t) = \beta_{ds}(t, t_s) \cdot k_h \cdot \varepsilon_{cd,0},$$

$$\beta_{ds}(t, t_s) = \frac{(t - t_s)}{(t - t_s) + 0.04\sqrt{h_0^3}},$$

where t is the age of the concrete at the moment considered (in days); t_s is the age of the concrete (days) at the beginning of drying shrinkage (or swelling). Normally this is at the end of curing; h_0 is the notional size (mm) of the cross-section. The factor k_h is a coefficient depending on the notional size according to the following table:

h_0 (mm)	k_h
100	1.0
200	0.85
300	0.75
≥500	0.50

The basic drying shrinkage strain is calculated from

$$\varepsilon_{cd,0} = 0.85\left[\left(220 + 110 \cdot \alpha_{ds1}\right) \cdot exp\left(-\alpha_{ds2} \cdot \frac{f_{cm}}{f_{cmo}}\right)\right] \cdot 10^{-6} \cdot \beta_{RH},$$

$$\beta_{RH} = 1.55\left[1 - \left(\frac{RH}{RH_0}\right)^3\right],$$

where α_{ds1} and α_{ds2} are coefficients that depends on the type of cement and equal to

$$\alpha_{ds1} = \begin{cases} 3 \text{ for the cement Class S} \\ 4 \text{ for the cement Class N} \\ 5 \text{ for the cement Class R,} \end{cases}$$

$$\alpha_{ds2} = \begin{cases} 0.13 \text{ for the cement Class S} \\ 0.12 \text{ for the cement Class N} \\ 0.11 \text{ for the cement Class R.} \end{cases}$$

RH is the ambient relative humidity (%) and $RH_0 = 100\%$; f_{cm} is the mean compressive strength (MPa), f_{cmo}=10MPa. The autogenous shrinkage strain follows

$$\varepsilon_{ca}(t) = \beta_{as}(t)\varepsilon_{ca}(\infty),$$

where $\varepsilon_{ca}(\infty) = 2.5(f_{ck} - 10)\cdot 10^{-6}$, and

$$\beta_{as}(t) = 1 - \exp\left(-0.2t^{0.5}\right),$$

where t is given in days.

The details of the calculation using this method is listed in the table on next page.

Details of Calculation of Shrinkage using *EuroCode 2* Method

Nr	Member	h	b	h_0	k_h	f_{cm}	f_{ck}	$\varepsilon_{ca,\infty}$	RH	β_{RH}	$\varepsilon_{cd,0}$	t	t_0	β_{as}	ε_{ca}	β_{ds}	ε_{cd}	ε_{sh}
		mm				Mpa		-	%	-		days		-				
1	*REF-R3*	175	253	103.446	1	42.21	34.21	-6.052E-05	78	-0.814	-3.829E-04	26	7	0.64	-3.869E-05	0.31	-1.191E-04	-1.578E-04
2	*REF-R4*	175	253	103.446	1	42.21	34.21	-6.052E-05	78	-0.814	-3.829E-04	25	7	0.63	-3.825E-05	0.30	-1.147E-04	-1.530E-04
3	*REF-R5*	175	253	103.446	1	42.21	34.21	-6.052E-05	78	-0.814	-3.829E-04	23	7	0.62	-3.733E-05	0.28	-1.055E-04	-1.428E-04
4	*S3-025-FA*	175	253	103.446	1	46.21	38.21	-7.053E-05	87	-0.529	-2.382E-04	23	7	0.62	-4.350E-05	0.28	-6.560E-05	-1.444E-04
5	*S3-040-FA*	175	253	103.446	1	46.21	38.21	-7.053E-05	87	-0.529	-2.382E-04	26	7	0.64	-4.509E-05	0.31	-7.408E-05	-1.590E-04
6	*S4-025-FA*	175	253	103.446	1	48.07	40.07	-7.517E-05	90	-0.420	-1.852E-04	24	7	0.62	-4.695E-05	0.29	-5.328E-05	-1.503E-04
7	*S4-040-FA*	175	253	103.446	1	46.21	38.21	-7.052E-05	87	-0.529	-2.382E-04	33	7	0.68	-4.816E-05	0.38	-9.095E-05	-1.881E-04
8	*S5-025-FA*	175	253	103.446	1	46.21	38.21	-7.052E-05	87	-0.529	-2.382E-04	27	7	0.65	-4.557E-05	0.32	-7.672E-05	-1.636E-04
9	*S5-040-FA*	175	253	103.446	1	48.07	40.07	-7.517E-05	90	-0.420	-1.852E-04	44	7	0.73	-5.522E-05	0.47	-8.663E-05	-2.232E-04
10	*S4-025-SB*	175	253	103.446	1	42.21	34.21	-6.052E-05	78	-0.814	-3.829E-04	27	7	0.65	-3.911E-05	0.32	-1.234E-04	-1.625E-04
11	*S4-040-SB*	175	253	103.446	1	48.07	40.07	-7.517E-05	90	-0.420	-1.852E-04	31	7	0.67	-5.049E-05	0.36	-6.725E-05	-1.809E-04
12	*S4-025-FW*	175	253	103.446	1	42.21	34.21	-6.052E-05	78	-0.814	-3.829E-04	28	7	0.65	-3.952E-05	0.33	-1.275E-04	-1.670E-04
13	*S4-040-FW*	175	253	103.446	1	48.07	40.07	-7.517E-05	90	-0.420	-1.852E-04	36	7	0.70	-5.253E-05	0.41	-7.554E-05	-1.990E-04